Dynamics and manipulation of nuclear architecture and gene expression

Katharina Thanisch

München 2015

Erstgutachter:	Prof. Dr. Heinrich Leonhardt
Zweitgutachter:	PD Dr. Stefan Müller
Tag der Abgabe:	14.01.2015
Tag der mündlichen Prüfung:	11.03.2015

Dynamics and manipulation of nuclear architecture and gene expression

Dissertation

an der Fakultät für Biologie

der Ludwig-Maximilians-Universität München

vorgelegt von

Katharina Thanisch aus Zell Mosel

München, den 14.01.2015

Table of contents

List of figures

Abstract

The spatiotemporal organisation and dynamics of chromatin are key to genome function. Most nuclei exhibit a conserved architecture with active euchromatin localised in the nuclear interior between the inactive perinuclear, perinucleolar and pericentromeric heterochromatin (HC) domains. Spatial chromatin arrangements are not fixed but change during development and differentiation, as exemplified by the nuclear inversion of rod photoreceptors in nocturnal mammals. Remarkably, the repositioning of genes to the inactive compartment often correlates with transcriptional repression, which can be mimicked by artificially tethering genes to the periphery. However, little is known about the mechanisms governing genome positioning and its functional consequences.

Based on a GFP-labelled designer transcription activator-like effector (dTALE) directed against the major satellite repeats, we developed fluorescent dTALEs as a new tool to spatiotemporally resolve the cell cycle-dependent dynamics of genomic sequences and unravel the interplay between the dTALE and the chromatin in living cells. Using *in vitro* DNA binding assays and fluorescence polarisation we confirm a tight dTALE-DNA interaction at the *oct4* locus and employ dTALEs to transcriptionally activate *oct4*.

Furthermore, we extended dTALE-based genome visualisation to targeted manipulation of spatial HC arrangements by tethering chromocenters (CCs) to the nuclear periphery, which caused CC disintegration and is compatible with cellular proliferation and differentiation.

To elucidate the mechanisms underlying peripheral HC anchorage, we investigated the HC organisation in different tissues and species and identified the nuclear envelope components Lamin C (LmC) and Lamin B receptor (LBR) as developmentally regulated tethers. Using mice ectopically expressing either LmC or LBR in rod nuclei, we demonstrate that LBR but not LmC rescues the inverted nuclear architecture and mediates peripheral HC tethering.

Finally, using a human artificial chromosome (HAC) in murine cells, we investigated how DNA sequence composition relates to chromatin positioning. Notably, chromosome segments corresponding to the main chromatin classes faithfully segregate and partially retain the pattern of lamina-association, which correlates with gene expression.

In conclusion, we developed a new set of dTALE-based methods to visualise and manipulate the nuclear architecture in living cells allowing better understanding of the relationship between genome positioning and function. Moreover, we show that distinct chromatin classes blueprint the nuclear architecture and demonstrate that differential nuclear envelope protein composition determines spatial heterochromatin arrangements and gene expression during differentiation and development.

Zusammenfassung

Die dynamische Organisation des Chromatins spielt eine wichtige Rolle in der Regulation der Zellkernfunktion. Charakteristisch für alle Zellkerne ist eine globale Segregation aktiver, euchromatischer (EC) und inaktiver, heterochromatischer (HC) Bereiche. In den meisten Zellkernen ist das EC im Kerninneren organisiert, während sich das HC in der Peripherie des Zellkerns und der Nukleoli sowie in den perizentromerischen Bereichen befindet. Diese räumliche Anordnung ist jedoch veränderbar. Insbesondere während der Entwicklung und Differenzierung kommt es zu weitgehenden Restrukturierungen, z.B. in den Stäbchenzellen nachtaktiver Tiere, deren Zellkernarchitektur mit ihrer Differenzierung invertiert. Zudem ändert sich die Position mancher Gene in Abhängigkeit von ihrem transkriptionellen Status und eine ektopische Rekrutierung an die Kernperipherie resultiert häufig in transkriptioneller Repression. Die Grundlagen der räumlichen Chromatinanordnung und die Abhängigkeiten zwischen Position und Funktion sind jedoch weitgehend unbekannt.

Basierend auf einem GFP-markierten designer transcription activator-like effector (dTALE), der spezifisch die Sequenz der repetitiven major satellite DNA bindet, haben wir fluoreszente dTALEs als neue Methode zur Visualisierung der zellzyklusabhängigen Positionierung genomischer Sequenzen etabliert. Interessanterweise ist die dTALE-Chromatin-Bindung gleichzeitig hochaffin und dynamisch reguliert. Durch *in vitro* DNA-Bindestudien und Fluoreszenzpolarisierungsexperimente konnten wir die hohe Affinität der Bindung auch am *oct4* Lokus nachweisen und dTALEs zur transkriptionellen Aktivierung von *oct4* nutzen.

Darüber hinaus haben wir die dTALE-basierte Visualisierung auf die Manipulation der räumlichen Anordnung genomischer Sequenzen erweitert, indem wir Chromozentren (CC) artifiziell an die Kernperipherie rekrutieren. Es ist bemerkenswert, dass trotz peripherer Lokalisierung und Auflösung der sphärischen CC-Struktur weder Proliferation noch Differenzierung beeinträchtigt werden.

Um die Grundlagen der peripheren HC-Assoziation besser zu verstehen, haben wir die HC-Organisation in verschiedenen Geweben und Spezies untersucht und die Kernhüllenproteine Lamin C (LmC) und Lamin B Rezeptor (LBR) als entwicklungsabhängig regulierte Verankerungsmoleküle identifiziert. Mittels transgener Mäuse, die eines der beiden Proteine ektopisch in Stäbchenzellen exprimieren, zeigen wir, dass LBR jedoch nicht LmC allein die Inversion der Zellkernarchitektur unterbinden kann.

Letztlich haben wir den Einfluss der Sequenzkomposition auf die Chromatinanordnung mittels eines humanen artifiziellen Chromosoms (HAC) in Mauszellen untersucht. Interessanterweise verhalten sich HAC Segmente hinsichtlich ihrer Segregation, Laminaassoziation und transkriptionellen Regulation weitgehend wie die ihnen entsprechenden Chromatinklassen.

Zusammenfassend haben wir neue TALE-basierte Methoden zur Visualisierung und Manipulation der Zellkernarchitektur entwickelt um die Abhängigkeiten zwischen Genompositionierung und Funktion besser zu verstehen. Darüberhinaus zeigen wir, dass distinkte Chromatinklassen eine Art Blaupause für die Zellkernarchitektur darstellen und die Proteinzusammensetzung der Kernmembran mitbestimmend für die HC-Anordnung während der Differenzierung und Entwicklung ist.

1 Introduction

More than 130 years ago, chromosomes were first described by Walther Flemming as stained bodies appearing during cell division (Flemming, 1882). Stimulated by the notion that chromosomes physically carry the genetic information (Wilson, 1925), chromosome behaviour, structure and dynamics were intensively studied to uncover how this information is stored, expressed and passed on. With the breakthrough of the discovery of the genetic code in the 1950ths, however, the focus shifted assuming DNA sequence information is holding the keys to functional genome output. This seemingly straightforward relationship, however, emerged to be fairly more complicated. Cells of a multicellular organism are homogenous in their DNA sequence, arise from one single cell, but are phenotypically highly divers. Cellular identity is acquired, maintained and inherited owing to differential genome usage. Differential gene expression is imposed by hierarchical levels of regulation, which do not affect the primary sequence and are therefore referred to as epigenetic. Most epigenetic mechanisms regulating gene expression and ensuring cellular identity are intimately linked to chromatin structural plasticity. Evidence is emerging that besides one-dimensional (1D)-aspects such as chemical DNA and histone modifications, histone variants, nucleosome remodelling or non-coding RNAs, also three-dimensional (3D)-processes such as long-range interactions and genome positioning impact on the spatiotemporal control of genome accessibility and function.

1.1 Principles of chromatin organisation

In eukaryotes, higher order 3D-organisation of the linear DNA sequence is accomplished by complexing DNA with RNA and proteins into chromatin, ensuring compaction within the spatial confines of the nucleus while maintaining its dynamic properties for regulated chromatin access. The basic building unit of chromatin is the nucleosome core particle, an octameric complex comprising two copies each of the histones H2A, H2B, H3 and H4 around which 147 base pairs (bp) of DNA are wrapped 1.7 times (Luger et al., 1997). Adjacent nucleosomes are arranged into a linear array of nucleosomes regularly spaced by a linker sequence of 10-50 bp, resembling a “beads-on-a-string” fibre of 11 nm diameters (Olins and Olins, 1974; 2003). Interactions between the nucleosomes promoted by association of the linker histone H1 as well as additional chromatin trans-acting proteins and RNAs drive further assembly into higher order structures.

1.1.1 Eu- and heterochromatin

Gene activity is influenced by the state of the local chromatin environment and the regulatory elements within. Based on its differential compaction during interphase, chromatin is commonly classified into active eu- and inactive heterochromatin (EC and HC, respectively) (Heitz, 1928). EC and HC are distinctly marked by GC content, gene density, and, repeat composition (Korenberg and Rykowski, 1988; Chen and Manuelidis, 1989; Bernardi, 1989; Dillon and Festenstein, 2002).

Active genes mainly reside within the decondensed and more accessible EC, characterised by a high GC content and short interspersed nuclear elements (SINE) repeats of the B1 class. Condensed HC, instead, is highly ordered in nucleosomal arrays, less accessible, poor in genes and GC content, and enriched in long interspersed nuclear elements (LINE) repeats of the L1 and L2 class. HC can be further subdivised into facultative (fHC) and constitutive heterochromatin (cHC). While fHC mainly contains developmentally regulated, tissue-specific genes competent to interconvert between active and inactive states depending on the spatiotemporal context, cHC remains condensed throughout the cell cycle and is largely transcriptionally inert except for early developmental and pathological situations (Grewal and Jia, 2007; Almouzni and Probst, 2011; Fadloun et al., 2013; Smith and Meissner, 2013). The main component of cHC are tandemly clustered repeats preferentially formed at centromeric and telomeric regions (Grewal and Jia, 2007). While telomeric DNA, which protects chromosomal ends together with telomere-associated proteins from fusion and degradation, consists of conserved, 6 bp TTAGGG-repeats (Chan and Blackburn, 2004), centromeric regions are enriched in AT-rich satellite repeats, which rapidly evolve and notably vary in sequence composition, complexity, repeat unit length, and abundance in different organisms (Plohl et al., 2012). In humans, the centromeric domain is associated with 171 bp alphoid repeats, whereas in mice it comprises minor and major satellite (ms) repeats (Manuelidis, 1978; Wu and Manuelidis, 1980; Pardue and Gall, 1970; Wong and Rattner, 1988). Minor satellites of ~120 bp unit length cluster in comparatively small, 0.6 megabases (Mb) stretches at the centromere. The 234 bp ms-repeats, instead, form large pericentromeric arrays of up to ~6 Mb (Vissel and Choo, 1989; Kipling et al., 1991) and thus constitute a convenient model for studying HC (Figure 1A). Ms-repeats play an important role in the formation and maintenance of HC (Probst and Almouzni, 2008; Probst et al., 2010; Almouzni and Probst, 2011; Jachowicz et al., 2013). Pericentromeric HC is essential for safeguarding genome integrity and ensuring proper chromosome segregation in mitosis (Peters et al., 2001; Peng and Karpen, 2008; Bulut-Karslioglu et al., 2012; Almouzni and Probst, 2011).

1.1.2 Global arrangements of eu- and heterochromatin in conventional nuclei

EC and HC adopt distinct spatial arrangements within the nucleus. In mitotic chromosomes, EC and HC reside in alternating R- and G-bands, whereas during interphase they decondense into distinct spatial compartments (Figure 1). In mouse interphase nuclei, pericentromeric regions of multiple acrocentric chromosomes cluster in dense spherical structures, intensely stained by DAPI, which are referred to as chromocenters (CCs) (Guenatri et al., 2004; Joseph et al., 1989). In conventional nuclei, CCs adjoin both the nuclear periphery and the borders of the nucleoli. LINE-rich HC encircles the CCs, forms a layer beneath the nuclear envelope (NE) and at the margins of the nucleoli. SINE-rich EC is distributed between the perinuclear, perinucleolar and pericentromeric HC domains (Figure 1, B).

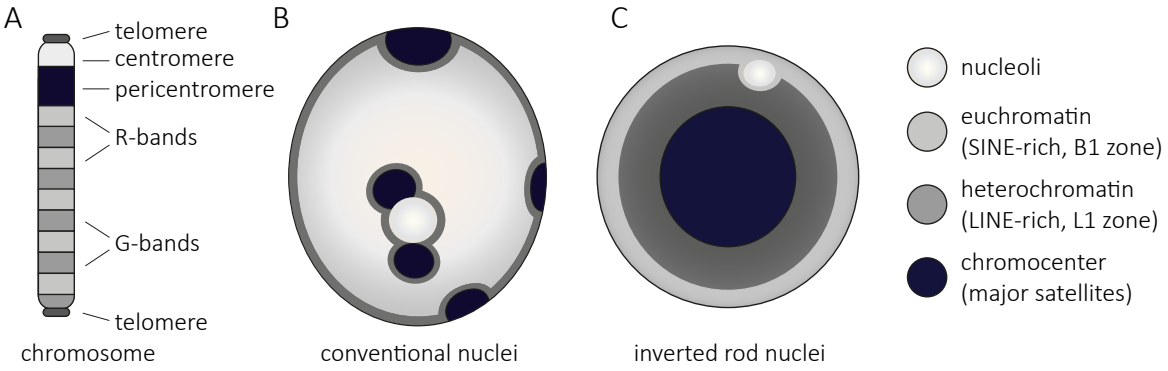

Figure 1: Conventional and inverted nuclear architecture. (A) Linear succession of alternating chromosome bands of LINE-rich heterochromatin (HC, G-bands) and SINE-rich euchromatin (EC, R-bands) on mitotic chromosomes. (B, C) Schematic representation of the spatial arrangement of the main chromatin classes (pericentromeric, LINE-rich and SINE-rich chromatin) in mouse conventional (B) and inverted rod (C) nuclei. (B) In conventional nuclei, pericentromeric major satellite (ms) repeats cluster in spherical bodies, called chromocenters (CCs). LINE-rich HC lines the CCs, the nucleoli and forms a layer beneath the nuclear envelope. SINE-rich EC positions between the heterochromatic domains. (C) In inverted rod nuclei, CCs fuse to form one large, internal CC surrounded by concentric shells of LINE-rich HC and SINE-rich EC.

1.2 Spatial distribution of chromatin in inverted rod nuclei

Although the genome is dynamically repositioned following each cell cycle, the global distribution of the main chromatin classes (pericentromeric, LINE-rich and SINE-rich chromatin) is usually maintained. An unique exception to this evolutionary conserved nuclear architecture is observed in rod photoreceptor nuclei of nocturnal mammals (Solovei et al., 2009). Rods adopt a so-called inverted architecture, where CCs coalesce into one big, internal CC surrounded by radial, concentric shells of LINE-rich HC and SINE-rich EC, thus confining gene activities to a thin, outer shell (Carter-Dawson and LaVail, 1979; Helmlinger et al., 2006; Solovei et al., 2009) (Figure 1, C).

The inverted nuclear architecture forms postmitotically during terminal rod differentiation by two parallel processes. First, CCs detach from the periphery and fuse. Second, LINE-rich HC is decompacted, detaches from the nuclear envelope and aggregates to form a shell around the internal CC. Importantly, fusion of satellites repeats from multiple chromosomes and their lining by LINE-rich HC is a common phenomena observed during differentiation (Solovei et al., 2004b; Brero et al., 2005). Inversion of rod cells represents an extreme example of this process. The radial orientation of HC favours the parallel arrangement of chromatin folds thereby increasing the overall mass density as well as the refractive index of the nuclear interior (Figure 2A). Consequently, aggregated HC serves as a microlense, reducing photon loss and adapting vision to low light conditions. The inverted nuclear architecture is, however, evolutionary disfavoured as it diminishes both inter- and intrachromosomal contacts. This is evidenced by the fact that rod inversion correlates with nocturnality in primary mammals but is reconverted back to a conventional nuclear architecture upon returning to diurnality (Solovei et al., 2009).

Importantly, at all stages of rod differentiation, a clear spatial separation of EC and HC is preserved irrespective of the dramatic chromatin reshuffling. So far, the mechanisms, which maintain the main chromatin classes spatially separated as well as the molecular basis underlying peripheral HC release during inversion, remain elusive.

1.3 Epigenetic regulation of the genome

Differential compaction of chromatin is key to regulated access by transcription factors (TFs). In cooperation with a network of epigenetic processes, TFs bind promoters to effectuate transcriptional output, tune the chromatin landscape and shape cellular functions (Dillon and Festenstein, 2002; Kouzarides, 2007; Voss and Hager, 2014). Amongst others, chemical modifications of DNA and histones, incorporation of histone variants, chromatin remodelling, non-coding RNAs, and genomic short and long – range interactions constitute the epigenetic repertoire, which in a hierarchical series of events establishes and heritably maintains expression patterns. In the following, histone and DNA modifications are presented in more detail.

1.3.1 Histone post-translational modifications (PTMs) and DNA methylation

Histones are highly enriched in the basic amino acids arginine and lysine, which, due to their positive charge, tightly interact with DNA and are at the same time highly amenable to post-translational modifications (PTMs) including acetylation, phosphorylation, sumoylation,

ubiquitination and different degrees of methylation (Kouzarides, 2007). Genome-wide analysis revealed a plethora of distinct chromatin states possessing a unique histone signature (Ernst and Kellis, 2010). Mainly modifications of globular histone fold domains directly affect histone-histone and histone-DNA interactions, whereas modifications of the flexible amino (N)-terminal tails flanking the histone fold motifs and protruding from the core particle indirectly affect chromatin compaction by attracting reader proteins.

Differential histone modification patterns can be correlated with the chromatin state. Active genes are enriched in euchromatic histone modifications such as lysine trimethylation of H3K4 (H3K4me3) and H3K36 (H3K36me3), with the former peaking at the transcription start site (TSS) and the latter covering the gene body and enhancers (Santos-Rosa et al., 2002; Kim et al., 2005). Furthermore, active regions are commonly marked by extensive lysine acetylation and serine phosphorylation, which is excluded from heterochromatic regions. Heterochromatic regions instead are enriched in repressive marks, such as H3K27me3, H4K20me3 and H3K9me2/3, which are indicative for fHC and cHC, respectively (Kouzarides, 2007). Heterochromatinisation is often initiated by repressive histone modifications and subsequently reinforced by DNA methylation.

DNA methylation is a postreplicative modification prevailing at the C5 position of cytosine in CpG dinucleotides. Deposition and maintenance of methylation is catalysed by DNA methyltransferases (Dnmts) and is vital to normal development (Okano et al., 1999; Li et al., 1992). Classically a considered stable modification, DNA methylation recently emerged to be dynamically regulated with a fraction of the modified bases subjected to sequential oxidation by a family of ten-elven translocation (Tet) enzymes and thereby poised for erasure (Kriaucionis and Heintz, 2009; Tahiliani et al., 2009; He et al., 2011; Ito et al., 2011; Pfaffeneder et al., 2011).

1.3.2 Epigenetic establishment of eu- and heterochromatin

Cytosines in the context of CpG dinucleotides are scarcely distributed within the bulk genome accounting only for about 1-4% of all genomic bases. Global methylation frequencies, however, are high with 70-80% of CpGs being methylated. The majority of methylated cytosines (5mC) remain methylated with exception to specific contexts such as global erasure during fertilisation or local selective changes occurring during differentiation and development.

Clusters of CpGs, so called CpG-islands, predominant within the promoters of house keeping and developmentally regulated genes close to the transcriptional start sites (TSS),

however, are constitutively hypomethylated creating permissive chromatin states (Deaton and Bird, 2011) with exception to pathologic situations.

In pathologic situations, DNA methylation is globally reduced and CpG islands become hotspots of aberrant hypermethylation leading to promoter silencing (Goelz et al., 1985; Jones and Baylin, 2002). In normal, physiological conditions, instead, multiple mechanisms antagonising DNA methylation maintain promoters transcriptionally permissive. Amongst others, Dnmts can be actively removed from promoter sites and binding can be prevented by R-loop formation of the nascent transcript (Smith and Meissner, 2013). Additionally, active removal of methylation marks likely involves Tet activity (Smith and Meissner, 2013).

Evidence emerged that dynamic interactions of TFs, often in coordination with enhancer elements, actively counteract heterochromatinisation. Accordingly, artificial introduction of TF binding sites favours local demethylation while its removal enhances methylation (Macleod et al., 1994; Brandeis et al., 1994). Establishment of H3K4me3 by histone methyltransferases (HMTs) such as Set domain containing (SetD) 1A, SetD1B, myeloid/lymphoid leukaemia (MLL) imposes a transcriptionally permissive state and sustains further opening of chromatin by recruitment of nucleosome remodelers and additional activating factors such as histone acetyltransferases (HATs) (Smith and Meissner, 2013).

Embryonic stem cells (ESCs) are characterised by a transcriptionally permissive, open chromatin state with a high ratio of euchromatic versus heterochromatic histone PMTs and a hyperdynamic configuration of the nucleosome core particle (Meshorer and Misteli, 2006; Mattout and Meshorer, 2010). In addition, ESCs harbour a ‘bivalent’ chromatin state at developmentally regulated genes with large heterochromatic domains marked by H3K27me3 and smaller euchromatic, H3K4me3-enriched domains. These opposing modifications keep TFs at a ‘poised’, low level allowing for rapid activation/silencing in response to stimuli (Bernstein et al., 2006; Azuara et al., 2006).

Upon differentiation, bivalent states are resolved to solely H3K4me3 (for expressed genes) or solely H3K27me3 (for repressed genes) diminishing chromatin plasticity (Meshorer and Misteli, 2006). Key TFs governing pluripotency of ESCs, such as Octamer binding TF 4 (Oct4, also known as Pou5F1), Nanog (Tír na nÓg (Irish): land of the ever young) or Sex-determining region (SRY)-Box2 (Sox2) are rapidly silenced while lineage specific gene programs are established. Cooperative heterochromatinisation of pluripotency-associated promoter regions is triggered by binding of repressive TFs, followed by recruitment of the chromatin remodeler lymphoid-specific helicase (LSH) to re-establish a regular nucleosome array, G9a-dependent H3K9me3 formation and heterochromatin protein 1 (HP1)

association. Finally, *de novo* methylation by Dnmt3a and 3b confers stable silencing (Smith and Meissner, 2013).

Silencing of constitutive, pericentromeric HC has been closely associated with H3K9me3, which triggers a cascade to consolidate heterochromatinisation (Bannister and Kouzarides, 2011; Lachner et al., 2001; Lehnertz et al., 2003; Schotta et al., 2004). Following H3K9me3 formation by the activity of suppressor of variegation (Suv) 39h1/h2 enzymes, chromo-domain containing proteins such as HP1 bind and subsequently recruit additional repressive factors (Maison and Almouzni, 2004; Bannister and Kouzarides, 2011; Lachner et al., 2001).

Once HC is established, chromatin compaction is self-reinforced in a series of events requiring cooperative action of HP1 with other epigenetic modifiers: H4K20 methylation by Suv4-20h1/h2 (Schotta et al., 2004; Hahn et al., 2013), DNA methylation by Dnmt3b (Lehnertz et al., 2003) and further H3K9me3 accumulation generating a positive feedback loop for HC stability and spreading (Maison and Almouzni, 2004). cHC at pericentromeric repeats is subsequently established by recruitment of methylcytosine-binding protein MeCP2, histone deacetylases (HDACs) and additional HMTs (Fuks et al., 2000; Jones et al., 1998; Nan et al., 1998).

Constitutive silencing of repetitive sequences, such as ms-repeats and transposable elements, ensures genome integrity by suppressing recombination events, is essential for proper chromosomal alignment to prevent aberrant chromosome segregation, and maintains transcriptional repression (Peters et al., 2001; Peng and Karpen, 2008; Bulut-Karslioglu et al., 2012). The physiological importance of proper HC silencing for normal development is evidenced by malignancies such as the autosomal-recessive immunodeficiency, centromeric instability and facial anomaly (ICF) syndrome, caused by mutations in Dnmt3b (Okano et al., 1999; Xu et al., 1999).

1.4 Domain organisation of the genome

Starting from the chromatin fibre, chromatin is organised in complex topological hierarchies to adopt a higher order 3D-structure. Chromatin is structurally refined in long distance loops and chromosomal domains, which shape the chromosome compartments within which euchromatic, transcriptionally active regions are segregated from the heterochromatic, transcriptionally inert ones (Bickmore, 2014) (Figure 2).

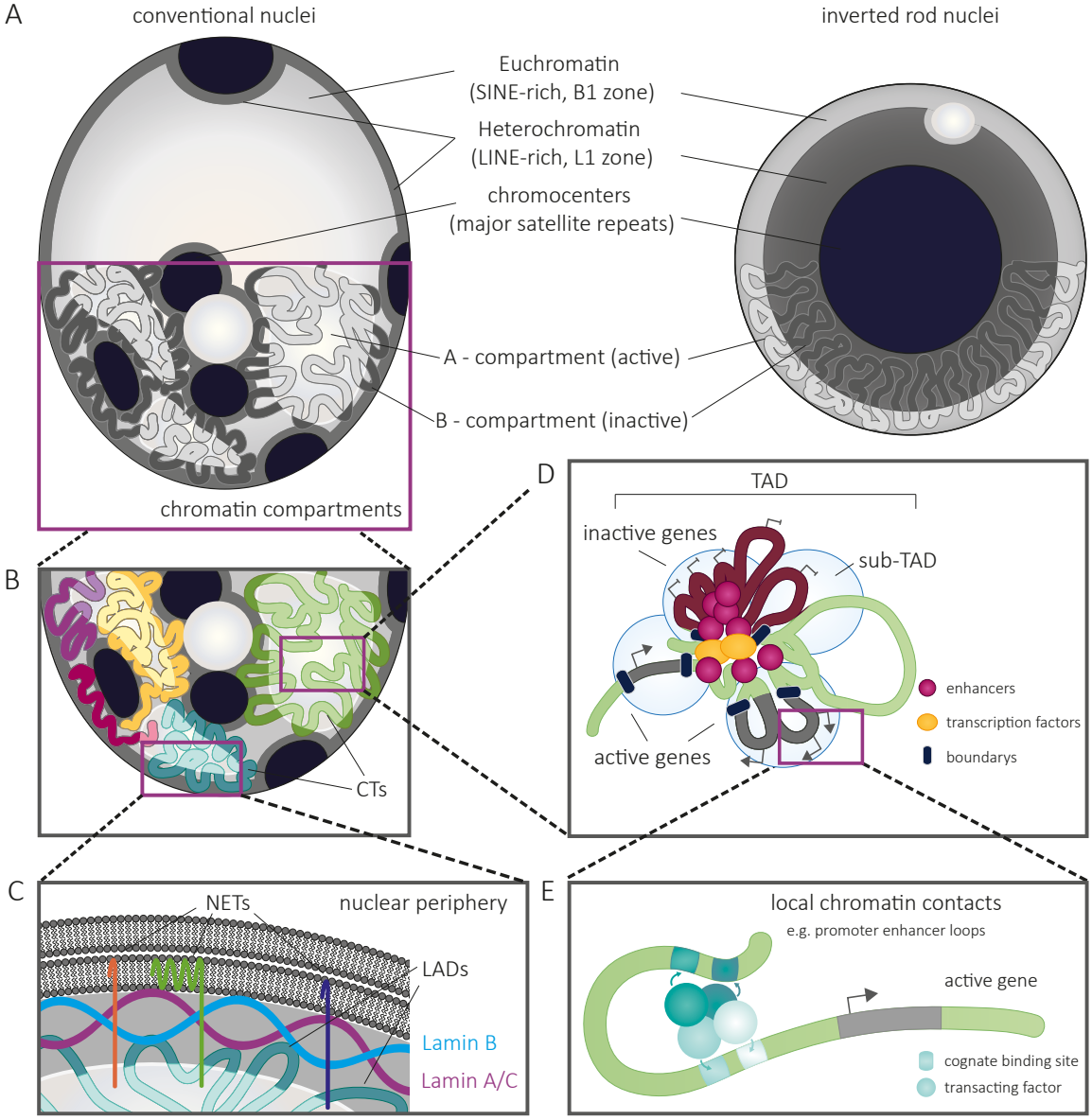

Figure 2: Hierarchical levels of genome organisation. (A) Spatial arrangements of the main chromatin classes in conventional and inverted nuclei (upper part). Chromatin segregates into two active (or open) and inactive (or closed) A and B compartments (lower part) corresponding to the euchromatic and heterochromatic zones, respectively. (B) Chromosomes (yellow, magenta, red, cyan and green) occupy distinct chromosome territories (CTs) and weave back and forth between the two compartments depending on the transcriptional status of the region. (C) Repressed chromatin domains associated with the nuclear lamina nuclear (Lamina-associating domains, LADs) coincidence with inactive B compartments. (D) CTs are shaped by the relative arrangement of topologically associating domains (TADs), which usually depend on their transcriptional status. TADs are interaction domains, which define groups of sequences with a high tendency to cluster and are relatively insulated from their genomic neighbours by boundaries enriched for architectural proteins such as CTCF, Mediator and Cohesin. Within TADs, actively expressed genes and distal enhancer come in close proximity and

share similar sets of TFs at transcription factories. Silent genes in between the active regions loop out. Architectural proteins facilitate loop formation to form sub-TADs. (E) Within sub-TADs, local DNA contacts, e.g. by means of looping, control the communication between regulatory elements.

1.4.1 A and B compartments correspond to eu- and heterochromatin

The domain organisation of the genome is imposed by transcriptional activity. Heterochromatic sequences show an inherent tendency to cluster due to self-associating forces and action of chromatin-binding proteins. Thereby they drive the global separation of the silencing compartment from the active, euchromatic compartment (Gibcus and Dekker, 2013).

At the level of genomic analysis, chromosome folding can be assessed by a number approaches related to chromosome conformation capture (3C) (Dekker et al., 2002; Simonis et al., 2006; Lieberman-Aiden et al., 2009; Zhang et al., 2012; Sexton et al., 2012). 3C-techniques (3C, 4C, 5C and Hi-C) determine the frequencies of physical interactions and proximities of genomic loci thereby allowing for estimations of contact probabilities among large sets of genomic loci. A snapshot of the 3D chromosomal conformation is generated by formaldehyde crosslinking, followed by fragmentation, intramolecular ligation, and detection by either PCR or deep sequencing (Hakim and Misteli, 2012). Especially Hi-C enables for quantitative probing of genome-wide contacts with high resolution.

Hi-C interaction maps infer that chromatin spatially segregates into two active (A) and inactive (B) compartments, which correspond to EC and HC, respectively (Lieberman-Aiden et al., 2009) (Figure 2, A). This functional organisation of chromatin is conserved across species (Lieberman-Aiden et al., 2009; Zhang et al., 2012; Sexton et al., 2012). Within A and B compartments interactions are preferentially enriched throughout the genome whereas associations between the compartments are depleted, with distinct boundaries separating interactions between alternating compartments. Within compartment B, pairs of loci exhibit an increased interaction frequency compared to compartment A, which is indicative for more compacted chromatin (Lieberman-Aiden et al., 2009). Compartment A instead correlates with the presence of genes, high transcriptional activity, is more accessible to DNase digestion and overlaps with euchromatic marks.

Folding of chromosomes within compartments is non-homogenous, but can be further partitioned into subcompartments of discrete chromosome domains (CDs) (Figure 2). CDs form predominately within but are not limited to one chromosome. Compartments are defined by proximity of CDs with similar activities, resulting in alternate transcriptionally active and inactive blocks on mitotic chromosomes. However, these blocks do not display on and

off states but a continuum of different transcriptional activities (Imakaev et al., 2012; Rao et al., 2014). Depending on genomic segment, cell type and species, domain size varies roughly between 100 kb in flies to 1 Mb in humans (Cavalli and Misteli, 2013). Different types of active and inactive domains have been identified so far, which were classified regarding DNA methylation status, frequency of interaction (e.g., topology associated domains (TADs)), protein composition (e.g. sub-TADs), spatial distribution (e.g., lamina-associated domains (LADs) or nucleolus-associated domains (NADs)) and replication timing (replication domains), amongst others (Bickmore and van Steensel, 2013; Rao et al., 2014).

1.4.2 A and B compartments correspond to early and late replication domains

Compartmentalisation according to transcriptional activity is closely matched by the spatiotemporal order of replication. Microscopically, DNA replication can be visualised at discrete sites, termed replication foci. Replication foci are formed by large numbers of synchronously firing replicons and appear in characteristic patterns during S-phase (Nakamura et al., 1986; Nakayasu and Berezney, 1989; O'Keefe et al., 1992; Dimitrova and Berezney, 2002).

The *in vivo* dynamics of replication foci can be studied by fluorescently tagging proliferating cell nuclear antigen (PCNA), a central component of the DNA replication machinery (Leonhardt et al., 2000). In mammals, foci of one to ten co-activated origins replicate Mb-sized chromosomal segments within 45-60 min (Berezney et al., 2000). At a given time, 10–15 % of the thousands of individual replication sites are simultaneously active during S-phase (Hatton et al., 1988). Pulse-chase experiments following cells through multiple divisions reveal constancy of foci size, shape and intensity implying that replication foci constitute a structural unit (Sadoni et al., 2004). Adjacent foci assemble dynamically and replicate sequentially owing to a proposed domino effect (Leonhardt et al., 2000; Sporbert et al., 2002).

The spatial distribution of replication foci throughout the nucleus appears to be maintained by constraint chromatin motion within the nucleus and stable anchorage of replication foci, e.g. by structures such as the nuclear periphery (Leonhardt et al., 2000; Sporbert et al., 2002; Ragoczy et al., 2006; Steglich et al., 2012).

The temporal profile of replication is evolutionary conserved and developmentally regulated (Rhind and Gilbert, 2013; Hiratani et al., 2008). Global compartmentalisation of

replicating chromatin during S-Phase manifests in early, mid, mid-late and late replication patterns, is linked to the transcriptional status of the region and spatially confined to the respective compartment. Early replicating euchromatic, transcriptional active, gene-rich chromatin appears as small foci dispersed in the nuclear interior leaving out regions at the nucleolar and nuclear periphery, which is referred to as early S-phase pattern. In contrast, heterochromatic, gene-poor and transcriptionally less active regions replicate in foci at both perinucleolar and perinuclear compartments in mid to late S-phase. fHC is replicated in mid S-phase and followed by the onset of cHC replication in mid-late S-phase, which persists throughout late S-phase (Rhind and Gilbert, 2013). In mouse cells replicating cHC appears in a large horseshoe like pattern surrounding the CCs (Figure 3).

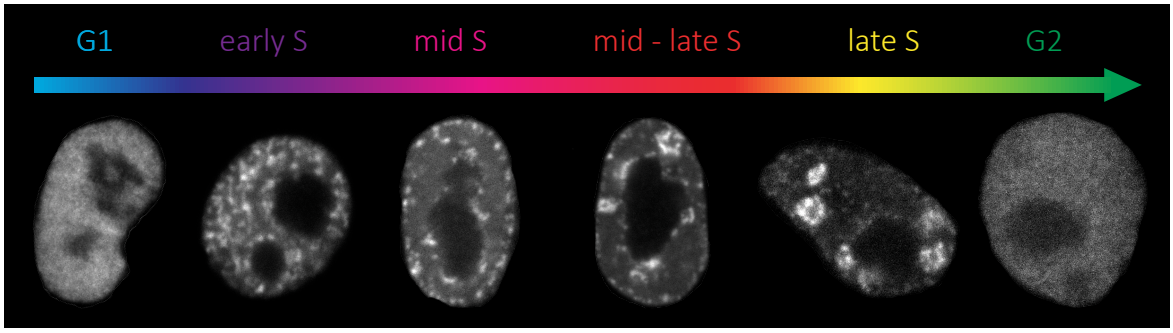

Figure 3: Spatiotemporal segregation of DNA replication. S-phase patterns of murine ESCs expressing PCNA-mRFP. During early S-phase, euchromatin is replicated appearing as small foci in the nuclear interior excluding both nuclear and nucleolar peripheral regions. Subsequently, perinuclear and perinucleolar regions are replicated from mid to late S Phase. FHC replicates first (mid S-phase pattern), followed by cHC appearing as horseshoe like pattern around the CCs (mid-late S-phase), which persists throughout S-phase (late S phase pattern).

Global analysis demonstrated the segmentation of chromosomes into Mb-sized replication domains, which likely represent a unit of large scale chromatin folding (Hiratani et al., 2008). Replication domains closely match A and B compartments (Lieberman-Aiden et al., 2009; Ryba et al., 2010). Early replicating EC is confined to the active A, whereas late replicating HC only appears in the inactive B compartment. During G1 phase as chromatin becomes anchored, nuclear compartments form by self-assembly of replication domains with distinct origin-suppressed boundaries, which demarcate the two compartments (Ryba et al., 2010; Moindrot et al., 2012). Timing of replication is suggested to correlate with chromatin compaction, as less compacted chromatin folding within the A compartment allows for earlier access of replication-initiation factors.

1.4.3 B compartments coincidence with lamina-associating domains (LADs)

A special class of repressive interaction domains is formed by anchorage of repressed chromosomal regions to the nuclear lamina (NL), which lines the nuclear envelope (Figure 2, C). Based on DNA adenine methyltransferase (Dam) identification (DamID) with a Dam coupled to a nuclear laminar protein (e.g. Lamin B1), Lamina-associating domains (LADs) where identified (Pickersgill et al., 2006; Guelen et al., 2008; Peric-Hupkes et al., 2010; van Bemmel et al., 2013).

LADs are confined to the compacted HC of the B compartment and rarely intermingle with the euchromatic compartment. Following disassembly of the NL, LADs show a clear banding throughout the condensed pro- and metaphase chromosomes, which alternates with bands corresponding to the euchromatic A compartment (Kind et al., 2013). With an average size of 0.5 Mb, LADs cover about 40 % of the genome and have sharp borders marked by boundary elements such as binding sites for the CCCTC-binding factor (CTCF) (Guelen et al., 2008; Peric-Hupkes et al., 2010).

While 80 % of all LADs are largely invariant between different pluripotent and differentiated cell types (constitutive LADs or cLADs), the remaining facultative lamina-contacts appear to be lineage-specific (facultative LADs or fLADs) (Peric-Hupkes et al., 2010). cLADs are nearly 'gene-deserts' and show features of cHC, whereas fLADs contain developmentally regulated genes enriched in fHC. Genes within fLADs loose NL association upon or prior to their activation during differentiation, whereas genes no longer expressed acquire NL contacts (Peric-Hupkes et al., 2010). Consistently, massive parallel integration of thousands of reporters revealed a striking decrease in transcriptional activity when inserted into LAD regions (Akhtar et al., 2013). Taken together, this implies that the NL constitutes an environment restrictive for transcription, in contrast to the nuclear interior, which is more permissive. LADs probably silence transcription by hindering access of TFs. Indeed, tethering a genomic region to the nuclear periphery can diminish gene expression (Finlan et al., 2008; Reddy et al., 2008; Dialynas et al., 2010), although this represents not a general phenomenon (Finlan et al., 2008; Kumaran and Spector, 2008). The determinants of LAD association remain, however, largely unknown. There is evidence, that certain sequences such as $(GA)_n$ repeats or Ying-Yang 1 (YY1) motifs play a role in targeting fLADs to the periphery (Zullo et al., 2012; Harr et al., 2015). Similarly, cLADs are characterised by the presence of A/T rich isochores (Meuleman et al., 2013). Besides sequence dependency, chromatin modifications, such as H3K9me2, which is specifically enriched at LADs, are likely to be involved in LAD specification. Consistently, knockout of H3K9 methyltransferases results in genome-wide loss of NL interactions in *C. elegans* (Towbin et al., 2012). Similarly,

in human cells, LADs can be destabilised and repositioned towards the nuclear interior by the acidic-activation domain of the viral protein VP16, which is associated with decreased levels in H3K9me2. LAD-NL contact frequencies are regulated by the histone methyltransferase G9a, which establishes H3K9me2 (Kind et al., 2013). While their mobility is largely confined during interphase, LADs are highly dynamic following mitosis, when contacts with the NL are re-established in a stochastic manner. Thus, LAD positioning is not epigenetically inherited (Kind et al., 2013).

As for the nuclear periphery, perinucleolar associations of specific chromosomal sequences, additionally to the expected ribosomal DNA (rDNA) loci, have been observed and termed nucleolar associated domains (NADs) (Nemeth et al., 2010; van Koningsbruggen et al., 2010). Exhibiting large congruency in their patterns, both LADs and NADs possibly represent a similar, if not the same, kind of chromatin. Taken together, these findings suggest that the nuclear periphery has a pivotal role in the spatial genome organisation and the modulation of gene expression. The mechanisms, however, which are responsible for peripheral HC/LAD association, remain largely elusive.

1.5 Chromosome territories (CTs) and their spatial arrangements

Chromosomes weave back and forth within and between active and inactive compartments depending on the transcriptional status of the genomic region but their spatial positioning is largely confined to distinct chromosome territories (CTs) (Cremer and Cremer, 2001) (Figure 2, B). First evidenced by microirradiation and fluorescence *in situ* hybridisation (FISH) experiments (Cremer et al., 1982; Manuelidis, 1985; Lichter et al., 1988; Pinkel et al., 1988), chromosomal arrangements into individual CTs was recently corroborated by 3C-analysis (Simonis et al., 2006; Lieberman-Aiden et al., 2009; Zhang et al., 2012; Sexton et al., 2012; Kalhor et al., 2011). Most of the captured genomic interactions are intrachromosomally restricted. However, a certain degree of interchromosomal contacts is observed, mainly occurring between clusters of active domains, whereas inactive clusters are confined to their own CT. Intermixing mainly occurs in the territorial peripheries possibly building platforms for functional interactions such as transcriptional regulation (Branco and Pombo, 2006; Simonis et al., 2006; Lieberman-Aiden et al., 2009; Kalhor et al., 2011; Boyle et al., 2011).

1.5.1 CT neighbourhoods

Chromosomes exhibit a high variability regarding their relative positioning with respect to

each other. While neighbourhood relationships are confined during interphase, CT neighbourhoods change from interphase to interphase and mix progressively with each mitosis as demonstrated by chromosome painting and bleaching experiments (Walter et al., 2003; Bolzer et al., 2005). Accordingly, CTs do not have fixed positions but rather have preferred orientations in particular cell types or developmental contexts, a concept which can be extended to the level of single genes (Cremer and Cremer, 2010; Mayer et al., 2005; Rajapakse et al., 2009).

1.5.2 Gene-content dependent radial distribution and CTs polarisation

Chromosomes adopt a polarised, radial positioning (Cremer and Cremer, 2001). Radial positioning relative to the nuclear interior or the periphery is mainly determined by gene-content (Croft, 1999; Cremer and Cremer, 2001; Cremer et al., 2003; Boyle et al., 2001). Small, gene-dense CTs tend to localise towards the interior, while large, less gene-dense CTs occupy more peripheral positions. Convincing evidence was provided by FISH experiments comparing the localisation of the two human chromosomes HSA18 and HSA19, similar in size but opposing in gene-content. While the gene-poor HSA18 preferentially localises peripherally, the gene-rich HSA19 positions towards the nuclear interior (Croft, 1999; Cremer et al., 2001; 2003). Similar to CTs themselves, single genes and genomic segments distribute non-randomly and adopt a polarised positioning according to gene-density and transcriptional activity. Within CTs, gene-rich chromosomal segments display a general tendency to localise internally, whereas gene-poor segments reside towards the CT periphery (Kupper et al., 2007; Goetze et al., 2007; Nagano et al., 2013).

1.5.3 Topological associating domains (TADs) as basic units of CTs

At subcompartment level, a unit of chromatin organisation termed TAD (topological associated domains) has been recently identified (Dixon et al., 2012; Sexton et al., 2012). TADs represent interaction domains in which genomic loci show a higher interaction frequency than outside of the domain and are relatively insulated from their genomic neighbours.

Being conserved across species, invariant between different cell types and tiling most of the genome, TADs represent constitutive hardwired, organisational blocks of the 3D-nuclear architecture subordinate to the CT (Dixon et al., 2012; Sexton et al., 2012; Nora

et al., 2012; Hou et al., 2012) (Figure 2, D). Several adjacent TADs typically belong to either A or B compartments, but can also span boundaries and adopt different chromatin states. One example for spatial segregation of oppositely regulated neighbourhoods in adjacent TADs is observed on the inactive X chromosome (Nora et al., 2012). Organisation of the antagonising long non-coding transcripts *Xist* and *Tsix*, which control X-chromosome inactivation at the X-inactivation centre, together with their known positive regulators in separate TADs allows for the maintenance of two opposing chromatin microenvironments in close proximity (Nora et al., 2012).

Differently to chromatin compartments, TADs do not result in alternating transcriptional patterns when successively ordered along a mitotic chromosome (Dekker et al., 2013). Most probably, TADs correspond to the replication foci described before. TADs emerge to be dependent on binding of the architectural proteins CTCF, Mediator and Cohesin, which are present within and enriched at the boundaries of TADs (Phillips-Cremins et al., 2013). Likewise, those insulators separate LADs from non-LADs (or interLADs) and early from late replication foci (Sexton et al., 2012; Dixon et al., 2012; Nora et al., 2012). Moreover, these architectural proteins coordinately facilitate loop formation to build up sub-TADs and long-range enhancer-gene interactions at TAD boundaries, mediating long-range gene regulation (Phillips-Cremins et al., 2013; Sanyal et al., 2012). Two different types of loops were revealed coinciding either with Mediator/Cohesin or CTCF and Cohesin. While the former is restricted to ESC-specific enhancer-promoter loops overlapping with TF binding, the latter is proposed to have a scaffolding function for chromosome folding. Domains are dynamic with changing gene activities, for instance at the *Hox* gene cluster, where upon progressive transcriptional activation a second domain forms into which actively transcribed genes are transferred (Noordermeer et al., 2014). Based on these findings, gene activity appears to be defined by the microenvironment of a close neighbourhood, restricting interactions to the regulatory elements within and thereby insulating genes from the rest of the genome (Figure 2, D and E).

1.6 Role of the nuclear periphery in spatial genome organisation

Eukaryotic nuclei are surrounded by the nuclear envelope (NE), a double membrane structure, composed of an inner and outer nuclear membrane (INM and ONM, respectively). Interspersed with nuclear pores, the NE creates connectivity between cytosol and nucleoplasm enabling for transport and communication while at the same time confining chromatin within the 3D nuclear space and providing an anchoring site for HC/LADs.

Organisation of HC at the periphery is performed by the nuclear envelope (NE) and associated proteins (Figure 4, see also 1.4.3).

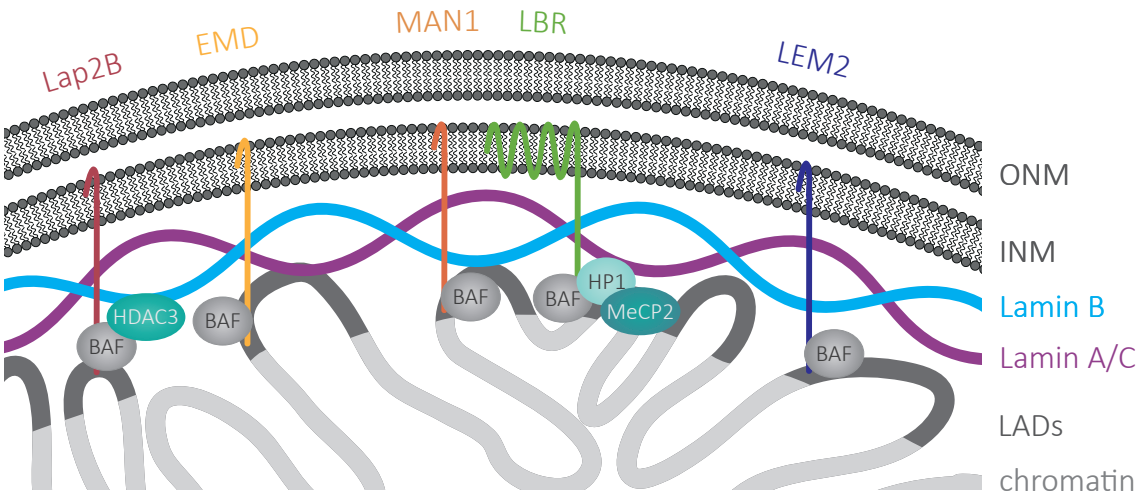

Figure 4: Schematic view of the nuclear periphery. Lamins form a proteinaceous meshwork underlying the inner nuclear membrane (INM) of the nuclear envelope (NE). Peripheral association of heterochromatic genomic regions (Lamina-associating domains, LADs) is established by interactions of Lamins with INM proteins, such as Lap2B, EMD, MAN, LEM2 or LBR, either directly, e.g. by interaction of the Tudor domain of LBR with HC, or indirectly through nucleoplasmic factors such as BAF, HP1, MeCP2 or HDAC3.

The INM is underlined by a proteinaceous type V intermediate filament meshwork, composed of A- and B-type Lamins (Prokocimer et al., 2009; Dechat et al., 2010). A- and B-type Lamins are suggested to build separate networks, which can overlap and interconnect. Lamins have a conserved structure with a short N-terminal head domain, a carboxy (C) - terminal immunoglobulin (Ig) - fold tail domain and a central alpha-helical domain subdivised in four heptad regions designated as coils. The coils mediate self-assembly of Lamins to adopt a superhelical structure, which further polymerises in a head-to-tail fashion to form filaments (Dechat et al., 2010) (Figure 5).

While at least one of the B-type Lamins Lamin B1 (LB1) or Lamin B2 (LB2) is constitutively expressed, the expression of A-type Lamins is developmentally regulated (Benavente et al., 1985; Schatten et al., 1985; Lehner et al., 1987). Mice depleted in LB1 die at birth (Vergnes et al., 2004), while Lamin A (LmA) knock-out results in postnatal growth retardation and muscular dystrophy due to disruption of the NE integrity (Sullivan et al., 1999). Vertebrate A-type lamins exist in two differentially spliced isoforms LmA and Lamin C (LmC), which are sequentially and structurally almost identical, but differently processed (Fisher et al., 1986; McKeon et al., 1986; Lin and Worman, 1993) (Figure 5). Due a CAAX-box motif present within the 74 last residues lacking in LmC, LmA is subjected to posttranslational farnesylation and carboxymethylation. Later, the modified residues are cleaved off releasing LmA from the nuclear membrane.

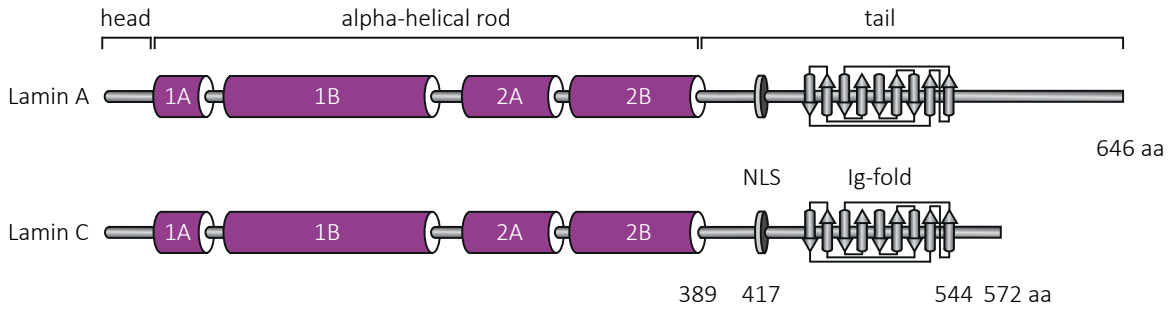

Figure 5: Domain structure and function of Lamins. Schematic representation of Lamin A and Lamin C polypeptide chains. According to the tripartite organisation of all intermediate filaments, Lamins comprise a short globular N-terminal head domain, a central alpha-helical rod domain (magenta) characterised by four heptad repeat regions (1A, 1B, 2A, and 2B) and a globular C-terminal tail domain containing the nuclear localisation signal (NLS) and the immunoglobulin (Ig)- fold domain (grey, the nine ß-strands of the Ig-fold domain are depicted). Coiled coil interactions of the alpha-helical rod domain mediate homodimer formation, which are further assembled head-to-tail by overlapping of the rod domains. The N-terminal domain assists in stabilisation of the assembled polymer while the Ig-fold tail is involved in partner protein binding.

While most of the A-type lamins are integrated in the polymerising NL, a fraction is found within the nucleoplasm (Dechat et al., 2010). Lamin filaments serve as scaffolds conferring mechanical stability, maintain cellular shape and structure. Moreover, both peripheral and nucleoplasmic Lamins play a role in various nuclear processes such as DNA repair and replication, gene expression, proliferation, differentiation, and chromatin organisation (Dechat et al., 2010; Gesson et al., 2014).

Mutual interactions between peripheral Lamins and a repertoire of INM proteins (also referred to as NE transmembrane proteins or NETs) ensure NE integrity. Together with nucleoplasmic factors, such as Barrier-to-autointegration factor (BAF), chromatin modifiers and HC-associated proteins, peripheral Lamins and NETs create a platform for the dynamic anchorage of LADs thereby facilitating both developmental gene regulation and cell state changes (Malik et al., 2010) (Figure 4).

The set of NETs is constantly increasing and highly divers in different cell types, with over 60 members identified so far (Wong et al., 2014; Malik et al., 2010). NET composition at the periphery changes dynamically upon development, external stimulus and in pathological situations (Korfali et al., 2010; Olins and Olins, 2004; Olins et al., 2000; Gaines et al., 2008; Scaffidi and Misteli, 2006).

NETs include single or two transmembrane (TM) LEM-domain containing (LEM) proteins Emerin (EMD), Lamina-associated polypeptide (LAP) 2B, LEM2, MAN1 (Lin et al., 2000; Wilson and Foisner, 2010) and the so-called Lamin B receptor (LBR), an eight TM protein (Worman et al., 1988; 1990). LBR fulfils multifunctional roles at the NE including regulation of membrane growth as well as chromatin tethering and facilitates developmental processes such as myelopoeisis (Olins et al., 2010; Cohen et al., 2008; Subramanian et al., 2012) (Figure 6).

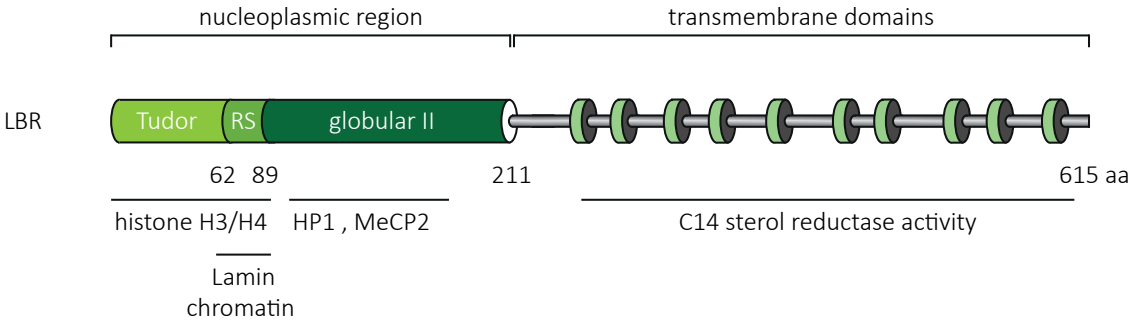

Figure 6: Domain structure and functions of LBR. Schematic representation of the LBR polypeptide chain. LBR comprises a C-terminal eight transmembrane domain, which mediates anchorage of LBR in the INM and exhibits C14 sterol reductase activity as well as a N-terminal nucleoplasmic region. Within the N-terminal region, the tudor domain is implicated in histone H3/H4 binding, while Lamin and HC interactions are mediated by the arginine/serine (RS) domain. Binding to HC-associated proteins such as HP1 and MeCP2 are mediated by the globular II domain.

Anchorage in the INM is provided by its C-terminal eight transmembrane (TM) domain, which additionally has sterol reductase activity and is involved in cholesterol biosynthesis (Ye and Worman, 1994; Silve et al., 1998; Waterham et al., 2003). The N-terminal domain facing the nucleoplasm binds to B-type lamins and directly interacts with epigenetic factors including heterochromatic H3K40me2, HP1 and Methyl-cytosine binding protein 2 (MeCP2) (Pyrpasopoulou et al., 1996; Ye et al., 1997; Guarda et al., 2009; Gaines et al., 2008; Olins et al., 2010; Makatsori et al., 2004; Hirano et al., 2012).

The diversity and physiological relevance of the nuclear periphery for proper nuclear function is emphasised by a plethora of heterogeneous and phenotypically diverse human developmental disorders, collectively termed laminopathies. Laminopathies are caused by loss or mutations in the associated genes of lamins and INM proteins (Capell and Collins, 2006; Worman, 2012). These include neuropathies, lipodystrophies and muscular dystrophies like the autosomal-dominant Emery-Dreifuss muscular dystrophy (AD-EDMD), often involving mutations in either LmA or EMD (Bonne et al., 1999; Bione et al., 1995) and premature aging syndromes, such as the Hutchinson-Gilford progeria syndrome (HGPS) caused by mutated LmA.

Expression of dysfunctional LmA in HGPS patient cells severely affects nuclear shape and chromatin tethering, resulting in loss of peripheral HC (Shumaker et al., 2006). Consistently, ChIP-seq analysis of HPGS patient cells revealed global reductions of genome-lamina contacts as well as changes in repressive histone methylation patterns (McCord et al., 2013). Moreover, mutations in LmA manifest in chromosome positioning changes with repositioning of the gene-poor HSA18 towards the interior, altered chromatin compaction and gene expression status (Meaburn et al., 2007; Mewborn et al., 2010).

Mutations in LBR cause fatal Greenberg skeletal dysplasia (Waterham et al., 2003) and Pelger-Huët Anomaly, which is associated with abnormal nuclear shape, impaired

nuclear lobulation and HC organisation in granulocytes (Shultz et al., 2003; Hoffmann et al., 2007). A similar phenotype is observed in mice lacking functional LBR, which are additionally affected by ichthyosis (Shultz et al., 2003; Cohen et al., 2008). Affected granulocytes exhibit an abnormal ovoid nuclear shape, diminished NE, hypolobulation and clumping of peripheral HC accompanied by repositioning towards the nuclear interior (Hoffmann et al., 2002; Zwerger et al., 2008) (Hoffmann et al., 2002; Zwerger et al., 2008). Conversely, stimulation of LBR expression following *in vitro* granulopoeisis favours lobulation and excessive NE production (Olins et al., 1998; Olins and Olins, 2009).

Considering the striking similarities between laminopathy-associated nuclear abnormalities and the inverted nuclear architecture of rod cells, it is likely that nuclear envelope composition is decisive for the nuclear architectural type adopted. Although peripheral association of chromatin has been implicated in higher order nuclear structure, spatial genome organisation and the modulation of gene expression, the mechanisms, which underlie peripheral tethering of heterochromatic LADs and govern nuclear inversion, are still not understood.

1.7 Chromatin dynamics in the nucleus

1.7.1 Chromatin mobility

Chromatin is no static but rather a dynamic entity. Composition and positioning of nucleosomes as well as epigenetic marks are frequently subjected to changes and many of the interactions of chromatin with nuclear proteins, such as TFs or HC-binding proteins, are highly transient (Phair and Misteli, 2001; Voss and Hager, 2014).

Dynamics of TF-chromatin interactions are mutually regulated and interdependent. On the one hand, TFs have to induce local chromatin remodelling and decompaction to bind and effectuate transcriptional output. On the other hand, chromatin compaction regulates TF binding as HC renders target regions inaccessible to TFs. Likewise, chromatin compaction regulates access of replication-initiation factors to the alternate compartments thereby controlling replication timing. Interestingly, EC and HC compartments as well as domains (e.g. LADs) are dynamic and to some extent cell-type specific (Lieberman-Aiden et al., 2009; Zhang et al., 2012; Kind et al., 2013; Noordermeer et al., 2014). While representing relatively stable entities within one cell cycle, LADs are not inherited throughout consecutive cell cycles (Kind et al., 2013). Conversely, loops and TADs are reproducible between different cells and cycles but can vary within one cell cycle (Gibcus and Dekker, 2013).

Globally, chromatin dynamics is restricted to occasional slow, long-range movements. Long-range movements are often accompanied by reorganisational changes mainly occurring during development, where they require passage through mitosis, or postmitotic differentiation. Locally, instead, chromatin is frequently subjected to rapid short-range movements. These movements are constraint, depend on adenosine triphosphate (ATP) levels and temperature (Soutoglou and Misteli, 2007; Dion and Gasser, 2014). Constraints of chromosome motion are imposed by the chromosome structure itself, e.g. by the centromere (Gartenberg et al., 2004; Shelby et al., 1996), presence of subnuclear structures, such as nucleoli, NE, nuclear speckles or Cajal bodies (Hemmerich et al., 2011), or by anchorage to subnuclear structures, such as the periphery (Chubb et al., 2002; Kind et al., 2013).

During the cell cycle, the overall chromatin mobility is relatively low except for early G1 phase, when positional changes of subchromosomal domains occur (Kind et al., 2013; Walter et al., 2003; Bolzer et al., 2005). Later in interphase, chromatin dynamics is limited to short-range movements, thereby maintaining a relatively stable, global genome topology. In general, HC is far more restricted in mobility than EC. Movements are largely confined within the respective compartments (Soutoglou and Misteli, 2007; Kind et al., 2013; Lieberman-Aiden et al., 2009). Accordingly, mobility of transgenes at the periphery or the nucleoli is significantly decreased compared to interior localisations (Chubb et al., 2002).

Positional changes of genes have been reported to correlate with changes in transcriptional activity. During differentiation, some genes adopt more internal or peripheral positions depending on whether they are expressed or not (Kosak et al., 2002; Williams et al., 2006; Takizawa et al., 2008; Jost et al., 2011; Peric-Hupkes et al., 2010), which is essentially due to positioning within the alternate compartments. Within LADs, most genes are silent and thousands of genes dislodge from the NL upon activation during differentiation (Peric-Hupkes et al., 2010). However, this does not apply to all genes and the NL is not exclusively restrictive for transcription (Hübner et al., 2013; Joffe et al., 2010). Similarly, manipulation of spatial genome arrangements by forced reposition of single genes to the nuclear periphery results in some, but not all cases, in decreased transcription (Finlan et al., 2008; Reddy et al., 2008; Dialynas et al., 2010; Kumaran and Spector, 2008). *Vice versa*, targeted activation correlates with loss of peripheral LAD association or active repositioning of genes (Kind et al., 2013; Chuang et al., 2006; Dundr et al., 2007). Strikingly, transcriptional activity of thousands of integrated reporters reflects the chromatin domain organisation as it largely depends on chromatin compaction and the microenvironment (Akhtar et al., 2013).

A typical example of large-scale movements and reorganisation observed during differentiation is CC fusion during myotube formation (Brero et al., 2005) or neuron maturation (Solovei et al., 2004b; 2009). Dramatic changes in the global genome organisation are also observed during ESC differentiation, when the hyperactive, globally decondensed chromatin state becomes more compacted while genome plasticity diminishes. Repressive chromatin states increase, initially small replication domains coalesce (Hiratani et al., 2008) and a clear peripheral heterochromatic rim forms. Concomitantly, the overall dynamics decreases (Joffe et al., 2010). Taken together, these findings highlight the importance of a dynamic chromatin landscape for modulating genome function.

1.7.2 Visualisation of chromatin dynamics

Advanced fluorescent microscopy provides a powerful tool to visualise the spatiotemporal organisation and dynamics of chromatin. *In vivo* protein dynamics can be observed by life time imaging of overexpressed or endogenously tagged fluorescent fusions or indirectly with fluorescent fusions of functionalised heavy-chain-only antibodies, referred to as chromobodies or nanobodies (Rothbauer et al., 2006; Romer et al., 2011).

The dynamic interplay of nuclear proteins with chromatin can be studied by diffusion-based methods such as fluorescence recovery after photobleaching (FRAP) or fluorescence loss in photobleaching (FLIP) (Figure 7).

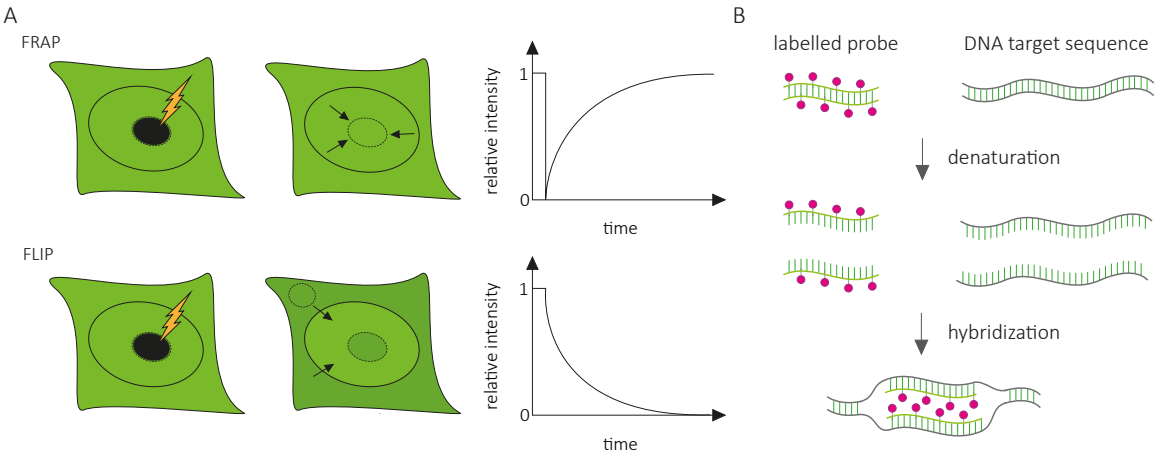

Figure 7: Kinetic microscopy and fluorescence *in situ* hybridisation methods. (A) Principle of fluorescence recovery after photobleaching (FRAP) and fluorescence loss in photobleaching (FLIP). In FRAP, recovery is measured within a bleached region over the time. Recovery rates depend on protein mobility. In FLIP, a region is repeatedly bleached and loss of fluorescence is measured in another region. (B) Principle of fluorescence *in situ* hybridisation (FISH). In FISH, a DNA probe, which is often directly labelled, is used to reveal specific, complementary DNA sequences following fixation and denaturation.

By applying a strong laser pulse, irreversible bleaching of fluorescent fusion proteins is induced perturbing the dynamic equilibrium of fluorescent proteins within the cell. In FRAP,

fluorescence recovery, i.e. restoration of a steady-state equilibrium by diffusion of bleached and unbleached proteins, is monitored over time. Information about the binding kinetics can be extracted, as the rate of recovery correlates with the protein mobility. Mobility depends on both size and interactions of the investigated proteins. In FLIP experiments, fluorescence loss is measured in an area distant from a region subjected to repeated bleaching. Hence, damage by photobleaching in the area of interest is reduced and spatial information about the immobile protein fraction can be obtained (Phair and Misteli, 2001).

Compared to the analysis of protein dynamics, the means of sequence-specific genome visualisation are limited. Traditionally, specific chromatin sequences are visualised by FISH, which relies on detection of target DNA sequences by base pairing with nucleic acid probes in fixed cells following denaturation (Figure 7, B). Elaborate techniques enabled for detection of whole chromosomes, chromosome arms, specific regions such as telomeres or centromeres, and single genes. Moreover, combinations of different fluorophores allowed for simultaneous visualisation of multiple chromosomal targets and multi-colour detection of an entire set of CTs (Bolzer et al., 2005). Due to its dependency on fixed chromatin, however, FISH can only provide static snapshots.

First live visualisation of native chromatin was enabled by replication labelling with fluorophor-conjugated deoxyuridine triphosphates (dUTPs) (Pepperkok and Ansorge, 1995; Zink et al., 1998; Bornfleth et al., 1999; Manders et al., 1999; Schermelleh et al., 2001) revealing the different S-phase patterns of the main chromatin classes.

Furthermore, genetic tagging enabled the indirect tracking of the surrounding, native genetic elements. Insertion of *lac* operator (LacO) arrays along with the expression of a green fluorescent protein (GFP)-fused lac repressor revealed the constraint movements of chromosomes (Marshall et al., 1997; Robinett et al., 1996). Moreover, repositioning of LacO-tagged loci from the periphery to the nuclear interior upon transcriptional activation provided first links between chromatin activity and nuclear positioning (Tumbar and Belmont, 2001; Chuang et al., 2006). Similarly, motion of specific cellular structures, such a telomeric repeats, was revealed by telomeric integration of LacO arrays (Jegou et al., 2009).

Direct tracing of native endogenous loci, however, is not possible by these approaches. Alternative methods take advantage of labelled peptide nucleic acid (PNA) probes, which specifically associate with the highly repetitive hexanucleotide sequence of telomeres (Molenaar et al., 2003). Recently, the cell cycle dependent dynamics of LADs were assessed using the so-called ^{m6}A-tracer technology (Kind et al., 2013). With the ^{m6}A-tracer technology, peripherally associated sequences are highlighted by a GFP-DpnI

truncation, which binds to methylated adenines generated by a coexpressed a Dam enzyme.

Chromatin can be indirectly visualised by fluorescent fusion proteins, which specifically bind certain DNA sequences, like the centromere protein (CENP) CENPB, which binds centromeric CENP-boxes, or proteins, which bind specific chromatin modification. For instance, 5mC can be revealed by GFP-methylcytosine binding domain (MBD) fusions, whereas hydroxymethylated cytosines can be revealed with Tet fusions. Similarly, histone PTMs can be highlighted by fluorescent fusions of readers such as Suv39h1/h2. Moreover, fluorescent histone fusions can be used for *in vivo* chromosomal counterstaining (Kanda et al., 1998) and to assess the chromatin mobility. Accordingly, GFP-H2B fusions in combination with photobleaching experiments revealed the local motion of chromatin with the restriction of large-scale movements to early G1 phase (Walter et al., 2003).

However, the described *in vivo* methods do not enable for the targeted visualisation of pre-defined sequences. Sequence-specific targeting and visualisation of repetitive sequences was first accomplished *in vivo* using recombinant zinc finger (ZF) based DNA recognition proteins (Lindhout et al., 2007). However, as sequence-specificity of zinc finger proteins (ZFPs) is hard to engineer, there is a need for alternative approaches enabling live visualisation of specific genomic sequences.

1.8 Modular DNA-binding domains

Several platforms of DNA recognition modules exist, which serve as programmable scaffolds to target specific DNA sequences. Those include ZFPs (Figure 8) and transcription activator-like effectors (TALEs).

Cys_2His_2 zinc finger (ZF) domains, the predominant DNA binding motif occurring in the human proteome (Tupler et al., 2001), were the first modules on which proteins with user-defined target recognition were based (Gersbach and Perez-Pinera, 2014; Beerli and Barbas, 2002).

A single ZF is composed of an alpha-helix and two beta-strands. DNA contacts within the major groove are established through positions -1, 3 and 6 within the alpha-helix (Pavletich and Pabo, 1991) (Figure 8). The base triplet determining DNA sequence specificity can be engineered to bind predefined sequences and usually three to four ZFs are joined to achieve target specificity (Berg, 1988). However, ZF modules are context dependent as adjacent modules influence each other thus rendering predictions about specificity and activity of ZFPs difficult (Zhu et al., 2013; Persikov et al., 2014). This unreliability, along with a

bias towards GC-rich sequences and high costs, have favoured alternative platforms with more straightforward DNA recognition properties, such as transcription activator-like effectors (TALEs).

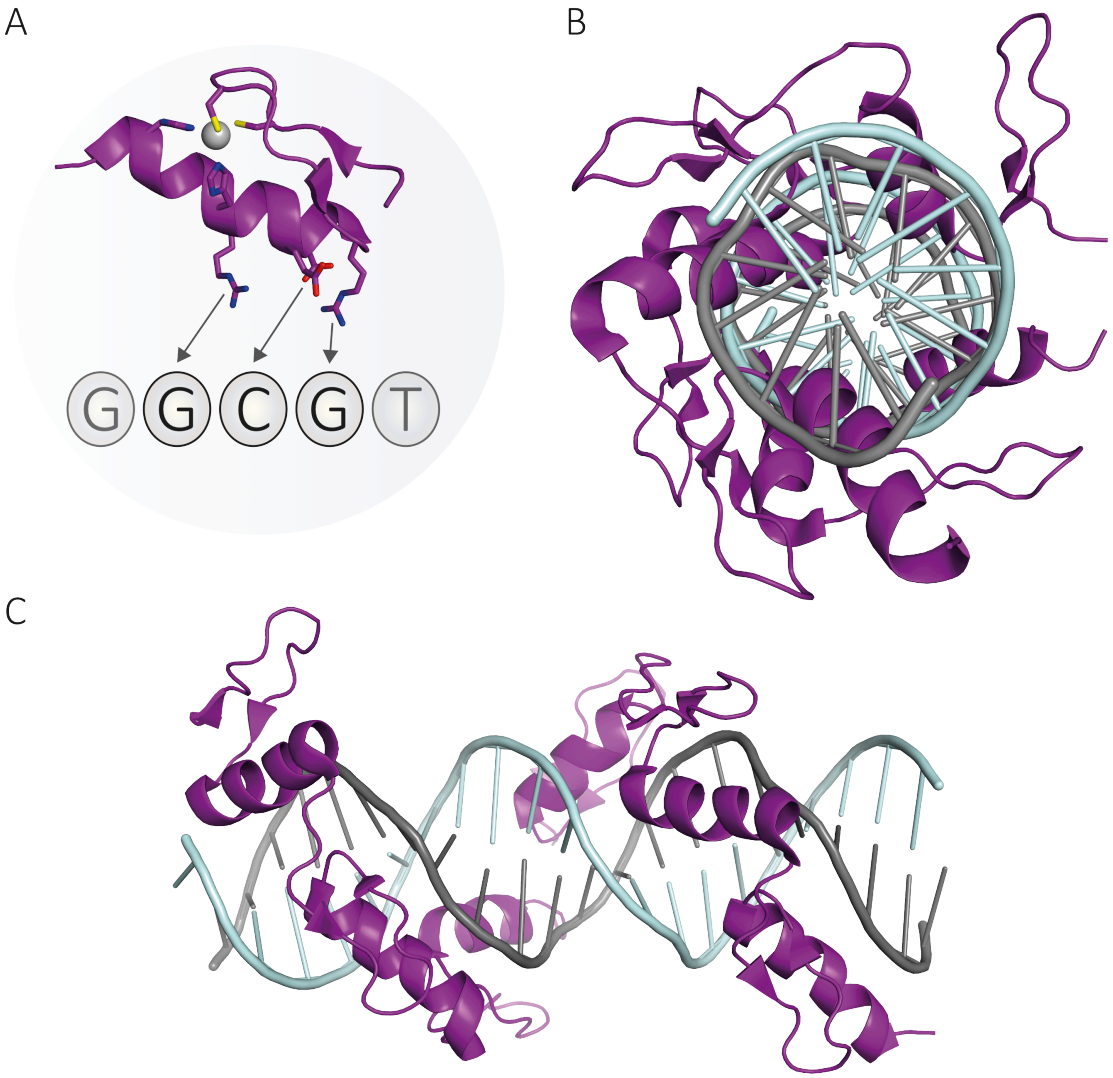

Figure 8: DNA recognition by zinc finger proteins (ZFPs). (A) Structure of a single ZF targeting the base triplet GCG (PDB 1p47). (B, C) ZFP consisting of 3 ZF bound to DNA. (B) Top view. (C) Side view.

1.8.1 Transcription activator-like effectors (TALEs)

TALEs are the key effectors determining pythopathogenicity of *Xanthomonas* species. Infection by the many *Xanthomonas* pathovars is a thread to agriculture, as they elicit diseases in a wide variety of plants, including several major crop and ornamental species (Mansfield et al., 2012). *Xanthomonas* bacteria typically invade plants through natural openings, such as stomata or hydathodes, and wounds, multiply in the intercellular spaces of the plant tissue or the xylem and inject the effector proteins via a Type III secretion (T3S)

system into the plant cell. Upon translocation to the cell nucleus, TALEs bind host gene promoters to suppress cellular defence mechanisms and activate host gene expression to the benefit of the pathogen (Boch and Bonas, 2010) (Figure 9).

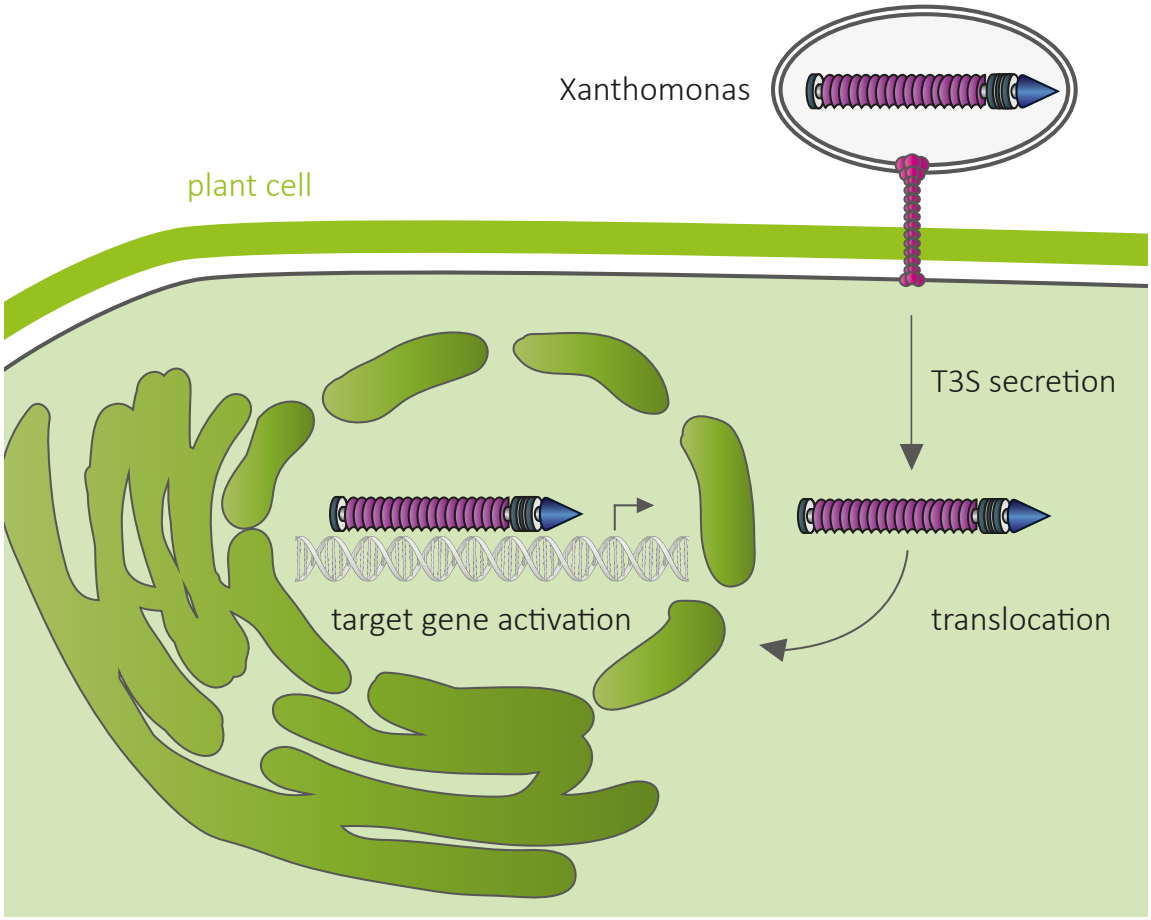

Figure 9: Model of TALE infection in plant cells. *Xanthomonas* species secret TALEs into the cell cytoplasm by a T3S system. Upon translocation into the nucleus, TALEs bind target promoters to manipulate host gene expression.

TALEs exhibit a conserved structure divisible into modular functional domains (Figure 10, A). The N-terminal domain (NTD) harbours a secretion signal directing injection of the TALEs into the cytoplasm (Buttner et al., 2004). The C-terminal domain (CTD) contains nuclear localisation signals (NLS) required for translocation into the nucleus (Van den Ackerveken et al., 1996; Szurek et al., 2001) as well as an acidic transcriptional activation domain (AD) in the far C-terminal region (Marois et al., 2002) enabling for eukaryotic transcriptional activation. Sequence-recognition and target binding is mediated by the central DNA repeat domain.

The DNA repeat domain is composed of canonical tandem arrayed repeats, consisting each of 33 to 35, typically 34 amino acids (aa), which are largely invariable except for positions 12 and 13, termed repeat variable diresidues (RVDs).

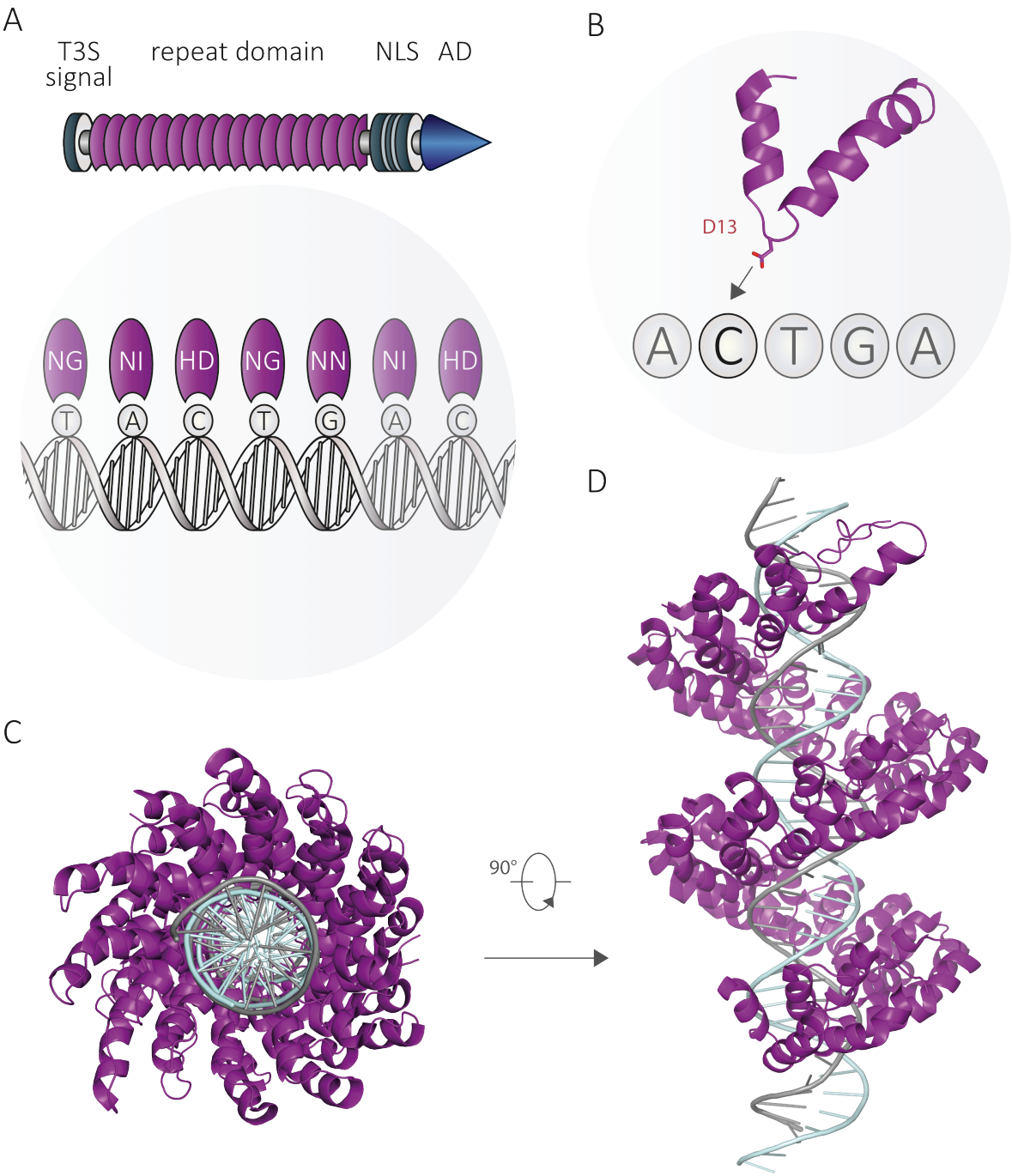

Figure 10: TALE structure and mode of DNA recognition. (A) TALE domain organisation. The central repeat domain is flanked by an N-terminal domain harbouring a T3S secretion signal and a C-terminal domain with localisation signals (NLS, light grey) as well as an activation domain (AD, blue). DNA recognition is mediated by the central repeat domain (individual repeats represented by purple ellipses). The most common RVD code for DNA base recognition is NI for adenine (A), HD for cytosine (C), NG for thymine (T) and NN for guanine (G). Note that NG also recognises methyl cytosine (5mC) (RVDs in white). Single letter code for amino acids. (B) Structure of an individual repeat with the base-specifying residue (D). (C, D) Superhelical TALE structure tracing along the DNA (TALE PthXo1, PDB 3ugm). (C) Top view. (D) Side view.

The canonical repeats are surrounded by sequentially divers non-canonical repeats at the C- and N-terminal borders. C-terminal to the last canonical repeat, a non-canonical ‘half repeat’, sequentially identical to a half canonical one, concludes the effector binding

element. While further non-canonical repeats adjacent to the half repeat do not significantly affect TALE binding properties, N-terminal non-canonical repeats exert a strong effect by forming multiple non-specific contacts to the DNA immediately 5' to the target sequence (de Lange et al., 2014). This region also engages binding of an invariant thymine base bound by the so-called T_0 repeat usually preceding the canonical repeats, as it is required for full TALE activity (Kay et al., 2007; Boch et al., 2009; Moscou and Bogdanove, 2009; Lange et al., 2014). Specific sequence recognition of DNA (Moscou and Bogdanove, 2009; Boch et al., 2009) and DNA-RNA hybrids (Yin et al., 2012), however, is achieved by the RVDs within the canonical repeats and governed by a simple cipher, which was decoded by bioinformatic and experimental approaches (Moscou and Bogdanove, 2009; Boch et al., 2009; Streubel et al., 2012; Yin et al., 2012; Yang et al., 2014). Although there are more than 20 different types of RVDs, the most common RVD code of base recognition is NI for adenine (A), HD for cytosine (C), NG for thymine (T) and as recently reported for methylated cytosine (5mC), and NN for guanine (G) (single letter code for amino acids) (Boch et al., 2009; Moscou and Bogdanove, 2009; Bogdanove and Voytas, 2011; Streubel et al., 2012; Yang et al., 2014; Deng et al., 2012b). This straightforward correlation with one repeat binding to one DNA base paved the way for the generation of custom designer TALEs (dTALEs) against virtually any user-defined sequence by simply aligning individual repeats of defined RVD composition (Figure 10, A).

Crystallographic studies of DNA-bound TALEs revealed that actually only RVD 13 is base-specifying, while RVD 12 is engaged in loop stabilisation (Deng et al., 2012a; Mak et al., 2012). Individual repeats adopt a left-handed helical hairpin structure with the RVDs residing within a central DNA binding loop flanked by two helical regions (Figure 10, B). Being neutral in charge, self-association of the repeats drives the assembly of a right-handed, superhelical TALE structure tracking the complete length of the target DNA along the major groove (sense strand) (Figure 10, C and D). As the TALE, which naturally can bind up to 34 bp, has to follow the structure of the DNA helix, it is highly interesting how TALEs search for and acquire cognate DNA contacts. From the structural data, it is plausible that target recognition is based on rapid DNA association and dissociation, with initial contacts being established by the N-terminal flanking region, followed by sequential sampling of the nucleotide bases by the RVDs of the canonical repeat domain, thereby achieving superhelical winding around the DNA as long as appropriate RVD to target sequence complementarity is provided (Mak et al., 2013).

1.8.2 TALE fusion proteins for genome engineering

The predictable and modular nature of TALEs as DNA binding scaffolds has made them a valuable tool with broad biotechnological applicability. Reprogramming of base specificity is straightforward and solely determined by RVD composition, since individual repeats are functionally independent modules irrespective of their position within the array and their neighbouring context (Deng et al., 2012a; Mak et al., 2012). dTALE assembly is rapidly achieved in a medium or high-throughput fashion at low costs based on several strategies, including 'Golden Gate' cloning (Cermak et al., 2011; Morbitzer et al., 2011), high-throughput solid-phase assembly (Reyon et al., 2012; Briggs et al., 2012), and ligation-dependent cloning methods (Schmid-Burgk et al., 2013).

One of the main applications of dTALEs is in fusion with nucleases, nickases, recombinases or transposases for genome engineering purposes (Joung and Sander, 2013; Mercer et al., 2012; Beurdeley et al., 2013; Gabsalilow et al., 2013; Owens et al., 2013). The most frequent dTALE-based architecture for genome engineering is C-terminal fusion with the FokI nuclease (TALEN). TALENs are used in pairs to target the two complementary strands separated by a spacer thereby allowing for FokI dimerisation and introduction of a double-strand break (DSB). Repair of DSBs is mediated either by non-homologous end joining (NHEJ) or homologous recombination (HR). The error-prone, NHEJ pathway leads to a high frequency of deletions and insertions next to the DSB eventually resulting in disruption of gene function. In presence of a homologous template, either a sister chromatid or an exogenously introduced repair donor containing sequences homologous to the target site, sealing of DSBs can be achieved while simultaneously enabling for introduction of specific sequences or mutations (Figure 11).

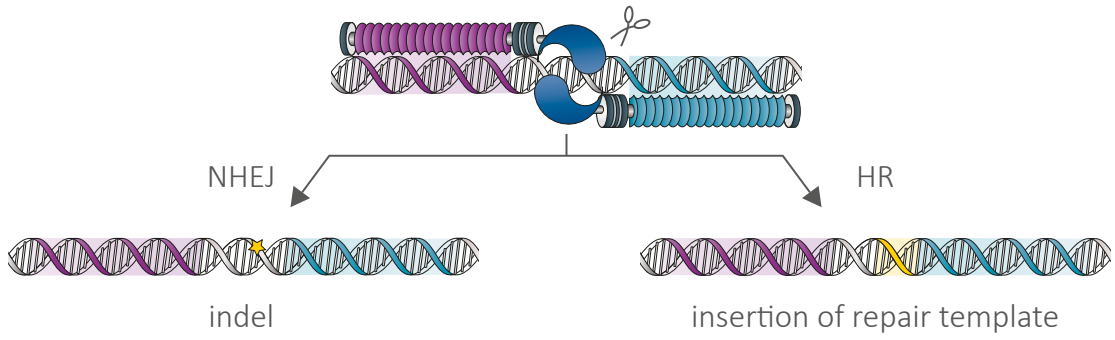

Figure 11: TALENs for genome engineering. Two C-terminal TALE FokI nuclease fusions targeting the two complementary strands, separated by a spacer. Following introduction of a double-strand break, the lession is sealed either by non-homologous end-joining (NEHJ) or, in presence of a homologous repair template, by homologous recombination (HR). NHEJ results in random mutations, insertion or deletions (indels), whereas HR allows for targeted modifications by recombination with the repair template.

Due to the ease of the technology, targeted modifications have been generated in a great variety of cell types and organisms, including human somatic and pluripotent stem cells, mice, rats, worms, fruit flies, and zebrafish, amongst others (Joung and Sander, 2013). Serving as a scaffold to which various effector domains can be coupled, TALEs might enable targeted manipulations of both the genome and epigenome, e.g. in fusion with activation domains, or epigenetic modifiers. Moreover, TALE-GFP fusions hold a great potential for sequence-specific genome visualisation in living cells similarly to ZFPs. Thus, TALEs present promising tools to manipulate and trace the spatiotemporal genome organisation.

1.9 Aims of this work

The spatiotemporal organisation and dynamics of chromatin are key to genome regulation. This thesis focuses on different methods to trace and manipulate overall topological genome arrangements and activate gene expression.

First, we wanted to employ dTALEs for targeted activation of the pluripotency factor *oct4* and study the *in vitro* dTALE binding properties and affinities.

To specifically target and trace endogenous DNA sequences in living cells, I sought to repurpose dTALEs in fusion with GFP as a new tool for genome visualisation. To demonstrate the feasibility of the approach, I aimed at following the cell cycle dependent dynamics of CCs using a dTALE directed against the ms-repeats. In addition, I wanted to gain first insights about the dTALE binding properties *in vivo* and address the kinetics of the dTALE-DNA interaction.

Another aim of mine was to exploit TALE-chromatin recognition for targeted nuclear repositioning of endogenous loci thereby establishing a new model system to study the role of spatial genome arrangements on cell cycle progression and differentiation.

The nuclear periphery plays an important role in peripheral HC association. The molecular mechanisms underlying peripheral tethering and loss of HC association during rod inversion, however, remain largely elusive. Preliminary immunostaining data pointed to LmA/C and LBR as putative peripheral HC tethers. Both or at least one of the two proteins is constitutively expressed in all cell types with exception to rods, where both proteins are missing. To assess the potential involvement in peripheral HC anchorage, I aimed at examining whether ectopic expression of LmC or LBR in rod cells can rescue the inverted nuclear architecture. Therefore, I wanted to establish transgenic mouse models, ectopically expressing either of the two candidate genes by a rod-specific promoter. The role of the proteins in HC tethering will be assessed on their ability to revert the inverted nuclear architecture of rod nuclei to a conventional one.

In addition to peripheral association, the mechanisms, which maintain the spatial separation of the different chromatin classes, are not fully understood yet. Based on human artificial chromosomes (HAC) stably integrated in mouse conventional and inverted rod cell backgrounds as a model system, we sought to assess whether primary sequence composition drives correct positioning in the nucleus. In particular, we wanted to test whether segments corresponding to the main chromatin classes represented on the HAC properly segregate, acquire normal lamina-association and transcriptional regulation as compared to their mouse counterparts. By assessing the transcriptional status of HAC

genes, I wanted to gain insights into the interdependencies of the degree of lamina-association and transcriptional activity of genic HAC regions in different cellular contexts.

2 Results

2.1 Targeted transcriptional activation of silent oct4 pluripotency gene by combining designer TALEs and inhibition of epigenetic modifiers

5368–5377 Nucleic Acids Research, 2012, Vol. 40, No. 12 Published online 2 March 2012
doi:10.1093/nar/gks199

Targeted transcriptional activation of silent *oct4* pluripotency gene by combining designer TALEs and inhibition of epigenetic modifiers

Sebastian Bultmann[1], Robert Morbitzer[2], Christine S. Schmidt[1], Katharina Thanisch[1], Fabio Spada[1], Janett Elsaesser[2], Thomas Lahaye[2,*] and Heinrich Leonhardt[1,*]

[1]Department of Biology, Center for Integrated Protein Science Munich (CIPSM) and [2]Department of Biology, Institute of Genetics, 82152 Planegg-Martinsried, Ludwig Maximilians University Munich, Germany

Received September 22, 2011; Revised and Accepted February 13, 2012

ABSTRACT

Specific control of gene activity is a valuable tool to study and engineer cellular functions. Recent studies uncovered the potential of transcription activator-like effector (TALE) proteins that can be tailored to activate user-defined target genes. It remains however unclear whether and how epigenetic modifications interfere with TALE-mediated transcriptional activation. We studied the activity of five designer TALEs (dTALEs) targeting the *oct4* pluripotency gene. In vitro assays showed that the five dTALEs that target distinct sites in the *oct4* promoter had the expected DNA specificity and comparable affinities to their corresponding DNA targets. In contrast to their similar in vitro properties, transcriptional activation of *oct4* by these distinct dTALEs varied up to 25-fold. While dTALEs efficiently upregulated transcription of the active *oct4* promoter in embryonic stem cells (ESCs) they failed to activate the silenced *oct4* promoter in ESC-derived neural stem cells (NSCs), indicating that as for endogenous transcription factors also dTALE activity is limited by repressive epigenetic mechanisms. We therefore targeted the activity of epigenetic modulators and found that chemical inhibition of histone deacetylases by valproic acid or DNA methyltransferases by 5-aza-2′-deoxycytidine facilitated dTALE-mediated activation of the epigenetically silenced *oct4* promoter in NSCs. Notably, demethylation of the *oct4* promoter occurred only if chemical inhibitors and dTALEs were applied together but not upon treatment with inhibitors or dTALEs only. These results show that dTALEs in combination with chemical manipulation of epigenetic modifiers facilitate targeted transcriptional activation of epigenetically silenced target genes.

INTRODUCTION

The ability to specifically manipulate the expression of endogenous genes by engineered designer transcription factors has wide-ranging applications in basic and applied biology (1–4). Availability of suitable DNA-binding scaffolds that can be tailored to bind user-defined target sequences has been the major limitation in the generation and application of designer transcription factors. Recent studies however demonstrated that transcription activator-like effector proteins (TALEs) from the plant pathogenic bacterial genus *Xanthomonas* contain a DNA-binding domain that can be adjusted to bind any desired target sequence with high specificity (5–9). The TALE DNA-binding domain is composed of tandem arranged 33–35 amino acid repeats, with each repeat binding to one base (10,11). Base preferences of repeats are specified by residues 12 and 13, known as the repeat variable diresidues (RVDs), that determine preferential pairing with A (NI), C (HD), G (NK) and T (NG) nucleotides, respectively. The use of this TALE code facilitates the assembly of TALE repeat arrays that bind any desired DNA sequence (12).

A recent study investigated a large number of dTALEs and found that most, but not all, activated the desired target promoters (5). Notably, the epigenetically controlled *oct4* and *c-myc* gene could not be upregulated by their matching dTALEs, suggesting that epigenetic modifications affect dTALE-mediated gene activation.

We systematically investigated the application of dTALEs to the murine pluripotency gene *oct4* to clarify

*To whom correspondence should be addressed. Tel: +49 89 2180 74740; Fax: +49 89 2180 74702; Email: lahaye@biologie.uni-muenchen.de
Correspondence may also be addressed to Heinrich Leonhardt. Tel: +49 89 2180 74232; Fax: +49 89 2180 74236; Email: h.leonhardt@lmu.de

The authors wish it to be known that, in their opinion, the first two authors should be regarded as joint First Authors.

how epigenetic modifications affect their performance. The inspection of five dTALEs that bind to distinct DNA sequences within the *oct4* promoter revealed similar affinities to their DNA targets but up to 25-fold differences in their efficiency as transcriptional activators. Further studies revealed that dTALE-mediated activation of a silent *oct4* promoter in neural stem cells (NSCs) can be drastically improved by treatment with the histone deacetylase (HDAC) inhibitor valproic acid (VPA) and the DNA methyltransferase inhibitor 5-aza-2′-deoxycytidine (5azadC). These data suggest that chromatin modifications that are involved in transcriptional gene silencing, hinder dTALE-mediated gene activation and that simultaneous inhibition of HDACs and DNA methyltransferases may overcome this limitation of dTALE technology.

MATERIALS AND METHODS

Construction of plasmids

A Gateway cassette from pGWB5 (13) was amplified (forward primer: 5′-GGGGCGATCGCACAAGTTTGTACAAAAAAGCTGAACGAG-3′; reverse primer: 5′- GGGGCGGCCGCAACCACTTTGTACAAGAAAGCTGAACG-3′), thereby adding AsiSI and NotI restriction sites. This fragment was cloned via AsiSI and NotI into pCAG_mCh (14) generating pCAG_mCh_GW. The VP16AD was amplified from RSV

E2F1-VP16 (15) (forward primer: 5′GGGGGTCTCTCACCATGGATCCTGCCCCCCCGACCGATGTCAGC-3′; reverse primer:5′-GGGGGTCTCCCTTCTACCCACCGTACTCGTCAATTCCAAGG-3′), thereby adding a BamHI restriction site to the 5′ end and cloned into pENTR-D- TOPO (Invitrogen) generating pENTR-D-BamHI_VP16AD. TALE repeat arrays were generated via multi-fragment cut-ligation using golden gate cloning (16) and ligated either into pENTR-D-TALE-Δrep-*Bpi*I-A or pENTR-D-TALE-Δrep-*Bpi*I-AC-VP16AD. All entry clones were transferred by LR recombination (Invitrogen) into the expression vector pCAG_mCh_GW.

The *oct4* reporter construct (p*oct4*-GFP) was generated by inserting the XhoI/AvrII fragment of GOF-18 (17) which includes the basepairs −1 to −4716 upstream of the transcriptional start site of *oct4* together with a linker oligo (5′-CCTAGGTGAGCCGTCTTTCCACCAGGCCCCCGGCTCGGGGTGCGATCGCCGCCCATGG-3′) into pGL-3 basic (Promega) cut with XhoI/NcoI. Subsequently, the Luciferase ORF was removed by cutting with KasI/FseI and the eGFP ORF (amplified with: forward primer: 5′-AAAGGCGCCAGTGAGCAAGGGCG-3′; reverse primer: 5′-AAAGGCCGGCCTTACTTGTACAGCTCGTCC-3′) was inserted.

The promoter mutants *TB83*, *TB68*, *TB60* and *TB31* were generated by site-directed mutagenesis using a *Asi*SI/*Aat*II derived sub-cloned *poct4-GFP* fragment as template with either forward primer: 5′-TCTCCCACCCCCACAGCTCTGCTCCTTTGGGGAGGGAGAGGTGAAAC-3′, 5′-GCTCTGCTCCTCCACCCACCCAGGGGTTGGGGAGGGAGAGGTGAAACCG-3′,″ 5′-CCTCCACCCACCCAGGGGGCGGGGCCTTGGGGAGGGAGAGGTGAAACCG-3′ or 5′-GGTCAAGGCTAGAGGGTGGGATTGGGTTGGGGAGGGAGAGGTGAAACCG-3′ together with reverse primer: 5′-GAAACTGAGGCGAGCGCTATCTG-3′, thereby deleting TB83, TB68; TB60 and TB31 and inserting them individually at the position of TB31.

Immunofluorescence staining

For immunostaining, ogNSCs were grown on cover slips and transiently transfected with the T-83VP16 construct for Oct4 stainings or untransfected for Pax6, Nestin and Olig2 stainings. Cells were fixed with 2.0% or 3.7% formaldehyde in phosphate-buffered salie (PBS) and permeabilized in PBS containing 0.2% Triton X-100. The Oct4 staining was performed using a goat primary antibody against the murine Oct4 (goat; 1:1000, Santa Cruz) and a secondary anti-goat antibody coupled to Alexa Fluor 647 (1:2000, Molecular Probes). The neural stem cell markers Pax6 (rabbit; 1:1000, Millipore), Nestin (mouse monoclonal, Rat-401; 1:10, Developmental Studies Hybridoma Bank, University of Iowa) and Olig2 (rabbit; 1:500, Millipore) were detected with secondary antibodies conjugated to Alexa Fluor 488 (Molecular Probes). The antibodies were diluted in PBS containing 0.02% Tween 20 and 2% bovine serum albumin (BSA). Cells were counterstained with DAPI and mounted in Vectashield (Vector Laboratories). Images were acquired with a Zeiss Axioplan 2 fluorescence microscope equipped with a Plan-NEOFLUAR 40×/1.3 oil objective (Zeiss).

Cell culture, transfection and fluorescence-activated cell sorting

HEK293T cells (18) were cultured in Dulbecco's modified Eagle's medium (DMEM) supplemented with 50 μg/ml gentamicin and 10% fetal bovine serum (FBS). For expression of fusion proteins, HEK293T cells were transfected with polyethylenimine (Sigma). ogESCs were cultured as described (19). ogNCSs were cultured in N2B27 medium supplemented with 20 ng/ml FGF-2 and EGF. NSCs and ESCs were transfected using Lipofectamin 2000 (Invitrogen) according to the manufacturer's instructions and sorted with a fluorescence-activated cell sorting (FACS) Aria II instrument (Becton Dickinson).

Generation of transgenic cell lines

ogESCs were generated by transfecting wt J1 ESCs (20) with the p*oct4*-GFP reporter construct and repeated sorting for eGFP expression. Finally, single cell sorting was used to obtain a clonal transgenic cell line.

Derivation of NSCs from ESCs

ogESCs were differentiated into ogNSCs as previously described (21–23). In brief, 3.5×10^5 cells were plated in a 25 cm^2 culture flask with N2B27 medium containing 1000 U/ml of LIF (ESGRO, Millipore). The next day the medium was exchanged against N2B27 without LIF to initiate differentiation into the neural lineage. After 7 days cells were plated in Euromed-N (Euroclone)

supplemented with 20 ng/ml EGF and FGF2 (Peprotech). After 5 days, neurospheres were collected and plated in gelatin-coated flasks in N2B27 medium containing 20 ng/ml EGF and FGF2 to allow outgrowth of NSCs.

Treatment of ogNSCs with epigenetic inhibitors

VPA sodium salt (Sigma-Aldrich) was dissolved in PBS at a concentration of 250 mM and sterile filtered. 5-aza-2′-deoxycytidine (Sigma-Aldrich) was dissolved in PBS at a concentration of 30 mM. Trichostatin A (TSA; Sigma-Aldrich) was dissolved in dimethyl sulfoxide (DMSO) at a concentration of 5 mM. Cells were transfected with the T-83 construct as described above. Medium was changed after 12 h against medium containing dilutions of the respective inhibitor or combination thereof as indicated in Figure 4 and respective legend. Cells were cultured for additional 36 h followed by FACS and quantitative real-time-polymerase chain reaction (qRT-PCR).

In vitro methylation and reporter gene assay

In vitro methylation of p*oct4*-GFP was performed using M.SssI (New England Biolabs). Forty-five units of enzyme were incubated with 45 µg of plasmid DNA in the presence of 160 µM SAM overnight. After 3 h of incubation, fresh SAM (160 µM) was added to ensure complete methylation. Methylation status of the plasmid after *in vitro* methylation was tested by digestion with MspI and HpaII (Fermentas). For the reporter gene assay HEK293T cells were plated in six-well plates and grown to 70% confluence. Subsequently, cells were co-transfected with the reporter plasmid and the respective dTALE construct. Forty-eight hours after transfection cells were lysed in PBS containing 0.5% NP40 and mammalian protease inhibitors. The lysate was cleared by centrifugation and eGFP and mCherry fluorescence was measured with a Tecan Infinite M1000 plate reader.

RNA Isolation, cDNA synthesis and qRT-PCR

Isolation of RNA and reverse transcription was carried out as described previously (19). Real-time PCR analysis was performed on the 7500 Fast Real-Time PCR System (Applied Biosystems) at standard reaction conditions using either the TaqMan Gene Expression Master Mix (Applied Biosystems) or the *Power* SYBR Green PCR Master Mix (Applied Biosystems). The following TaqMan Gene expression assays were used: gapdh (Assay ID: Mm99999915_g1), oct4 (Assay ID: Mm00658129_gH) and nanog (Assay ID: Mm01617 761_g1). Primer sequences for SYBR Green PCRs: gapdh (For 5′catggccttccgtgttccta 3′ Rev 5′cttcaccaccttctt gatgtcatc 3′); tet1 (for 5′ccaggaagaggcgactacgtt 3′ Rev 5′ ttagtgttgtgtgaacctgatttattgt 3′) and hnf4a (for 5′ caagaggtccatggtgtttaagg 3′, Rev 5′ cggctcatctccgctagct 3′). Relative mRNA levels were normalized to gapdh and calculated with the comparative CT Method ($^{\Delta\Delta}$CT Method).

In vitro DNA-binding assays

In vitro DNA-binding assays were performed as described previously (24,25) with the following modifications. Two differentially fluorescently labeled DNA substrates corresponding to position − 39 to +18 (A) and −88 to −31 (B) relative to the TSS of the *oct4* promoter (Figure 3) were used in direct competition. Substrates were prepared by annealing 5′ ATTO550 or ATTO647N labeled lower strand with the respective unlabeled upper strand oligonucleotide. For competition assays, 200-nM ATTO647N-labeled substrate A and ATTO550-labeled substrate B were added and incubated at room temperature (RT) for 1 h with constant mixing. Fluorescence intensities were measured with a Tecan Infinite M1000 plate reader using the following excitation/emission wavelengths: 490 ± 10 nm / 511 ± 10 nm for eGFP, 550 ± 15 nm / 580 ± 15 nm for ATTO550 and 650 ± 10 nm / 670 ± 10 nm for ATTO647N. The measurements were normalized using standard curves from purified eGFP and ATTO-dye-labeled oligonucleotides. Moreover, a control set of each substrate with distinct fluorophores was used for normalization.

Fluorescence polarization measurements

DNA affinity was determined by fluorescence polarization measurements. eGFP-dTALE fusion proteins were purified as described above and eluted from the Sepharose beads by addition of 250 mM imidazol. Different concentrations of GFP-dTALE fusion proteins were incubated with their specific ATTO647N-labeled substrates (1 nM). After incubation for 30 min, at RT fluorescence polarization was measured with a Tecan Infinite M1000 plate reader using 635 nm for excitation and 670 ± 10 nm for emission. The data of fluorescence polarization over protein concentration were fitted with $y = \frac{y_{max} \cdot x}{K_d + x}$ using gnuplot (http://www.gnuplot.info).

DNA methylation analysis

For the analysis of DNA methylation levels at the *oct4* promoter genomic DNA was isolated using the NucleoSpin Triprep Kit (Macherey-Nagel). Bisulfite treatment was performed using the EZ DNA Methylation-Gold™ Kit (Zymo Research Corporation) according to the manufacturer's protocol. Subsequently, the *oct4* promoter sequence was amplified in a semi-nested PCR using the primers:

F1: 5′-ATGGGTTGAAATATTGGGTTTATTTA-3′
F2: 5′-GTAAGAATTGAGGAGTGGTTTTAG-3′
R1: 5′ACCCTCTAACCTTAACCTCTAAC 3′
R2 = R1 with 5′biotin

The biotinylated PCR products of the second PCR were analyzed by pyrosequencing (Varionostic GmbH, Ulm, Germany). The pyrosequencing covered five CpG sites of which the average methylation level was calculated. DNA methylation levels of major satellite repeats and *H19* promoter was performed as previously described (25).

RESULTS

Design and construction of five dTALEs targeting the murine oct4 promoter

We generated five dTALEs each targeting a distinct 19-bp sequence of the murine pluripotency gene *oct4* to test whether the position of the target sequence influences the efficiency of dTALE-mediated promoter activation. These five dTALEs targeted sequences upstream or downstream of the Sp1/Sp3/hormone responsive element (HRE) box (Figure 1A, Supplementary Figure S1). DNA-binding TALE repeat arrays were generated by Golden Gate cloning as described previously (6) and transferred to mammalian expression vectors by Gateway recombination (Supplementary Figure S1A). To monitor transfection efficiency and expression levels, mCherry (26) was fused to the N-terminus of the dTALEs. Furthermore, we replaced the transcriptional activation domain (AD) of the *Xanthomonas* wild-type TALE protein (wtdTALEs) with the VP16 AD from the herpes simplex virus (VP16dTALEs) and compared the activity of these two distinct dTALE architectures.

dTALEs targeting distinct sites in the *oct4* promoter have similar affinities in vitro but differ strongly in their in vivo performance as transcriptional activators

The activity of the different dTALEs was first analyzed in a transient reporter gene assay. HEK293T cells were co-transfected with an *oct4* promoter-driven *eGFP* reporter (p*oct4-eGFP*) and a constitutively expressed *dTALE* construct. Expression was analyzed by fluorescence measurement 48 h after transfection. Notably, the VP16dTALEs activated the *oct4* promoter to significantly higher levels than the corresponding wtdTALEs (Figure 1C), despite the fact that the latter were expressed at slightly higher levels (Supplementary Figure S2). The most distal dTALE (T-83) yielded the strongest transcriptional activation with both, the wtdTALE and VP16dTALE architecture (Figure 1B and C). To test whether the variable efficiency of the dTALEs with distinct repeat arrays is caused by the location of the target sites within the promoter, we replaced base pairs −31 to −102 of the *oct4* reporter construct which contain the target sites of four of the five dTALEs, with a shorter sequence containing one dTALE target site only. The resulting four reporter constructs have the respective dTALE target site at the same position (Figure 2A). Transcriptional activation of these four mutated reporter constructs by the corresponding VP16dTALEs was greatly reduced as compared to the activation level of the wild-type *oct4* reporter. Three of the four VP16dTALEs induced similar eGFP expression levels (Figure 2B) while T-60 exhibited a slightly stronger activation in the mutated promoter. The enhanced activity of T-60 is possibly due to the overlap of its target site with the SP1 site in the wild-type promoter, which also results in a relatively higher background in cells transfected only with the mutated reporter construct containing the T-60 binding site (Figure 2C). The dTALEs used in this study were designed to target different sequences within the promoter region of *oct4*. The distinct RVD compositions of these dTALE repeat arrays might result in different binding affinity, causing the observed difference in transcriptional activation. We therefore determined the affinity and specificity of our dTALEs *in vitro* using fluorescently labeled DNA substrates and eGFP–dTALE fusion proteins. We found specific binding of all five dTALEs to their respective DNA substrates (Figure 3A and B). Dissociation constants were determined by fluorescence polarization and all dTALEs tested yielded affinities for their specific substrates, with K_d values in the low nanomolar to high picomolar range (Figure 3C). Notably, the dTALE T-83, which was the strongest transcriptional activator *in vivo*, had a comparably low affinity *in vitro*. Together, these data strongly suggest that the observed variations in dTALE-mediated activation of the *oct4* promoter are not due to inherent differences in their binding affinity.

dTALEs activate methylated reporter plasmids

In addition to positional effects, we tested whether the epigenetic state of the promoter might influence the efficiency of dTALE-mediated transcriptional activation. We methylated the p*oct4*-GFP plasmid *in vitro* (Supplementary Figure S3A) and determined its inducibility by dTALEs. All dTALEs induced eGFP expression from the methylated *oct4* promoter, yet to lower levels as compared to the unmethylated reporter (Figure 1D). Notably, the relative differences in the activity of the highly potent T-83 and the other dTALEs were up to 25-fold and thus more pronounced with the methylated as compared to the unmethylated reporter construct (Figure 1D). These results indicate that dTALEs can activate heavily methylated promoter sequences, albeit to a reduced extent, and suggest that the lack of correlation between *in vitro* binding affinity and *in vivo* activity of dTALES may reflect their different ability to overcome other repressive epigenetic marks at the target locus.

dTALEs hyperactivate endogenous oct4 expression in embryonic stem cells

To test the ability of dTALEs to activate the endogenous *oct4* gene we generated mouse embryonic stem cells (ESCs) stably carrying the p*oct4-GFP* reporter construct (ogESCs). ogESCs were tested with T-83 fused to the VP16 AD (VP16 T83), the most efficient dTALE, and compared with mCherry control vector. Transfected mCherry-positive cells were selected using FACS and total RNA was isolated followed by reverse transcription and qRT-PCR. FACS analysis showed that ogESCs transfected with the VP16 T-83 had a 3–4-fold higher mean eGFP fluorescence intensity compared to control transfected cells (Supplementary Figure S4A). Transcription of the endogenous *oct4* was induced about 2-fold as determined by qRT-PCR (Supplementary Figure S4B). The relatively low induction rate is likely due to the high basal level of *oct4* transcription in ESCs and the negative feedback of Oct4 on its own promoter (27).

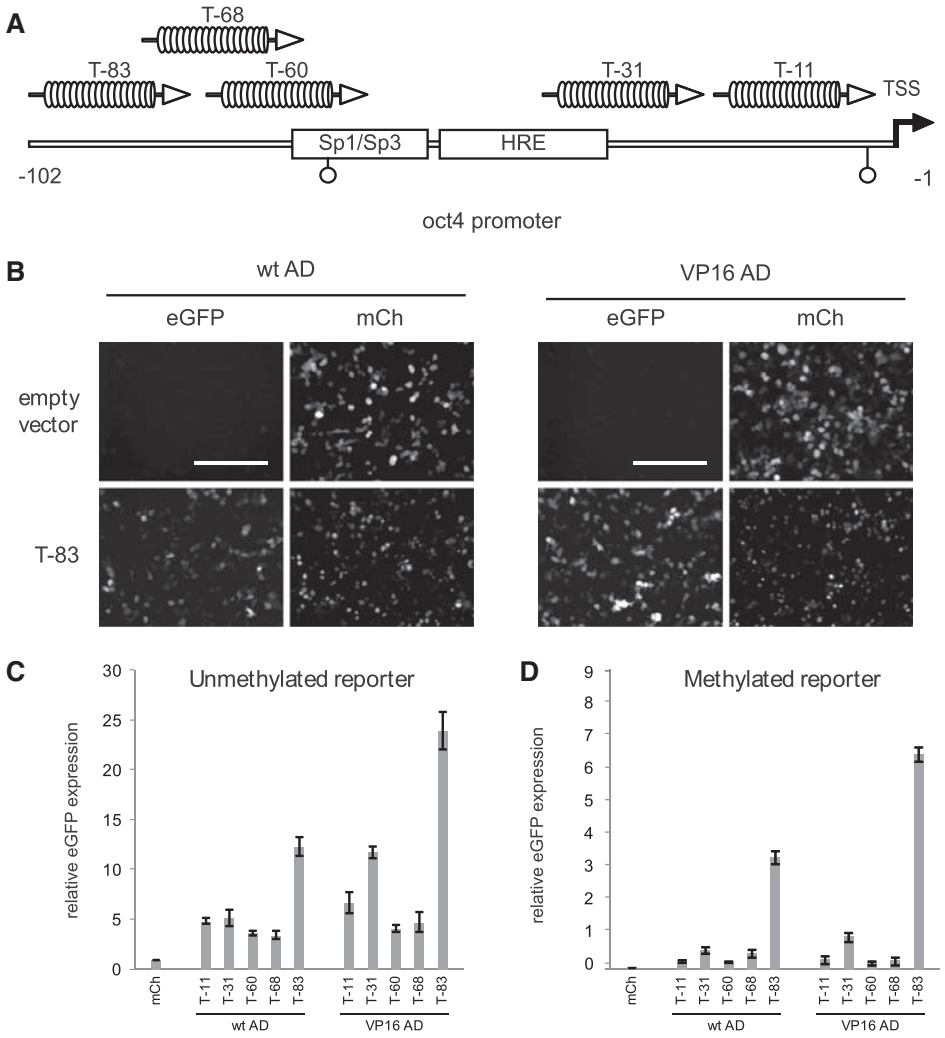

Figure 1. Activation of a transgenic *oct4* reporter construct by *dTALEs* in HEK293T cells. (**A**) Schematic representation of the 102-bp fragment upstream of the transcriptional start site (TSS) of the *oct4* promoter, including the binding site of the Sp1/Sp3 transcription factors, the hormone responsive element (HRE) and two CpG sites (open circles). *oct4*-specific dTALEs are depicted in correspondence of the location of their target sequence and designated according to the distance between the 5′ end of their target sequence and the TSS. (**B**) Fluorescence microscopy images of HEK293T cells co-transfected with the p*oct4- GFP* reporter construct and the T-83 *dTALE* constructs. Left panel shows cells transfected with the T-83 dTALE fused to the wild-type AD (wt AD). Right panel shows cells transfected with the T-83 dTALE fused to the VP16 AD. Scale bar = 200 µm. (**C**) Transcriptional activation of the unmethylated p*oct4-GFP* reporter construct by *oct4*-specific dTALEs. eGFP expression was normalized to cells co-transfected with a control plasmid encoding the fluorescent protein mCherry (mCh) and *poct4-GFP* reporter construct. (**D**) Transcriptional activation of the *in vitro* methylated p*oct4-GFP* reporter construct by *oct4*-specific dTALEs. eGFP expression was normalized to cells co-transfected with a control plasmid (mCh) and *poct4-GFP* reporter construct. To allow for a direct comparison of expression levels in (C) and (D) the data observed on the methylated promoter were normalized to the mCherry values observed with the unmethylated promoter (C). Error bars in (C) and (D) represent standard deviation from three independent experiments.

Activation of *oct4* in neural stem cells depends on inhibition of repressive epigenetic mechanisms

To test whether dTALEs can also activate a transcriptionally silent endogenous *oct4* promoter, we differentiated ogESCs into NSCs. During this differentiation process the *oct4* locus is epigenetically silenced and NSCs no longer express *oct4* (28). Analysis by immunofluorescence showed that all cells were positive for the NSC markers (21) Pax6, Nestin and Olig2 (Supplementary Figure S5), indicating successful *in vitro* differentiation from ogESCs to ogNSCs. The ogNSCs were transfected with the vector encoding the dTALE VP16 T-83 or a control vector encoding mCherry. Forty-eight hours after transfection cells were analyzed by flow cytometry. In contrast to the experiments with ogESCs, the dTALE VP16 T-83 activated neither the transgenic p*oct4-eGFP* reporter nor the endogenous *oct4* promoter in ogNSCs (Figure 4A and B). This could be due to the different epigenetic states of the *oct4* promoter in ESCs and NSCs. Whereas the *oct4* promoter in ESCs is active and apparently accessible to dTALEs, *oct4* is not expressed in NSCs and the promoter

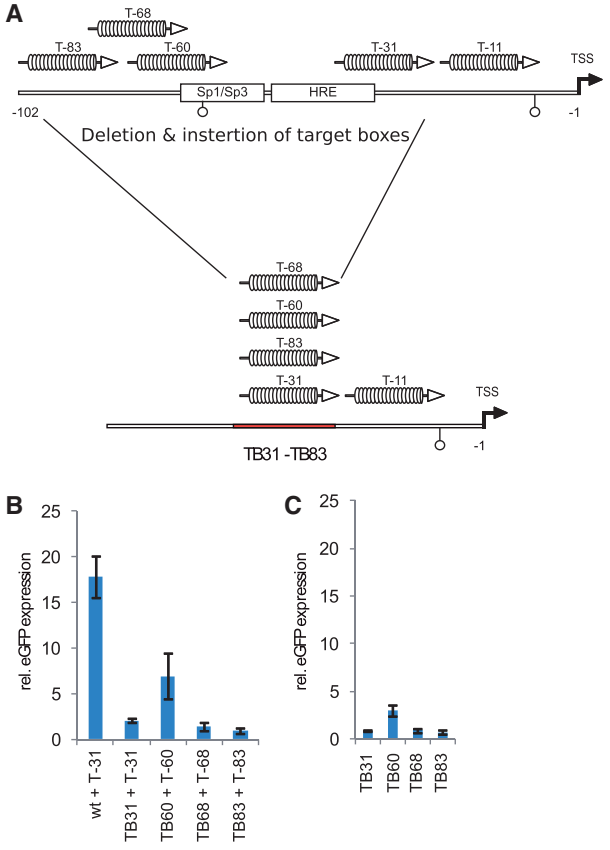

Figure 2. The location of a dTALE target sequence within the *oct4* promoters can affect its functionality. (**A**) Schematic representation of an *oct4* promoter deletion construct in which base pairs −31 to −102 relative to the TSS were deleted and the target sequences of the four dTALEs were inserted yielding the reporter constructs TB31, TB60, TB68 and TB83. (**B**) Transcriptional activation of the reporter constructs TB31, TB60, TB68 and TB83 by corresponding dTALEs. (**C**) Background activity of the mutated reporter constructs in cells co-transfected with respective reporter and mCherry control.

might be less prone to dTALE-mediated activation. Therefore, we envisaged that inhibiting the repressive epigenetic modifiers that prevent activation of the *oct4* promoter in NSCs could allow dTALE-mediated activation of *oct4*. To test this hypothesis, we used the HDAC inhibitors TSA (29) or VPA (30) as well as the DNA methyltransferase (Dnmt) inhibitor 5-aza-2'-deoxycytidine (5azadC) (31) to interfere with two major epigenetic mechanisms by which transcriptional silencing of genes is achieved in mammals. Twelve hours after transfection with VP16 T-83, ogNSCs were treated with the respective inhibitor for additional 36 h. Treatment with 5azadC or VPA but not TSA significantly increased relative eGFP expression in cells transfected with VP16 T-83 (Figure 4A and Supplementary Figure S6A–C). Similarly, endogenous *oct4* transcript levels were induced up to 60% as compared to the levels in ogESCs. However, a combination of 5azadC and VPA did not show additive nor synergistic effects (Figure 4A and B). Treatment with the inhibitors alone did not result in transcriptional activation of the reporter nor the endogenous *oct4* gene (Figure 4A and B), demonstrating that the observed activation was due to the synergistic action of the dTALE and the inhibitors. Cells transfected with the *dTALE VP16 T-83* and treated with VPA, 5azadC or combinations of both showed not only increased *oct4* transcript levels but also Oct4 protein (Figure 4F). Moreover, treatment of *VP16 T-83* transfected cells with VPA, 5azadC or combinations of both exhibited up-regulation of the Oct4 target genes *nanog* and *tet1* (Figure 4C and D) (32–34). By contrast, genes that are not part of the Oct4 regulatory network were not influenced by treatment with inhibitors and/or expression of dTALE VP16 T-83 on transcript (Supplementary Figure S7A).

As both, 5azadC and VPA, have been reported to induce DNA demethylation (31,35) we investigated the effects of these inhibitors on the DNA methylation levels of the *oct4* promoter. Interestingly, in all samples that were treated with the inhibitors only and/or transfected with the control plasmid no change in DNA methylation levels was observed. However, expression of the dTALE VP16 T-83 together with VPA and/or 5azadC treatment caused a reduction of DNA methylation at the *oct4* promoter by ~30% (Figure 4E). Treatment with inhibitors alone or in combination with the dTALEs did not influence methylation levels at the *h19* locus and major satellite repeats, showing that the observed effect is specific for the *oct4* promoter (Supplementary Figure S7B and S7C). These results suggest a synergistic effect of dTALEs and epigenetic inhibitors in mammalian cells.

DISCUSSION

Variable efficiency of different dTALEs in transcriptional activation

In eukaryotic cells, transcriptional activation involves the concerted action of multiple factors recognizing target sites at different positions of gene promoters. The possibility to generate dTALEs that bind different sites within the promoter of target genes opens new possibilities to probe and optimize conditions for targeted transcriptional activation. We designed a panel of dTALEs targeting distinct sites in the murine *oct4* promoter and compared their performance *in vitro* and *in vivo*. Expression of dTALE T-83 resulted in a 2-fold increase of the *oct4* mRNA in ESCs. Previous studies reported a number of dTALEs targeting distinct promoters (5–7,36,37). However, none of these studies has systematically investigated whether the relative position of a dTALE target site within a promoter affects its functionality. We engineered five dTALEs, each targeting a distinct 19-bp sequence within the *oct4* promoter. All dTALEs yielded K_d values in the low nanomolar to high picomolar range and were expressed at similar levels but differed largely in their efficiency *in vivo*. Remarkably T-83, the dTALE with one of the lowest binding affinity, showed the highest efficiency in *oct4* promoter activation. Our data obtained with recombinant *oct4* promoter constructs showed that deletions in the native *oct4* promoter severely affected

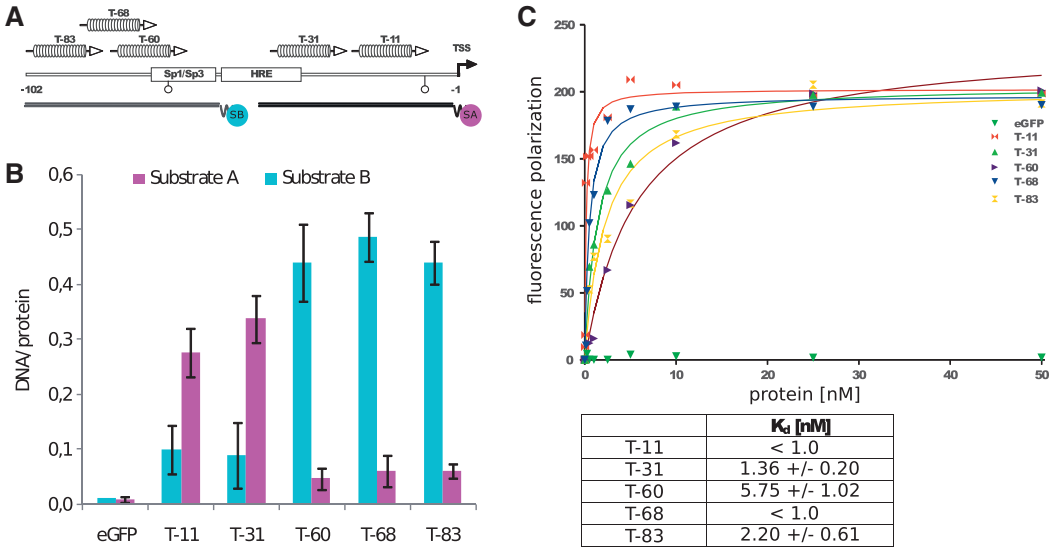

	K_d [nM]
T-11	< 1.0
T-31	1.36 +/- 0.20
T-60	5.75 +/- 1.02
T-68	< 1.0
T-83	2.20 +/- 0.61

Figure 3. (**A**)DNA-binding properties of oct4 eGFP-dTALE fusion proteins *in vitro*. Schematic representation of the 102-bp upstream of the transcriptional start site (TSS) of the *oct4* promoter, including the binding site of the Sp1/Sp3 transcription factors, the hormone responsive element (HRE) and two CpG sites (open circles). oct4 eGFP–dTALE fusion proteins are depicted at the position of their target sequence and numbered according to the distance between the 5′ end of their target sequence and the TSS of the *oct4* gene. Binding assays were performed using fluorescently labeled double-stranded DNA substrates corresponding to position −39 to +18 [substrate A (SA)] and −88 to −31 [substrate B (SB)] relative to the TSS of the oct4 gene. Note that substrate A includes the targeting sequences of dTALEs T-11 and T-31 and substrate B includes the targeting sequences of dTALEs T-60, T-68 and T-83. (**B**) DNA binding of eGFP-dTALE fusions to the specific substrate in competition with the respective unspecific substrate. Shown are fluorescent intensity ratios of bound labeled DNA substrate/eGFP-dTALE fusions. eGFP was used as negative control. Values represent means and ±SEM from three independent experiments. (**C**) DNA affinity measurements of the five dTALEs as measured by fluorescence polarization. Upper panel shows the data points acquired for each dTALE and the corresponding fitted curves. The table contains the K_d values for each dTALE calculated from the fittings using gnuplot and the function $f(x) = \frac{Y_{max} * x}{K_d + x}$.

dTALE performance, indicating that the presence of a specific binding site is not sufficient for efficient activation of transcription. These results suggest that the different capacity of dTALEs to activate transcription is less determined by their intrinsic DNA-binding properties but rather by their interactions at target promoters. Studies with the viral transactivator VP16 had previously indicated position-dependent interactions of the VP16 activation domain, possibly with basal transcription factors (38). Therefore, it is likely that also dTALEs are involved in complex interactions at the promoter of target genes that may either hinder or promote transcriptional activation.

As multiple *cis*- and *trans*-acting factors and epigenetic modifications are involved in the regulation of promoter activity, it will be difficult to predict the efficiency of a dTALE *in silico*. Hence, it seems important to construct and test multiple dTALEs for a given target promoter to obtain the most effective transcriptional activator. In the past, the assembly of genes that encode custom-designed repeat arrays was challenging and thus construction of multiple dTALEs targeting one promoter was not a realistic task. However, this is no longer a bottleneck since the recently established hierarchical ligation-based 'Golden Gate' cloning approaches facilitate rapid generation of genes encoding TALE repeat arrays (5,6,9,36,37,39,40).

Another potential bottleneck in the selection of efficient dTALEs is the analysis of promoter activation by RT-PCR or comparable assays. By contrast, promoter–reporter fusions constructs facilitate rapid quantitative comparison of multiple dTALEs but may not adequately reflect the transcriptional regulation of the corresponding endogenous genes. In this context, it should be noted that the dTALE (T-83), performing best on plasmid reporters, also most efficiently activated the chromosomal *oct4* promoter (Supplementary Figure S6E). Thus, promoter–reporter fusions may greatly facilitate the screening of different dTALE repeat arrays and experimental conditions that can then be verified and optimized in a second step by monitoring transcription of the endogenous genes.

Transcriptional activation by dTALEs is facilitated by epigenetic inhibitors

In a recent study, dTALEs were shown to activate an episomal *oct4* reporter but not the endogenous *oct4* promoter (5). Similarly, we observed a lack of dTALE-mediated *oct4* activation in NSCs, where the promoter is silent. In ESCs, however, where the *oct4* promoter is active, our dTALE clearly increased *oct4* transcription, suggesting that dTALE activity depends on the epigenetic state of the promoter. These results are consistent with the reported multistep inactivation of the *oct4* promoter that occurs during cellular differentiation after implantation and involves H3K9 as well as DNA methylation. This tight epigenetic control apparently safeguards against

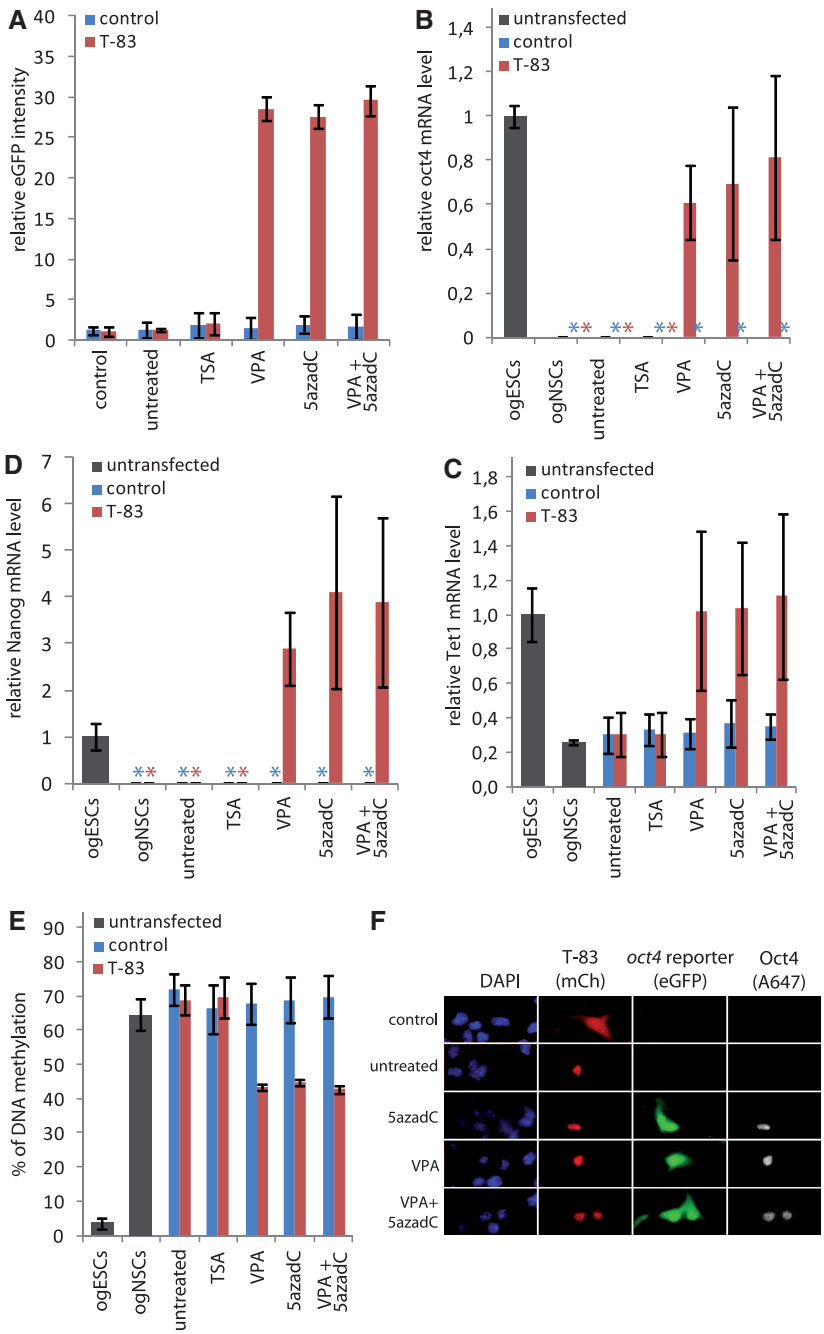

Figure 4. Activation of the endogenous *oct4* gene in NSCs requires inhibition of repressive epigenetic mechanisms. (**A**) Relative eGFP intensities as measured by flow cytometry of mCherry-positive ogNSCs transfected with the VP16 T-83 *dTALE* construct (T-83). Cells transfected with control plasmid (blue) or T-83 (red) were untreated or treated with TSA (30 nM), VPA (620 µM), 5azadC (10 nM) or a combination of VPA (310 µM) and five azadC (5 nM). (**B**) Relative levels of endogenous *oct4* mRNA measured by quantitative real-time PCR of transfected, mCherry-positive ogNSCs from (A) as well as untransfected ogNSCs and ogESCs as a reference. (**C**) DNA methylation levels of the *oct4* promoter in samples from (A) and of ogESCs as well as ogNSCs as reference. Percentage of methylation represents the average of five CpG sites in the proximal part of the *oct4* promoter. (**D**, **E**) Relative mRNA levels of *tet1* and *nanog* as determined by quantitative real-time PCR of samples from (A) and of ogESCs as well as ogNSCs as reference. (**F**) Fluorescence microscopy images of ogNSCs transfected with the T-83 construct in combination with 5azadC treatment (10 nM) or no drug. Samples were stained for Oct4 protein (A647) and counterstained with DAPI. mCherry channel shows cells transfected with T-83. eGFP channel shows expression of the *oct4* reporter transgene. Scale bar represents 25 µm. For images of samples treated with the other inhibitors, see Supplementary Figure S4. Error bars represent standard deviation from two to three independent experiments. Asterisks indicate samples where no mRNA was detectable by quantitative real-time PCR.

inappropriate reactivation of the *oct4* gene and thus prevents uncontrolled proliferation and cancer (41–43).

We found that chemical inhibition of repressive epigenetic modifiers like Dnmts and HDACs enabled dTALE-mediated transcriptional activation of silent *oct4* in NSCs. Interestingly, of the two HDAC inhibitors tested only VPA but not TSA treatment allowed efficient transcriptional activation of *oct4* by dTALEs. A similar difference between the two inhibitors was previously reported for cellular reprogramming and *oct4* promoter activation (44). One possible explanation for the different efficacy of the two inhibitors could be their different target specificities (45). Interestingly, VPA was shown to specifically affect the proximal region of the *oct4* promoter (46) where also the T-83 dTALE binds. This might also explain why inhibitor treatment of cells transfected with T-31, the dTALE with the next greatest activity in the reporter assays, did not facilitate the activation of *oct4* (Supplementary Figure S6E).

Previous studies reported that high concentrations of VPA and/or 5azadC induce demethylation and reactivation of silent genes (35,47,44,46,38). Under our experimental conditions, however, these inhibitors induced DNA demethylation of the *oct4* promoter only in combination with dTALEs, indicating a synergistic effect. A possible explanation could be that binding of the dTALE interferes with maintenance of DNA methylation and, thus, in combination with the epigenetic inhibitors leads to reduction of methylation levels. Such a synergistic effect would be consistent with the recent realization that DNA methylation is rather dynamic and functionally linked to other epigenetic pathways (48). The synergy between low concentrations of epigenetic inhibitors and dTALEs suggests that silent target genes could be activated without genome-wide demethylation and thus avoid unwanted side effects.

In summary, we demonstrated that combining dTALEs with DNA methylation and/or HDAC inhibitors facilitates selective activation of the endogenous *oct4* pluripotency gene. As in turn also Oct4 target genes are reactivated, dTALEs could be used for reprogramming of somatic cells to induced pluripotent stem cells (iPSCs). It remains to be investigated whether single or combinations of several dTALEs are more efficient than present reprogramming strategies involving the Oct4 protein itself. However, in contrast to native transcription factors, dTALEs can be specifically directed against single genes or selected combinations of target genes and thereby allow dissection of complex transcription networks to identify key factors in biological processes like pluripotency and differentiation. The combination with epigenetic inhibitors may, in some cases, facilitate the activation of tightly repressed genes and further expand the utility of dTALEs in basic and applied biosciences.

SUPPLEMENTARY DATA

Supplementary Data are available at NAR Online: Supplementary Figures 1–7.

ACKNOWLEDGEMENTS

We thank Luca Gentile and Hans R. Schöler (Max Planck Institute for Molecular Biomedicine, Münster) for providing the GOF-18 construct, DG Johnson (Howard Hughes Medical Institute, Durham) for providing the E2F1-VP16 fusion and Kerry Tucker (Ruprecht-Karls-University,Heidelberg) for providing wt J1 ESCs. Furthermore, we thank Fabian Köhler and Tobias Anton for help with the reporter gene assays. We thank Alex Buschle for help with the immunofluorescence staining and Carina Frauer for advice on the DNA binding assays. CSS and KT gratefully acknowledge the International Max Planck Research School for Molecular and Cellular Life Sciences (IMPRS-LS). H.L., T.L., S.B. and F.S. conceived the study. H.L., T.L., F.S., S.B. and R.M. designed the experiments. S.B. performed the cell biological experiments and DNA methylation analysis. K.T. performed the DNA binding assays. R.M. and J.E. established a collection of plasmids for assembly of *dTALE* genes. RM designed and cloned the dTALEs used in this study. CSS isolated RNA samples, performed the expression analysis and DNA methylation analysis. S.B., F.S., T.L. and H.L. wrote the manuscript.

FUNDING

The Deutsche Forschungsgemeinschaft (SPP 1356 and SFBs 646/TR5) to H.L.; grants from the 2Blades foundation to T.L.; The Elite Network of Bavaria (International Doctorate Program NanoBioTechnology) to C.S.S.; S.B. is a fellow of the graduate school Life Science Munich (LSM). Funding for open access charge: The Deutsche Forschungsgemeinschaft.

Conflict of interest statement. None declared.

REFERENCES

1. Klug,A. (2010) The discovery of zinc fingers and their development for practical applications in gene regulation and genome manipulation. *Q. Rev. Biophys.*, **43**, 1–21.
2. Segal,D.J. (2011) Toward controlling gene expression at will: selection and design of zinc finger domains recognizing each of the 5'-GNN-3' DNA target sequences. *Proc. Natl. Acad. Sci. USA*, **96**, 2758–2763.
3. Cathomen,T. and Joung,J.K. (2008) Zinc-finger nucleases: the next generation emerges. *Mol. Ther.*, **16**, 1200–1207.
4. De Francesco,L. (2011) Move over ZFNs. *Nat. Biotechnol.*, **29**, 681–684.
5. Zhang,F., Cong,L., Lodato,S., Kosuri,S., Church,G.M. and Arlotta,P. (2011) Efficient construction of sequence-specific TAL effectors for modulating mammalian transcription. *Nat. Biotechnol.*, **29**, 149–153.
6. Morbitzer,R., Elsaesser,J., Hausner,J. and Lahaye,T. (2011) Assembly of custom TALE-type DNA binding domains by modular cloning. *Nucleic Acids Res.*, **39**, 5790–5709.
7. Miller,J.C., Tan,S., Qiao,G., Barlow,K.A., Wang,J., Xia,D.F., Meng,X., Paschon,D.E., Leung,E., Hinkley,S.J. *et al.* (2011) A TALE nuclease architecture for efficient genome editing. *Nat. Biotechnol.*, **29**, 143–148.
8. Mahfouz,M.M., Li,L., Shamimuzzaman,M., Wibowo,A., Fang,X. and Zhu,J.-K. (2011) De novo-engineered transcription activator-like effector (TALE) hybrid nuclease with novel DNA binding specificity creates double-strand breaks. *Proc. Natl. Acad. Sci. USA*, **108**, 2623–2628.

9. Cermak,T., Doyle,E.L., Christian,M., Wang,L., Zhang,Y., Schmidt,C., Baller,J.A., Somia,N.V., Bogdanove,A.J. and Voytas,D.F. (2011) Efficient design and assembly of custom TALEN and other TAL effector-based constructs for DNA targeting. *Nucleic Acids Res.*, **39**, e82.
10. Boch,J., Scholze,H., Schornack,S., Landgraf,A., Hahn,S., Kay,S., Lahaye,T., Nickstadt,A. and Bonas,U. (2009) Breaking the code of DNA binding specificity of TAL-type III effectors. *Science*, **326**, 1509–1512.
11. Moscou,M.J. and Bogdanove,A.J. (2009) A simple cipher governs DNA recognition by TAL effectors. *Science*, **326**, 1501.
12. Bogdanove,A.J., Schornack,S. and Lahaye,T. (2010) TAL effectors: finding plant genes for disease and defense. *Curr. Opin. Plant Biol.*, **13**, 394–401.
13. Nakagawa,T., Kurose,T., Hino,T., Tanaka,K., Kawamukai,M., Niwa,Y., Toyooka,K., Matsuoka,K., Jinbo,T. and Kimura,T. (2007) Development of series of gateway binary vectors, pGWBs, for realizing efficient construction of fusion genes for plant transformation. *J. Biosci. Bioeng.*, **104**, 34–41.
14. Niwa,H., Yamamura,K. and Miyazaki,J. (1991) Efficient selection for high-expression transfectants with a novel eukaryotic vector. *Gene*, **108**, 193–199.
15. Johnson,D.G. (1994) Oncogenic capacity of the E2F1 Gene. *Proc. Natl. Acad. Sci. USA*, **91**, 12823–12827.
16. Engler,C., Gruetzner,R., Kandzia,R. and Marillonnet,S. (2009) Golden gate shuffling: a one-pot DNA shuffling method based on type IIs restriction enzymes. *PLoS One*, **4**, e5553.
17. Yeom,Y., Fuhrmann,G., Ovitt,C., Brehm,A., Ohbo,K., Gross,M., Hubner,K. and Scholer,H. (1996) Germline regulatory element of Oct-4 specific for the totipotent cycle of embryonal cells. *Development*, **122**, 881–894.
18. DuBridge,R.B., Tang,P., Hsia,H.C., Leong,P.M., Miller,J.H. and Calos,M.P. Analysis of mutation in human cells by using an Epstein–Barr virus shuttle system. *Mol. Cell. Biol.*, **7**, 379–387.
19. Szwagierczak,A., Bultmann,S., Schmidt,C.S., Spada,F. and Leonhardt,H. (2010) Sensitive enzymatic quantification of 5-hydroxymethylcytosine in genomic DNA. *Nucleic Acids Res.*, **38**, e181.
20. Li,E., Bestor,T.H. and Jaenisch,R. (1992) Targeted mutation of the DNA methyltransferase gene results in embryonic lethality. *Cell*, **69**, 915–926.
21. Conti,L., Pollard,S.M., Gorba,T., Reitano,E., Toselli,M., Biella,G., Sun,Y., Sanzone,S., Ying,Q.-L., Cattaneo,E. *et al.* Niche-independent symmetrical self-renewal of a mammalian tissue stem cell. *PLoS Biol.*, **3**, e283.
22. Ying,Q.-L., Stavridis,M., Griffiths,D., Li,M. and Smith,A. (2003) Conversion of embryonic stem cells into neuroectodermal precursors in adherent monoculture. *Nat. Biotechnol.*, **21**, 183–186.
23. Ying,Q.L. and Smith,A.G. (2003) Defined conditions for neural commitment and differentiation. *Methods Enzymol.*, **365**, 327–341.
24. Rottach,A., CFrauer,C., Pichler,G., Bonapace,I.M., Spada,F. and Leonhardt,H. (2010) The multi-domain protein Np95 connects DNA methylation and histone modification. *Nucleic Acids Res.*, **38**, 1796–1804.
25. Frauer,C., Rottach,A., Meilinger,D., Bultmann,S., Fellinger,K., Hasenöder,S., Wang,M., Qin,W., Söding,J., Spada,F. *et al.* (2011) Different binding properties and function of CXXC zinc finger domains in Dnmt1 and Tet1. *PLoS One*, **6**, e16627.
26. Shaner,N.C., Campbell,R.E., Steinbach,P.A., Giepmans,B.N.G., Palmer,A.E. and Tsien,R.Y. (2004) Improved monomeric red, orange and yellow fluorescent proteins derived from Discosoma sp. red fluorescent protein. *Nat. Biotechnol.*, **22**, 1567–1572.
27. Pan,G., Li,J., Zhou,Y., Zheng,H. and Pei,D. (2006) A negative feedback loop of transcription factors that controls stem cell pluripotency and self-renewal. *FASEB J.*, **20**, 1730–1732.
28. Kim,J.B., Zaehres,H., Wu,G., Gentile,L., Ko,K., Sebastiano,V., Araúzo-Bravo,M.J., Ruau,D., Han,D.W., Zenke,M. *et al.* (2008) Pluripotent stem cells induced from adult neural stem cells by reprogramming with two factors. *Nature*, **454**, 646–650.
29. Yoshida,M., Kijima,M., Akita,M. and Beppu,T. (1990) Potent and specific inhibition of mammalian histone deacetylase both *in vivo* and *in vitro* by trichostatin A. *J. Biol. Chem.*, **265**, 17174–17179.
30. Göttlicher,M., Minucci,S., Zhu,P., Krämer,O.H., Schimpf,A., Giavara,S., Sleeman,J.P., Lo Coco,F., Nervi,C., Pelicci,P.G. *et al.* (2001) Valproic acid defines a novel class of HDAC inhibitors inducing differentiation of transformed cells. *EMBO J.*, **20**, 6969–6978.
31. Santi,D.V., Garrett,C.E. and Barr,P.J. (1983) On the mechanism of inhibition of DNA-cytosine methyltransferases by cytosine analogs. *Cell*, **33**, 9–10.
32. Chen,X., Fang,F., Liou,Y.-C. and Ng,H.-H. (2008) Zfp143 regulates Nanog through modulation of Oct4 binding. *Stem Cells*, **26**, 2759–2767.
33. Koh,K.P., Yabuuchi,A., Rao,S., Huang,Y., Cunniff,K., Nardone,J., Laiho,A., Tahiliani,M., Sommer,C.A., Mostoslavsky,G. *et al.* (2011) Tet1 and Tet2 regulate 5-hydroxymethylcytosine production and cell lineage specification in mouse embryonic stem cells. *Cell Stem Cell*, **8**, 200–213.
34. Rodda,D.J., Chew,J.-L., Lim,L.-H., Loh,Y.-H., Wang,B., Ng,H.-H. and Robson,P. (2005) Transcriptional regulation of nanog by OCT4 and SOX2. *J. Biol. Chem.*, **280**, 24731–24737.
35. Dong,E., Chen,Y., Gavin,D.P., Grayson,D.R. and Guidotti,A. (2010) Valproate induces DNA demethylation in nuclear extracts from adult mouse brain. *Epigenetics*, **5**, 730–735.
36. Geißler,R., Scholze,H., Hahn,S., Streubel,J., Bonas,U., Behrens,S.-E. and Boch,J. (2011) Transcriptional activators of human genes with programmable DNA-specificity. *PloS One*, **6**, e19509.
37. Weber,E., Gruetzner,R., Werner,S., Engler,C. and Marillonnet,S. (2011) Assembly of designer TAL effectors by Golden Gate cloning. *PLoS One*, **6**, e19722.
38. Hagmann,M., Georgiev,O. and Schaffner,W. (1997) The VP16 paradox: herpes simplex virus VP16 contains a long-range activation domain but within the natural multiprotein complex activates only from promoter-proximal positions. *J. Virol.*, **71**, 5952–5962.
39. Li,T., Huang,S., Zhao,X., Wright,D.A., Carpenter,S., Spalding,M.H., Weeks,D.P. and Yang,B. (2011) Modularly assembled designer TAL effector nucleases for targeted gene knockout and gene replacement in eukaryotes. *Nucleic Acids Res.*, **39**, 6315–6325.
40. Scholze,H. and Boch,J. (2011) TAL effectors are remote controls for gene activation. *Curr. Opin. Microbiol.*, **14**, 47–53.
41. Feldman,N., Gerson,A., Fang,J., Li,E., Zhang,Y., Shinkai,Y., Cedar,H. and Bergman,Y. (2006) G9a-mediated irreversible epigenetic inactivation of *Oct-3/4* during early embryogenesis. *Nat. Cell Biol.*, **8**, 188–194.
42. Gidekel,S., Pizov,G., Bergman,Y. and Pikarsky,E. (2003) Oct-3/4 is a dose-dependent oncogenic fate determinant. *Cancer Cell*, **4**, 361–370.
43. Looijenga,L.H.J., Stoop,H., de Leeuw,H.P.J.C., de Gouveia Brazao,C.A., Gillis,A.J.M., van Roozendaal,K.E.P., van Zoelen,E.J.J., Weber,R.F.A., Wolffenbuttel,K.P., van Dekken,H. *et al.* (2003) POU5F1 (OCT3/4) identifies cells with pluripotent potential in human germ cell tumors. *Cancer Res.*, **63**, 2244–2250.
44. Huangfu,D., Maehr,R., Guo,W., Eijkelenboom,A., Snitow,M., Chen,A.E. and Melton,D.A. (2008) Induction of pluripotent stem cells by defined factors is greatly improved by small-molecule compounds. *Nat. Biotechnol.*, **26**, 795–797.
45. Kim,T.-Y., Bang,Y.-J. and Robertson,K. (2006) Histone deacetylase inhibitors for cancer therapy. *Epigenetics*, **1**, 14–23.
46. Teng,H.F., Kuo,Y.-L., Loo,M.R., Li,C.L., Chu,T.W., Suo,H., Liu,H.S., Lin,K.H. and Chen,S.L. (2011) Valproic acid enhances *Oct4* promoter activity in myogenic cells. *J. Cell. Biochem.*, **110**, 995–1004.
47. Al-Salihi,M., Yu,M., Burnett,D.M., Alexander,A., Samlowski,W. and Fitzpatrick,F.A. (2011) The depletion of DNA methyltransferase-1 and the epigenetic effects of 5-aza-2'deoxycytidine (decitabine) are differentially regulated by cell cycle progression. *Epigenetics*, **6**, 1021–1028.
48. Bhutani,N., Burns,D.M. and Blau,H.M. (2011) DNA demethylation dynamics. *Cell*, **146**, 866–872.

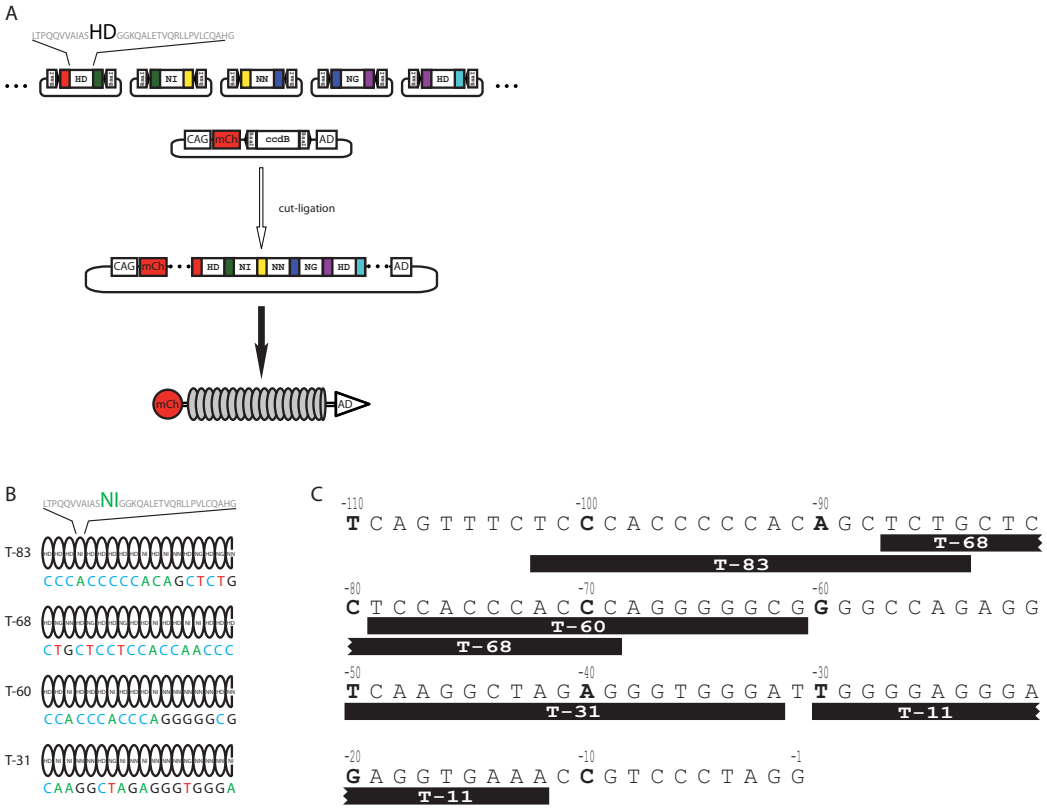

D

ATGGTGAGCAAGGGCGAGGAGGATAACATGGCCATCATCAAGGAGTTCATGCGCTTCAAGGTGCACATGGAGGGCTCCGTGAACGGCCACGAGTTCGAGATCGAGGGCGAGGGCG
AGGGCCGCCCCTACGAGGGCACCCAGACCGCCAAGCTGAAGGTGACCAAGGGTGGCCCCCTGCCCTTCGCCTGGGACATCCTGTCCCCTCAGTTCATGTACGGCTCCAAGGCCTAC
GTGAAGCACCCCGCCGACATCCCCGACTACTTGAAGCTGTCCTTCCCCGAGGGCTTCAAGTGGGAGCGCGTGATGAACTTCGAGGACGGCGGCGTGGTGACCGTGACCCAGGACTC
CTCCCTGCAGGACGGCGAGTTCATCTACAAGGTGAAGCTGCGCGGCACCAACTTCCCCTCCGACGGCCCCGTAATGCAGAAGAAGACCATGGGCTGGGAGGCCTCCTCCGAGCGGA
TGTACCCCGAGGACGGCGCCCTGAAGGGCGAGATCAAGCAGAGGCTGAAGCTGAAGGACGGCGGCCACTACGACGCTGAGGTCAAGACCACCTACAAGGCCAAGAAGCCCGTGCA
GCTGCCCGGCGCCTACAACGTCAACATCAAGTTGGACATCACCTCCCACAACGAGGACTACACCATCGTGGAACAGTACGAACGCGCCGAGGGCCGCCACTCCACCGGCGGCATGG
ACGAGCTGTACAAGAGCGGCCTGAGGAGCAGAGCCCAGGCGAGCAACAGCGCCGTGGACGCCACCATGGGCGATCGCACAAGTTTGTACAAAAAAGCAGGCTCCGCGGCCGCCCC
CTTCACCATGGATCCCATTCGTTCGCGCACACCAAGTCCTGCCCGCGAGCTTCTGCCCGGACCCCAACCCGATGGGGTTCAGCCGACTGCAGATCGTGGGGTGTCTCCGCCTGCCGG
CGGCCCCCTGGATGGCTTGCCCGCTCGGCGGACGATGTCCCGGACCCGGCTGCCATCTCCCCCTGCCCCCTCACCTGCGTTCTCGGCGGGCAGCTTCAGTGACCTGTTACGTCAGTT
CGATCCGTCACTTTTTAATACATCGCTTTTTGATTCATTGCCTCCCTTCGGCGCTCACCATACAGAGGCTGCCACAGGCGAGTGGGATGAGGTGCAATCGGGTCTGCGGGCAGCCG
ACGCCCCCCCACCCACCATGCGCGTGGCTGTCACTGCCGCGCGGCCGCCGCGCGCCAAGCCGGCGCCGCGACGACGTGCTGCGCAACCCTCCGACGCTTCGCCGGCCGCGCAGGTGG
ATCTACGCACGCTCGGCTACAGCCAGCAGCAACAGGAGAAGATCAAACCGAAGGTTCGTTCGACAGTGGCGCAGCACCACGAGGCACTGGTCGGCCATGGGTTTACACACGCGCA
CATCGTTGCGCTCAGCCAACACCCGGCAGCGTTAGGGACCGTCGCTGTCAAGTATCAGGACATGATCGCAGCGTTGCCAGAGGCGACACACGAAGCGATCGTTGGCGTCGGCAAAC
AGTGGTCCGGCGCACGCGCTCTGGAGGCCTTGCTCACGGTGGCGGGAGAGTTGAGAGGTCCACCGTTACAGTTGGACACAGGCCAACTTCTCAAGATTGCAAAACGTGGCGGCGT
GACCGCAGTGGAGGCAGTGCATGCATGGCGCAATGCACTGACGGGTGCCCCCCTGAACCTTACGCCGCAGCAGGTGGTGGCCATCGCCAGCCACGATGGCGGCAAGCAGGCGCTGG
AGACGGTGCAGCGGCTGCTTCCGGTGCTGTGCCAGGCCCATGGCCTGACCCCGGAGCAGGTGGTGGCCATCGCCAGCCACGATGGCGGCAAGCAGGCGCTGGAGACGGTGCAGCGA
TTGTTGCCGGTGCTGTGCCAGGCCCATGGCCTGACCCCGGAGCAGGTGGTGGCCATCGCCAGCCACGACGGTGGCAAGCAGGCGCTGGAGACTGTCCAGCGGCTGTTGCCGGTGCT
GTGCCAGGCCCATGGCCTGACCCCGGAGCAGGTGGTGGCCATCGCCAGCAATATTGGTGGCAAGCAGGCGCTTGAGACGGTGCAGCGGCTGTTGCCGGTGCTGTGCCAGGCCCATG
GCCTGACCCCGCAGCAGGTGGTGGCCATCGCCAGCCACGACGGTGGCAAGCAGGCTCTGGAGACGGTGCAGCGGCTGTTGCCGGTGCTGTGCCAGGCCCATGGCCTGACCCCGGAG
CAGGTGGTGGCCATCGCCAGCCACGACGGGGGCAAGCAGGCGCTGGAGACGGTGCAGCGGCTGTTGCCGGTGCTGTGCCAGGCCCATGGCCTGACCCCGCAGCAGGTGGTGGCCAT
CGCCAGCCACGACGGCGGCAAGCAGGCGCTGGAGACGGTGCAGGCGCTGTTGCCGGTGCTGTGCCAGGCCCATGGCCTGACCCCGGAGCAGGTGGTGGCCATCGCAAGCCACGACG
GTGGCAAGCAGGCGCTGGAGACGGTGCAGGCGCTGTTGCCGGTGCTGTGCCAGGCCCATGGCCTGACCCCGGAGCAGGTGGTGGCAATCGCCAGCCACAACGGTGGCAAGCAGGC
GCTGGAGACGGTGCAGCGGCTGTTGCCGGTGCTGTGCCAGGCCCATGGCCTGACCCCGCAACAGGTGGTAGCCATCGCCAGCAATATTGGTGGCAAGCAGGCGCTGGAGACGGTGC
AGCGGCTGTTGCCGGTGCTGTGCCAGGCCCATGGCCTGACACCCCAGCAGGTGGTAGCGATCGCCAGCCACGACGGTGGCAAGCAGGCGCTGGAGACGGTGCAGCGGCTGCTCCG
GTGCTGTGCCAGGCCCATGGCCTGACCCCGGAGCAGGTGGTGGCCATCGCCAGCAATATTGGTGGCAAGCAGGCGCTGGAGACGGTGCAGCGATTGTTGCCGGTGCTGTGCCAGGC
CCATGGCCTGACCCCGGAGCAGGTGGTGGCCATCGCCAGCAATAATGGTGGCAAGCAGGCGCTGGAGACTGTCCAGCGGCTGTTGCCGGTGCTGTGCCAGGCCCATGGCCTGACCC
CGGAGCAGGTGGTGGCCATCGCCAGCCACGACGGTGGCAAGCAGGCGCTTGAGACGGTGCAGCGGCTGTTGCCGGTGCTGTGCCAGGCCCATGGCCTGACCCCGGAGCAGGTGGTG
GCCATCGCCAGCAATGGCGGTGGCAAGCAGGCTCTGGAGACGGTGCAGCGGCTGTTGCCGGTGCTGTGCCAGGCCCATGGCCTGACCCCGGAGCAGGTGGTGGCCATCGCCAGCCA
CGACGGGGGCAAGCAGGCGCTGGAGACGGTGCAGCGGCTGTTGCCGGTGCTGTGCCAGGCCCATGGCCTGACCCCGCAGCAGGTGGTGGCCATCGCCAGCAATGGCGGCGGCAAGC
AGGCGCTGGAGACGGTGCAGGCGCTGTTGCCGGTGCTGTGCCAGGCCCATGGCCTGACACCCCAGCAGGTGGTGGCCATCGCCAGCAATaatGGCGGCAGGCCGGCGCTGGAGAGC
ATTGTTGCCCAGTTATCTCGCCCTGATCCGGCGTTGGCCGCGTTGACCAACGACCACCTCGTCGCCTTGGCCTGCCTCGGCGGACGTCCTGCGCTGGATGCAGTGAAAAAGGGATT
GCCGCACGCGCCGGCCTTGATCAAAAGAACCAATCGCCGTATTCCCGAACGCACATCCCATCGCGTTGCCGACCACGCGCAAGTGGTTCGCGTGCTGGGTTTTTTCCAGTGCCACT
CCCACCCAGCGCAAGCATTTGATGACGCCATGACGCAGTTCGGGATGAGCAGGCACGGGTTGTTACAGCTCTTTCGCAGAGTGGGCGTCACCGAACTCGAAGCCCGCAGTGGAAC
GCTCCCCCCAGCCTCGCAGCGTTGGGACCGTATCCTCCAGGCATCAGGGATGAAAAGGGCCAAACCGTCCCCTACTTCAACTCAAAGCGCCGGATCAGGCGTCTTTGCATGCATTCG
CCGATTCGCTGGAGCGTGACCTTGATGCGCCTAGCCCAATGCACGAGGGAGATCAGACGCGGGCAAGCAGCCGTAAACGGTCCCGATCGGATCGTGCTGTCACCGGTCCCTCCGCA
CAGCAATCGTTCGAGGTGCGCGTTCCCGAACAGCGCGATGCGCTGCATTTGCCCCTCAGTTGGAGGGTAAAACGCCCGCGTACCAGTATCGGGGGCGGCCTCCCGGATCCTGCCCC
CATTACCGACGTCAGCCTGGGAGACGAACTCCGCCTGGACGGCGAGGAGGTGGATATGACGCCCGCCGACGCCCTGGACGACTTCGACTTGGAGATGCTGGGGGACGTGGAGTCCC
CCTCCCCGGGAATGACCCACGACCCCGTCTCGTATGGGGCTTTGGACGTGGACGATTTTGAGTTTGAACAGATGTTTACCGATGCCATGGGCATTGACGACTTTGGGGGGTAG

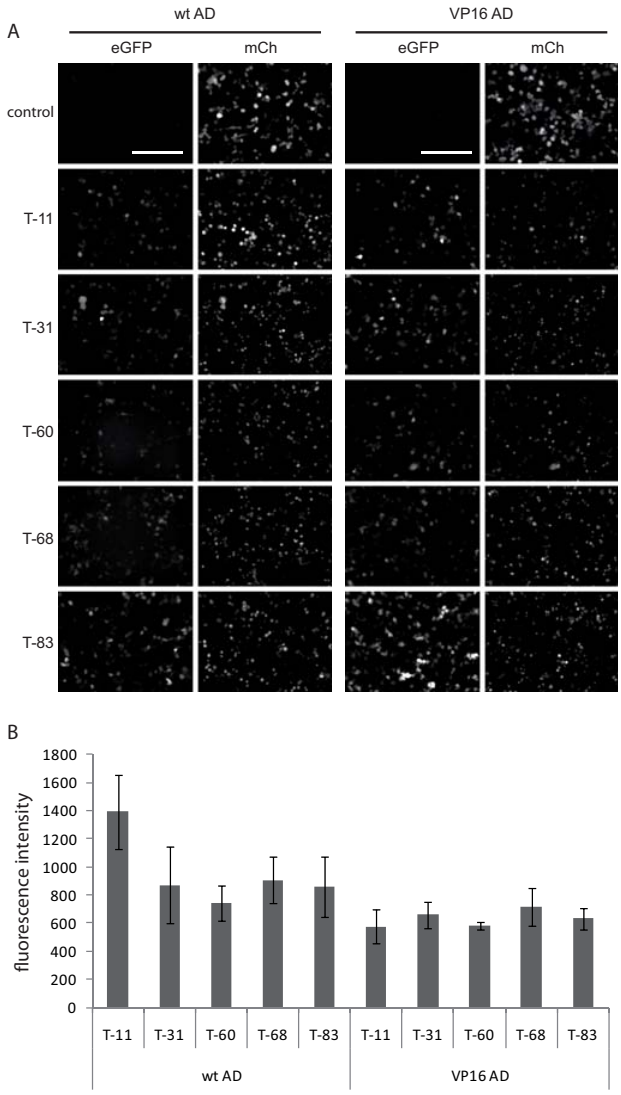
A
wt AD
VP16 AD
eGFP
mCh
eGFP
mCh
control
T-11
T-31
T-60
T-68
T-83

B
fluorescence intensity
1800
1600
1400
1200
1000
800
600
400
200
0
T-11
T-31
T-60
T-68
T-83
T-11
T-31
T-60
T-68
T-83
wt AD
VP16 AD

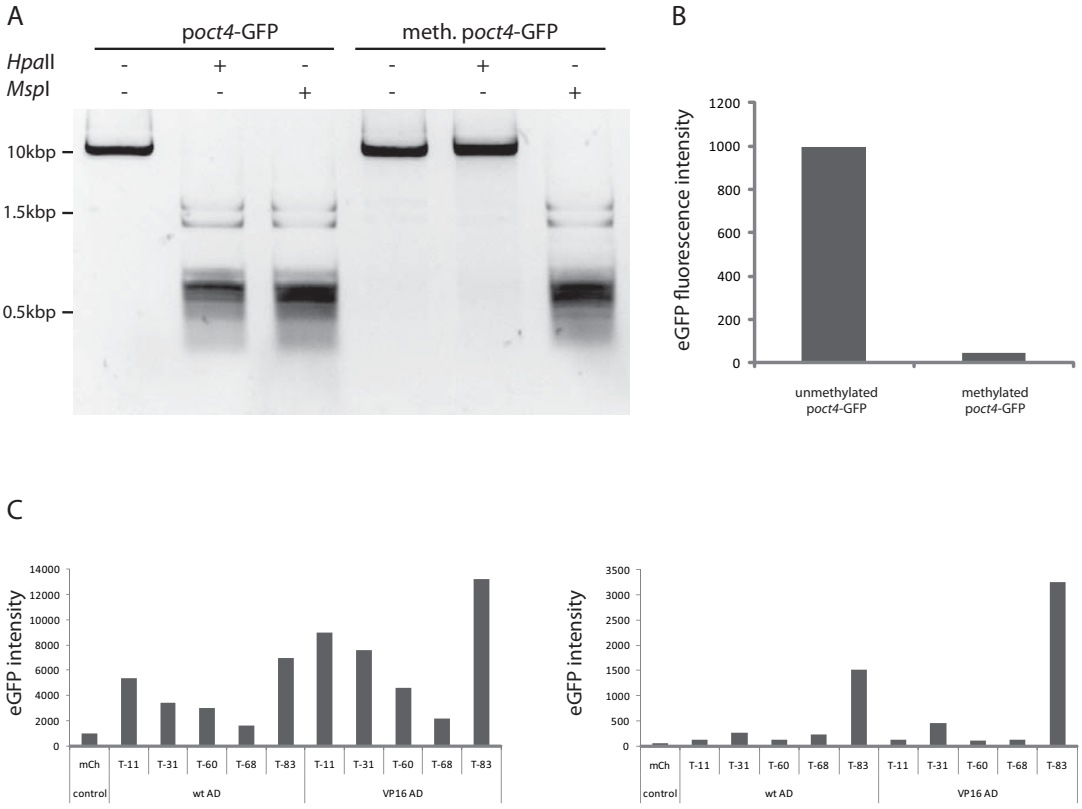
A
poct4-GFP
meth. poct4-GFP
HpaII
MspI
10kbp
1.5kbp
0.5kbp
B
eGFP fluorescence intensity
unmethylated poct4-GFP
methylated poct4-GFP
C
eGFP intensity
mCh
T-11
T-31
T-60
T-68
T-83
control
wt AD
VP16 AD

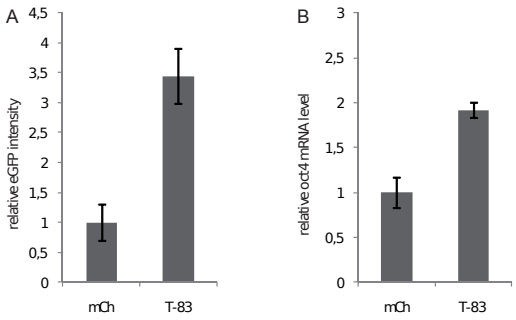
A
4,5
4
3,5
3
2,5
2
1,5
1
0,5
0
relative eGFP intensity
mCh
T-83
B
3
2,5
2
1,5
1
0,5
0
relative oct4 mRNA level
mCh
T-83

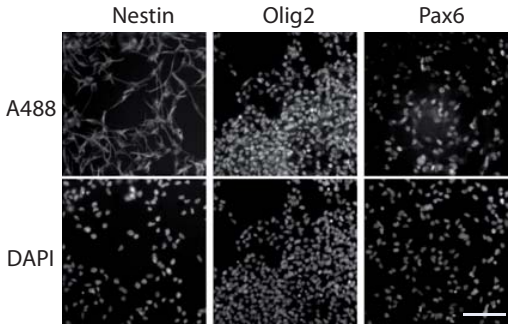
Nestin
Olig2
Pax6
A488
DAPI

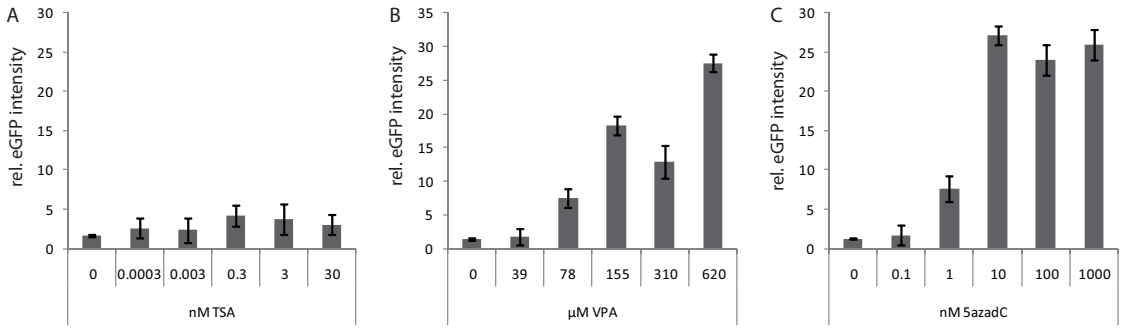
A
rel. eGFP intensity
0
5
10
15
20
25
30
0
0.0003
0.003
0.3
3
30
nM TSA
B
rel. eGFP intensity
0
5
10
15
20
25
30
35
0
39
78
155
310
620
µM VPA
C
rel. eGFP intensity
0
5
10
15
20
25
30
0
0.1
1
10
100
1000
nM 5azadC

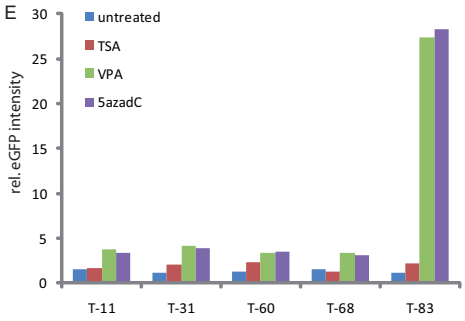
E
rel. eGFP intensity
0
5
10
15
20
25
30
untreated
TSA
VPA
5azadC
T-11
T-31
T-60
T-68
T-83

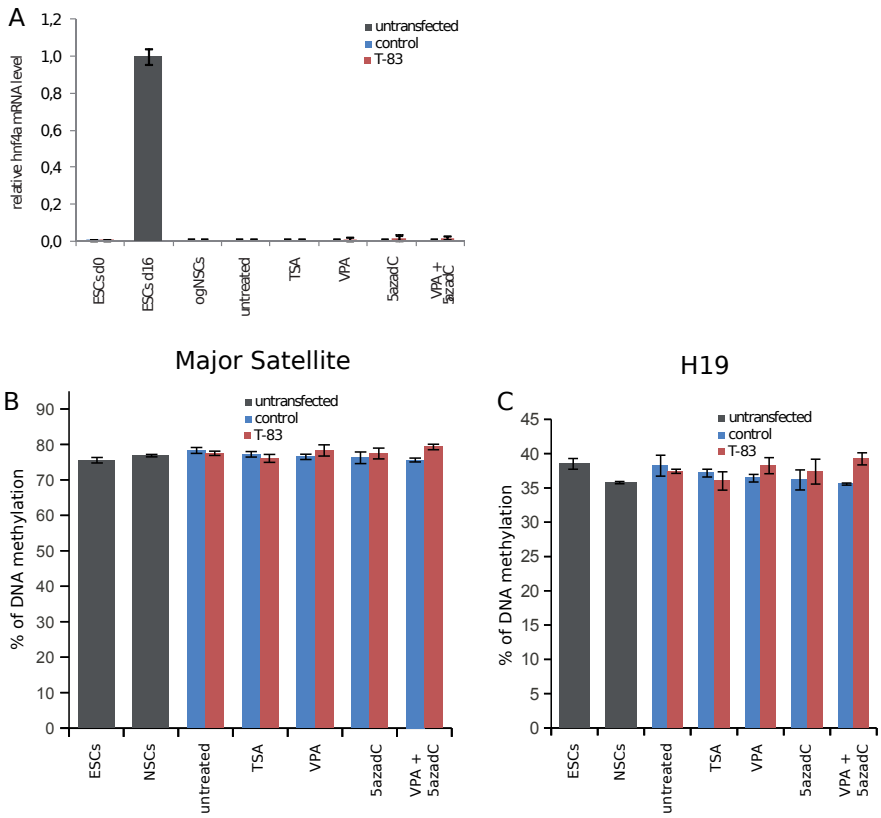
A
relative hnf4a mRNA level
1,2
1,0
0,8
0,6
0,4
0,2
0,0
untransfected
control
T-83
ESCs d0
ESCs d16
ogNSCs
untreated
TSA
VPA
5azadC
VPA + 5azadC
B
Major Satellite
% of DNA methylation
90
80
70
60
50
40
30
20
10
0
untransfected
control
T-83
ESCs
NSCs
untreated
TSA
VPA
5azadC
VPA + 5azadC
C
H19
% of DNA methylation
45
40
35
30
25
20
15
10
5
0
untransfected
control
T-83
ESCs
NSCs
untreated
TSA
VPA
5azadC
VPA + 5azadC

2.2 Targeting and tracing of specific DNA sequences with dTALEs in living cells

Published online 25 December 2013

Nucleic Acids Research, 2014, Vol. 42, No. 6 ***e38***
doi:10.1093/nar/gkt1348

Targeting and tracing of specific DNA sequences with dTALEs in living cells

Katharina Thanisch[1], Katrin Schneider[1], Robert Morbitzer[2], Irina Solovei[1], Thomas Lahaye[2], Sebastian Bultmann[1,*] and Heinrich Leonhardt[1,*]

[1]Department of Biology II, Humanbiology and Bioimaging, Center for Integrated Protein Science Munich (CIPSM), Ludwig Maximilians University Munich, 82152 Planegg-Martinsried, Germany and [2]Department of Biology I, Genetics, Ludwig Maximilians University Munich, 82152 Planegg-Martinsried, Germany

Received August 30, 2013; Revised November 5, 2013; Accepted December 4, 2013

ABSTRACT

Epigenetic regulation of gene expression involves, besides DNA and histone modifications, the relative positioning of DNA sequences within the nucleus. To trace specific DNA sequences in living cells, we used programmable sequence-specific DNA binding of designer transcription activator-like effectors (dTALEs). We designed a recombinant dTALE (msTALE) with variable repeat domains to specifically bind a 19-bp target sequence of major satellite DNA. The msTALE was fused with green fluorescent protein (GFP) and stably expressed in mouse embryonic stem cells. Hybridization with a major satellite probe (3D-fluorescent *in situ* hybridization) and co-staining for known cellular structures confirmed *in vivo* binding of the GFP-msTALE to major satellite DNA present at nuclear chromocenters. Dual tracing of major satellite DNA and the replication machinery throughout S-phase showed co-localization during mid to late S-phase, directly demonstrating the late replication timing of major satellite DNA. Fluorescence bleaching experiments indicated a relatively stable but still dynamic binding, with mean residence times in the range of minutes. Fluorescently labeled dTALEs open new perspectives to target and trace DNA sequences and to monitor dynamic changes in subnuclear positioning as well as interactions with functional nuclear structures during cell cycle progression and cellular differentiation.

INTRODUCTION

Covalent DNA and histone modifications play a key role in epigenetic gene regulation and have been intensively investigated over the past decades. While there is no doubt that higher order chromatin structures and nuclear genome organization also play important roles, they are far less amenable to systematic analysis due to their transient and fragile nature that can only be studied in the cellular context.

Multicolor fluorescent *in situ* hybridization (FISH) enabled the simultaneous visualization of multiple DNA sequences in fixed cells and indicated the territorial organization of all chromosomes in interphase nuclei (1). In general, the subnuclear distribution of chromosomal segments within the nucleus and with respect to chromosome territories seems to correlate with their gene density and transcriptional activity (2–4). Besides these general principles of genome organization, there is by now good evidence for spatial (re-)organization of the genome during differentiation (5). These changes in genome organization during cellular differentiation might be caused by changes in transcriptional activity, DNA and histone modifications as well as altered proteome composition. For example, the dramatic genome reorganization during myogenesis was linked to the expression of methylcytosine binding proteins (6). Likewise, developmental expression patterns of the nuclear envelope proteins Lamin A/C (LamA/C) and the Lamin B receptor (LBR) control peripheral tethering of facultative heterochromatin and gene expression patterns (7). To what extent and in which cases the relative nuclear position of genes is cause or consequence of transcriptional activity remains to be clarified.

*To whom correspondence should be addressed. Tel: +49 89 2180 74232; Fax: +49 89 2180 74236; Email: h.leonhardt@lmu.de
Correspondence may also be addressed to Sebastian Bultmann. Tel: +49 89 2180 74233; Fax: +49 89 2180 74236; Email: bultmann@bio.lmu.de
Present Address:
Thomas Lahaye, ZMBP-General Genetics, University of Tübingen, 72076 Tübingen, Germany.
Robert Morbitzer, ZMBP-General Genetics, University of Tübingen, 72076 Tübingen, Germany.

One challenge in addressing these basic questions is the temporal resolution, as changes in genome organization might be fast and transient. To study the dynamics of chromosomal loci, Lac operator repeats were inserted and traced with Lac repressor green fluorescent protein (GFP) fusion proteins (8). With this genetic tag, rapid movements of a DNA chromosome region were observed in response to gene activation (9,10). However, this method is limited to artificially inserted bacterial DNA sequences and thus not applicable to native endogenous DNA sequences. Alternatively, chromosome dynamics in general can be monitored with histone GFP fusions (11), but with this approach, specific DNA sequences cannot be distinguished.

A well-established technology to create recombinant specific DNA binding modules is based on the Cys_2His_2 zinc finger (ZF) domains and their 3-bp DNA recognition code (12–14). These domains can be combined to polydactyl zinc finger proteins (PZF) that bind user-defined DNA target sequences. PZF have been used for tracing and manipulating specific DNA sequences *in vivo* (15,16) as well as for gene activation and genome engineering (17–21). Nevertheless, PFZ target choice is biased toward GC-rich sequences, and fusion of individual ZF modules can influence their individual binding specificity, making the generation of PZF for a desired sequence a laborious and cost-intensive process (22).

However, in the past years, a new technology has emerged that overcomes several of the limitations associated with the use of PZF as artificial DNA binding domains. Transcription activator-like effector proteins (TALEs) from the plant pathogen genus *Xanthomonas* contain a DNA binding domain that can be adjusted to bind any desired target sequence with high specificity (23–27). The central TALE DNA binding domain is composed of tandem arranged 33–35 amino acid repeats, with each repeat binding to one base. The base preference of the individual repeats is specified by amino acids 12 and 13, referred to as repeat variable diresidues (RVDs) (28,29). This straightforward correlation between RVD and bound nucleotide allows the fast and efficient generation of DNA binding modules for any user-defined target sequence leading to a broad application of designer TALEs (dTALEs) in genome engineering and as artificial transcription factors (23–27,30–32).

Here we describe the application of dTALEs as a tool for targeting and tracing of repetitive DNA sequences in living cells. We show that dTALEs can be used to visualize the dynamics of major satellite repeats in mouse embryonic stem cells (ESCs) throughout the cell cycle and to characterize their *in vivo* binding kinetics.

MATERIALS AND METHODS

Plasmid construction

H2B C-terminally fused to monomeric red fluorescent protein (H2B-mRFP) was described previously (33). The coding sequences of Cbx1 (NM_007622.3) and Cbx 5 (NM_007626.3) were amplified by polymerase chain reaction from pGST-Cbx1 (34) and wild-type E14 cDNA (35), respectively, placed under the control of the cytomegalovirus (CMV) promoter, and fused with mRFP by replacing the ligase I cDNA in the pCMV-mRFP-ligase I plasmid described previously (36). *TALE* genes were cloned in pEXPR IBA3 (IBA, Göttingen) by BsaI cut-ligation (enhanced GFP (eGFP), TALE N/C-terminal regions) and BpiI cut-ligation (TALE DNA binding domain), respectively. Therefore, the BpiI restriction site of pEXPR IBA3 was removed by site-directed mutagenesis using primers P1 and P2. Furthermore, the 3' BsaI overlap of the multiple cloning site was changed from GCGC to AAGG by site-directed mutagenesis using primers P3 and P4. eGFP (27), TALE N- and C-terminal regions were amplified with primers P5 and P6, P7 and P8, and P9 and P10, respectively. Thereby BsaI restriction sites and appropriate overlaps were added and the parts were subsequently assembled in pEXPR IBA3 by BsaI cut-ligation resulting in pEXPR IBA3 eGFP TALE N/C. The DNA binding domain was assembled as described in (24) and cloned via BpiI cut-ligation into the pre-assembled pEXPR IBA3 eGFP TALE N/C to generate the GFP-msTALE.

P1 pEXPR-IBA3 BpiI* F
GGATTGGGAAGATAATAGCAGGCATGC
P2 pEXPR-IBA3 BpiI* R
GCATGCCTGCTATTATCTTCCCAATCC
P3 pEXPR-IBA3 BsaI GCGC-AAGG F
CCATGGTCTCAAAGGTTGGAGCCACCCGC
P4 pEXPR-IBA3 BsaI GCGC-AAGG R
GCGGGTGGCTCCAACCTTTGAGACCATGG
P5 GFP F
TTTGGTCTCTAATGGTGAGCAAG
P6 GFP R
GTCTCAGGTGAAATCGCCCAT
P7 AvrBs3 N-term BsaI F
TTTGGTCTCTCACCATGGATCCCATTCGTTCGCG
CAC
P8 AvrBs3 N-term BsaI ATAA R
AAAGGTCTCATTATGGGAAGACCGCGTAAGGT
TCAGG
P9 AvrBs3 C-term BsaI ATAA F
TTTGGTCTCTATAAGGGAAGACGGCGCTGGAG
P10 AvrBs3 C-term (till BamHI) BsaI AAGG R
TTTGGTCTCCCTTAGGATCCGGGAGGCCGCCCC

Cell culture, transfection and fluorescence-activated cell sorting

HEK 293T cells were cultured and transfected as described before (27). J1 ESCs (37) were maintained on gelatin-coated dishes in Dulbecco's modified Eagle's medium supplemented with 16% fetal bovine serum (Biochrom), 0.1 mM ß-mercaptoethanol (Invitrogen), 2 mM L-glutamine, 1× MEM non-essential amino acids, 100 U/ml penicillin, 100 µg/ml streptomycin (PAA Laboratories GmbH), 1000 U/ml recombinant mouse LIF (Millipore), 1 µM PD032591 and 3 µM CHIR99021 [Axon Medchem, (38)]. Transfections in ESCs were performed using Lipofectamin 2000 (Invitrogen) according to the manufacturer's instructions. Fluorescence-activated cell sorting (FACS) was performed with an FACS Aria II (Becton Dickinson).

Generation of transgenic cell lines

ESCs stably carrying the GFP-msTALE construct were generated by transfecting wt J1 ESCs (37) followed by G418 antibiotic selection (750 μg/ml) and repeated sorting for eGFP expression. To obtain clonal transgenic cell lines, single cell sorting was performed. Single cell clones were analyzed by high content imaging using the Operetta system (PerkinElmer). 4′,6-diamidino-2-phenylindole (DAPI) and eGFP fusion proteins were excited, and the emission was recorded using standard filter sets and 200 ms exposure. For each well, nine different fields were imaged and analyzed with the Harmony analysis software. Double transgenic cell lines were generated by transfecting the stable GFP-msTALE cell line with mRFP-PCNA and H2B-mRFP followed by repeated sorting for eGFP and RFP expression.

Immunoprecipitation and western blot

Immunoprecipitation was performed as described before (39). One p100 of HEK293T cells transiently transfected with the GFP-msTALE fusion protein or stable GFP-msTALE ESCs, respectively, was harvested and lysed. GFP fusions were pulled down using the GFP-Trap (40) (Chromotek) and subjected to western blotting using a mouse monoclonal anti-GFP antibody (Roche, 11814460001). For comparison of protein levels, stable GFP-msTALE ESCs were lysed in Radio-Immunoprecipitation Assay (RIPA) buffer. Lysate from 750 000 cells was subjected to western blotting using a mouse monoclonal anti-GFP (Roche, 11814460001), rabbit polyclonal anti-CBX1 (Abcam, ab10478) and rabbit polyclonal anti-CENPB (Abcam, ab25743).

Immunofluorescence staining and microscopy

Immunostaining and 3D-FISH were performed as described previously (41). Briefly, cells cultured on coverslips were fixed with 4% paraformaldehyde for 10 min, washed with PBST (PBS, 0.01% Tween20) and permeabilized with 0.5% Triton X-100. Both primary and secondary antibodies were diluted in blocking solution (PBST, 4% bovine serum albumin). Coverslips with cells were incubated with primary and secondary antibody solutions in dark humid chambers for 1–2 h at room temperature; washings after primary and secondary antibodies were done with PBST. For immuno-FISH, both primary (anti-GFP) and secondary antibodies were applied first; subsequently, cells were postfixed with 4% paraformaldehyde and pre-treated for hybridization. Hybridization was carried out for 2 days at 37°C; posthybridization washings included 2 × Saline Sodium Citrate (SSC) at 37°C and 0.1 × SSC at 61°C (41). The probe for major satellite repeats was generated by polymerase chain reaction using mouse Cot1 DNA (primers: 5′-GCG AGA AAA CTG AAA ATC AC and 5'-TCA AGT CGT CAA GTG GAT G), labeled with Cy3-dUTP by nick-translation, and dissolved in hybridization mixture (50% formamide, 10% dextran sulfate, 1 × SSC) at a concentration of 10–20 ng/μl. For nuclear DNA counterstaining, DAPI was added to the secondary antibody solution to the final concentration 2 μg/ml. Coverslips were mounted in antifade medium (Vectashield, Vector Laboratories) and sealed with colorless nail polish.

Following primary antibodies were used: anti-GFP (Roche, 11814460001), anti-lamin B1 (Santa Cruz Biotechnology, sc-6217), anti-nucleophosmin (B23, Sigma-Aldrich, B0556), anti-kinetochores (Euroimmun AG, CA 1611-0101) and anti-H4K20me3 (Abcam, ab9053). The secondary antibodies were anti-rabbit conjugated to DyLight fluorophore 594 (Jackson ImmunoResearch, 711-505-152), anti-mouse conjugated to Alexa 488 and 555 (Invitrogen, A21202 and A31570), anti-goat conjugated to Cy3 (Jackson ImmunoResearch, 706-166-148) or Alexa 647 (Invitrogen, A21447) and anti-human conjugated to Cy3 (Jackson ImmunoResearch, 309-165-003). Single optical sections or stacks of optical sections were collected using a Leica TCS SP5 confocal microscope equipped with Plan Apo 63×/1.4 NA oil immersion objective and lasers with excitation lines 405, 488, 561 and 633 nm. Dedicated plug-ins in ImageJ program were used to compensate for axial chromatic shift between fluorochromes in confocal stacks, to create RGB images/stacks and to arrange them into galleries (42,43).

Live cell microscopy, fluorescence loss in photobleaching and quantitative fluorescence recovery after photobleaching analysis

Live cell imaging, fluorescence loss in photobleaching (FLIP) and fluorescence recovery after photobleaching (FRAP) experiments were performed on an Ultra*VIEW* VoX spinning disc microscope (PerkinElmer) as described before (44). Photobleaching was performed using two iterations with the acousto-optic tunable filter (AOTF) of the 488 nm laser line set to 100% transmission. For acquisition of FRAP or FLIP experiments, the 488 nm laser line was set to 20% transmission.

In FRAP experiments, a circular bleach region of 2.5 × 2.5 μm, covering one chromocenter (CC) per cell, was chosen. After 20 prebleach frames with a time interval of 200 ms, CCs in five cells were bleached (~650 ms). Then 150 postbleach frames were recorded with a time interval of 200 ms followed by 800 postbleach frames with a time interval of 500 ms. The mean intensity of this circular region was measured over time. Data correction, double normalization and calculation of the half time recovery ($t_{1/2}$) and the mobile fraction (*MF*) were performed as described before (45). The outline of the nucleus for the evaluation was determined using images obtained with bright field illumination. The results of 14 cells were averaged.

In FLIP experiments, approximately half of the cell was bleached in a rectangular region. Like in the FRAP experiments, multiple cells were bleached in parallel. After initial five prebleach frames with a time interval of 4 s, 40 bleach cycles were performed. Each bleach cycle consisted of a bleaching event of ~700 ms followed by 10 time frames with a time interval of 4 s. In each frame, a z-stack of 7 μm with a step size of 1 μm was recorded to check for axial drift. To evaluate the data, the mean intensity of a circular region of 20 × 20 pixel was determined over time.

The region covered either a CC in the unbleached half of a cell, in which the other half was repeatedly bleached [Figure 3B (1)], or in a neighboring unbleached cell [Figure 3B (2)]. Afterward, the background was subtracted from these results. The measurements were performed in Fiji (46) followed by calculations in Excel.

In long-term imaging experiments, a z-stack of 10.8–14.4 µm with a step size of 1.2 µm was recorded every 15 min for ~20 h. To avoid photodamage of the cells, the AOTF of the laser was set to low transmission values of 6–10%.

RESULTS AND DISCUSSION

Generation of a GFP-msTALE highlighting major satellite DNA in mouse cells

To test whether dTALEs are suitable to trace DNA sequences *in vivo*, we generated an N-terminal GFP fusion construct directed against the 19-bp sequence 5'-TGGCG AGAAAACTGAAAAT-3' of the murine major satellite repeat sequence using a golden-gate cloning-based approach (Supplementary Figure S1) (24). The 234-bp units of the major satellite repeat are present in 1000–10 000 copies per chromosome located in the centromeric periphery (47). Major satellite repeats constitute the major part of mouse CCs. These heterochromatin regions are clustered centromeres of acrocentric chromosomes located at the nuclear periphery and around the nucleoli (Figure 1A) (48). The distinct subnuclear localization and high copy number of major satellite repeats constitute an ideal model system to test the applicability of dTALEs for *in vivo* tracing of DNA sequences.

Using the dTALE directed against the major satellite repeat (GFP-msTALE), we generated a stable mouse ESC line by antibiotic selection followed by repeated FACS sorting. After single cell sorting, we established a clone that exhibited correct protein size of the GFP-msTALE compared with a transient transfection in HEK293T cells (Figure 1B). The cell line expressed relatively low levels of the GFP-msTALE compared with the endogenous heterochromatin-associated protein Cbx1 and the kinetochore binding protein CenpB (Supplementary Figure S2). To address the specificity of the TALE binding to the major satellite repeats, we performed fluorescence *in situ* hybridization on 3D-preserved cells (3D-FISH) (Figure 1C). Using a directly labeled probe directed against the major satellites combined with immunostaining, we observed strict co-localization of the GFP-msTALE with the major satellite foci. To further characterize the stable ESC line, the subnuclear localization of the GFP-msTALE in relation to several makers of nuclear structures was assessed. In interphase cells, the GFP signal exhibited a focal pattern co-localizing with DAPI-stained CCs as well as with trimethylated histone 4 lysine 20 (H4K20me3), a marker for constitutive heterochromatin highly enriched in major satellite repeats (46) (Figure 1D, upper panel). Furthermore, we found that kinetochores are localized in the periphery of the GFP foci consistent with the expected relative organization of CCs (Figure 1D, middle panel). Immunolabeling against nucleophosmin (B23), a marker enriched in nucleoli and lamin B1, revealed that the GFP foci localize around the nucleoli and in the nuclear periphery (Figure 1D, lower panel). For direct comparison, we transiently expressed two heterochromatin proteins (RFP-Cbx1 and RFP-Cbx5, also known as heterochromatin protein 1 beta and alpha), which co-localized with the GFP-msTALE at CCs (Supplementary Figure S3A and B) until G2 phase, when binding of both Cbx1 and Cbx5 is abolished (49). Taken together, these data demonstrate that the GFP-msTALE correctly highlights the localization of the major satellite DNA *in vivo*.

The GFP-msTALE enables DNA sequence tracing during the cell cycle *in vivo*

After establishing the correct localization of the GFP-msTALE, we analyzed its behavior during cell cycle progression. We generated double transgenic cell lines also expressing H2B-RFP (Supplementary Figure S3C) to visualize whole chromatin in combination with GFP-msTALE-bound CCs. To distinguish the different phases of DNA replication, we stably transfected the GFP-msTALE ESC line with the S-phase marker RFP-PCNA (50) and acquired time series over 20 h demonstrating the suitability of the approach for live cell imaging. We observed progression throughout S-phase with the GFP-msTALE exhibiting the typical focal pattern expected for major satellite DNA (Figure 2A, Supplementary Movie S1). Importantly, the GFP-msTALE was located at mid to late S-phase replication foci, correlating well with the replication of CCs (45,50) (Figure 2A and B).

Next, we analyzed the localization of the GFP-msTALE through mitosis. Although the dTALE still localized to chromosomes until mid prophase, it largely dissociated in mid to late prophase and reassociated in early telophase (Figure 2C). Residual binding in metaphase was visible on contrast enhancement and with higher expression levels (Supplementary Figure S3). It should be noted that while this work was under review, a smaller TALE construct targeting another major satellite repeat sequence was described that exhibited more stable DNA binding throughout mitosis (51). These results indicate that the chromatin condensation during mitosis might affect binding of the dTALE to its target sequences, an observation in line with the hypothesis that chromatin environment can influence dTALE binding and activity (27,52).

Analysis of *in vivo* protein dynamics reveals a strong but dynamic association of the GFP-msTALE with CCs

The observation that the dTALE is not associated with condensed chromosomes during mitosis prompted us to investigate the *in vivo* DNA binding kinetics of the GFP-msTALE in more detail. To quantify the binding dynamics of the GFP-dTALE in living cells, we performed FRAP and FLIP experiments. Both methods were used in a complementary approach (53,54), with intensity measurements focusing on single CCs, the prominent binding sites of the GFP-msTALE. For the FRAP experiment, we bleached a small circular region including one CC and quantified the recovery in this region over time (Figure 3A and C). The faster the recovery, the more transient is the binding dynamics. In contrast, for the FLIP

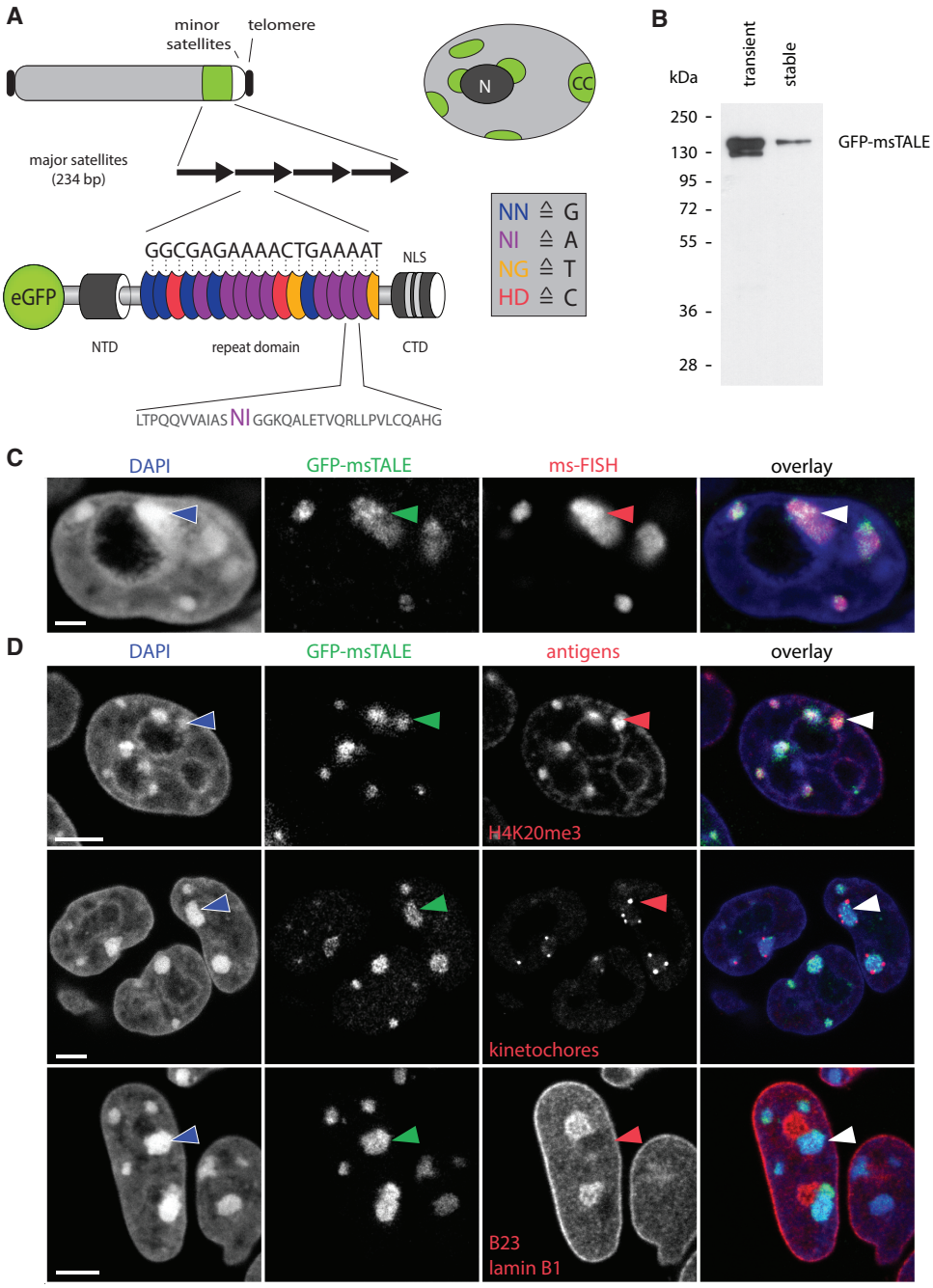

Figure 1. Localization of the GFP-msTALE to major satellite repeats in mouse pericentromeric heterochromatin. (**A**, top) Schematic representation of an acrocentric mouse chromosome with telomeres (black), major satellites (green), minor satellites (white) and the long arm of the chromosome (light gray). Overview of a nucleus showing multiple heterochromatin centers (CC, green), where the major satellite DNA is clustered. CCs localize next to the nuclear periphery and the nucleoli (dark gray, N) and are surrounded by less condensed chromatin (light gray). (A, bottom) Schematic representation of the GFP-msTALE aligned to its binding site within the major satellite repeats (black arrows). The dTALE is composed of an N-terminal domain (NTD), a C-terminal domain (CTD) bearing nuclear localization signals (NLS) and a central repeat domain. DNA target recognition is mediated by the RVDs within each TALE repeat (blue, purple, yellow and red ellipses for RVDs binding to the bases G, A, T and C, respectively, single letter code for amino acids and nucleotide bases). A representative repeat sequence with RVDs (purple) is shown below as close-up (single letter code for amino acids). The complete sequence is shown in Supplementary Figure S1. Note that the msTALE is lacking the C-terminal activation domain. For visualization and immunoprecipitation, the dTALE is N-terminally fused to GFP. (**B**) GFP-Trap pull-down from HEK293T cells transiently transfected with the GFP-msTALE construct (transient) and a J1 ESC clone stably expressing the GFP-msTALE (stable). Immunodetection by an anti-GFP antibody. (**C**) 3D-immuno-FISH on stable GFP-msTALE ESCs with probe directed against major satellite repeats (ms-FISH). Because the GFP signal is strongly reduced by 3D-FISH procedure, an anti-GFP antibody was used to visualize GFP-msTALE localization. Note strict co-localization of the GFP signal (green) and the FISH probe (red). Nuclei were counterstained with DAPI (blue).

(continued)

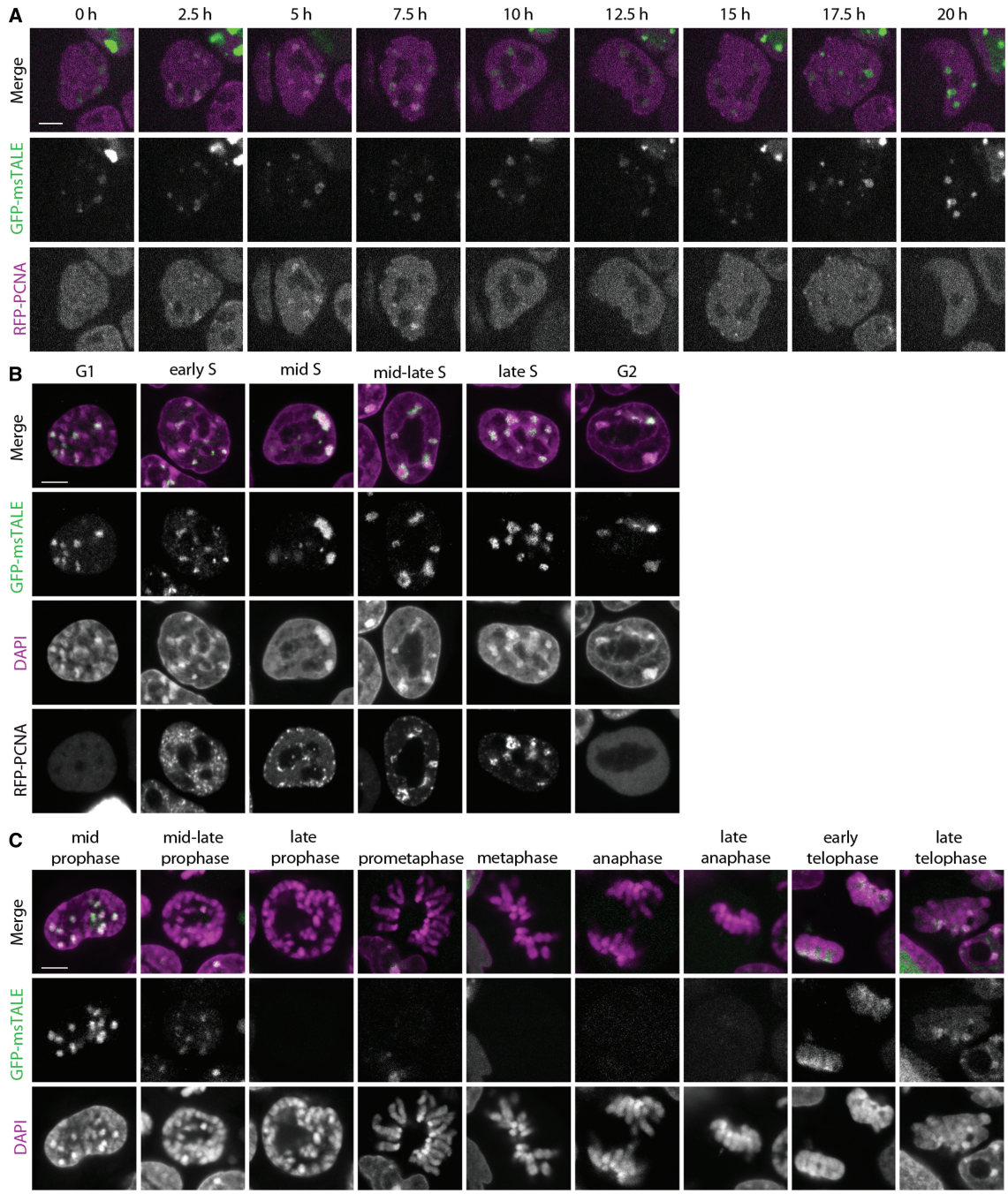

Figure 2. Cell cycle-dependent distribution of GFP-msTALE. (**A**) Live cell imaging of replicating stable GFP-msTALE cell line (green) stably transfected with RFP-PCNA (magenta). (**B**) Single confocal sections of fixed and RFP-PCNA co-transfected GFP-msTALE stable cell line (green) during DNA replication. DNA is visualized by DAPI (magenta). (**C**) Single confocal sections of fixed GFP-msTALE cell line (green) during mitosis. DNA is visualized by DAPI (magenta). Scale bars: 5 µm.

Figure 1. Continued
Arrowhead points at one of the CCs. (**D**) Immunostaining of ESCs stably expressing the GFP-msTALE (green). Upper panel, antibodies against heterochromatin (anti-H4K20me3, red) mark GFP-positive CCs. Middle panel, human antiserum binding to kinetochores reveals kinetochore clusters (red) at the surface of CCs. Lower panel, CCs marked with GFP-msTALE show a characteristic intranuclear localization abutting nuclear periphery or adjacent to the nucleoli (both shown in red). Nuclei were counterstained with DAPI (blue). Arrowheads mark one of the CCs in each exemplified nucleus. All images are single optical confocal sections. Scale bars: C, 5 µm; D, 2 µm.

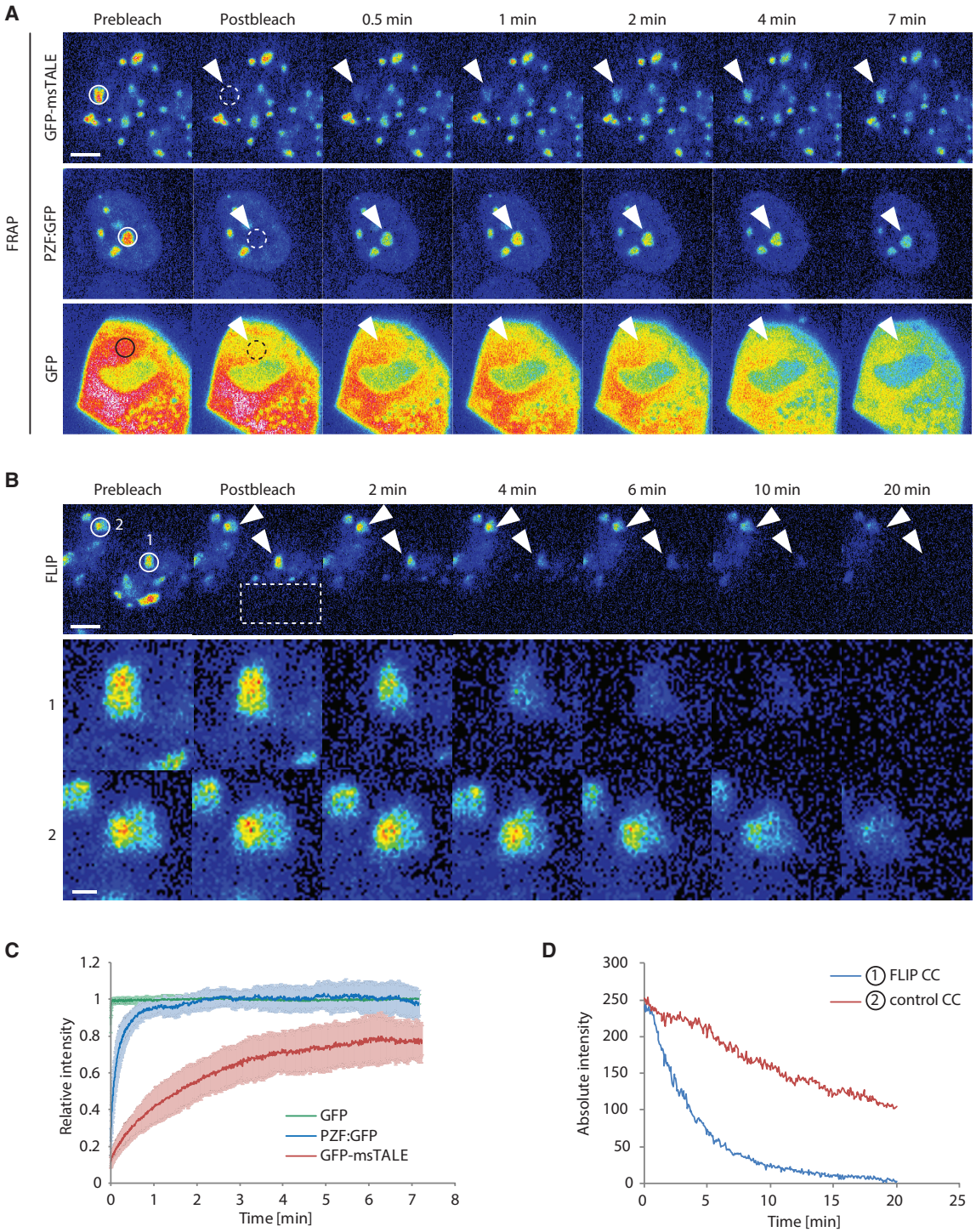

Figure 3. Comparative analysis of the dynamics of GFP, GFP-msTALE and PZF:GFP by FRAP and FLIP. Continuous lines indicate the intensity measurement areas, whereas dashed lines indicate the bleached regions. The arrowheads point to the intensity measurement areas in the postbleach time points. These regions are magnified by a factor of four in the lower panel of (B). Scale bars: 5 µm (upper panel) and 1 µm (lower panel, (B)). (**A**) Representative FRAP experiment for GFP, the stable GFP-msTALE cell line and PZF:GFP. A circular region (dashed line) with a diameter of 2.5 µm was bleached. (**B**) Representative FLIP experiment of the GFP-msTALE. A rectangular region indicated by the dashed line was repeatedly bleached. CCs in the unbleached half of the bleached cell (1) and in an unbleached reference cell (2) are highlighted. (**C**) Quantitative evaluation of FRAP experiments (average of 12–14 cells) comparing GFP-msTALE, PZF:GFP and GFP. Error bars represent standard deviation. (**D**) Representative background corrected, absolute intensities of two CCs in a bleached cell (1, blue line) and an unbleached reference cell (2, red line) illustrated in (B).

experiment we bleached half of the nucleus repeatedly and quantified the intensity of a CC in the unbleached half (Figure 3B and D). On protein dissociation from the binding site in the unbleached region and diffusion into the bleached region, a reduction of signal intensity in the unbleached half of the nucleus can be observed. The faster the signal decreases, the more transient is the binding dynamics. Thus, the binding dynamics of GFP-dTALEs can be analyzed without inducing damage at these sites by photobleaching. As the bleached regions and the measured region are separate from each other, this approach also takes into account the mobility between different compartments (55,56).

In our quantitative FRAP experiments with the GFP-msTALE, we observed a gradual slow increase in intensity over 7 min (Figure 3C). Even after this time, an immobile, not yet recovered fraction of ~20% was still detectable, indicating a strong binding of the dTALE to the major satellites. Unlike freely diffusing proteins such as GFP (44), no fast initial recovery of GFP-msTALE was detected in the bleached area (Figure 3A). Also the signal intensity outside CCs was rather low, indicating that most of the GFP-msTALE was bound to chromosomes. The stable interaction of GFP-msTALE with major satellites DNA seen in the FRAP experiments becomes directly evident from the complementary FLIP experiments. Even on repeated bleaching, GFP-msTALE fluorescence was detectable at the unbleached CCs within the same nucleus for up to 20 min (Figure 3D, line 1). Notably, reference measurement of CCs in the adjacent cell (Figure 3D, line 2) revealed a continuous loss of fluorescence (~50% over 20 min) because of image acquisition with these microscope settings, so that the actual dissociation of GFP-msTALE from CCs (Figure 3D, line 1) is even slightly slower. For comparison, we tested the ZF-based PZF:GFP binding to the major satellite repeats (15) and obtained a fast initial recovery together with a 10 times lower half time recovery value in FRAP experiments as well as a faster loss of fluorescence in FLIP experiments (Figure 3A and C and Supplementary Figure 4B) exhibiting less stable binding than the TALE construct.

In vitro studies revealed that dTALEs have K_d values in the low nanomolar to high picomolar range (27,57), indicating a strong binding affinity of dTALEs to DNA. Our *in vivo* binding studies demonstrate that dTALEs also strongly bind their target DNA sequence in a chromatin context, but not in a static mode, and reveal a rather dynamic interplay with chromatin. The depletion of GFP-msTALE from highly condensed chromatin during mitosis could be due to conformational changes of the DNA substrate weakening the binding or preventing rebinding that shifts the dynamic equilibrium toward the unbound state. This is consistent with the recent observation that condensation may affect binding and access of nuclear proteins to chromatin (33).

In summary, we could show that dTALEs can be engineered to bind and highlight repetitive DNA sequences *in vivo*. With the example of a dTALE designed to target the major satellite repeats in mouse cells, we showed that fluorescent dTALEs are suitable for live cell imaging of specific DNA sequences throughout the cell cycle. Moreover, we found that dTALEs can detect changes in chromatin condensation and that a dynamic interplay between dTALE and chromatin exists. In this study, we targeted repetitive DNA sequences; with more sensitive detection as used in single molecule tracing setups, eventually single copy genes might also become traceable.

Fluorescently labeled dTALEs open new perspectives to trace specific endogenous DNA sequences at high temporal and spatial resolution in living cells. Strict sequence dependent localization, higher affinity and easy assembly of dTALEs give this method an advantage over previous techniques based on overexpression of chromatin binding factors or ZF arrays in tracing and targeting of specific DNA sequences in living cells. This novel application of dTALEs will help to identify and elucidate cell cycle and development-specific changes in genome organization and chromatin dynamics.

SUPPLEMENTARY DATA

Supplementary Data are available at NAR Online.

ACKNOWLEDGEMENTS

The authors thank Dr Bert J. van der Zaal [Institute of Biology Leiden (IBL), Leiden University, Leiden] for providing the PZF:GFP construct. They thank Thomas Pyttel for generating the Cbx1 and Cbx5 expression constructs. Furthermore, they thank Dr Boris Joffe for comments and suggestions.

FUNDING

The Deutsche Forschungsgemeinschaft [SFB924 to T.L., SO1054 to I.S. and SFB646 to H.L.]; the Two Blades Foundation (to T.L.); the Nanosystems Initiative Munich [to H.L.]; the Bundesministerium für Bildung und Forschung [EpiSys to H.L.]; The International Max Planck Research School for Molecular and Cellular Life Sciences (IMPRS-LS) (to K.T. and K.S.); The Bundesministerium für Bildung und Forschung [3D-SR, in part to K.T.]. Funding for open access charge: Deutsche Forschungsgemeinschaft.

Conflict of interest statement. T.L. is a co-inventor of a patent application regarding the use of TALEs.

REFERENCES

1. Bolzer,A., Kreth,G., Solovei,I., Koehler,D., Saracoglu,K., Fauth,C., Muller,S., Eils,R., Cremer,C., Speicher,M.R. *et al.* (2005) Three-dimensional maps of all chromosomes in human male fibroblast nuclei and prometaphase rosettes. *PLoS Biol.*, **3**, e157.
2. Mahy,N.L., Perry,P.E. and Bickmore,W.A. (2002) Gene density and transcription influence the localization of chromatin outside of chromosome territories detectable by FISH. *J. Cell Biol.*, **159**, 753–763.
3. Branco,M.R. and Pombo,A. (2006) Intermingling of chromosome territories in interphase suggests role in translocations and transcription-dependent associations. *PLoS Biol.*, **4**, e138.
4. Osborne,C.S., Chakalova,L., Brown,K.E., Carter,D., Horton,A., Debrand,E., Goyenechea,B., Mitchell,J.A., Lopes,S., Reik,W.

et al. (2004) Active genes dynamically colocalize to shared sites of ongoing transcription. *Nat. Genet*., **36**, 1065–1071.
5. Joffe,B., Leonhardt,H. and Solovei,I. (2010) Differentiation and large scale spatial organization of the genome. *Curr. Opin. Genet. Dev*., **20**, 562–569.
6. Brero,A., Easwaran,H., Nowak,D., Grunewald,I., Cremer,T., Leonhardt,H. and Cardoso,M. (2005) Methyl CpG-binding proteins induce large-scale chromatin reorganization during terminal differentiation. *J. Cell Biol*., **169**, 733–743.
7. Solovei,I., Wang,A.S., Thanisch,K., Schmidt,C.S., Krebs,S., Zwerger,M., Cohen,T.V., Devys,D., Foisner,R., Peichl,L. *et al*. (2013) LBR and lamin A/C sequentially tether peripheral heterochromatin and inversely regulate differentiation. *Cell*, **152**, 584–598.
8. Robinett,C.C., Straight,A., Li,G., Willhelm,C., Sudlow,G., Murray,A. and Belmont,A.S. (1996) In vivo localization of DNA sequences and visualization of large-scale chromatin organization using lac operator/repressor recognition. *J. Cell Biol*., **135**, 1685–1700.
9. Tumbar,T. and Belmont,A.S. (2001) Interphase movements of a DNA chromosome region modulated by VP16 transcriptional activator. *Nat. Cell Biol*., **3**, 134–139.
10. Gasser,S.M. (2002) Visualizing chromatin dynamics in interphase nuclei. *Science*, **296**, 1412–1416.
11. Kanda,T., Sullivan,K.F. and Wahl,G.M. (1998) Histone-GFP fusion protein enables sensitive analysis of chromosome dynamics in living mammalian cells. *Curr. Biol*., **8**, 377–385.
12. Klug,A. (2010) The discovery of zinc fingers and their development for practical applications in gene regulation and genome manipulation. *Q. Rev. Biophys*., **43**, 1–21.
13. Pabo,C.O., Peisach,E. and Grant,R.A. (2001) Design and selection of novel Cys2His2 zinc finger proteins. *Annu. Rev. Biochem*., **70**, 313–340.
14. Segal,D.J. and Barbas,C.F. III (2000) Design of novel sequence-specific DNA-binding proteins. *Curr. Opin. Chem. Biol*., **4**, 34–39.
15. Lindhout,B.I., Fransz,P., Tessadori,F., Meckel,T., Hooykaas,P.J. and van der Zaal,B.J. (2007) Live cell imaging of repetitive DNA sequences via GFP-tagged polydactyl zinc finger proteins. *Nucleic Acids Res*., **35**, e107.
16. Casas-Delucchi,C.S., Becker,A., Bolius,J.J. and Cardoso,M.C. (2012) Targeted manipulation of heterochromatin rescues MeCP2 Rett mutants and re-establishes higher order chromatin organization. *Nucleic Acids Res*., **40**, e176.
17. Cathomen,T. and Joung,J.K. (2008) Zinc-finger nucleases: the next generation emerges. *Mol. Ther*., **16**, 1200–1207.
18. Urnov,F.D., Miller,J.C., Lee,Y.L., Beausejour,C.M., Rock,J.M., Augustus,S., Jamieson,A.C., Porteus,M.H., Gregory,P.D. and Holmes,M.C. (2005) Highly efficient endogenous human gene correction using designed zinc-finger nucleases. *Nature*, **435**, 646–651.
19. Porteus,M.H. and Carroll,D. (2005) Gene targeting using zinc finger nucleases. *Nat. Biotechnol*., **23**, 967–973.
20. Segal,D.J., Dreier,B., Beerli,R.R. and Barbas,C.F.III. (1999) Toward controlling gene expression at will: selection and design of zinc finger domains recognizing each of the 5'-GNN-3' DNA target sequences. *Proc. Natl Acad. Sci. USA*, **96**, 2758–2763.
21. Joung,J.K. and Sander,J.D. (2012) TALENs: a widely applicable technology for targeted genome editing. *Nat. Rev. Mol. Cell Biol*., **14**, 49–55.
22. DeFrancesco,L. (2011) Move over ZFNs. *Nat. Biotechnol*., **29**, 681–684.
23. Zhang,F., Cong,L., Lodato,S., Kosuri,S., Church,G. and Arlotta,P. (2011) Efficient construction of sequence-specific TAL effectors for modulating mammalian transcription. *Nat. Biotechnol*., **29**, 149–153.
24. Morbitzer,R., Elsaesser,J., Hausner,J. and Lahaye,T. (2011) Assembly of custom TALE-type DNA binding domains by modular cloning. *Nucleic Acids Res*., **39**, 5790–5799.
25. Miller,J.C., Tan,S., Qiao,G., Barlow,K.A., Wang,J., Xia,D.F., Meng,X., Paschon,D.E., Leung,E., Hinkley,S.J. *et al*. (2011) A TALE nuclease architecture for efficient genome editing. *Nat. Biotechnol*., **29**, 143–148.
26. Mahfouz,M.M., Li,L., Piatek,M., Fang,X., Mansour,H., Bangarusamy,D.K. and Zhu,J.K. (2012) Targeted transcriptional repression using a chimeric TALE-SRDX repressor protein. *Plant Mol. Biol*., **78**, 311–321.
27. Bultmann,S., Morbitzer,R., Schmidt,C.S., Thanisch,K., Spada,F., Elsaesser,J., Lahaye,T. and Leonhardt,H. (2012) Targeted transcriptional activation of silent oct4 pluripotency gene by combining designer TALEs and inhibition of epigenetic modifiers. *Nucleic Acids Res*., **40**, 5368–5377.
28. Boch,J., Scholze,H., Schornack,S., Landgraf,A., Hahn,S., Kay,S., Lahaye,T., Nickstadt,A. and Bonas,U. (2009) Breaking the code of DNA binding specificity of TAL-type III effectors. *Science*, **326**, 1509–1512.
29. Moscou,M. and Bogdanove,A. (2009) A simple cipher governs DNA recognition by TAL effectors. *Science*, **326**, 1501.
30. Cermak,T., Doyle,E., Christian,M., Wang,L., Zhang,Y., Schmidt,C., Baller,J., Somia,N., Bogdanove,A. and Voytas,D. (2011) Efficient design and assembly of custom TALEN and other TAL effector-based constructs for DNA targeting. *Nucleic Acids Res*., **39**, 7879.
31. Mussolino,C., Morbitzer,R., Lutge,F., Dannemann,N., Lahaye,T. and Cathomen,T. (2011) A novel TALE nuclease scaffold enables high genome editing activity in combination with low toxicity. *Nucleic Acids Res*., **39**, 9283–9293.
32. Bogdanove,A.J. and Voytas,D.F. (2011) TAL effectors: customizable proteins for DNA targeting. *Science*, **333**, 1843–1846.
33. Martin,R.M. and Cardoso,M.C. (2010) Chromatin condensation modulates access and binding of nuclear proteins. *FASEB J*., **24**, 1066–1072.
34. Nielsen,A.L., Oulad-Abdelghani,M., Ortiz,J.A., Remboutsika,E., Chambon,P. and Losson,R. (2001) Heterochromatin formation in mammalian cells: interaction between histones and HP1 proteins. *Mol. Cell*, **7**, 729–739.
35. Sharif,J., Muto,M., Takebayashi,S., Suetake,I., Iwamatsu,A., Endo,T.A., Shinga,J., Mizutani-Koseki,Y., Toyoda,T., Okamura,K. *et al*. (2007) The SRA protein Np95 mediates epigenetic inheritance by recruiting Dnmt1 to methylated DNA. *Nature*, **450**, 908–912.
36. Mortusewicz,O., Rothbauer,U., Cardoso,M.C. and Leonhardt,H. (2006) Differential recruitment of DNA Ligase I and III to DNA repair sites. *Nucleic Acids Res*., **34**, 3523–3532.
37. Li,E., Bestor,T. and Jaenisch,R. (1992) Targeted mutation of the DNA methyltransferase gene results in embryonic lethality. *Cell*, **69**, 915–926.
38. Ying,Q.L., Wray,J., Nichols,J., Batlle-Morera,L., Doble,B., Woodgett,J., Cohen,P. and Smith,A. (2008) The ground state of embryonic stem cell self-renewal. *Nature*, **453**, 519–523.
39. Meilinger,D., Fellinger,K., Bultmann,S., Rothbauer,U., Bonapace,I., Klinkert,W., Spada,F. and Leonhardt,H. (2009) Np95 interacts with de novo DNA methyltransferases, Dnmt3a and Dnmt3b, and mediates epigenetic silencing of the viral CMV promoter in embryonic stem cells. *EMBO Rep*., **10**, 1259–1264.
40. Rothbauer,U., Zolghadr,K., Muyldermans,S., Schepers,A., Cardoso,M.C. and Leonhardt,H. (2008) A versatile nanotrap for biochemical and functional studies with fluorescent fusion proteins. *Mol. Cell Proteomics*, **7**, 282–289.
41. Solovei,I. and Cremer,M. (2010) 3D-FISH on cultured cells combined with immunostaining. *Methods Mol. Biol*., **659**, 117–126.
42. Ronneberger,O., Baddeley,D., Scheipl,F., Verveer,P.J., Burkhardt,H., Cremer,C., Fahrmeir,L., Cremer,T. and Joffe,B. (2008) Spatial quantitative analysis of fluorescently labeled nuclear structures: problems, methods, pitfalls. *Chromosome Res*., **16**, 523–562.
43. Walter,J., Joffe,B., Bolzer,A., Albiez,H., Benedetti,P.A., Muller,S., Speicher,M.R., Cremer,T., Cremer,M. and Solovei,I. (2006) Towards many colors in FISH on 3D-preserved interphase nuclei. *Cytogenet. Genome Res*., **114**, 367–378.
44. Schneider,K., Fuchs,C., Dobay,A., Rottach,A., Qin,W., Wolf,P., Alvarez-Castro,J.M., Nalaskowski,M.M., Kremmer,E., Schmid,V. *et al*. (2013) Dissection of cell cycle-dependent dynamics of Dnmt1 by FRAP and diffusion-coupled modeling. *Nucleic Acids Res*., **41**, 4860–4876.
45. Schermelleh,L., Haemmer,A., Spada,F., Rosing,N., Meilinger,D., Rothbauer,U., Cardoso,M.C. and Leonhardt,H. (2007) Dynamics

of Dnmt1 interaction with the replication machinery and its role in postreplicative maintenance of DNA methylation. *Nucleic Acids Res.*, **35**, 4301–4312.
46. Schindelin,J., Arganda-Carreras,I., Frise,E., Kaynig,V., Longair,M., Pietzsch,T., Preibisch,S., Rueden,C., Saalfeld,S., Schmid,B. *et al.* (2012) Fiji: an open-source platform for biological-image analysis. *Nat. Methods*, **9**, 676–682.
47. Vissel,B. and Choo,K.H. (1989) Mouse major (gamma) satellite DNA is highly conserved and organized into extremely long tandem arrays: implications for recombination between nonhomologous chromosomes. *Genomics*, **5**, 407–414.
48. Comings,D.E. (1980) Arrangement of chromatin in the nucleus. *Hum. Genet.*, **53**, 131–143.
49. Mateescu,B., England,P., Halgand,F., Yaniv,M. and Muchardt,C. (2004) Tethering of HP1 proteins to chromatin is relieved by phosphoacetylation of histone H3. *EMBO Rep.*, **5**, 490–496.
50. Leonhardt,H., Rahn,H.P., Weinzierl,P., Sporbert,A., Cremer,T., Zink,D. and Cardoso,M.C. (2000) Dynamics of DNA replication factories in living cells. *J. Cell Biol.*, **149**, 271–280.
51. Miyanari,Y., Ziegler-Birling,C. and Torres-Padilla,M.E. (2013) Live visualization of chromatin dynamics with fluorescent TALEs. *Nat. Struct. Mol. Biol.*, **20**, 1321–1324.
52. Deng,D., Yan,C., Pan,X., Mahfouz,M., Wang,J., Zhu,J.K., Shi,Y. and Yan,N. (2012) Structural basis for sequence-specific recognition of DNA by TAL effectors. *Science*, **335**, 720–723.
53. Ishikawa-Ankerhold,H.C., Ankerhold,R. and Drummen,G.P. (2012) Advanced fluorescence microscopy techniques–FRAP, FLIP, FLAP, FRET and FLIM. *Molecules*, **17**, 4047–4132.
54. Phair,R.D. and Misteli,T. (2001) Kinetic modelling approaches to in vivo imaging. *Nat. Rev. Mol. Cell Biol.*, **2**, 898–907.
55. Cole,N.B., Smith,C.L., Sciaky,N., Terasaki,M., Edidin,M. and Lippincott-Schwartz,J. (1996) Diffusional mobility of Golgi proteins in membranes of living cells. *Science*, **273**, 797–801.
56. Koster,M., Frahm,T. and Hauser,H. (2005) Nucleocytoplasmic shuttling revealed by FRAP and FLIP technologies. *Curr. Opin. Biotechnol.*, **16**, 28–34.
57. Meckler,J.F., Bhakta,M.S., Kim,M.S., Ovadia,R., Habrian,C.H., Zykovich,A., Yu,A., Lockwood,S.H., Morbitzer,R., Elsaesser,J. *et al.* (2013) Quantitative analysis of TALE-DNA interactions suggests polarity effects. *Nucleic Acids Res.*, **41**, 4118–4128.

Supplementary Figure 1: Nucleotide and amino acid sequence of the GFP-msTALE. The entire open reading frame of the fusion protein is shown: GFP is highlighted in green, repeat divariable residues (RVD) within each TALE repeat are highlighted in blue, purple, yellow and red for RVDs binding to the bases G, A, T and C, respectively. Single letter code is used for amino acids and nucleotide bases.

Supplementary Movie 1: Cell-cycle dependent distribution of GFP-msTALE. Live cell imaging of replicating stable GFP-msTALE cell line (green) cotransfected with RFP-PCNA (magenta).

Supplementary Figure 2: Expression of the stably integrated GFP-msTALE construct is relatively low compared to endogenous protein levels of major satellite associated proteins. Western blot showing protein levels of the GFP-msTALE, CenpB and Cbx1 in the stable GFP-msTALE ES cell line.

Supplementary Figure 3: Live cell imaging of GFP-msTALE together with chromatin associated proteins (A) Live cell imaging of replicating stable GFP-msTALE cell line (green) cotransfected with RFP-Cbx1 (magenta). (B) Live cell imaging of replicating stable GFP-msTALE cell line (green) cotransfected with RFP-Cbx5 (magenta). (C) Live cell imaging of replicating stable GFP-msTALE cell line (green) stably transfected with H2B-RFP (magenta). Arrowheads point towards one representative chromocenter. Scale bars: 5 µm.

Supplementary Figure 4: Comparative analysis of the dynamics of the GFP-msTALE , the PZF:GFP and GFP. (A) Representative FLIP experiments of the stable GFP-msTALE cell line and PZF:GFP (FLIP of the GFP-msTALE taken from Figure 3B for direct comparison). A rectangular region indicated by the dashed line was repeatedly bleached. Chromocenters in the unbleached half of the bleached cell (1) and in an unbleached reference cell (2) are highlighted. Continuous lines indicate the intensity measurement areas, whereas dashed lines indicate the bleached regions. Arrowheads point to the intensity measurement areas in the postbleach time points. These regions are magnified by a factor of four in the lower panels for both stable GFP-msTALE ESC line and the PZF:GFP. Scale bars: 5 µm (upper panels), 1 µm (lower panels). (B) Kinetic properties of GFP, GFP-msTALE and PZF:GFP analyzed by FRAP. N indicates the number of analyzed cells, *MF* the mobile fraction and $t_{1/2}$ the half time of recovery. Mean values ± standard deviation are listed.

Supplementary Figure 1

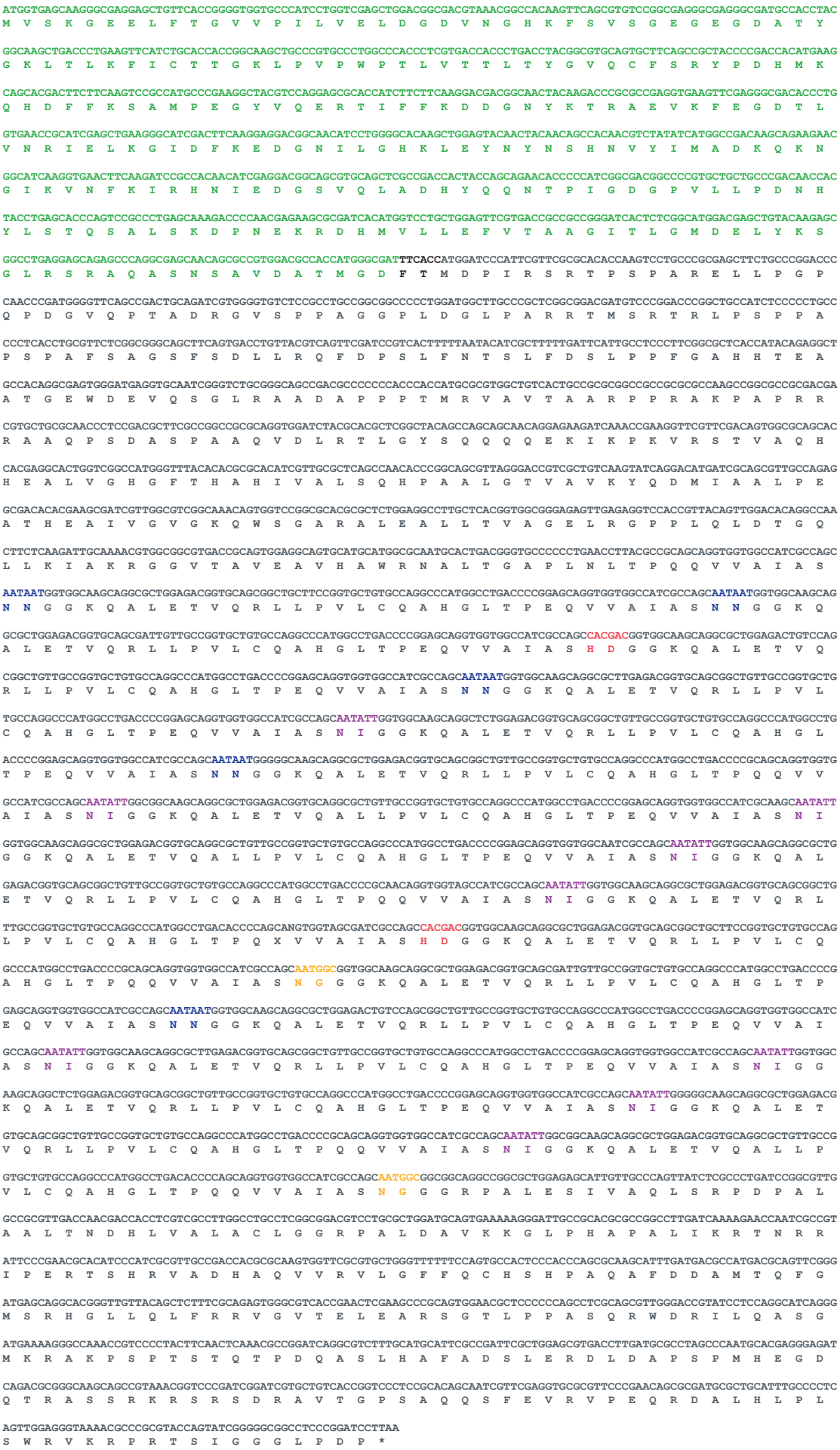

Supplementary Figure 2

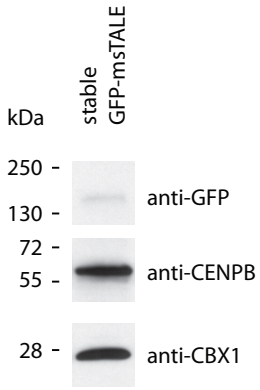

Supplementary Figure 3

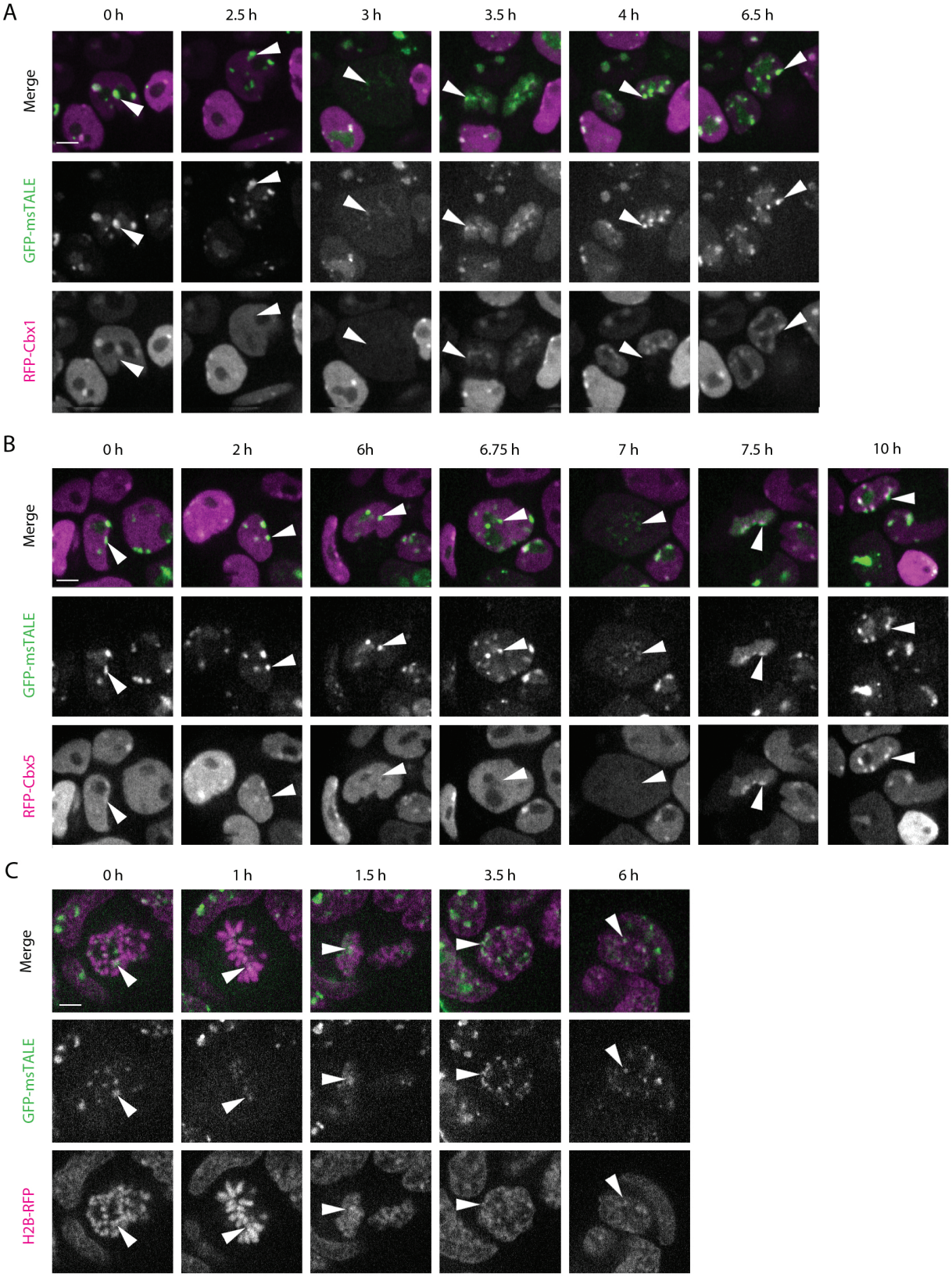

Supplementary Figure 4

A

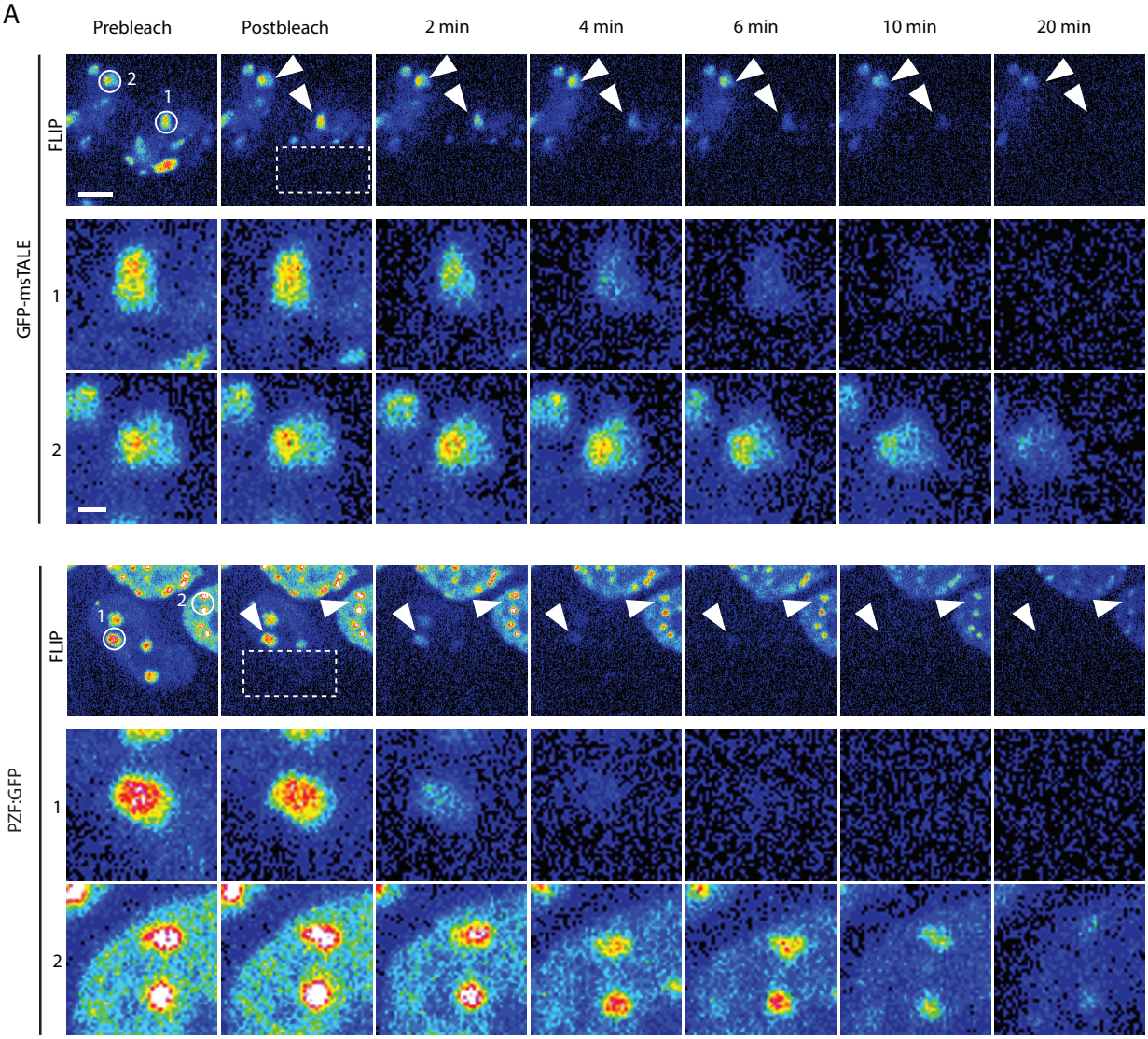

B

	N	*MF* [%] ± SD	$t_{1/2}$[s]
GFP	12	1.0±0.3	0.1±0.1
GFP-msTALE	14	0.7±0.1	77.8±21.2
PZF:GFP	12	1.0±0.1	6.9±3.5

2.3 Targeted manipulation of spatial heterochromatin arrangements

Katharina Thanisch, Irina Solovei and Heinrich Leonhardt

Abstract

The spatiotemporal organisation of chromatin is key to genome function and is dynamically remodelled during development and differentiation. Yet, the interrelationship of genome positioning and function remains largely unclear. Here, we employ fluorescently tagged designer transcription activator-like effectors (dTALEs) in combination with a GFP-nanotrap to manipulate the overall nuclear architecture by tethering chromocenters to the nuclear periphery. Artificial tethering results in disintegration of chromocenters and association of the major satellite repeats with the nuclear periphery in a patched pattern. Notably, forced subnuclear reposition of pericentromeric heterochromatin appears not to be essential for cellular proliferation and does not prevent myotube differentiation. Our results reveal the high plasticity of the nuclear architecture and indicate that pericentromeric heterochromatin is functionally not strictly dependent on its subnuclear positioning. This new model system provides a powerful means for studying cause and consequence relationship of spatial genome positioning and its function.

Introduction

Epigenetic control of gene expression is intimately linked to dynamic genome positioning. Globally, genomic arrangements are conserved among most cell types. Eu- and heterochromatin is spatially segregated in the nuclei (Misteli, 2007; Lieberman-Aiden et al., 2009) with the active euchromatin localised internally between the repressive perinuclear, perinucleolar and pericentromeric heterochromatin compartment (Guelen et al., 2008; Zhang et al., 2007).

Differential association with intranuclear compartments has been correlated to gene expression, as genes can dynamically position to or away from the nuclear periphery (Kosak et al., 2002; Williams et al., 2006; Takizawa et al., 2008; Jost et al., 2011; Peric-Hupkes et al., 2010) or chromocenters (CCs), clusters of pericentromeric major satellite repeats (ms-repeats) (Brown et al., 1997; 1999; Skok et al., 2001; Roldan et al., 2005; Merkenschlager et al., 2004; Clowney et al., 2012), depending on whether they are repressed or not. Likewise, artificial tethering to the nuclear lamina often suffices to repress transcription (Finlan et al., 2008; Reddy et al., 2008; Dialynas et al., 2010; Kumaran and Spector, 2008), while targeted activation correlates with release of lamina-associating domains (LADs) and internal gene reposition (Kind et al., 2013; Chuang et al., 2006; Dundr et al., 2007).

Large-scale changes in the nuclear architecture occur during development and differentiation (Probst et al., 2007; Solovei et al., 2004b; Brero et al., 2005; Solovei et al., 2009) and are connected to alterations in gene expression, epigenetic modifications and protein composition. In differentiating and postmitotic neurons, differential expression of chromatin-binding proteins facilitates the progressive clustering of pericentromeric regions (Brero et al., 2005; Clowney et al., 2012; Solovei et al., 2013), thereby driving the consolidation and further separation of the eu- and heterochromatic compartments (Gibcus and Dekker, 2013). In the extreme example of rod photoreceptor nuclei of nocturnal mammals, absence of the developmentally regulated tethers Lamin A/C and LBR causes nuclear inversion involving extensive chromatin remodelling with release of peripheral LADs and CC fusion (Solovei et al., 2009; 2013). Importantly, remodelling does not impede with transcriptional regulation, yet the hierarchical relationships between transcriptional activity, chromatin condensation and its spatial arrangements remain elusive.

Live cell approaches to spatiotemporally visualise the dynamics of genome remodelling have been limited until the recent advent of programmable DNA binding technologies (Lindhout et al., 2007; Miyanari et al., 2013; Ma et al., 2013; Thanisch et al., 2014; Chen et al., 2013; Anton et al., 2014). Here, we repurpose transcription activator-like effectors (TALEs) in combination with the GFP-nanotrap, a GFP-binding protein (GBP) fused to Lamin B1 (LB1) (Rothbauer et al., 2006) as a tool to perturb spatial heterochromatin arrangements and assess how ectopic CC reposition impacts on cellular function. We demonstrate that nuclear chromatin arrangements can be drastically altered by tethering CCs to the periphery without affecting cellular proliferation and differentiation.

Materials and methods

Plasmids

The GFP-msTALE, GFP-binding protein (GBP) N-terminally fused to LB1 (GBP-LB1) and H2B C-terminally fused to monomeric red fluorescent protein (H2B-mRFP) were described previously (Thanisch et al., 2014; Rothbauer et al., 2008; Martin and Cardoso, 2010). GBP-LB1-mRFP was generated by inserting the PCR-amplified LB1 from GBP-LB1 using EcoRV and BamHI endonucleases.

Cell culture, transfection and fluorescence-activated cell sorting

J1 ESCs were cultured as described previously (Thanisch et al., 2014). Pmi28 primary mouse myoblasts were cultured and differentiated as described previously (Kaufmann et al., 1999). For differentiation experiments, poly-L-lysine coated coverslips were used.

Transfections were performed using Lipofectamine 2000 (Invitrogen) according to the manufacturers instructions. Transgenic and double transgenic cell lines were generated as described previously (Thanisch et al., 2014). Fluorescence-activated cell sorting (FACS) was performed with an FACS Aria II (Becton Dickinson).

Immunofluorescence staining and FISH

Immunostaining and 3D-FISH were performed as described previously (Solovei and Cremer, 2010). In brief, cells cultured on coverslips were fixed for 10 min with 4% paraformaldehyde, washed with PBST (PBS, 0.01% Tween20) and permeabilised with 0.5% Triton X-100. Antibodies were diluted in blocking solution (PBST, 4% bovine serum albumin). For antigen detection, fixed and permeabilised cells were incubated with primary and secondary antibody solutions in dark, humid chambers for 1–2 h at room temperature. Following primary and secondary antibody detection, washings were performed with PBST. For immuno-FISH, antigen detection with both primary (anti-GFP) and secondary antibodies was performed first. Cells were post fixed with 4% paraformaldehyde and pre-treated for hybridisation. Hybridisation was performed for 2 days at 37°C. Post hybridisation washings were carried out with 2 x Saline Sodium Citrate (SSC) at 37°C and 0.1 x SSC at 61°C (Solovei and Cremer, 2010). The FISH probe for ms repeat detection was generated by polymerase chain reaction using mouse Cot1 DNA (Invitrogen) as a template and the primers 5'-GCG AGA AAA CTG AAA ATC AC-3' and 5'-TCA AGT CGT CAA GTG GAT G-3'. The probe was directly labelled with Cy3-dUTP by nick-translation, and dissolved in hybridisation mixture (50% formamide, 10% dextran sulfate, 1 x SSC) at a concentration of 10–20 ng/ml. Nuclear DNA counterstaining was performed by adding DAPI to the secondary antibody solution (final concentration 2mg/ml). Coverslips were mounted in Vectashield antifade (Vector Laboratories) and sealed with colourless nail polish.

Primary antibodies used in this study: anti-GFP (Roche, 11814460001), anti-lamin B1 (Santa Cruz Biotechnology, sc-6217), anti-Nup153 (Abcam, ab24700), anti-nucleophosmin (B23, Sigma-Aldrich, B0556), anti-kinetochores (Euroimmun AG, CA 1611-0101) and anti-H4K20me3 (Abcam, ab9053). The secondary antibodies were anti-rabbit conjugated to DyLight fluorophor 649 (Jackson ImmunoResearch, 711-496-152), anti-mouse conjugated to Alexa 555 and 647 (Invitrogen, A31570 and A31571), anti-goat conjugated to Cy3 (Jackson ImmunoResearch, 705-166-147) and anti-human conjugated to Cy3 (Jackson ImmunoResearch, 309-165-003). For 3D-SIM, cells were grown on precision coverslips, thickness no. 1.5H (170 µm ± 5 µm, Marienfeld Superior) using immersion oil with a

refractive index of 1.514 to minimise spherical aberration.

Microscopy and image acquisition

For confocal microscopy, single optical sections or stacks of optical sections were acquired on a Leica TCS SP5 confocal microscope equipped with a Plan Apo 63x / 1.4 NA oil immersion objective and lasers with excitation lines 405, 488, 561 and 633 nm. ImageJ plugins were used to compensate for axial chromatic shift between fluorophores in confocal stacks, create RGB images/stacks and arrange them into galleries (Ronneberger et al., 2008; Walter et al., 2006).

High-resolution 3D-SIM microscopy was performed as described previously (Schermelleh et al., 2008) and a DeltaVision OMX V3 3D-SIM microscope (Applied Precision Imaging, GE Healthcare) equipped with a 60×/1.42 NA PlanApo oil objective and sCMOS cameras (Olympus). Images were obtained with a z-step size of 125 nm. Reconstruction and image deconvolution was applied to the SI raw data using the SoftWorX 4.0 software package (Applied Precision).

Live cell imaging was performed on an UltraVIEW VoX spinning disc microscope (PerkinElmer) as described before (Schneider et al., 2013). In long-term imaging, a z-stack of 13.5 mm with a step size of 1.5 µm was recorded every 15 min for approx. 24 h. To minimise photo damage of the cells, the acousto-optic tunable filter (AOTF) of the laser was adjusted to low transmission values (6–10%).

Results and Discussion

Development of a sequence-specific tool for targeted manipulation of chromatin positioning

Our method of targeted reposition of genomic loci is based on programmable sequence-specific DNA recognition by dTALEs in combination with the high affinity binding of chromobodies (Boch et al., 2009; Moscou and Bogdanove, 2009; Rothbauer et al., 2006). To explore whether CCs can be immobilised at the nuclear periphery, we employed a GFP-msTALE, targeted against the ms-repeats (Thanisch et al., 2014) (Figure 1b), together with the GFP-nanotrap, a GFP-binding protein (GBP) fused to the nuclear lamina component Lamin B1 (LB1) (Rothbauer et al., 2006) (Figure 1c). CCs are spherical bodies formed by blocks of pericentromeric ms-repeats (Figure 1a), which can be readily revealed by their intense 4',6-diaminidino-phenolindole (DAPI) staining. Their high copy number and distinct

subnuclear localisation at the nuclear periphery and the margins of the nucleoli makes them an ideal model system for targeted manipulation of the chromatin organisation.

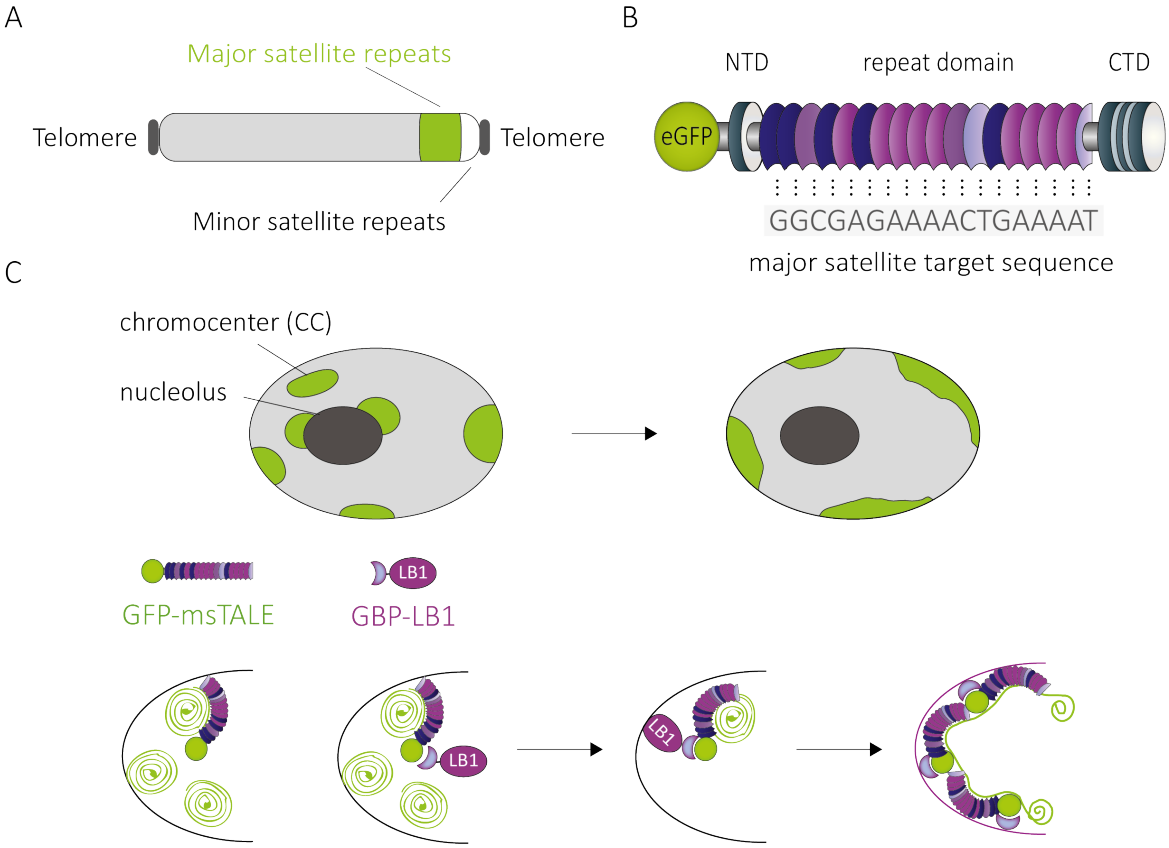

Figure 1: Visualisation and repositioning of the major satellite repeats. (A) Cartoon of a murine acrocentric chromosome with telomeres (black), minor satellite repeats (white), major satellite (ms) repeats (green) and the long arm of the chromosome (grey). (B) Schematic representation of the GFP-msTALE aligned to its DNA target site within the ms-repeat. The GFP-msTALE is subdivised in an N-terminal domain (NTD), a central DNA binding repeat domain and a C-terminal domain (CTD) comprising nuclear localisation sequences. For visualisation and manipulation, the TALE is N-terminally fused to GFP. (C) Model for TALE-mediated tethering of the chromocenters to the periphery. The chromocenters (CCs, green), focal structures of clustered ms-repeats, are highlighted by the GFP-msTALE. Upon expression of the GFP-nanotrap, a GFP-binding nanobody (GBP) fused to the nuclear lamina protein LaminB1 (GBP-LB1), CCs are ectopically repositioned to the periphery.

Indeed, ectopic tethering drastically changed the chromatin distribution with the disappearance of DAPI-stained spherical CCs and an increase in peripheral heterochromatin (Figure 2, DAPI staining). These results are similar to those observed for peripheral tethering of ms-repeats in early developing embryos, where ms-repeats are not yet forming CCs (Jachowicz et al., 2013).

To explore the degree of nuclear reorganisation, we assessed the relation of ectopically tethered CCs to nuclear structures and histone modifications by immunostainings. Staining against LB1 revealed that CCs highlighted by the GFP-msTALE colocalised with the nuclear lamina and were smeared beneath the nuclear envelope (Figure 2, A). Strikingly, increased peripheral heterochromatin association did not affect the nuclear lamina, as no changes in LB1 distribution were observed (Figure 2, A).

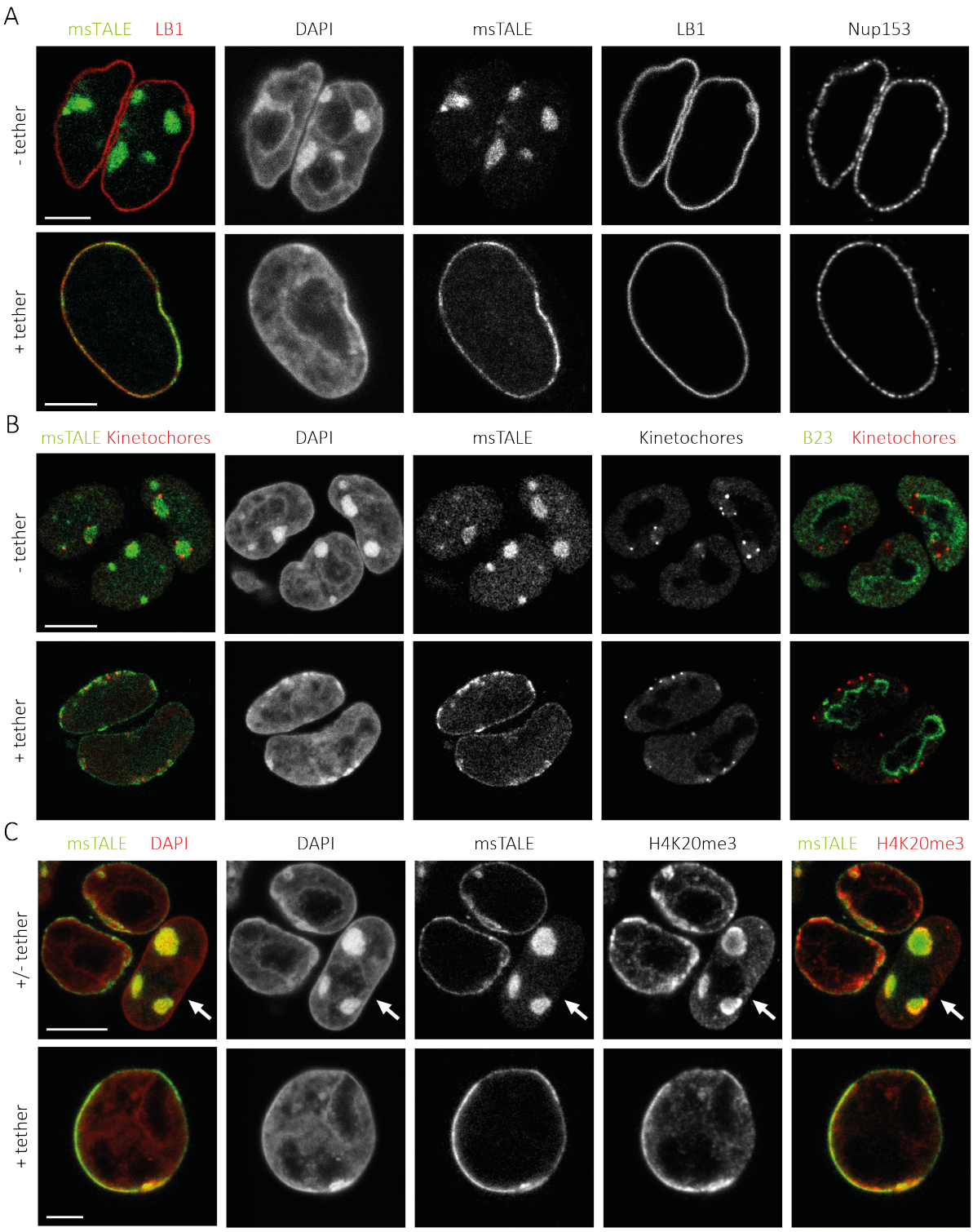

Figure 2: Chromocenter positioning in relation to nuclear structures and histone marks. Immunostaining of murine ESCs stably expressing the GFP-msTALE with and without GBP-LB1 (+/- tether, upper and lower panels, respectively). (A-B) CCs marked by the GFP-msTALE show a characteristic perinuclear (anti-LB1, red) and perinucleolar (anti-B23, red) localisation (upper panels). (A) Upon tethering, CCs appear as flat structures squashed against the periphery (anti-LB1, red). Nuclear pore distribution is not affected (anti-Nup153). (B) Upon tethering, nucleoli follow the repositioned CCs (anti-B23, red). Kinetochores cluster at the surface of the CCs irrespective of the subnuclear positioning (anti-CREST, red, upper and lower panels) (C) Antibodies against heterochromatin (anti-H4K20me3) highlight spherical (upper panel, nuclei marked by arrows) and peripherally tethered CCs (msTALE). Scale bars: A, 5µm; B, 10µm; C, 10 for upper and 5 µm for lower panels.

Similarly, nuclear pores, which are surrounded by a transcriptionally permissive microenvironment in yeast (Schmid et al., 2006; Taddei et al., 2006) and have been reported to be excluded from sites of peripherally tethered integrated reporters (Reddy et al., 2008), were not redistributed by ectopic CC tethering (Figure 1, A). While some genes albeit their positioning at the nuclear periphery have been reported to retain their transcriptional competence (Hewitt et al., 2004; Kim et al., 2004), it still remains unclear whether a similar active domain is found around nuclear pores in the metazoan system (Akhtar and Gasser, 2007).

We next analysed the consequences of peripheral CC tethering on nucleoli and centromere distribution. In control nuclei, CCs adjoin multiple nucleoli and proximal centromeres cluster on the surface of the CCs as revealed by staining against the nucleolar marker B23 and kinetochores (Figure 2B, upper panel). Upon tethering, focal CC enrichment at the nucleoli is abrogated (Figure 2B, lower panel). However, we observe an increased fusion of nucleoli to form large nucleoli, which tend to tightly associate with the nuclear periphery (Figure 2B, lower panel). Similarly, centromere clusters persist at the surface of the CCs irrespective of their subnuclear localisation and flattened appearance (Figure 2B, lower panel).

H3K40me3, a histone posttranslational modification specific for constitutive heterochromatin usually enriched at the nuclear periphery and CCs, was found exclusively peripheral following ectopic tethering (Figure 2, C). Importantly, the histone modification pattern at the periphery was unaffected suggesting that peripheral association of CCs does not alter the chromatin modification state of the heterochromatic compartment.

To directly analyse the extent of reposition and the organisation of the tethered CCs, we performed 3D-immuno-FISH.

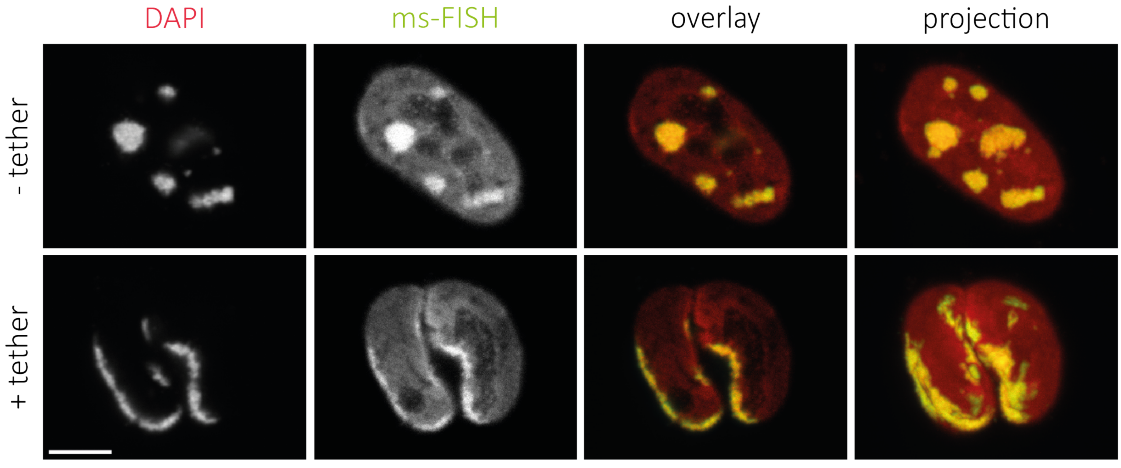

Figure 3: Chromocenter positioning in normal and tethered nuclei. 3D-immuno-FISH with a probe directed against the ms-repeats (green). DAPI counterstain (red). Single confocal sections and maximum intensity projections. Scale bar: 5 µm.

To further characterise the fine-structure of the tethered CCs, we performed superresolution three-dimensional (3D) structured illumination microscopy (3D-SIM), which enables subdiffraction visualisation of nuclear structures (Schermelleh et al., 2008).

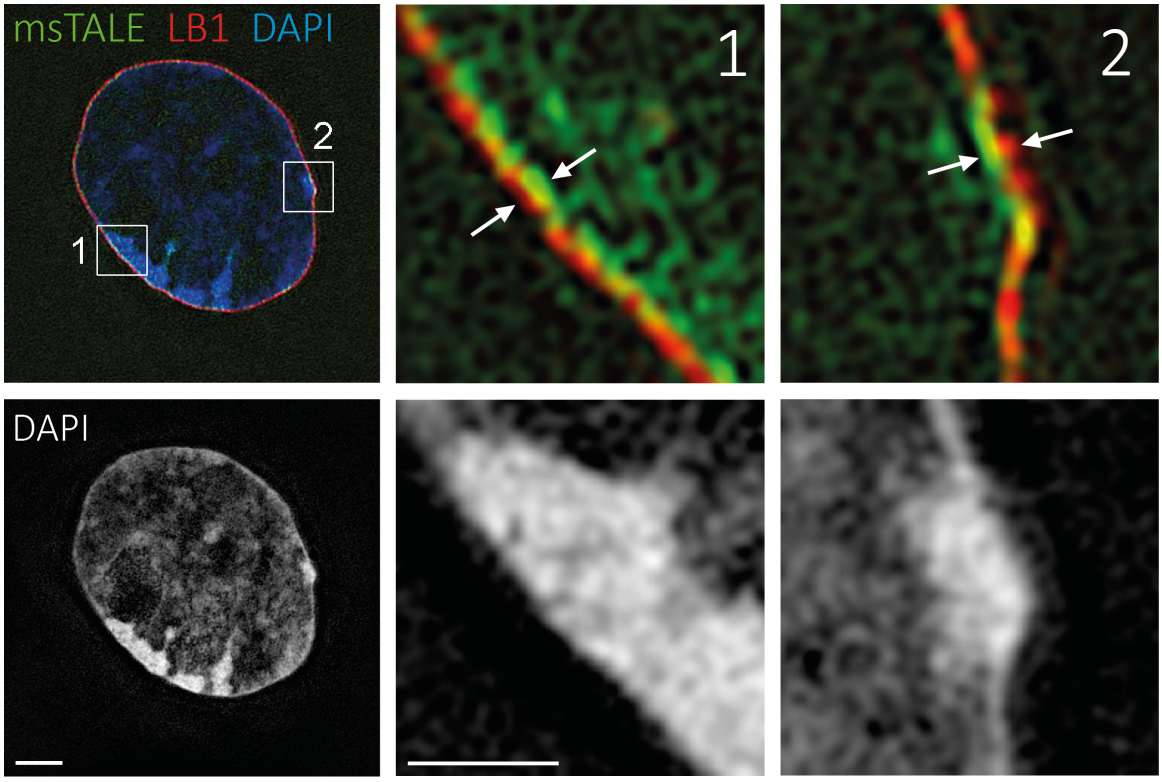

Figure 4: 3D-SIM highlights the fine-structure of peripherally tethered chromocenters. Mid z-section of a GFP-msTALE (green) and GBP-Lb1 coexpressing murine ESC. Immunostaining with an anti-LB1 antibody (red). DAPI counterstain (upper panel: blue, lower panel: grey). Eightfold magnification of boxed areas reveal a patch-like pattern of peripherally associated CCs. Scale bars: 5 µm; magnification: 1 µm.

Indeed, superresolution imaging confirmed the patched pattern of CCs upon peripheral tethering (Figure 4). Although CC structure is compromised, associations between ms-repeats persist at least partially, as the structures retain a three-dimensional shape (Figure 4, magnifications). Most likely, this stems from an inherent self-association of highly repetitive sequences supported by chromatin-binding proteins (e.g. MeCP2 (Brero et al., 2005), HP1 (Maison and Almouzni, 2004)), architectural proteins (e.g. Cohesin, CTCF (Parelho et al., 2008; Rubio et al., 2008; Wendt et al., 2008)) or chromatin modifiers (e.g. histone methyltransferases (HMTs) (Peters et al., 2001; Pinheiro et al., 2012; Hahn et al., 2013).

Consistently, knock-out of the H3K9me1-specific HMTs Prdm (PRDI-BF1 and RIZ homology domain containing protein) 3 and Prdm6 HMTs resulted in complete disruption of ms-repeat association along with peripheral relocalisation and a compromised nuclear lamina (Pinheiro et al., 2012). Instead reposition alone, as mediated by the TALE together with the GBP-LB1, does not result in extensive nuclear remodelling. Together, these results

indicate that our targeted recruitment system enables study of specific genomic loci and associated proteins at a different subnuclear context while preserving its epigenetic regulation and leaving other subnuclear structures, such as nucleoli and the nuclear lamina unaffected.

Peripheral chromocenter tethering is compatible with normal cellular proliferation

Given that artificial tethering of ms-repeats in early developing embryos is restricted to the 2-cell stage prior to CC formation and drastically interferes with subsequent cellular divisions (Jachowicz et al., 2013), we were prompted to investigate whether peripheral CC association can be established and maintained in ESCs.

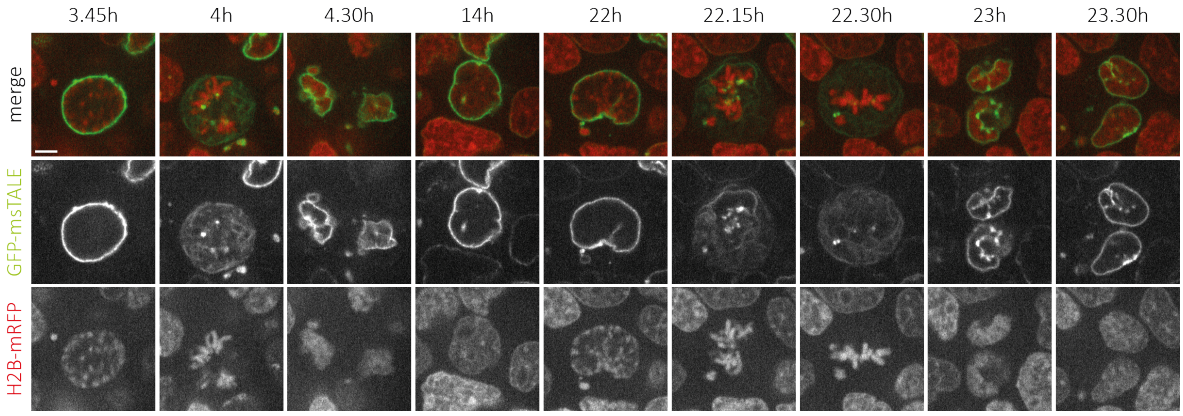

Figure 5: Peripheral lamina-association of CCs is maintain over consecutive cell cycles. Live cell imaging of peripheral CC tethering. CCs are highlighted by the GFP-msTALE (green) and recruited to the periphery by GBP-LB1. Bulk chromatin is visualised by H2B-mRFP. Scale bar: 5 µm.

Using live cell imaging, we followed the dynamics of CC tethering in ESCs stably coexpressing the GFP-msTALE and H2B-RFP (Thanisch et al., 2014), which were additionally transfected with the GFP-nanotrap (Figure 5, Supplemental video 1). During interphase, CCs are stably attached to the periphery due to presence of the GFP-nanotrap, whereas upon nuclear envelope breakdown and lamina dissociation, tethering is released. With the reassembling of the nuclear lamina at anaphase to telophase transition, peripheral lamina-association is re-established. Importantly, peripheral tethering did not interfere with cellular division in rapidly cycling ESCs and was maintained over consecutive cell cycles.

Consistent with previous findings for tethering of integrated reporters and LAD establishment, peripheral CC tethering depends on passage through mitosis and follows the dynamics of LB1 incorporation in late anaphase (Figure 6, Supplemental video 2). Importantly, these finding are consistent with previous results, demonstrating that peripheral tethering of test genes and LAD establishment depends on passage through mitosis (Reddy et al., 2008; Kumaran and Spector, 2008; Zullo et al., 2012; Kind et al., 2013).

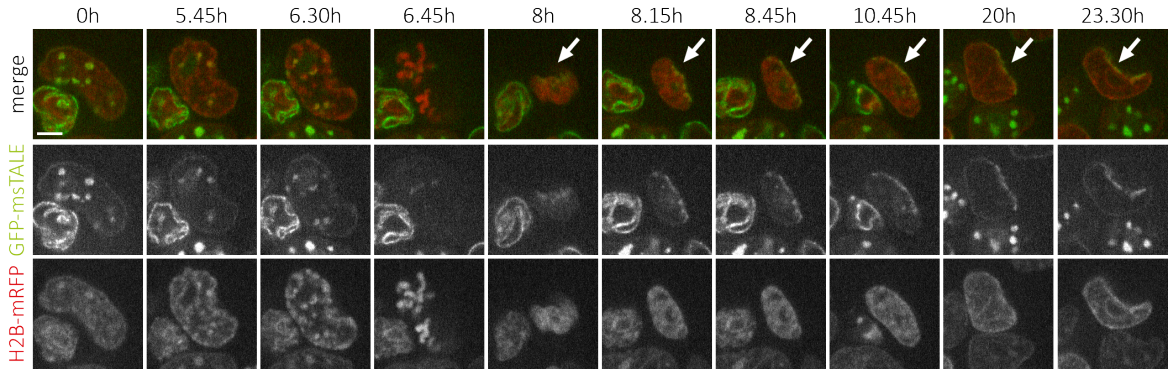

Figure 6: Peripheral lamina-association of CCs requires passage through mitosis. Live cell imaging of peripheral CC targeting. CCs are highlighted by the GFP-msTALE (green) and peripherally recruited by GBP-LB1. Prior to mitosis, CCs exhibit a characteristic spherical shape with a distinct subnuclear distribution at the boarders of the nucleoli and next to the periphery. Peripheral lamina-association is established during mitosis with the targeted recruitment of LB1 in late anaphase (8h timepoint). Arrows point to peripherally deposited CCs. Bulk chromatin is visualised by H2B-mRFP. Scale bar: 5 µm.

Moreover, we generated a bitransgenic ESC line, stably coexpressing GFP-msTALE and GFP-nanotrap, thereby directly demonstrating that stable CCs tethering can be maintained. Together, our results demonstrate, that CCs can be repositioned in ESCs and suggest that cellular proliferation is independent of subnuclear CC positioning.

Peripheral chromocenter tethering does not prevent cell differentiation

During cellular proliferation, CCs are reformed following each cell cycle, whereas extensive CCs fusion is a key characteristic of the profound changes in nuclear architecture observed during terminal differentiation of e.g. postmitotic neurons or myoblasts (Manuelidis, 1984; Solovei et al., 2004b; Brero et al., 2005; Solovei et al., 2009).

To address whether myoblasts with peripherally tethered CCs retain the potential to differentiate into myotubes, we first generated a Pmi28 cell line stably expressing the GFP-msTALE, which we transiently transfected with the GFP-nanotrap and subjected to *in vitro* differentiation. Additionally, H2B-mRFP was cotransfected as a reliable marker for transfection. Untransfected control nuclei, which underwent myotube differentiation showed a reduced number in CC foci of increased size indicating ongoing CC fusion (Figure 7, compare upper and lower panels). Notably, 65% of H2B-mRPF transfected myotubes completely lost CCs and revealed instead a peripheral rim of ms-repeats. This suggests that myotubes can still be formed irrespective of the subnuclear positioning of pericentromeric heterochromatin.

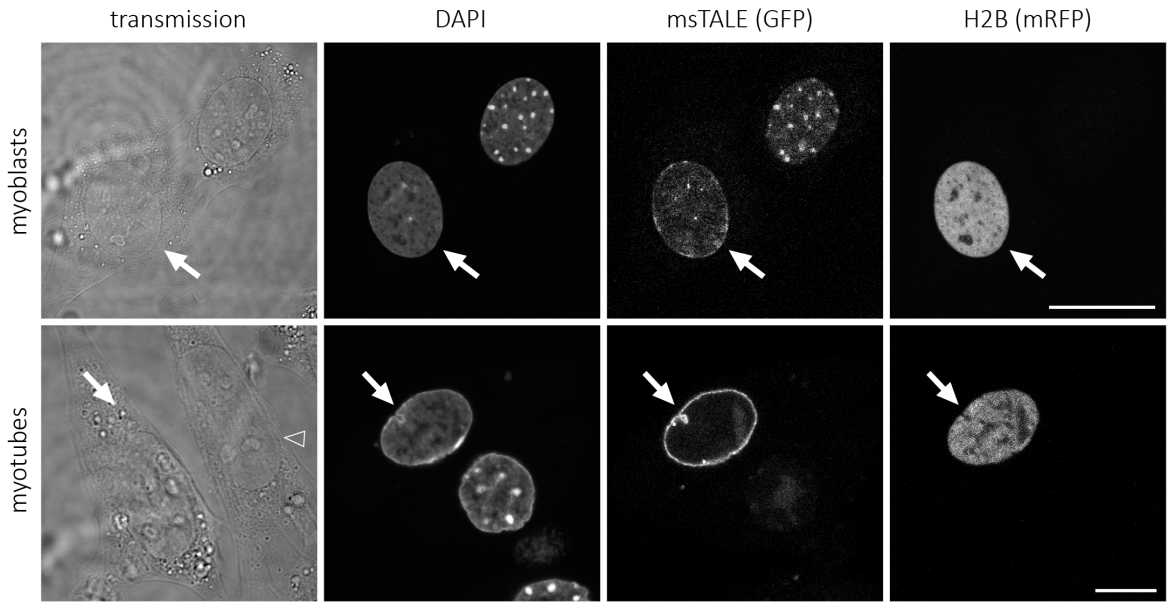

Figure 7: Peripheral chromocenter tethering does not prevent myotube differentiation. Cultured Pmi28 myoblasts stably expressing GFP-msTALE were cotransfected with GBP-LB1 and H2B-mRFP and *in vitro* differentiated into myotubes. Nuclei of myoblasts and myotubes were distinguished based on their appearance in transmission light. Myoblasts have very flat cytoplasm and nuclei. Differentiating myoblasts and myotubes are spindle shaped, their cytoplasm and nuclei become more voluminous, nuclei have smaller diameter. As a consequence of increased volume, nuclei of myotubes position well above the substrate. In addition, mature myotubes have multiple nuclei arranged linearly in the middle of the elongated tube-shaped cytoplasm. The upper panel shows two myoblast nuclei, one untransfected with normally formed CCs and the transfected one with CCs tethered to the nuclear periphery. The nucleoplasm in the transfected cell is marked by expression of H2B-mRFP (arrow). The lower panel shows two nuclei in a young myotube, one with normally formed CCs clearly visible by DAPI staining and one with peripherally tethered CCs (arrow). The latter nucleus was transfected (marked by H2B-mRFP expression, arrow) before fusion into the myotubes. Note that both myotube nuclei position well above the nuclei of a nearby myoblast, which is flattened on the substrate (arrowhead). DAPI counterstain. Optical confocal sections. Scale bars: 25 µm for upper and 10 µm for lower panels.

In summary, we demonstrate a high plasticity of spatial heterochromatin arrangements, as forced pericentromeric heterochromatin reposition to the nuclear periphery is compatible with cellular proliferation and differentiation. With the example of ectopic peripheral CC tethering, we show that by combining sequence-specific TALE-based recognition of genomic loci with the high affinity of the GFP-nanotrap, genomic loci can be repositioned to the nuclear periphery. As the GBP can be fused to distinctly subnuclear localised proteins, we present a versatile two-component system enabling for the targeted recruitment of genomic loci to defined subnuclear structures (Herce et al., 2013) and study of the interrelationship between genome positioning and transcriptional activity.

2.4 LBR and Lamin A/C sequentially tether heterochromatin and inversely regulate differentiation

Cell

LBR and Lamin A/C Sequentially Tether Peripheral Heterochromatin and Inversely Regulate Differentiation

Irina Solovei,[1] Audrey S. Wang,[2,3] Katharina Thanisch,[1] Christine S. Schmidt,[1] Stefan Krebs,[4] Monika Zwerger,[5] Tatiana V. Cohen,[6] Didier Devys,[7] Roland Foisner,[8] Leo Peichl,[9] Harald Herrmann,[5] Helmut Blum,[4] Dieter Engelkamp,[10] Colin L. Stewart,[2,3,*] Heinrich Leonhardt,[1,*] and Boris Joffe[1,*]

[1]Department of Biology II, Center for Integrated Protein Science Munich (CIPSM), Ludwig-Maximilians University Munich, Grosshadernerstrasse 2, 82152 Planegg-Martinsried, Germany
[2]Institute of Medical Biology, 8A Biomedical Grove, Singapore 138648, Republic of Singapore
[3]Department of Biological Sciences, National University of Singapore, Singapore 117543, Republic of Singapore
[4]Laboratory for Functional Genome Analysis (LAFUGA), Gene Center Munich, Ludwig-Maximilians University Munich, Feodor-Lynen-Strasse 25, 81377 Munich, Germany
[5]Department of Molecular Genetics, B065, German Cancer Research Center (DKFC), 69120 Heidelberg, Germany
[6]Children's National Medical Center, Center for Genetic Medicine, 111 Michigan Avenue, Washington, DC 20010-2970, USA
[7]Institut de Génétique et de Biologie Moléculaire et Cellulaire, CNRS UMR 7104, INSERM U 964, Université de Strasbourg, 67404 Illkirch, France
[8]Max F. Perutz Laboratories, Medical University of Vienna, Dr. Bohr-Gasse 9, 1030 Vienna, Austria
[9]Max Planck Institute for Brain Research, Deutschordenstrasse 46, 60528 Frankfurt am Main, Germany
[10]Transgenic Service Facility, BTE, Franz-Penzoldt-Centre, Friedrich-Alexander-University of Erlangen-Nürnberg, Erwin-Rommel-Strasse 3, 91058 Erlangen, Germany
*Correspondence: colin.stewart@imb.a-star.edu.sg (C.L.S.), h.leonhardt@lmu.de (H.L.), boris.joffe@lmu.de (B.J.)
http://dx.doi.org/10.1016/j.cell.2013.01.009

SUMMARY

Eukaryotic cells have a layer of heterochromatin at the nuclear periphery. To investigate mechanisms regulating chromatin distribution, we analyzed heterochromatin organization in different tissues and species, including mice with mutations in the lamin B receptor (*Lbr*) and lamin A (*Lmna*) genes that encode nuclear envelope (NE) proteins. We identified LBR- and lamin-A/C-dependent mechanisms tethering heterochromatin to the NE. The two tethers are sequentially used during cellular differentiation and development: first the LBR- and then the lamin-A/C-dependent tether. The absence of both LBR and lamin A/C leads to loss of peripheral heterochromatin and an inverted architecture with heterochromatin localizing to the nuclear interior. Myoblast transcriptome analyses indicated that selective disruption of the LBR- or lamin-A-dependent heterochromatin tethers have opposite effects on muscle gene expression, either increasing or decreasing, respectively. These results show how changes in NE composition contribute to regulating heterochromatin positioning, gene expression, and cellular differentiation during development.

INTRODUCTION

The nuclear localization of chromatin regions is highly ordered and plays an important role in the functional organization of the nucleus (Cremer and Cremer, 2010). The vast majority of eukaryotic nuclei display a conventional nuclear architecture with euchromatin predominantly occupying internal nuclear regions, whereas heterochromatin primarily underlies the nuclear envelope (NE) between the nuclear pores and around the nucleolus. Although the NE, which also includes the nuclear lamina underlying the inner nuclear membrane (INM), is regarded as a silencing compartment, recent studies expanded its role to a number of other cardinal biological processes, both in and outside the nucleus (Brachner and Foisner, 2011). Mutations in lamins and proteins associated with the NE cause a number of severe diseases (collectively named laminopathies) affecting diverse tissues and organ systems (Worman et al., 2010).

Targeting genes to the nuclear lamina and peripheral heterochromatin can strongly affect transcription (Deniaud and Bickmore, 2009). A growing body of evidence from *Drosophila* and *C. elegans* indicates that integrity of the lamina is indispensable for correctly positioning genes in the nucleus and regulating their transcriptional status (Mattout et al., 2011; Towbin et al., 2010). However, this does not explain the maintenance of peripheral heterochromatin in mammals because release of heterochromatin from the NE is not observed by the absence of either the A- or B-type lamins (Coffinier et al., 2011; Kim et al., 2011; Kubben et al., 2011; Sullivan et al., 1999; Yang et al., 2011).

A unique exception to chromatin organization in eukaryotes is found in rod photoreceptor cells of nocturnal mammals (Solovei et al., 2009). To reduce light loss in the retina (which is crucial for nocturnal vision), the positions of eu- and heterochromatin in their nuclei are inverted (Figure 1A). Euchromatin is predominately juxtaposed to the NE with only small islands of heterochromatin present at the periphery (Kizilyaprak et al., 2011;

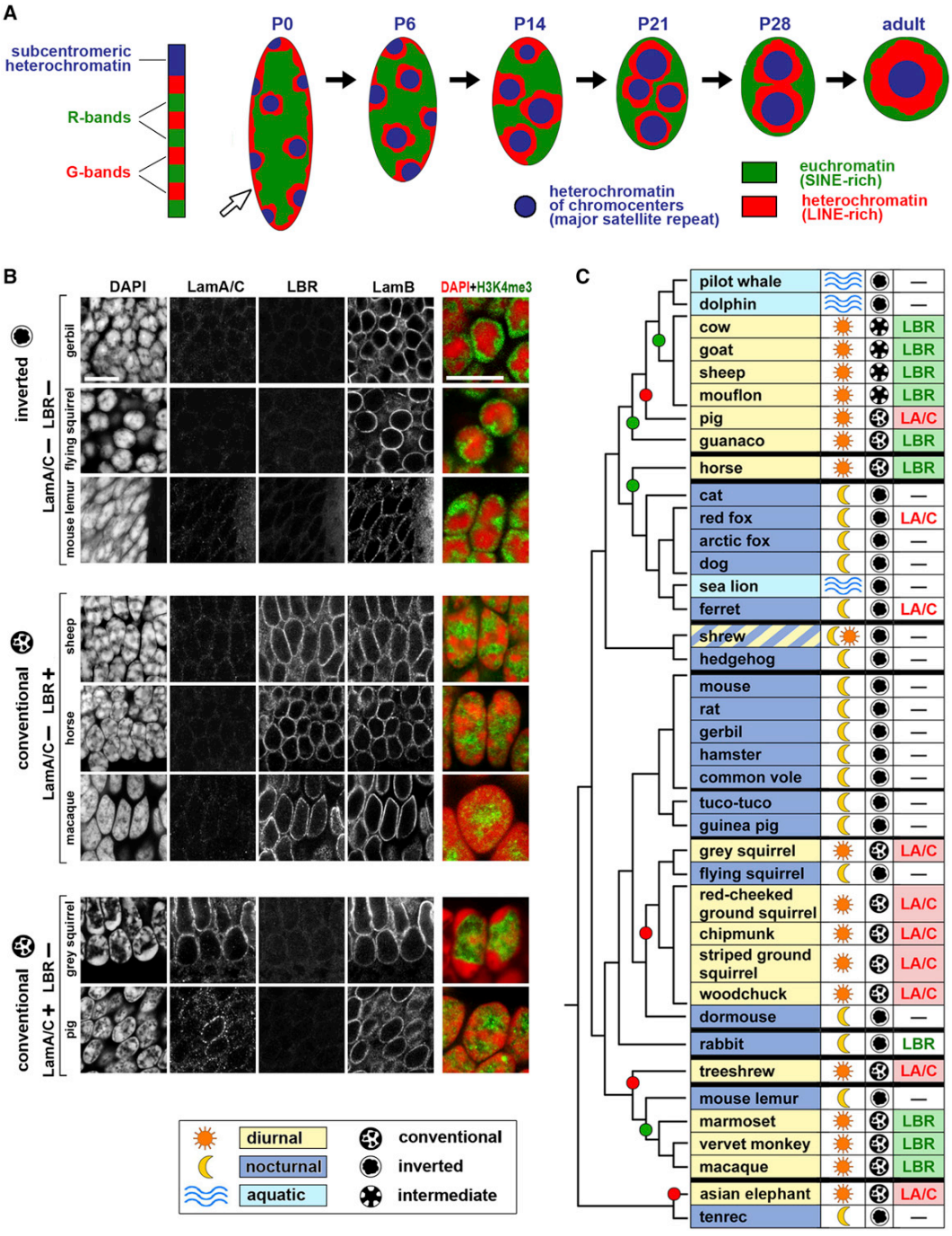

Figure 1. Correlation of Nuclear Architecture with Expression of LBR and LamA/C in Rod Cell Nuclei of Mammals

(A) Position of the main chromatin classes in mouse chromosomes (left) and during rod nuclei differentiation (right) (modified from Solovei et al., 2009). Initially, rod cells have a conventional nuclear architecture—most chromocenters abut the NE, and there is a layer of peripheral heterochromatin (empty arrow). During rod cell maturation, heterochromatin is released from the NE; slow remodeling (about 1 month) results in inversion of the positions of the three main chromatin classes.

(B) Expression of LBR, LamA/C, and lamin B in the rod nuclei of representative mammalian species. The right column shows rod nuclei of these species after euchromatin (green) and DAPI (red) staining.

(C) Phylogenetic distribution of LBR and LamA/C in rod nuclei of mammals. Bullets show reacquisition of LBR (green) and LamA/C (red). Note three exceptions (rabbit, red fox, and ferret). See Extended Experimental Procedures section for full scientific names of the species. Bar, 10 μm.

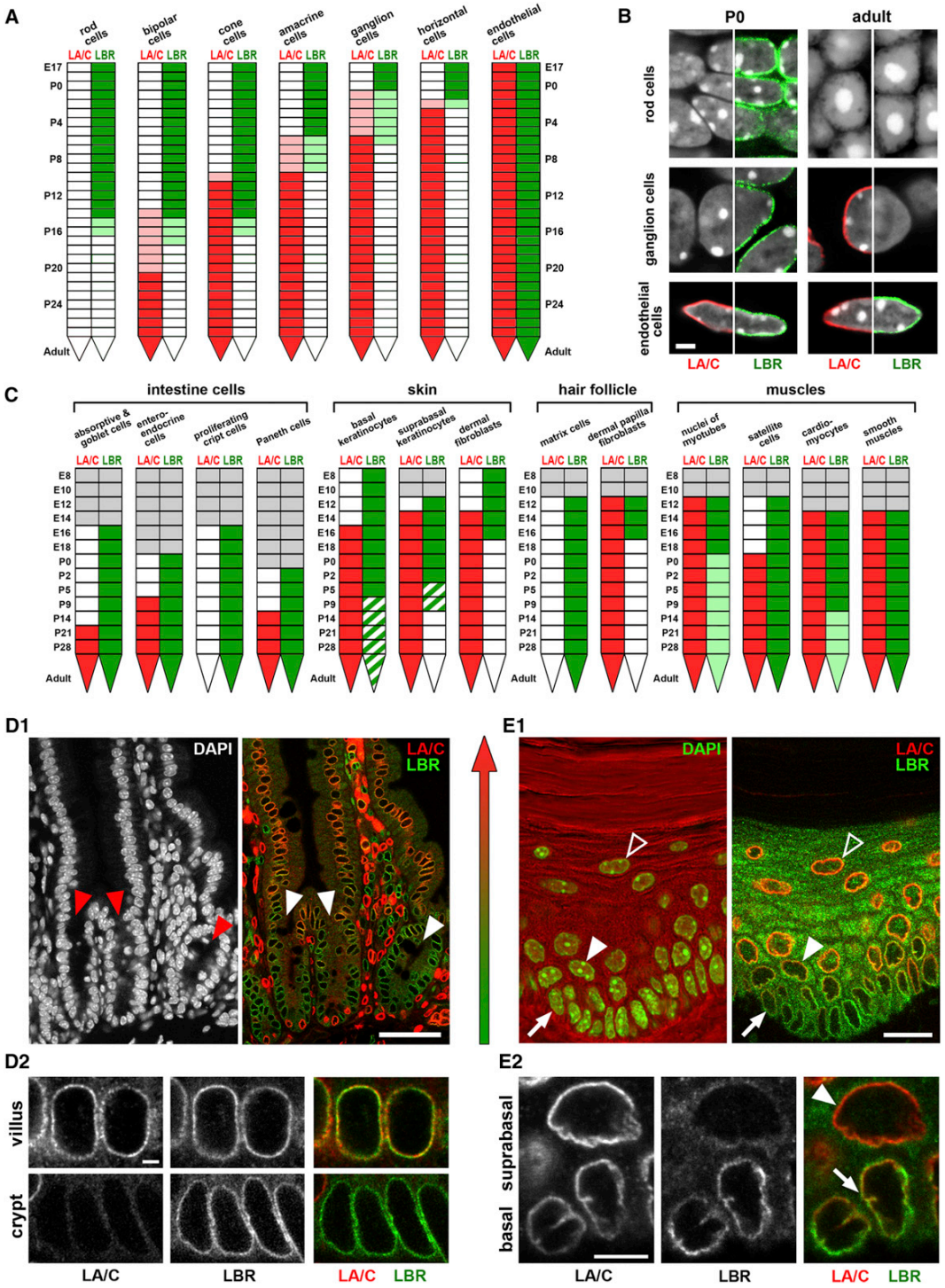

Figure 2. Coordinated Expression of LBR and LamA/C in WT Mice

In all panels, LBR is shown in green, and lamA/C (LA/C) is shown in red.

(A–C) Temporal coordination in retinal (A and B) and nonretinal (C) cell types. The stages at which a cell type cannot be identified are shown in gray; initial low lamA/C expression level is shown in pink, and light green marks a very low residual LBR level; hatched pattern symbolizes variation between nuclei in mixed populations (see Results, section "Expression of Lamin A/C and LBR Is Temporarily Coordinated: LBR Precedes LamA/C during Nuclear Differentiation").

(legend continued on next page)

Solovei et al., 2009). The inverted state develops postmitotically from a conventional one by a slow remodeling process lasting several weeks (Figure 1A). Inversion does not affect the high transcriptional activity of mammalian rods, which justifies their value as a model of spatial organization of mammalian nuclei in general.

We reasoned that the redistribution of peripheral heterochromatin in rod nuclei and its maintenance in other cells likely depend on the same mechanism, which we set out to decipher. Here, we show that, in mammals, there are two mechanisms tethering peripheral heterochromatin to the NE, an LBR-dependent mechanism and a lamin-A/C-dependent mechanism. They are used at early and late stages of differentiation, respectively, and have opposite effects on the expression of tissue-specific genes.

RESULTS

A preliminary immunohistochemical analysis of mouse retinas for a number of peripheral nuclear proteins in differentiated rod cells revealed a surprising coabsence of two predominant NE proteins, lamins A/C (LamA/C) and LBR. From our own and published data, it was clear that a lack of either LamA/C or LBR alone was insufficient for inversion. This led us to investigate whether inversion in rod nuclei requires the absence of both LamA/C and LBR.

Inversion Correlates with Absence of Lamin A/C and LBR in Mammalian Rod Cell Nuclei

The inverted nuclear architecture of rods is restricted to nocturnal mammals. Mammalian groups that reacquired a diurnal lifestyle (e.g., primates) also regained a conventional nuclear architecture in their rod nuclei (Solovei et al., 2009). If inversion requires the absence of both LBR and LamA/C, the rods of nocturnal mammals should not express either of these proteins, whereas the rods of diurnal mammals should have reacquired expression of at least one of them.

Using antibodies to LBR and LamA/C, we tested their expression in retinal cryosections from a broad panel of diurnal and nocturnal mammals. To avoid any misinterpretation due to epitope variation, we analyzed 39 species in which both antibodies were present in the NE in the endothelial cells of retinal blood capillaries. These cells always express both proteins and served as a reliable internal control. Mammals with inverted rod nuclei expressed neither LamA/C nor LBR (Figures 1B and 1C), whereas all mammals with a conventional chromatin pattern expressed either the LBR or LamA/C. Because the transition from nocturnal to diurnal lifestyle occurred in a number of mammalian taxa, each of the two proteins was independently reacquired several times (Figure 1C). Which of them was reacquired had no visible effect on the nuclear architecture.

Expression of Lamin A/C and LBR Is Temporarily Coordinated: LBR Precedes LamA/C during Nuclear Differentiation

The apparent interchangeability of LamA/C and LBR in mammalian rods raises the question of whether the two proteins have distinct functions in other tissues. To obtain cell-type-specific data on their expression, we analyzed nuclei from more than 30 different cell types in tissue sections from wild-type (WT) mice of different ages. Cells were identified by histological criteria and, when necessary, by using cell -type-specific antibodies (Figure S1 available online).

In the developing retina, the expression of both proteins in neuronal nuclei is temporarily coordinated (Figures 2A and 2B). At first, retinal neurons only express LBR. LamA/C then appears and replaces LBR 10–14 days after the birth of the respective neuronal cell type (i.e., after the last division of the cell-type-specific progenitor cells [see Rapaport et al., 2004]). In rods, LBR expression ceases after postembryonic day 14 (P14) without initiation of LamA/C expression.

Timelines for other representative tissues and cell types are shown in Figure 2C. In contrast to neurons (and cardiomyocytes), other cell types are constantly renewed by the differentiation of stem cells. In the intestinal epithelium and stratified epidermis (e.g., lips), the positions of cells at successive stages of differentiation are spatially ordered in a linear fashion. A graded staining pattern observed in these tissues (Figures 2D and 2E) clearly reveals temporal changes in expression of the two proteins.

Timelines for renewed cells (Figure 2C) actually show the differences in expression between cells that are at the same (differentiated) state but in mice of different ages rather than differences in the same cells arising with age, as in not-renewed cells. For instance, differentiated absorptive and goblet cells of the small intestine are LamA/C negative until P14, whereas in older mice, differentiated cells of these types express both LBR and LamA/C (Figures 2D1 and S1A). The crypt cells renewing the intestinal epidermis only express LBR at all ages (Figures 2D1 and S1B). The nuclei of hepatocytes and myotubes (striated muscle) lose most LBR around P9–P14 and P0, respectively. Still, they retain a weak LBR signal even as adults, whereas satellite cells that renew myotubes have a lifelong strong expression of LBR. The nuclei of cardiomyocytes lose most LBR by P9, retaining only residual LBR expression. Differentiated lymphoid and myeloid blood cells do not express LamA/C (Röber et al., 1990) but persistently express LBR. These results corroborate the role of LBR and LamA/C in maintaining peripheral heterochromatin: all cell types except rods always express at least one of these two proteins.

Nuclei Not Expressing Lamin A/C Undergo Inversion in LBR Null Mice

We studied mice carrying a native and a transgenic mutation in the *Lbr* gene, $Lbr^{ic/ic}$ (Shultz et al., 2003) and $Lbr^{GT/GT}$ (Cohen

(D and E) Spatiotemporal coordination in expression of LBR and LamA/C in the intestinal epithelium of the small gut (D) and stratified epidermis of the lip (E) tissues at low magnification (D1 and E1) and representative nuclei (D2 and E2). During differentiation, cells are shifted in the apical direction, therefore a clear "green to red" (LBR to LamA/C) gradient is observed in both tissues (D1 and E1). In (D1), arrowheads mark the entrances of three crypts. In (E), arrows mark basal keratinocytes; arrowheads indicate suprabasal keratinocytes expressing both proteins (solid arrowheads) or only LamA/C (apical strata, empty arrowheads). Bars: B and D2, 2 μm; D1, 50 μm; E1, 10 μm; and E2, 5 μm. See also Figure S1.

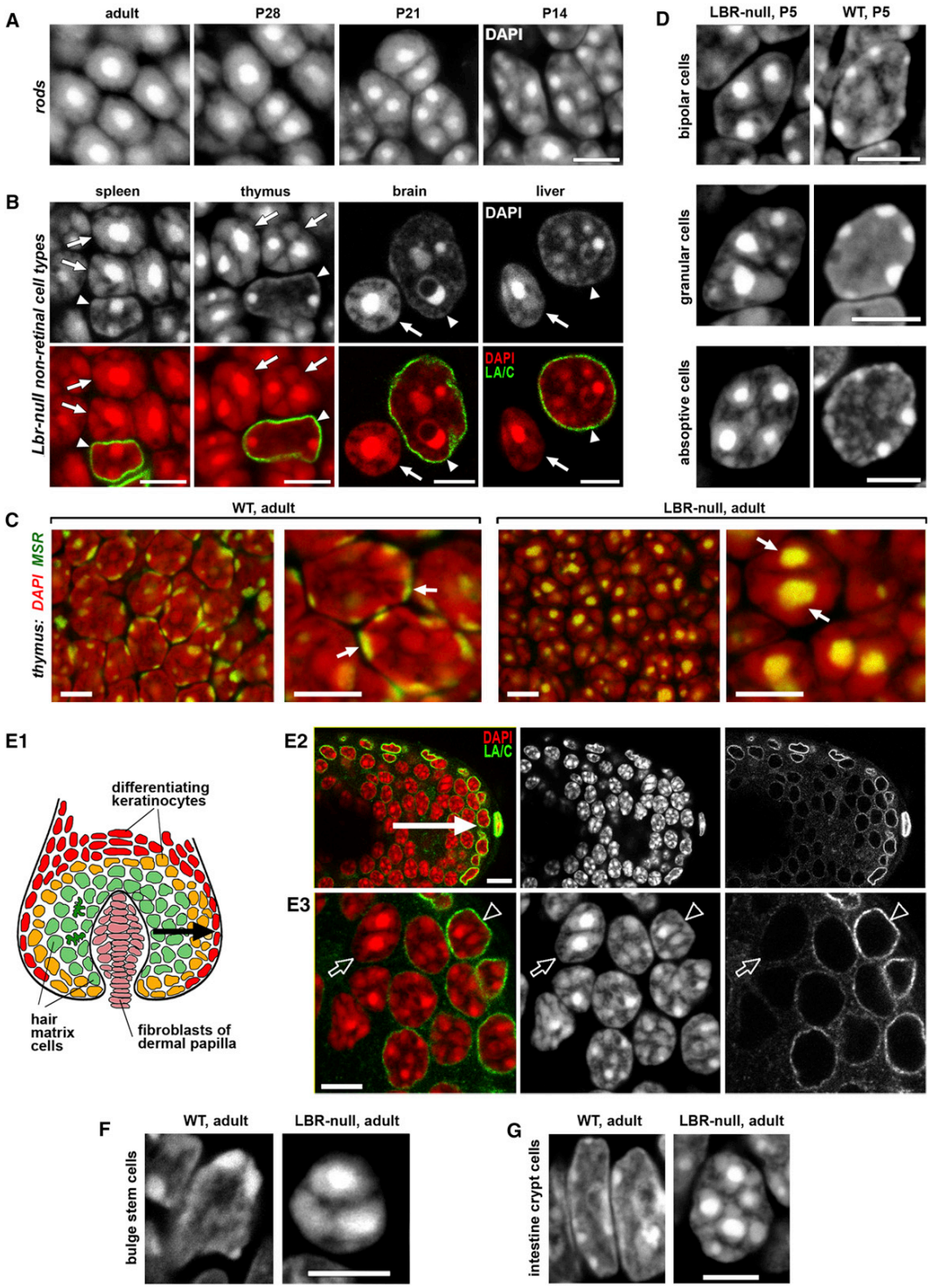

Figure 3. Inversion in LBR Null Cells Not Expressing LamA/C

(A) Representative images showing landmark stages of nuclear inversion in WT rods.

(B) Inverted nuclei in thymic and splenic lymphocytes, microglia (brain), and Kupffer (liver) cells. Inverted nuclei lack LamA/C (arrows), whereas neighboring nuclei expressing LamA/C (green) retain a normal nuclear architecture (arrowheads).

(legend continued on next page)

et al., 2008). We did not find any differences in nuclear architecture between these genotypes and therefore grouped them as LBR null mice. We reasoned that cells not expressing LamA/C in these mice, thus lacking both proteins, would be expected to invert. To search for inversion, we screened tissues from P5, P12–14, and adult LBR null mice. Several cell types (out of more than 30 identified) showed advanced inversion and were astonishingly similar to mature or maturating rod nuclei (c.f. Figures 3A and 3B). In all cases, inversion coincided with the absence of LamA/C (Figure 4) that was confirmed by a LamA/C signal in adjacent cells of other types. Inversion in nonrod cells was accompanied by the same changes in the nuclear positioning of the main chromatin classes and relevant nuclear structures as in rods (Figure S2).

For a semiquantitative description of the degree of inversion in nonretinal cells, we compared them to rods at different stages of differentiation. P14, P21, P28, and adult (AD) rods (Figures 1A and 3A) were used to describe the state of inversion in nonrod cell nuclei. Nonrod cells with advanced inversion (Figure 3B) had nuclei with one to five large chromocenters surrounded by LINE-rich chromatin, with little or no contact with the NE; they corresponded to P21/AD rods. A representative example is lymphocytes, which do not express LamA/C in WT mice (Röber et al., 1990). WT lymphocytes usually either have no internal chromocenters or only one. In LBR null lymphocytes, all chromocenters were internal (Figures 3B, 3C, S3A, and S3B).

For quantitative analysis, we compared inverted and noninverted nuclei (from LBR null and WT mice) in P5 and P46 thymic lymphocytes and P5 cerebellar granular cells. Using the numbers of peripheral (abutting the NE) and internal chromocenters as coordinates, we found that inverted and conventional nuclei occupy two nonoverlapping regions in the respective two-dimensional diagram (Figures S3B–S3D). Such differences were observed even for the moderately inverted lymphocyte nuclei and cerebellar granular neurons from P5 mice, showing that, if inversion occurs in a cell type, it affects all nuclei. These data also show that the essence of inversion is the loss of heterochromatin association with the NE (which also facilitates chromocenter fusion). Chromocenter numbers also decrease (ca. 1.5-fold in average), whereas the sizes of the two largest chromocenters increase.

The relationship between inversion and the dynamics of LBR and LamA/C expression during differentiation is directly visible in the hair follicle (Figure 3E). In the central part of a WT hair bulb, matrix cells do not express LamA/C and exhibit pronounced nuclear inversion (comparable to P14–21 rods) in LBR null mice. During differentiation, the cells migrate along the hair follicle toward its opening. Differentiated cells at the border of the bulb are LamA/C positive and display a conventional nuclear architecture, as do the nuclei of cells situated closer to the hair follicle opening.

In several cell types, Lam A/C expression does not start by P5 (Figures 3D and 4). At P5, these cells from LBR null mice have fewer chromocenters and a nuclear architecture corresponding to the P14/P21 stage of inversion in rods (c.f. Figures 3D and 3A). This was observed in the granular cells of the cerebellum, bipolar cells in the retina, podocytes (kidney), and absorptive cells of the small intestine (Figures 3D and S3E). By P14, LamA/C expression commences in these cell types, and in adult LBR null mice, nuclei of these cells do not differ from their WT counterparts.

Inverted nuclei were also present in the niches of the least differentiated and most rarely dividing stem cells (Greco and Guo, 2010), which presumably have enough time for inversion. We observed inverted nuclei in the hair bulge (Figure 3F) and at the bottom of the crypts of the small intestine (Figure 3G).

Loss of Lamin A/C Either Induces Inversion or Is Compensated by Prolonged LBR Expression

Lamin A/C$^{-/-}$ mice (*Lmna*-Zp3) generated for this study generally survive to P13–18. In P13 and P16 *Lmna*-KO mice, we examined all cell types that, by this age, normally express LamA/C, but not LBR (Figures 2C and 4). We observed advanced chromatin inversion in fibroblasts of the dermal papilla of hair follicles (Figure 5A). However, these were the only cell type where the nuclear architecture was affected (Figure 4). In other cell types, we observed a different phenotype: persistent expression of LBR beyond the stage at which it ceases in WT mice and, consequently, conventional nuclei (Figures 4, 5B1, and S4). A tissue-specific knockout (K14*Cre* *Lmna*$^{-/-}$) revealed that the compensatory ecchronic LBR expression was not silenced with age (3 months; Figures 5B2 and S4).

Lbr $^{-/-}$ *Lmna* $^{-/-}$ Mice Show Inversion in All Postmitotic Cell Types

Despite the absence of overt morphological defects, double null (*Lbr* $^{-/-}$ *Lmna* $^{-/-}$) pups die shortly after birth, and therefore, only P0 animals were studied. We focused attention on cell types that do not invert in any of the two single-gene knockouts (Figure 4), in particular, the colon epithelium and skin epidermis as they are readily identified in sections. Both cell types express LBR and LamA/C at birth. In the double nulls, these cells show a clear increase in chromocenter size (chromocenter fusion) and relocation of chromocenters from the periphery to the nuclear interior (Figures 5C and 5D). Similar changes occurred in all postmitotic cell types we identified (Figure 5E). Compared to WT, chromocenter fusion is strongly promoted in double null neurons; in particular, inversion in rods is greatly accelerated (Figures S5F and S5G).

(C) Thymic lymphocytes, FISH with major satellite repeat (MSR) probe specific for chromocenters (arrows).
(D) Transient inversion in bipolar cells (retina), granular cells (cerebellum), and absorptive cells (duodenum) from P5 mice (DAPI).
(E) Inversion and rescue of the nuclear architecture in the hair bulb matrix cells. (E1) Diagram of the hair bulb structure. Dividing cells of the hair matrix (green) and differentiating keratinocytes (orange and red) are shifted peripherally during differentiation (arrow). (E2) A section through hair bulb showing LamA/C-positive cells at the periphery, with the arrow showing the direction of centrifugal migration. Note the much stronger LamA/C staining in a fibroblast abutting the hair bulb. (E3) Representative region of a hair bulb: inverted nucleus not expressing LamA/C (arrow) and conventional architecture in nuclei expressing LamA/C (arrowhead).
(F and G) Inverted nuclei from hair bulge (F) and crypt (G). Bars, 5 μm. See Figures S2 and S3.

tissue	cell type		WT LBR	WT LA/C	nuclear pattern in LBR-null mice P5 and AD (P46)	nuclear pattern in *Lmna*-KO mice P16
brain	microglial cells		+	-	inverted	conventional
spleen	lymphocytes		+	-	inverted	conventional
	granulocytes		+	-	inverted	conventional
thymus	lymphocytes		+	-	inverted	conventional
intestine	crypt cells		+	-	inverted	conventional
hair	matrix keratinocytes		+	-	inverted	conventional
liver	Kupffer cells		+	-	inverted	conventional
retina	rod cells	(P5)	+	-	inverted	conventional
		(AD)	-	-	inverted	inverted
cerebellum	granular cells	(P5)	+	-	moderate inversion	conventional, rescued
		(AD)	-	+	conventional	
retina	bipolar cells	(P5)	+	-	moderate inversion	conventional, rescued
		(AD)	-	+	conventional	
intestine	absorptive cells	(P5)	+	-	moderate inversion	conventional, rescued
		(AD)	+	+	conventional	
kidney	podocytes	(P5)	+	-	moderate inversion	*not studied*
		(AD)	+	+	conventional	
retina	amacrine cells	(P5)	+	-	enhanced CC fusion	conventional, rescued
		(AD)	-	+	conventional	
	cone cells (1)	(P5)	+	-	enhanced CC fusion	conventional, rescued
		(AD)	-	+	enhanced CC fusion	
brain	cortical neurons		-	+	conventional	conventional, rescued
cerebellum	Purkinje cells		-	+	conventional	conventional, rescued
retina	ganglion cells		-	+	conventional	conventional, rescued
	horizontal cells		-	+	conventional	conventional, rescued
spleen	reticulocytes		-	+	conventional	conventional, rescued
thymus	epithelial cells		-	+	conventional	conventional, rescued
skin	keratinocytes (2)		+/-	+	conventional	conventional, rescued
	dermal fibroblasts		-	+	conventional	conventional, rescued
hair	fibroblasts of dermal papilla		-	+	conventional	inverted
kidney	epithelial cells of proximal and distal convoluted tubes		-	+	conventional	*not studied*
liver	hepatocytes		+ (w)	+	conventional	conventional, rescued
skeletal muscles	myotubes		+ (w)	+	conventional	conventional, rescued
	satellite cells		+	+	conventional	conventional
spleen	erythroblasts		+	+	conventional	conventional
	megacaryocytes		+	+	conventional	conventional
small intestine	Paneth cells (indiscernible in P5)		+	+	conventional	conventional
	smooth muscle cells		+	+	conventional	conventional
blood vessels	endothelial cells		+	+	conventional	conventional
heart	cardiomyocytes	(P5)	+	+	conventional	conventional, rescued
		(AD)	+ (w)	+	conventional	
connective tissue	chondroblasts / chondrocyte	(P5)	+	+	conventional	conventional, rescued
		(AD)	-	+	conventional	
	osteoblasts / osteocytes	(P5)	+	+	conventional	conventional, rescued
		(AD)	-	+	conventional	

Figure 4. Correlation of LBR and LamA/C Expression with the Nuclear Architecture in 34 Cell Types from WT, LamA/C-, and LBR Null Mice
LamA/C staining in cones (1) is notably weaker than in the majority of other retinal cells. Cone nuclei are comparable to a moderate inversion in WT retina, and chromocenter (CC) fusion tends to be enhanced in LBR null cones compared to WT. However, in difference to rod nuclei, peripheral heterochromatin is retained in cones. A proportion of basal keratinocytes (2) are LBR positive; other basal and all suprabasal keratinocytes are LBR negative. In adult mice, the nuclei of hepatocytes, cardiomyocytes, and myotubes (w) retain a very low level of LBR. In LamA/C KO mice, LBR expression is dramatically enhanced.

As expected, inversion is not complete in the nuclei of P0 double null cells because full inversion needs several weeks after cell cycle exit (Solovei et al., 2009). The levels of inversion observed in double null nuclei were comparable to that of the transient inversion in P5 LBR null mice (Figure 3D). The level of inversion varies between nuclei because some cells in P0 pups are postmitotic and some are cycling. Nevertheless, all identified postmitotic cell types showed a clear inversion, confirming that peripheral heterochromatin cannot be maintained in postmitotic cells in absence of both lamin A/C and LBR.

Ectopic LBR Expression Counteracts Rod Nuclei Inversion

Having shown that the absence of both LBR and LamA/C results in inversion, we set out to test whether their ectopic expression prevents inversion. We generated transgenic mice specifically expressing these proteins in rods (the only cell type where both proteins are absent) under the control of the neural retina leucine zipper (*Nrl*) promoter, which initiates transcription immediately after rod progenitors exit the cell cycle (Akimoto et al., 2006).

We generated two lines of Lbr-TER (Lbr transgenically expressed in rods) mice. In both lines, LBR was expressed in a proportion of retinal clones. In Lbr-TER1 mice, a proportion of nuclei show characteristic signs of LBR overexpression (cf. Olins et al., 2010). In the retina of 2-month-old mice homozygous for *Lbr* insert, LBR-expressing nuclei show a conventional architecture, in particular, a layer of peripheral heterochromatin (Figures 6A and 6C, arrows). These nuclei have two to seven (four or five in 77% of nuclei) chromocenters, with all chromocenters being located at the periphery (Figures 6A–6C). Nuclei not expressing LBR in the same retina were not different from WT and completely inverted (Figures 6A–6C, arrowheads). In Lbr-TER2 mice, LBR was weakly expressed, but they also showed a statistically significant retardation of inversion (Figures S5A–S5D). Thus, an adequate level of LBR expression is sufficient to maintain peripheral heterochromatin in rods.

LamA/C Needs a Mediator to Bind to Peripheral Chromatin

We expressed lamin C (LamC) in rods to avoid potential abnormalities in the posttranscriptional processing necessary for LamA, but not LamC. LamC-only mice are overtly normal (Fong et al., 2006), and LamC alone is sufficient to maintain peripheral heterochromatin (data not shown). We generated two lines expressing LamC in rod nuclei. In LamC-TER1, all rods expressed LamC, and in LamC-TER2, expression was very strong but only present in 70%–80% of the retinal clones. In contrast to LBR, transgenic LamC had no visible effects on rod nuclei (Figure S5E) at any age.

The inability of LamC to tether peripheral heterochromatin conforms to the notion that LamA/C predominantly binds chromatin indirectly, via a complex with LEM domain proteins (Brachner and Foisner, 2011). Therefore, we analyzed the expression of LEM domain proteins in WT retinas (Figure 6D) using antibodies against emerin, Man1, Lem2, and NE-associated isoforms of Lap2 (neLap2: β, γ, δ, and ε). Man1 and neLap2 are present in rods at all stages of differentiation, whereas Lem2 is not expressed in rods at any stage. In contrast, emerin is present in young rods but is silenced as inversion advances (Figure S6A). We also analyzed SCA7 (spinocerebral ataxia type 7) mice where mature, already fully inverted rods dedifferentiate and partially restore a conventional nuclear architecture (Helmlinger et al., 2006). Both LamA/C and emerin expression is initiated in rods from adult SCA7 mice (Figure S6A), whereas the expression status of neLap2, Man1, and Lem2 does not change.

To test the possible role of emerin, we studied emerin null (*Emd*-KO) mice. Earlier studies revealed that these mice are practically normal (Melcon et al., 2006; Ozawa et al., 2006). We reasoned that, if emerin is indeed an indispensable component of the LamA/C-dependent heterochromatin tether, its deletion in cells not expressing LBR should cause either (i) nuclear inversion, (ii) persistent LBR expression (the LamA/C tether replaced by the LBR tether), or (iii) emerin is replaced in the LamA/C tether by a functionally similar protein, e.g., other LEM domain protein.

We analyzed adult (6-month-old) $Emd^{-/-}$ mice and found neither nuclear inversion in any cell type nor persistent LBR expression. We also observed no prominent qualitative changes in the expression of other LEM domain proteins, with a noteworthy exception of the dermal papilla (hair) nuclei (Figures 6D and S6B) that invert in $Lmna^{-/-}$ mice. In adult WT mice, these nuclei strongly express emerin, whereas neLap2 expression was undetectable. In contrast, moderate but clear neLap2 expression was observed in $Emd^{-/-}$ mice, suggesting that, at least in one case, emerin deletion is compensated by another LEM domain protein. Importantly, our data showed that the expression of LEM domain proteins is cell-type- and developmentally stage-specific (Figures 6D and S6C). None of the LEM domain proteins are present in all cell types lacking LBR, and therefore, no individual LEM domain protein could be the universal mediator of the LamA/C-dependent peripheral heterochromatin tether.

Loss of LBR and LamA/C Inversely Affects Transcription in a Proportion of Muscle Genes in Early Myogenic Cells, but Not in Differentiated Muscle

To determine the functional roles of the two temporally distinct heterochromatin tethers, we analyzed the genome-wide effects of LBR and LamA/C deficiency on the transcriptome (Tables S1 and S2). We prepared primary cultures of myogenic cells derived from limb muscles of P15–P16 $Lmna^{-/-}$ and $Lbr^{-/-}$ mice and from their WT littermates as controls. To minimize artifacts due to culture, we harvested cells after the second passage. Transcription profiles confirmed the early-myogenic nature of the cells in our cultures (Table S3).

Gene Ontology (GO) enrichment analysis using GOrilla (Tables S4A and S4B) and GSEA software (data not shown) suggested that the loss of Lbr or LamA/C tends to have opposite effects on muscle-related genes, reducing their expression in $Lmna^{-/-}$ and increasing it in $Lbr^{-/-}$ myoblasts. To test this finding, we analyzed expression levels of all genes covered by two GOCs most relevant for our experiments: structural constituent of muscle (GO: 0008307) and striated muscle cell differentiation (GO: 0051146) (Tables S5A and S5B). This provided us with two relevant gene sets for statistical analysis, which we restricted to genes that had a nonzero expression level (FPKM > 0;

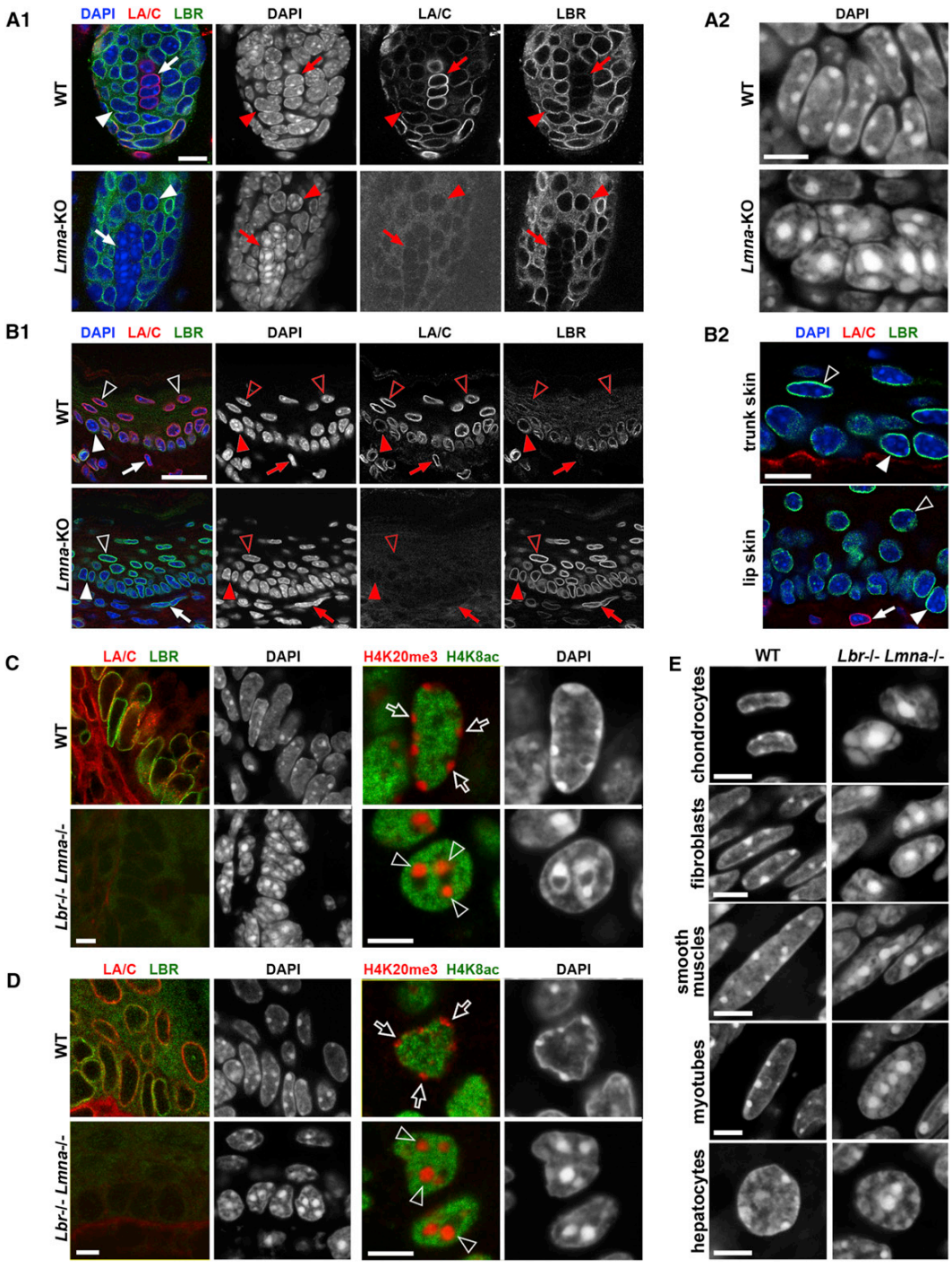

Figure 5. Nuclear Organization in *Lmna*$^{-/-}$ and *Lbr* $^{-/-}$ *Lmna* $^{-/-}$ Mice

(A) Inversion in the hair bulb of P16 *Lama*-KO mice. In contrast to the matrix cells (arrowheads), the fibroblasts of the dermal papilla (arrows) do not express LBR and invert in LamA/C KO mice.

(B) Compensation for LamA/C loss by persisting LBR expression in the skin. (B1) Lip skin of a P16 *Lmna*$^{-/-}$ mouse and WT littermate. Basal keratinocytes (solid arrowhead) express both LBR and LamA/C, whereas suprabasal keratinocytes (empty arrowheads) and dermal fibroblasts (arrow) express only LamA/C. In *Lama*-KO mice, both latter cell types express LBR (Figure S4). (B2) Compensation in suprabasal keratinocytes in both trunk (top) and lip skin (bottom) from a 3-month-old K14Cre-driven *Lmna*$^{-/-}$ (see also Figure S4). Note a fibroblast expressing LamA/C (arrow).

(legend continued on next page)

frequency of reads per Kb per Mio) in all studied transcriptomes to facilitate uniform comparison of genotypes and cell types.

Nearly 60% of the genes from the GOC structural constituent of muscle (41 genes with nonzero expression in our data) were strongly and similarly deregulated in myoblasts; expression was reduced by the loss of LamA/C and slightly increased by the loss of LBR (Figure 7A1). This pattern was also reproduced by nearly all genes individually deregulated in one or both KOs at a statistically significant level ($p < 0.05$; marked by colored bullets in Figure 7A1). More than 2-fold deregulation was observed in a large proportion of genes, irrespective of their expression level (Figure 7B1). In contrast to myoblasts, differences in expression levels in differentiated muscles were much smaller and without the reverse effect of LamA/C and LBR loss (Figures 7A2 and 7B2). Deletion of LBR, which is anyway nearly silenced during myotube differentiation (Figure 2C), had very little effect on their transcriptome. GOC striated muscle cell differentiation revealed the same trends (Figure S7) as the GOC structural constituent of muscle.

From a statistical perspective, the differences (i) between the KOs in myoblasts and (ii) between myoblasts and muscles of the same genotype were significant at the levels $p < 0.001$ for the first GOC and $p = 0.013$ or better for the second GOC (signed rank test). The differences between the two KOs in limb muscle transcriptomes were not statistically significant for either GOC. The correlation between gene expression levels in our cultures and in differentiating C2C12 cells progressively declined as differentiation proceeded (Table S6), which emphasizes that loss of *Lbr* and *Lmna* primarily affects the initial stages of differentiation.

DISCUSSION

By analyzing rod photoreceptor cells from 39 mammalian species and a wide range of mouse tissues from nine relevant transgenic mouse lines, we show here that LBR and/or lamin A/C are essential for tethering heterochromatin to the nuclear periphery. Absence of both proteins in postmitotic cells results in inversion of the nuclear architecture with heterochromatin relocalizing from the nuclear envelope to nuclear interior (Figure 7C). During development and cellular differentiation, LBR and LamA/C expression is sequential and coordinated. Initially, only LBR is expressed and is later replaced by LamA/C, with a few differentiated cell types expressing both proteins. In most cell types, deletion of LamA/C is compensated by prolonged expression of LBR. Deletion of both LBR and LamA/C causes inversion in all differentiated cell types in newborn mice. In mouse rods normally lacking LBR and LamA/C, transgenic LBR expression is sufficient to maintain peripheral heterochromatin, whereas LamC requires cofactor(s). Comparing $Lbr^{-/-}$, $Lmna^{-/-}$, and WT myoblast transcriptomes revealed that a sequential temporal usage of LBR and LamA/C tethers during development correlates with their opposite effects on the transcription of muscle-specific genes: a decrease and increase, respectively. However, in terminally differentiated muscle, the differences between transcriptomes were almost nonexistent.

Two Mechanisms Tether Peripheral Heterochromatin to the Nuclear Envelope in Mammals

Although both LBR and LamA/C are indispensable for heterochromatin tethering, the roles of these proteins are different. LBR is an integral protein of the INM, which preferentially binds to B-type lamins. The Tudor domain of LBR selectively interacts with heterochromatin (Makatsori et al., 2004; Olins et al., 2010; Hirano et al., 2012). LBR, the lamina (B-type lamins), and INM are sufficient to build a heterochromatin tether (Figure 7D); see also Clowney et al. (2012). However, B-type lamins seem to be dispensable because cells from mice, lacking both *Lmnb1* and *Lmnb2*, retain a conventional nuclear architecture in the absence of LamA/C (Kim et al., 2011; Yang et al., 2011; data not shown); this may be due to the retention of LBR, which has several transmembrane domains, at the INM.

In contrast to LBR, exogenous A-type lamin expression does not counteract inversion in rods. Although LamA/C may bind chromatin directly (Andrés and González, 2009; Kubben et al., 2012), it typically functions as a scaffold for other chromatin-interacting proteins, LEM-domain proteins in particular. The latter share three important properties with LBR: they are anchored in the INM, interact with lamins, and bind to chromatin and/or DNA through their binding partners (Brachner and Foisner, 2011). LEM domain proteins anchor heterochromatin to the NE in yeast, which have no lamins, and in *C. elegans*, which has a single lamin (Ikegami et al., 2010; Mattout et al., 2011; Towbin et al., 2010).

The LEM domain protein Lap2β was recently implicated in gene silencing at the nuclear periphery in mammals (Zullo et al., 2012). It forms a complex with histone deacetylase HDAC3 and cKrox, a protein binding to stretches of GA dinucleotides. Whereas HDAC3 promotes heterochromatinization, the LEM domain protein binds the whole complex to the NE. The activity of the complex is cell-type- and developmental-stage-specific (Zullo et al., 2012), which probably depends on post-translational modifications known to strongly affect the properties of LEM domain proteins (Tifft et al., 2009).

Lap2β doubtlessly contributes to peripheral heterochromatin tethering in differentiated cells but cannot completely account for all tethering. Lap2β does not target, to the nuclear periphery, all lamina-associated DNA sequences analyzed (Zullo et al., 2012). Our data reveal that neLap2 does not prevent inversion occurring in LBR null cells that are also null for LamA/C. In rods, neLap2 does not counteract inversion in combination with transgenically expressed LamA/C (and native B-type lamins). Also, B-type lamins themselves are dispensable for maintaining peripheral heterochromatin in the absence of LBR in

(C and D) Epithelial cells in the colon (C) and epidermal keratinocytes (D) of $Lbr^{-/-}$ $Lmna^{-/-}$ mice have a smaller number of chromocenters that are internal and larger (due to fusion) than in WT (left). Differences in the position and size of chromocenters are emphasized by differential staining of eu- and heterochromatin (H4K8ac and H4K20m3, respectively; right).

(E) Increased size and internalization of chromocenters in several cell types from double KO.

Bars: A1 and B2, 10 μm; A2 and C–E, 5 μm; B1, 25 μm. See also Figures S4 and S5.

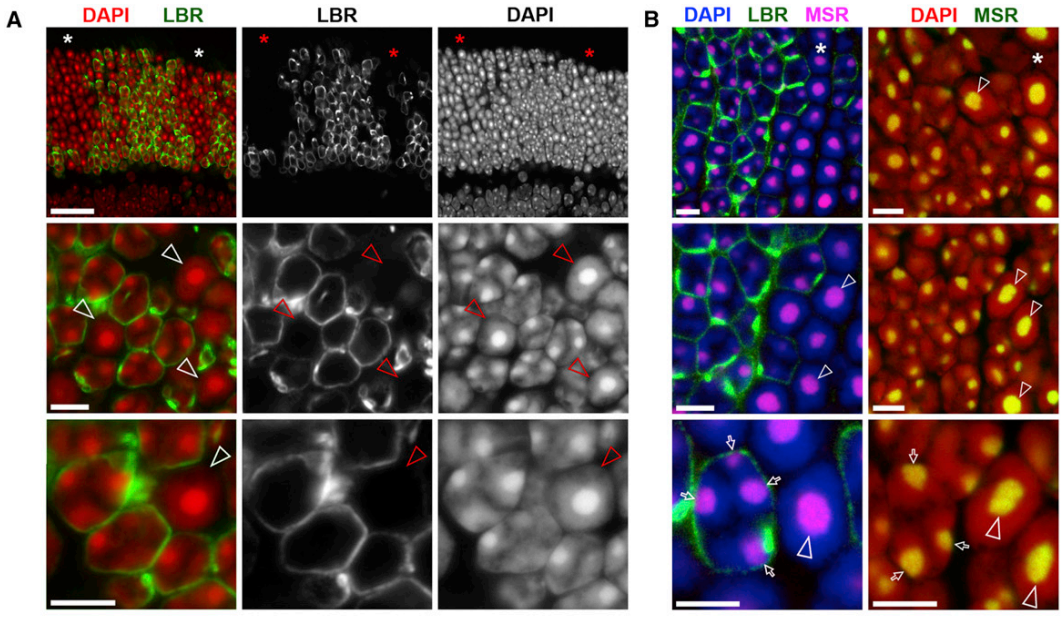

D

tissues	cell types	Lam A/C	LBR	neLap2	Man1	Lem2	Emerin
retina	rods	-	-	+	+	-	- (1)
	neuroretinal cells	+	-	+	+	-	+
	endothelial cells	+	+	+	+	+	+
skeletal muscles	myotube nuclei	+	+ (w)	- (2)	+	+	+
heart mucles	cardiomyocytes	+	+ (w)	- (2)	+	+	+
	fibroblasts	+	-	+	+	+	+
intestine: small	absorptive cells	+	+	+	+	+	-
	crypt cells	-	+	+	-	-	+
smooth muscles	various organs	+	+	+	+	+	+
liver	hepatocytes	+	+ (w)	+	+	-	-
	Kupffer cells	-	+	+	+	-	+
spleen	lymphocytes	-	+	+	-	-	+
	megakaryocytes	+	+	+	+	+	+
skin	basal keratinocytes	+	+	+	+	+	+
	suprabasal keratinocytes	+	-	+	+	+	+
	dermal fibroblasts	+	-	+	+	+	+
hair	matrix keratinocytes	-	+	+	-	-	+
	hairshaft keratinocytes	+	-	+	+	+	+
	dermal papilla cells	+	-	- / + (3)	+	+	+

Figure 6. Restoration of the Conventional Nuclear Architecture in Rods due to Transgenic Expression of LBR and Expression of LEM-Domain Proteins in a Panel of Tissues from WT and *Emd*-KO Mice

(A–C) Retina from a 2-month-old LBR-TER1 mouse homozygous for *Lbr* insertion. Border regions between LBR-positive and LBR-negative clones, showing inverted WT nuclei with a single central chromocenter (arrowheads) and nuclei that restored a conventional architecture with peripheral chromocenters (arrows); groups of WT nuclei are marked by asterisks.

(A) LBR staining (green) with DAPI counterstain (red).

(B) FISH with MSR probe.

(legend continued on next page)

nuclei from mice lacking both *Lmnb1* and *Lmnb2* (Kim et al., 2011; Yang et al., 2011; data not shown).

These facts emphasize the importance of LamA/C and also suggest a role for other LEM domain proteins in the LamA/C tether. Notably, emerin also binds to HDAC3, and its deletion reduces the level of HDAC3 at the nuclear periphery (Demmerle et al., 2012), whereas HDAC3 regulates heterochromatin levels (Bhaskara et al., 2010). The other LEM domain proteins have not yet been studied in this respect. At least in the dermal papilla cells (also affected by *Lmna* deletion), the loss of emerin results in increased expression of neLap, supporting a possible role for both emerin and neLap in peripheral heterochromatin tethering. However, even the absence of both emerin and neLap2 does not result in inversion in striated muscle. Our observations show that the pattern of LEM domain protein expression is cell type specific, with none of the LEM domain proteins being universally expressed in mammalian cells. This is in agreement with the reported broad functional overlap between LEM domain proteins in all organisms studied so far (Barkan et al., 2012; Huber et al., 2009; Mattout et al., 2011).

Clearly, the composition of the LamA/C-dependent peripheral heterochromatin tether requires further analysis. Nevertheless, our and published data support the notion that LEM-domain proteins cooperate with LamA/C in tethering peripheral heterochromatin to the NE in mammals (Figure 7D). Available data also suggest that different LEM domain proteins (probably combinations of these proteins) mediate heterochromatin binding to LamA/C, depending on the cell type and developmental stage. Indeed, in *C.elegans*, heterochromatic chromosome arms are targeted to the nuclear lamina by a complex of lamin with any of the two LEM domain proteins (Ikegami et al., 2010; Mattout et al., 2011). Targeting depends on histone methylation (Towbin et al., 2012)—that is, using the same repressive epigenetic marks that LBR binds to in mammals. This suggests that complexes of lamin and LEM domain proteins in mammals should also include proteins recognizing histone methylation.

Temporally Distinct Tethers Oppositely Affect Transcription of Tissue-Specific Genes and Cellular Differentiation

LamA/C is a known marker of the differentiated state (Zhang et al., 2011), whereas our data primarily link LBR expression to un- or early differentiated states. This difference in the timing of expression of LBR and LamA/C conforms to the opposite effects of *Lbr* and *Lmna* loss on transcription of many muscle-specific genes during the early stages of myotube differentiation. Loss of *Lbr* increases, whereas loss of *Lmna* decreases expression of these genes. This is consistent with the earlier findings on the delayed maturation of satellite and myotubes with myopathogenic mutations in *Lmna* (Melcon et al., 2006; Park et al., 2009; Bertrand et al., 2012). In agreement with previous studies (Kubben et al., 2011; Verhagen et al., 2012), loss of *Lbr* and *Lmna* had little effect on the transcriptomes of mature, fully differentiated skeletal muscle, though transgenic expression of LBR deregulates the differentiation of olfactory neurons (Clowney et al., 2012).

The same sequential pattern of LBR and LamA/C expression in diverse cell types suggests that peripheral heterochromatin tethers regulate differentiation in a broad range of tissues, e.g., mesodermal (osteogenic and adipogenic) or perhaps in all cell types. In mammalian cells, targeting chromatin to the NE mediates its silencing in a histone-deacetylation-dependent manner (Finlan et al., 2008), which concurs with HDAC3 associating with LEM domain proteins. Tellingly, the proximity of the myogenic master regulator gene *MyoD* to the nuclear periphery directly affects its binding to alternative transcription factors in mammalian cells (Melcon et al., 2006; Yao et al., 2011). This illustrates how changes in gene position can switch between regulatory pathways and regulate cellular differentiation. The versatility of chromatin binding by the LamA/C tether, suggested by our results, may explain how LamA/C contributes to the regulation of diverse genes and developmental processes, resulting in a plethora of phenotypically different syndromes when this protein is mutated.

EXPERIMENTAL PROCEDURES

Mice

WT mice were CD1 and C57BL/6. The LamA/C global knockout (Zp3-Lmna) was generated for this study (see Extended Experimental Procedures). Tissue samples studied were from P13 and P16 mice. Skin samples were also studied from a keratin-limited LamA/C knockout (driven by the keratin-14 promoter). LBR null mice were C57BL/6-ic^{J} (Jackson Laboratory Stock number 000529) (Shultz et al., 2003) and *Lbr*^{GT} (Cohen et al., 2008). Tissue samples of C57BL/6-ic^{J}/ic^{J} mice were provided by K. Hoffmann (Charite, Berlin): P5, P13, and P46 mutant mice and littermate controls. *Lbr*^{GT} mice were studied at P5, P14, and E12. Emerin null mice were generated by us previously (Melcon et al., 2006); two 6-month-old mice were studied. Lbr-TER and LamC-TER mice were generated by cloning the full complementary DNA (cDNA) sequences for mouse *Lbr* and lamin C into the pNRL-L-EGFP plasmid (Akimoto et al., 2006) to replace EGFP under the control of the *Nrl* promoter. DNA for microinjection was prepared, and transgenic mice were generated according to standard protocols. Retinas of R7E mice (Helmlinger et al., 2006) were studied at the ages of 2, 4, 6, 20, 43/46, 70, and 93 weeks. WT littermate controls were studied in parallel with genetically modified mice (4, 46, and 93 weeks for R7E mice).

Histological Study

Tissue samples were fixed in 4% paraformaldehyde, embedded in Jung tissue freezing medium, and studied after immunostaining cryosections using a Leica TCS SP5 confocal microscope as described earlier (Solovei et al., 2009). The antibodies used in this study are listed in Extended Experimental Procedures.

Transcriptome Analysis

Satellite cell cultures were derived from limb muscles of P15/P16 mice. The transcriptomes of two biological replicas (cultures derived from two different mice) of each analyzed genotype were sequenced following a standard protocol. KO myoblast transcriptomes were compared to transcriptomes of

(C) Differential staining of euchromatin (H4K8ac, green) and heterochromatin (H4K20me3, red).
(D) Expression of LEM domain proteins in WT and emerin KO mice. Different colors highlight differences in expression patterns between cell types; the only case where WT and Emd-KO are qualitatively different is highlighted in yellow. Emerin expression ceases during inversion (1); neLap2 expression ceases in striated muscles after P14 (2) (Figures S7B and S7C); neLap2 is absent in WT but present in *Emd*-KO (3) (Figure S7A); weak residual expression in adult (w).
Bars: A, top row, 25 μm; A and B, 5 μm; C1, 10 μm; C2, 2 μm. See also Figures S5 and S6.

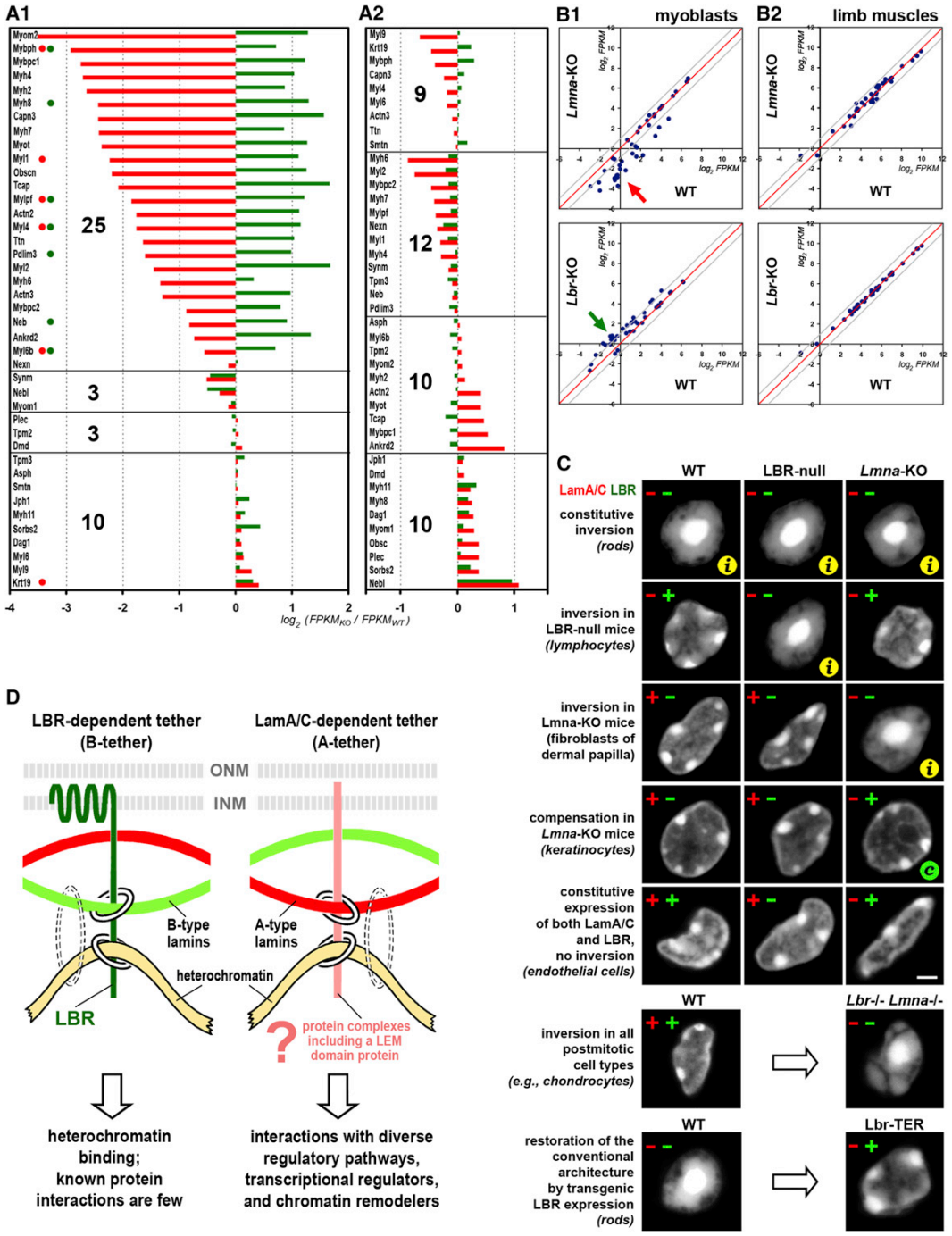

Figure 7. The Effect of Lbr and Lmna Loss on the Transcription of Muscle-Related Genes in Myoblasts and Differentiated Myotubes, with a Diagram Summarizing the Affected Pathways

(A) Genes from the GOC structural constituent of muscle: myoblasts (A1) and limb muscles (A2). The difference in transcription level (x axis) is expressed as logarithm of the fold change, ln ($FPKM_{KO}/FPKM_{WT}$), for *Lmna* (red) and *Lbr* (green). Numbers of genes with each of the four possible deregulation patters are shown in bold. Green and red bullets mark genes that are statistically significantly deregulated ($p < 0.05$ or better) in *Lmna* (red) and *Lbr* KO (green) knockouts. (B) Genes from the GOC structural constituent of muscle: myoblasts (B1) and limb muscles (B2). Each point represents a gene, with its expression levels (log_2 FPKM) in WT and a KO as coordinates. Gray lines mark a 2-fold reduction in expression (below the red line) and increased expression (above the red line). Arrows emphasize deregulation trends for *Lmna* (red) and *Lbr* (green).

(legend continued on next page)

WT littermates; in the case of *Lmna*-KO, RNA samples from three WT littermates were mixed before sequencing. Limb muscle transcriptomes were sequenced from two LBR$^{-/-}$, two LamA/C$^{-/-}$, and two WT mice, one littermate from each KO line. Sequencing depth was 35 Mio reads per RNA sample for myoblasts and 7.5 Mio reads per sample for limb muscles.

ACCESSION NUMBERS

The GEO accession numbers for the full myoblast transcriptome sequencing data reported in this paper are GSE37076 and GSM910296–GSM910307.

SUPPLEMENTAL INFORMATION

Supplemental Information includes Extended Experimental Procedures, seven figures, and six tables and can be found with this article online at http://dx.doi.org/10.1016/j.cell.2013.01.009.

ACKNOWLEDGMENTS

We are grateful to Stephen Young and Loren Fong (University of California, Los Angeles) for tissue samples of lamin-C-only mice, Yixian Zheng (Carnegie Institution for Science, Baltimore) for *Lmnb1/Lmnb2* double-knockout tissue samples, Anand Swaroop (National Eye Institute, Bethesda) for NRL-L-plasmid, and Barbara Knowles (Institute of Medical Biology, Singapore) for Zp3-Cre mice. We gratefully acknowledge the support by the DFG (SO1054/1 to IS, HE1853 to HH, SFB/TR5 to HL, and JO903/1 to BJ); by the German-Israeli-Foundation for Scientific Research and Development (111/2007 to HH); by the International Max Planck Research School for Molecular and Cellular Life Sciences (IMPRS-LS) to C.S.S. and K.T.; by BMBF (German agriculture network Phaenomics, 0315536F to H.B.); by Austrian Science Research Fund (FWF P22403-B12 to R.F.); and by the Singapore Biomedical Research Council and the Singapore Agency for Science, Technology, and Research (A*STAR) to C.L.S. and A.W.

Received: April 10, 2012
Revised: September 14, 2012
Accepted: January 7, 2013
Published: January 31, 2013

REFERENCES

Akimoto, M., Cheng, H., Zhu, D., Brzezinski, J.A., Khanna, R., Filippova, E., Oh, E.C., Jing, Y., Linares, J.L., Brooks, M., et al. (2006). Targeting of GFP to newborn rods by Nrl promoter and temporal expression profiling of flow-sorted photoreceptors. Proc. Natl. Acad. Sci. USA *103*, 3890–3895.

Andrés, V., and González, J.M. (2009). Role of A-type lamins in signaling, transcription, and chromatin organization. J. Cell Biol. *187*, 945–957.

Barkan, R., Zahand, A.J., Sharabi, K., Lamm, A.T., Feinstein, N., Haithcock, E., Wilson, K.L., Liu, J., and Gruenbaum, Y. (2012). Ce-emerin and LEM-2: essential roles in Caenorhabditis elegans development, muscle function, and mitosis. Mol. Biol. Cell *23*, 543–552.

Bertrand, A.T., Renou, L., Papadopoulos, A., Beuvin, M., Lacène, E., Massart, C., Ottolenghi, C., Decostre, V., Maron, S., Schlossarek, S., et al. (2012). DelK32-lamin A/C has abnormal location and induces incomplete tissue maturation and severe metabolic defects leading to premature death. Hum. Mol. Genet. *21*, 1037–1048.

Bhaskara, S., Knutson, S.K., Jiang, G., Chandrasekharan, M.B., Wilson, A.J., Zheng, S., Yenamandra, A., Locke, K., Yuan, J.L., Bonine-Summers, A.R., et al. (2010). Hdac3 is essential for the maintenance of chromatin structure and genome stability. Cancer Cell *18*, 436–447.

Brachner, A., and Foisner, R. (2011). Evolvement of LEM proteins as chromatin tethers at the nuclear periphery. Biochem. Soc. Trans. *39*, 1735–1741.

Clowney, E.J., LeGros, M.A., Mosley, C.P., Clowney, F.G., Markenskoff-Papadimitriou, E.C., Myllys, M., Barnea, G., Larabell, C.A., and Lomvardas, S. (2012). Nuclear aggregation of olfactory receptor genes governs their monogenic expression. Cell *151*, 724–737.

Coffinier, C., Jung, H.J., Nobumori, C., Chang, S., Tu, Y., Barnes, R.H., II, Yoshinaga, Y., de Jong, P.J., Vergnes, L., Reue, K., et al. (2011). Deficiencies in lamin B1 and lamin B2 cause neurodevelopmental defects and distinct nuclear shape abnormalities in neurons. Mol. Biol. Cell *22*, 4683–4693.

Cohen, T.V., Klarmann, K.D., Sakchaisri, K., Cooper, J.P., Kuhns, D., Anver, M., Johnson, P.F., Williams, S.C., Keller, J.R., and Stewart, C.L. (2008). The lamin B receptor under transcriptional control of C/EBPepsilon is required for morphological but not functional maturation of neutrophils. Hum. Mol. Genet. *17*, 2921–2933.

Cremer, T., and Cremer, M. (2010). Chromosome territories. Cold Spring Harb. Perspect. Biol. *2*, a003889.

Demmerle, J., Koch, A.J., and Holaska, J.M. (2012). The nuclear envelope protein emerin binds directly to histone deacetylase 3 (HDAC3) and activates HDAC3 activity. J. Biol. Chem. *287*, 22080–22088.

Deniaud, E., and Bickmore, W.A. (2009). Transcription and the nuclear periphery: edge of darkness? Curr. Opin. Genet. Dev. *19*, 187–191.

Finlan, L.E., Sproul, D., Thomson, I., Boyle, S., Kerr, E., Perry, P., Ylstra, B., Chubb, J.R., and Bickmore, W.A. (2008). Recruitment to the nuclear periphery can alter expression of genes in human cells. PLoS Genet. *4*, e1000039.

Fong, L.G., Ng, J.K., Lammerding, J., Vickers, T.A., Meta, M., Coté, N., Gavino, B., Qiao, X., Chang, S.Y., Young, S.R., et al. (2006). Prelamin A and lamin A appear to be dispensable in the nuclear lamina. J. Clin. Invest. *116*, 743–752.

Greco, V., and Guo, S. (2010). Compartmentalized organization: a common and required feature of stem cell niches? Development *137*, 1586–1594.

Helmlinger, D., Hardy, S., Abou-Sleymane, G., Eberlin, A., Bowman, A.B., Gansmüller, A., Picaud, S., Zoghbi, H.Y., Trottier, Y., Tora, L., and Devys, D. (2006). Glutamine-expanded ataxin-7 alters TFTC/STAGA recruitment and chromatin structure leading to photoreceptor dysfunction. PLoS Biol. *4*, e67.

Hirano, Y., Hizume, K., Kimura, H., Takeyasu, K., Haraguchi, T., and Hiraoka, Y. (2012). Lamin B receptor recognizes specific modifications of histone h4 in heterochromatin formation. J. Biol. Chem. *287*, 42654–42663.

Huber, M.D., Guan, T., and Gerace, L. (2009). Overlapping functions of nuclear envelope proteins NET25 (Lem2) and emerin in regulation of extracellular signal-regulated kinase signaling in myoblast differentiation. Mol. Cell. Biol. *29*, 5718–5728.

Ikegami, K., Egelhofer, T.A., Strome, S., and Lieb, J.D. (2010). Caenorhabditis elegans chromosome arms are anchored to the nuclear membrane via discontinuous association with LEM-2. Genome Biol. *11*, R120.

Kim, Y., Sharov, A.A., McDole, K., Cheng, M., Hao, H., Fan, C.M., Gaiano, N., Ko, M.S., and Zheng, Y. (2011). Mouse B-type lamins are required for proper organogenesis but not by embryonic stem cells. Science *334*, 1706–1710.

Kizilyaprak, C., Spehner, D., Devys, D., and Schultz, P. (2011). The linker histone H1C contributes to the SCA7 nuclear phenotype. Nucleus *2*, 444–454.

Kubben, N., Voncken, J.W., Konings, G., van Weeghel, M., van den Hoogenhof, M.M., Gijbels, M., van Erk, A., Schoonderwoerd, K., van den Bosch, B., Dahlmans, V., et al. (2011). Post-natal myogenic and adipogenic developmental: defects and metabolic impairment upon loss of A-type lamins. Nucleus *2*, 195–207.

(C) Summary of the effect of the genotype on the nuclear architecture. Presence and absence of LBR and LamA/C in individual cell types are shown with green and red pluses and minuses; *i*, inversion; *c*, compensation by prolonged LBR expression. Bar, 2 μm.
(D) Proposed organization of the two tethers maintaining peripheral heterochromatin. Chromatin/DNA binding by lamins (dotted circles) is not sufficient for heterochromatin tethering but might synergistically enhance binding.
See also Figure S7.

Kubben, N., Adriaens, M., Meuleman, W., Voncken, J.W., van Steensel, B., and Misteli, T. (2012). Mapping of lamin A- and progerin-interacting genome regions. Chromosoma *121*, 447–464.

Makatsori, D., Kourmouli, N., Polioudaki, H., Shultz, L.D., McLean, K., Theodoropoulos, P.A., Singh, P.B., and Georgatos, S.D. (2004). The inner nuclear membrane protein lamin B receptor forms distinct microdomains and links epigenetically marked chromatin to the nuclear envelope. J. Biol. Chem. *279*, 25567–25573.

Mattout, A., Pike, B.L., Towbin, B.D., Bank, E.M., Gonzalez-Sandoval, A., Stadler, M.B., Meister, P., Gruenbaum, Y., and Gasser, S.M. (2011). An EDMD mutation in C. elegans lamin blocks muscle-specific gene relocation and compromises muscle integrity. Curr. Biol. *21*, 1603–1614.

Melcon, G., Kozlov, S., Cutler, D.A., Sullivan, T., Hernandez, L., Zhao, P., Mitchell, S., Nader, G., Bakay, M., Rottman, J.N., et al. (2006). Loss of emerin at the nuclear envelope disrupts the Rb1/E2F and MyoD pathways during muscle regeneration. Hum. Mol. Genet. *15*, 637–651.

Olins, A.L., Rhodes, G., Welch, D.B., Zwerger, M., and Olins, D.E. (2010). Lamin B receptor: multi-tasking at the nuclear envelope. Nucleus *1*, 53–70.

Ozawa, R., Hayashi, Y.K., Ogawa, M., Kurokawa, R., Matsumoto, H., Noguchi, S., Nonaka, I., and Nishino, I. (2006). Emerin-lacking mice show minimal motor and cardiac dysfunctions with nuclear-associated vacuoles. Am. J. Pathol. *168*, 907–917.

Park, Y.E., Hayashi, Y.K., Goto, K., Komaki, H., Hayashi, Y., Inuzuka, T., Noguchi, S., Nonaka, I., and Nishino, I. (2009). Nuclear changes in skeletal muscle extend to satellite cells in autosomal dominant Emery-Dreifuss muscular dystrophy/limb-girdle muscular dystrophy 1B. Neuromuscul. Disord. *19*, 29–36.

Rapaport, D.H., Wong, L.L., Wood, E.D., Yasumura, D., and LaVail, M.M. (2004). Timing and topography of cell genesis in the rat retina. J. Comp. Neurol. *474*, 304–324.

Röber, R.A., Sauter, H., Weber, K., and Osborn, M. (1990). Cells of the cellular immune and hemopoietic system of the mouse lack lamins A/C: distinction versus other somatic cells. J. Cell Sci. *95*, 587–598.

Shultz, L.D., Lyons, B.L., Burzenski, L.M., Gott, B., Samuels, R., Schweitzer, P.A., Dreger, C., Herrmann, H., Kalscheuer, V., Olins, A.L., et al. (2003). Mutations at the mouse ichthyosis locus are within the lamin B receptor gene: a single gene model for human Pelger-Huët anomaly. Hum. Mol. Genet. *12*, 61–69.

Solovei, I., Kreysing, M., Lanctôt, C., Kösem, S., Peichl, L., Cremer, T., Guck, J., and Joffe, B. (2009). Nuclear architecture of rod photoreceptor cells adapts to vision in mammalian evolution. Cell *137*, 356–368.

Sullivan, T., Escalante-Alcalde, D., Bhatt, H., Anver, M., Bhat, N., Nagashima, K., Stewart, C.L., and Burke, B. (1999). Loss of A-type lamin expression compromises nuclear envelope integrity leading to muscular dystrophy. J. Cell Biol. *147*, 913–920.

Tifft, K.E., Bradbury, K.A., and Wilson, K.L. (2009). Tyrosine phosphorylation of nuclear-membrane protein emerin by Src, Abl and other kinases. J. Cell Sci. *122*, 3780–3790.

Towbin, B.D., Meister, P., Pike, B.L., and Gasser, S.M. (2010). Repetitive transgenes in C. elegans accumulate heterochromatic marks and are sequestered at the nuclear envelope in a copy-number- and lamin-dependent manner. Cold Spring Harb. Symp. Quant. Biol. *75*, 555–565.

Towbin, B.D., González-Aguilera, C., Sack, R., Gaidatzis, D., Kalck, V., Meister, P., Askjaer, P., and Gasser, S.M. (2012). Step-wise methylation of histone H3K9 positions heterochromatin at the nuclear periphery. Cell *150*, 934–947.

Verhagen, A.M., de Graaf, C.A., Baldwin, T.M., Goradia, A., Collinge, J.E., Kile, B.T., Metcalf, D., Starr, R., and Hilton, D.J. (2012). Reduced lymphocyte longevity and homeostatic proliferation in lamin B receptor-deficient mice results in profound and progressive lymphopenia. J. Immunol. *188*, 122–134.

Worman, H.J., Ostlund, C., and Wang, Y. (2010). Diseases of the nuclear envelope. Cold Spring Harb. Perspect. Biol. *2*, a000760.

Yang, S.H., Chang, S.Y., Yin, L., Tu, Y., Hu, Y., Yoshinaga, Y., de Jong, P.J., Fong, L.G., and Young, S.G. (2011). An absence of both lamin B1 and lamin B2 in keratinocytes has no effect on cell proliferation or the development of skin and hair. Hum. Mol. Genet. *20*, 3537–3544.

Yao, J., Fetter, R.D., Hu, P., Betzig, E., and Tjian, R. (2011). Subnuclear segregation of genes and core promoter factors in myogenesis. Genes Dev. *25*, 569–580.

Zhang, J., Lian, Q., Zhu, G., Zhou, F., Sui, L., Tan, C., Mutalif, R.A., Navasankari, R., Zhang, Y., Tse, H.F., et al. (2011). A human iPSC model of Hutchinson Gilford Progeria reveals vascular smooth muscle and mesenchymal stem cell defects. Cell Stem Cell *8*, 31–45.

Zullo, J.M., Demarco, I.A., Piqué-Regi, R., Gaffney, D.J., Epstein, C.B., Spooner, C.J., Luperchio, T.R., Bernstein, B.E., Pritchard, J.K., Reddy, K.L., and Singh, H. (2012). DNA sequence-dependent compartmentalization and silencing of chromatin at the nuclear lamina. Cell *149*, 1474–1487.

EXTENDED EXPERIMENTAL PROCEDURES

Mammalian Retinas

The following list shows the correspondence between the scientific species names and the English names used in Figure 1C: pilot whale, *Globicephala melaena*; dolphin, *Lagenorhynchus acutus*; cow, *Bos Taurus*; goat, *Capra hircus*; sheep, *Ovis oreintalis aries*; mouflon, *Ovis musimon*; pig, *Sus scrofa*; guanaco, *Lama guanicole*; horse, *Equus caballus*; cat, *Felis catus* red fox, *Vulpes vulpes*; arctic fox, *Alopex lagopus*; dog, *Canis lupus familiaris*; sea lion, *Phocarctos hookeri*; ferret, *Mustela putorius*; shrew, *Sorex araneus*; hedgehog, *Erinaceus concolor*; mouse, *Mus musculus*; rat, *Rattus norvegicus*; gerbil, *Meriones unguiculatus*; hamster, *Phodopus campbelli*; common vole, *Microtus arvalis*; tuco-tuco, *Ctenomys talarum*; guinea pig, *Cavia porcellus*; gray squirrel, *Sciurus carolinensis*; flying squirrel, *Pteromys volans*; red-cheeked ground squirrel, *Spermophilus erythrogenys*; chipmunk, *Tamias sibiricus*; striped ground squirrel, *Xerus erythropus*; woodchuck, *Marmota monax*; dormouse, *Glis glis*; rabbit, *Oryctolagus cuniculus*; treeshrew, *Tupaia belangeri*; mouse lemur, *Microcebus myoxinus*; marmoset, *Callithrix jaccus*; vervet monkey, *Chlorocebus aethiops*; macaque, *Macaca fascicularis*; hyrax, *Procavia capensis*; tenrec, *Echinops telfairi*. In most cases, eyes were dissected immediately (sacrificed animals) or soon after death, the sclera was punctured or cut open to allow fixative access to the retina, and eyes were fixed in 4% formaldehyde in PBS for 12-24 hr. Further processing was carried out as described in the next paragraph.

Histological Studies on Mice

Mice were sacrificed for histological studies by cervical dislocation after isofluran narcosis or by CO_2 euthanasia. Tissues were excised and fixed in 4% formaldehyde in PBS for 12-24 hr, infiltrated with 30% sucrose, and embedded in Jung tissue freezing medium (Leica Microsystems). In most cases, tissues of different age or from control and mutant/genetically modified animals were embedded and cut together so that they could be stained identically and observed in the same section. Cryosections (16-20μm) were prepared using Cryostat Leica and immediately stored at −80°C. Sections immunostaining was performed as described in Eberhart et al. (2012). Before immunostaining, sections were dried at room temperature for 30 min, re-hydrated in sodium citrate buffer, and subjected to antigen retrieval by heating up to 80-85°C in a microwave. The duration of the heating was dependent on the antibody, as shown in the tables below. After antigen retrieval, section were incubated in 0.5% Triton X-100 for 1 hr. Primary and secondary antibodies were applied for 12-24 hr under glass chambers at room temperature; antibodies were diluted in blocking solution (1% BSA, 0.1% Triton X-100, 0.1% Saponin in PBS); washes between and after antibodies were done with 0.01% Triton X-100, 3 × 30 m, at 37°C.

Antibodies for Nuclear Proteins

ATXN7, rabbit, serum 1261 (D. Devys, Institut de Génétique et de Biologie Moléculaire et Cellulaire, Illkirch); BAF, FL-89 (Santa Cruz Biotechnology, SC-33787); B-23, nucleophosmin (Sigma, B 0556); Emerin (Novocastra, NCL-Emerin and Santa Cruz Biotechnology, SC-15378); H3K4me3 (Abcam, ab8580); H3K36me3 (Abcam, ab9050); H4 acetylated (Millipore, 06-866); H4K20me3 (Abcam, ab9053); LamA/C N-term (H. Herrmann, H. Zentgraf, DKFZ); LamA C-term and LamC C-term (T. Kolb, H. Herrmann, DKFZ); LamA/C (Millipore #05-714); LamB1 C-term (Santa Cruz Biotechnology, SC-6217); LamB2 (Invitrogen, 33-2100); Lap2α and neLap2 / panLap2 (R. Foisner, Medical University, Vienna); LBR N-term (M. Zwerger, H. Herrmann, DKFZ); LEMD2 (Atlas Antibodies AB, HPA017340); Man1 (Santa Cruz Biotechnology, SC-50458); U2 and U5 snRNP (O. Makarova, University of Leicester).

Antibodies for Cell Type Identification

Horizontal cells, CaBP D-28K (Sigma, C9848); Blood cells, CD45 (eBioscience, 13-0451); Amacrine cells, GABA (Sigma, A2052); Müller cells, GS (BD Biosciences, #610517); Paneth cells of intestine crypts, Lysozyme (DacoCytomation, A0099); Microglial cells in retina and brain, Lba-1 (WAKO, #019-19741); Myotubes satellite cells, PAX7 (Developmental Studies Hybridoma Bank); Bipolar cells, PKCalpha (Sigma, P4334); Intestine enteroendocrine cells, Secretin (Santa Cruz Biotechnology, SC-26630).

Fluorescence In Situ Hybridization

Retina fixation, preparation and pretreatment of cryosections, and fluorescence in situ hybridization (FISH) were carried out as described by Solovei (2010). Probe against mouse major satellite repeat (MSR) was generated by PCR using mouse Cot1 DNA and the following primers: For: 5′ GCGAGAAAACTGAAAATCAC 3′ and Rev: 5′ TCAAGTCGTCAAGTGGATG 3′. MSR probe was labeled by nick-translation using Cy3-dUTP and dissolved in hybridization mixture (50% formamide, 10% dextran sulfate, 1xSSC) at a concentration of 10-20 ng/μl.

Microscopy and Image Acquisition

Single optical sections or stacks of optical sections were collected using a Leica TCS SP5 confocal microscope equipped with Plan Apo 63x/1.4 NA oil immersion objective and lasers with excitation lines 405, 488, 561, 594 and 633 nm. Dedicated plug-ins in ImageJ program were used to compensate for axial chromatic shift between fluorochromes in confocal stacks, to create RGB stacks/images and to arrange them into galleries (Ronneberger et al., 2008; Walter et al., 2006). Chromocenter number in rod cells was scored on confocal image stacks using ImageJ program.

Generation and Genotyping of *Lmna* Knockout Mice

The *Lmna* conditional knockout allele contains loxP sites ~100 bp upstream exon 10 and downstream 3′-UTR of exon 12. For deletion of the *Lmna* 3′-terminus, we used mice (JAX stock 003651) in which *Cre* expression is controlled by the regulatory sequences of the mouse zona pellucida 3 (*Zp3*) gene, which directs expression exclusively in the growing oocytes resulting in floxed oocytes (Sun et al., 2008). Homozygous ($Lmna^{Flx/Flx}$) females were crossed with homozygous *Zp3* males. Female offspring harboring the Zp3-Cre allele were then crossed with WT males to obtain mice heterozygous for lamin A/C ($Lmna^{\Delta/+}$) which were crossed to obtain complete null ($Lmna^{\Delta/\Delta}$) mice.

Mice with K14-Cre allele (JAX stock 004782) express the Cre recombinase under the control of the human keratin 14 promoter. Male K14-Cre mice were crossed to $Lmna^{Flx/Flx}$ females; male offspring with the genotype $Lmna^{Flx/+,\ K14\text{-}Cre}$) were crossed with $Lmna^{Flx/+}$ females to obtain mice homozygous for LamA/C deletion specifically in the epidermis of the skin.

Generation and Genotyping of Lbr- and LamC-TER Mice

The mouse Lbr and lamin C coding sequences, GenBank accession numbers NM_133815.2 (base 129 to 2009) and NM_001111102.1 (base 30 to 1954) were cloned into the Nrl-L-EGFP construct, containing a 2.5-kb mouse Nrl promoter segment (−2408 to +115), to replace EGFP (Akimoto et al., 2006). Nrl-*Lbr* and *Nrl-LamC* transgenes were excised from plasmid DNA by EcoRI-*NotI* digestion. Preparation of DNA for microinjection and the production of transgenic mice were performed according to standard protocol (Nagy et al., 2003). Transgenic founder animals and their offspring were identified using quantitative real-time PCR (qPCR). Genomic DNA was extracted from tail snips using QIAamp DNA Mini Kit (QIAGEN). qPCR was performed on the 7500 Fast Real-Time PCR System (Applied Biosystems) with *Power* SYBR Green PCR Master Mix (Applied Biosystems). Transgene DNA levels were normalized to *Oct4* genomic reference; relative levels were calculated with the comparative C_T Method ($\Delta\Delta C_T$ method). Primers: Oct4 genomic reference, For: 5′ GAG AAG GAT GTG AGT GCC AAG AT 3′ and Rev: 5′ GGA ATG GGA ACA GGG AAA CA 3′; Lbr, For: 5′ GTG CTT ACC TCT ATG TTC GCT CTC T 3′ And Rev: 5′ AAC TCT CGG CCA ATG AAG AAG T 3′; LamC, For: 5′ CAG TGA GAA GCG CAC ATT GG 3′ and Rev: 5′ CAT CCA CTC GCC TCA GCA T 3′.

Satellite Cell Cultures and RNA Extraction

Two week old mice were sacrificed by CO_2 euthanasia. All four limbs were removed, muscles were isolated from the bones and washed for 20 min in 2% Penn/Strep antibiotic solution, then transferred in Hank's balanced salt solution. Next, sterile dispase (2.4U/ml) and collagenase (1%) enzyme solution (1:1 volume) was added and tissue was digested at 37°C in water bath for 30 min. An equal volume of DMEM 10% FBS (D10) was added and the solution was filtered through a 70μm, then through a 40μm sterile filter. Cells were centrifuged at 1200 rpm for 5 min and the pellet was rinsed with D10. Cells were cultured in collagen-plated T25 flasks overnight at 37°C. After 3 days (at 80% confluency) they were passaged onto 100 mm petri dishes and harvested after another 2 days (at 40%–50% confluency). D10 media was removed and cells were washed twice with PBS. Then 1 ml of Trizol was added in the dish and cells were scraped off. Solution was snap-frozen and stored at −80°C. For RNA extraction, cell lysates were vortexed briefly and 200 μl of chloroform was added. After a brief vortex, cell lysates were centrifuged at 13000 rpm for 15 min at 4°C. Clear supernatant was removed and precipitated with equal volume of 70% ethanol. RNA was extracted using QIAGEN RNeasy kit.

Transcriptome Sequencing and Data Analysis

Starting from 100 ng of total RNA, double-stranded cDNA was generated by the Ovation RNA-Seq v2 Kit (Nugen, San Carlos, CA) according to the manufacturer's protocol for myoblast samples. Briefly, total RNA was reversely transcribed into cDNA using a tagged random primer. The purified double-stranded cDNA was amplified by isothermal amplification enabled by RNase H cleavage of a chimeric RNA-DNA primer that allows for repeated re-priming and strand displacement (Dafforn et al., 2004). 200ng of the resulting double stranded cDNA were random-sheared by sonication (Bioruptor, Diagenode, Liege, Belgium; 30 on/off cycles of 30 s each) and subjected to end-repair and adaptor ligation to generate sequencing libraries for the Illumina Genome Analyzer. Each library was barcoded by a distinct 4 nucleotide sequence located at the 5′ end of each library insert in order to allow multiplex-sequencing. Six barcoded libraries representing duplicates of *Lmna*-KO, *Lbr*-KO and control WT were pooled and single-end sequenced on 6 lanes on the Illumina Genome Analyzer GAIIx yielding 217 million raw reads with a length of 84 bp. After demultiplexing, barcode trimming and quality filtering each library retained 25 to 30 million reads. For limb muscle samples 100ng of total RNA were used to generate strand-specific cDNA libraries using the Encore complete RNA-Seq Kit (Nugen, San Carlos, CA) according to the manufacturer's protocol. Briefly, after first strand synthesis with semi-random hexamers, depleted for rRNA priming sequences, second strand cDNA was tagged with dUTP and selectively digested after library generation. Six barcoded libraries representing duplicates of Lmna-KO, *Lbr*-KO and control WT were pooled and single-end sequenced on 2 lanes on the Illumina Genome Analyzer GAIIx yielding 86 million raw reads with a length of 90 bp. After demultiplexing, barcode trimming and quality filtering each library retained around 10 million reads. Reads were mapped to the mouse genome using the splice-junction mapper TOPHAT (Trapnell et al., 2009). The program module Cuffdiff from the CUFFLINKS package (Trapnell et al., 2010) was used to obtain normalized FPKM values and to identify differentially expressed genes by accounting for biological replicates (n = 2) and setting a false discovery rate of 0.05. For assessment of repeat expression, a RepeatMasker file was obtained from UCSC genome browser (http://genome.ucsc.edu), restricted to region not overlapping with annotated genes and the fpkm values were summarized to the different

repeat classes using Cuffdiff. All data handling steps were performed on a client-cluster grid with a local instance of the GALAXY (Goecks et al., 2010) platform.

Gene Ontology analysis was performed using GOrilla (Eden et al., 2009) and GSEA (Subramanian et al., 2005) software.

SUPPLEMENTAL REFERENCES

Chen, Y., Gelfond, J., McManus, L.M., and Shireman, P.K. (2011). Temporal microRNA expression during in vitro myogenic progenitor cell proliferation and differentiation: regulation of proliferation by miR-682. Physiol. Genomics *43*, 621–630.

Cheung, T.H., Quach, N.L., Charville, G.W., Liu, L., Park, L., Edalati, A., Yoo, B., Hoang, P., and Rando, T.A. (2012). Maintenance of muscle stem-cell quiescence by microRNA-489. Nature *482*, 524–528.

Dafforn, A., Chen, P., Deng, G., Herrler, M., Iglehart, D., Koritala, S., Lato, S., Pillarisetty, S., Purohit, R., Wang, M., et al. (2004). Linear mRNA amplification from as little as 5 ng total RNA for global gene expression analysis. Biotechniques *37*, 854–857.

Eberhart, A., Kimura, H., Leonhardt, H., Joffe, B., and Solovei, I. (2012). Reliable detection of epigenetic histone marks and nuclear proteins in tissue cryosections. Chromosome Res. *20*, 849–858.

Eden, E., Navon, R., Steinfeld, I., Lipson, D., and Yakhini, Z. (2009). GOrilla: a tool for discovery and visualization of enriched GO terms in ranked gene lists. BMC Bioinformatics *10*, 48.

Goecks, J., Nekrutenko, A., and Taylor, J.; Galaxy Team (2010). Galaxy: a comprehensive approach for supporting accessible, reproducible, and transparent computational research in the life sciences. Genome Biol. *11*, R86.

Nagy, A., Gertsenstein, M., Vintersten, K., and Behringer, R. (2003). Manipulating the Mouse Embryo-A Laboratory Manual (Cold Spring Harbor, NY: Cold Spring Harbor Laboratory Press).

Ronneberger, O., Baddeley, D., Scheipl, F., Verveer, P.J., Burkhardt, H., Cremer, C., Fahrmeir, L., Cremer, T., and Joffe, B. (2008). Spatial quantitative analysis of fluorescently labeled nuclear structures: problems, methods, pitfalls. Chromosome Res. *16*, 523–562.

Solovei, I. (2010). Fluorescence in situ hybridization (FISH) on tissue cryosections. Methods Mol. Biol. *659*, 71–82.

Subramanian, A., Tamayo, P., Mootha, V.K., Mukherjee, S., Ebert, B.L., Gillette, M.A., Paulovich, A., Pomeroy, S.L., Golub, T.R., Lander, E.S., and Mesirov, J.P. (2005). Gene set enrichment analysis: a knowledge-based approach for interpreting genome-wide expression profiles. Proc. Natl. Acad. Sci. USA *102*, 15545–15550.

Sun, Q.Y., Liu, K., and Kikuchi, K. (2008). Oocyte-specific knockout: a novel in vivo approach for studying gene functions during folliculogenesis, oocyte maturation, fertilization, and embryogenesis. Biol. Reprod. *79*, 1014–1020.

Trapnell, C., Pachter, L., and Salzberg, S.L. (2009). TopHat: discovering splice junctions with RNA-Seq. Bioinformatics *25*, 1105–1111.

Trapnell, C., Williams, B.A., Pertea, G., Mortazavi, A., Kwan, G., van Baren, M.J., Salzberg, S.L., Wold, B.J., and Pachter, L. (2010). Transcript assembly and quantification by RNA-Seq reveals unannotated transcripts and isoform switching during cell differentiation. Nat. Biotechnol. *28*, 511–515.

Walter, J., Joffe, B., Bolzer, A., Albiez, H., Benedetti, P.A., Müller, S., Speicher, M.R., Cremer, T., Cremer, M., and Solovei, I. (2006). Towards many colors in FISH on 3D-preserved interphase nuclei. Cytogenet. Genome Res. *114*, 367–378.

Zammit, P.S., Partridge, T.A., and Yablonka-Reuveni, Z. (2006). The skeletal muscle satellite cell: the stem cell that came in from the cold. J. Histochem. Cytochem. *54*, 1177–1191.

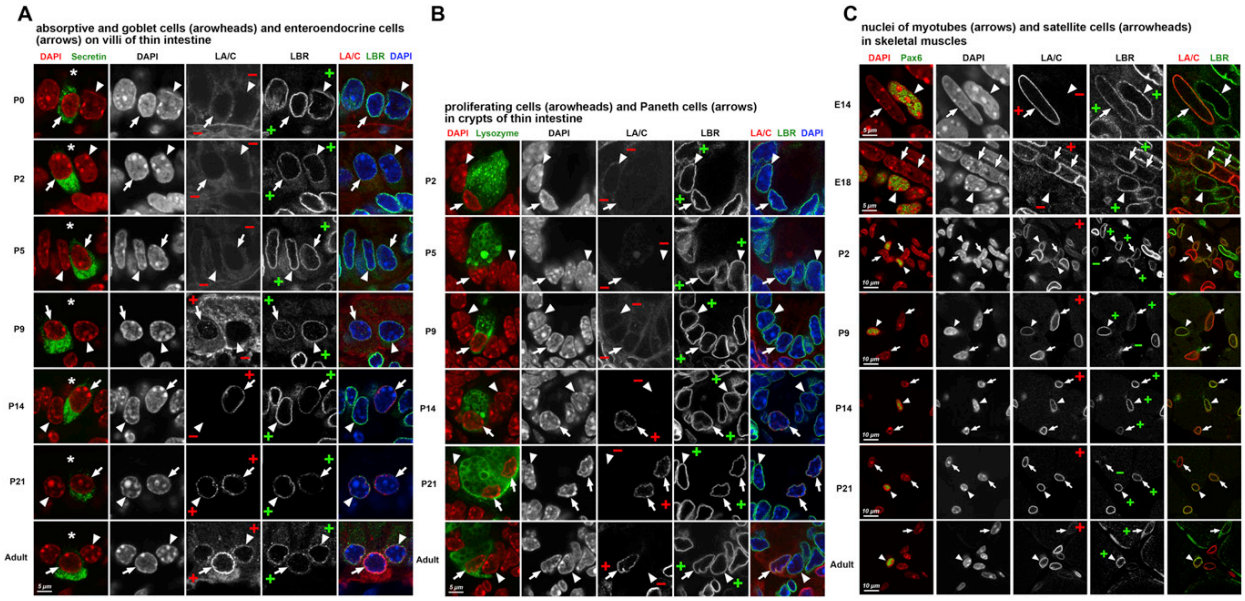

Figure S1. Expression of LBR and LamA/C in the Nuclei from Small Intestine and Skeletal Muscle in Mice of Different Age, Related to Figure 2C

(A) Absorptive cells (arrowheads) and enteroendocrine cells (marked by secretin expression, arrows). Goblet cells (not shown) do not differ from absorptive cells with regard to LBR and LamA/C expression.

(B) Crypt cells (arrowheads) and Paneth cells (arrows); the latter are marked by lysozyme expression.

(C) Nuclei of myotubes (arrows) and satellite cells (arrowheads). Presence and absence of LBR and LamA/C are marked by colored "+" and "-," respectively.

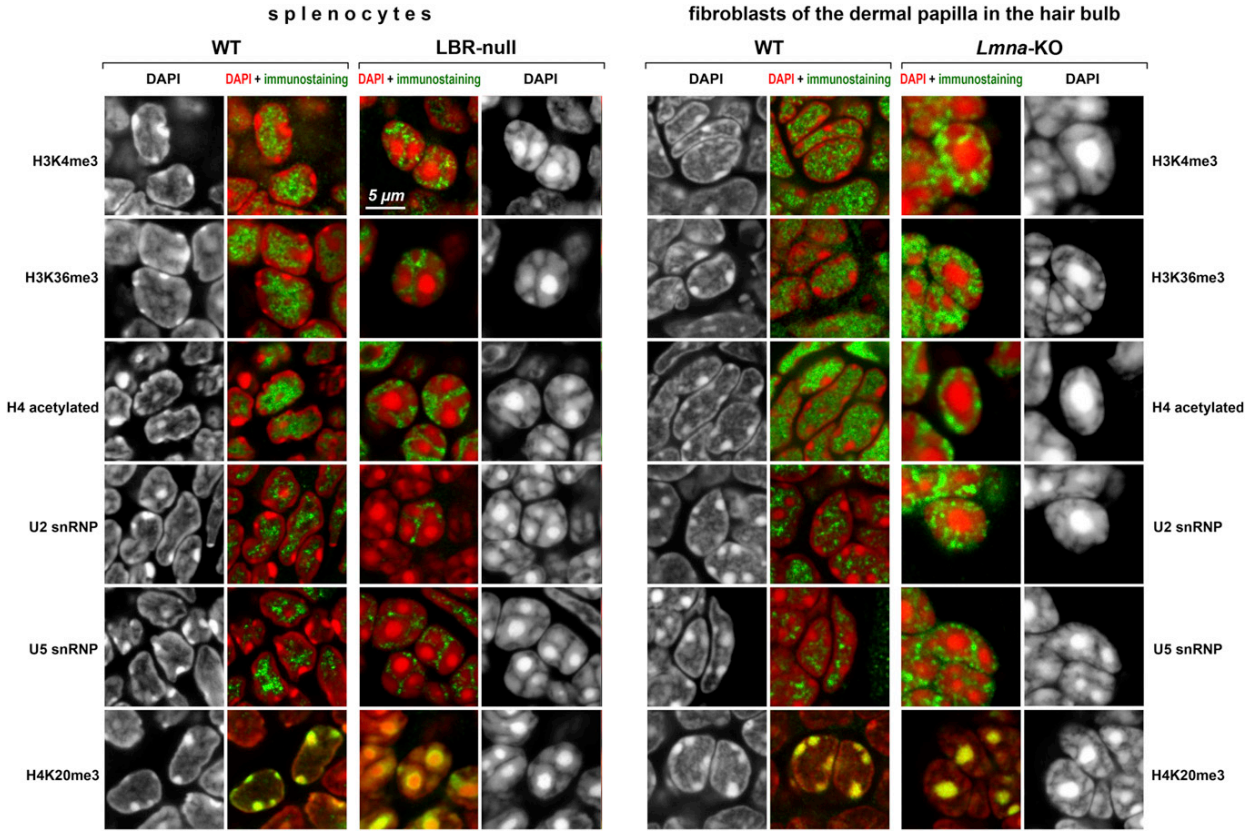

Figure S2. Nuclear Distribution of Eu- and Heterochromatin Markers in Representative Cell Types Undergoing Nuclear Inversion in LBR Null and *Lmna*-KO Mice, Related to Figures 3 and 5

Marker histone modifications for euchromatin (H3K4me3, H3K36me3, H4acetylated), heterochromatin (H4K20me3) and markers of splicing machinery (U2 and U5 snRNP) in nuclei that invert in LBR null and *Lmna*-KO mice. Note relocation of euchromatin markers and splicing machinery from the internal regions to the nuclear periphery and inverse shift of heterochromatin. The architecture of inverted nuclei of cells in LBR null and *Lmna*-KO mice corresponds to that of rod cells (c.f. Figure 1A and Solovei et al., 2009, Figures 2 and 3).

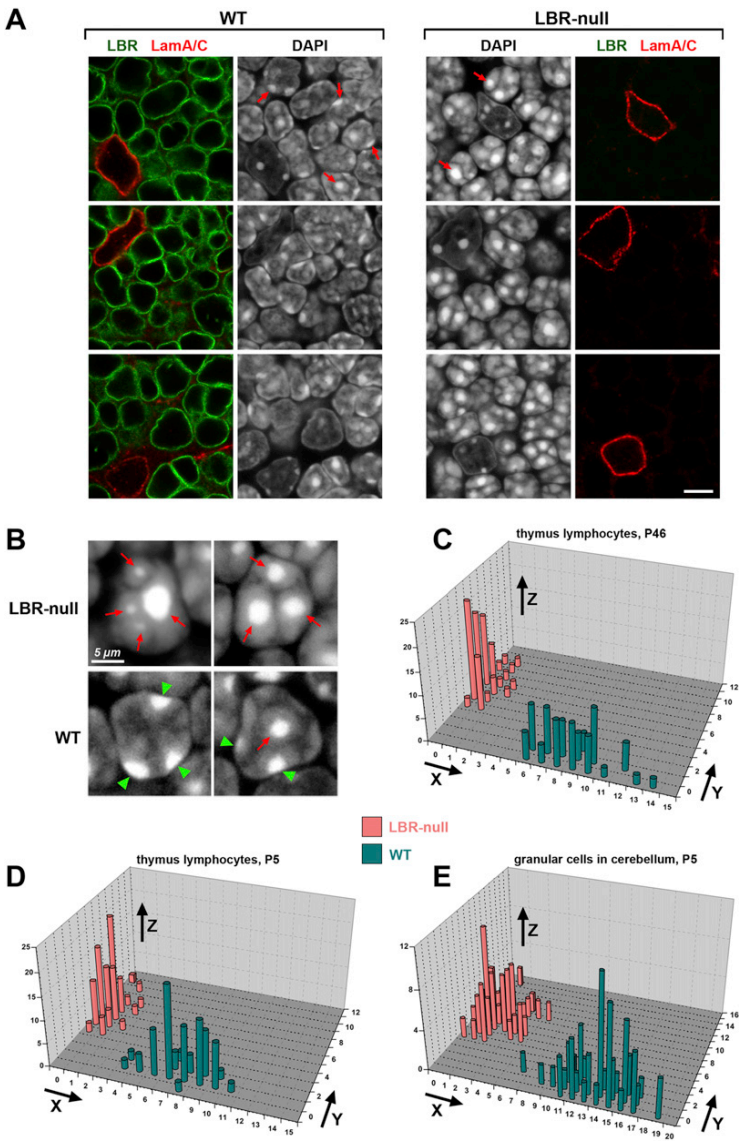

Figure S3. Comparison of the Organization of Inverted and Conventional Nuclei, Related to Figure 3

(A–D) Thymic lymphocytes from thymus of adult WT and LBR null mice.

(A) Cells only expressing LBR (green) are lymphocytes; the few cells expressing LamA/C (red) are stromal cells. Compared to WT (left), LBR null (right) lymphocytes have a smaller number of larger chromocenters. Nuclei of stromal cells have a conventional architecture and are not different between WT and LBR null.

(B) WT lymphocytes (bottom) have not more than one internal chromocenter (red arrow), the other are peripheral (green arrowheads). Peripheral chromocenters adjoin the nuclear border and actually have a hemispherical or discoid shape. LBR null lymphocytes have only spherical internal chromocenters (red arrows). Bars: 5μm.

(C–E) 2-dimensional distribution of frequency of internal and peripheral chromocenters in thymic lymphocytes and cerebellar granular cells (neurons). x axis: the number of peripheral chromocenters; y axis: the number of internal chromocenters; z-axis: percent of nuclei with the respective numbers of peripheral and internal chromocenters.

(C) lymphocytes from adult (P46) mice.

(D) lymphcytes from P5 mice.

(E) granular cells from P5 mice; these cells experience transient inversion during early postnatal development (see text, Figure 3D).

As inverted nuclei from LBR null (pink) and conventional nuclei from WT (blue) mice have different numbers of internal and peripheral chromocenters, they populate two non-overlapping regions of the diagram.

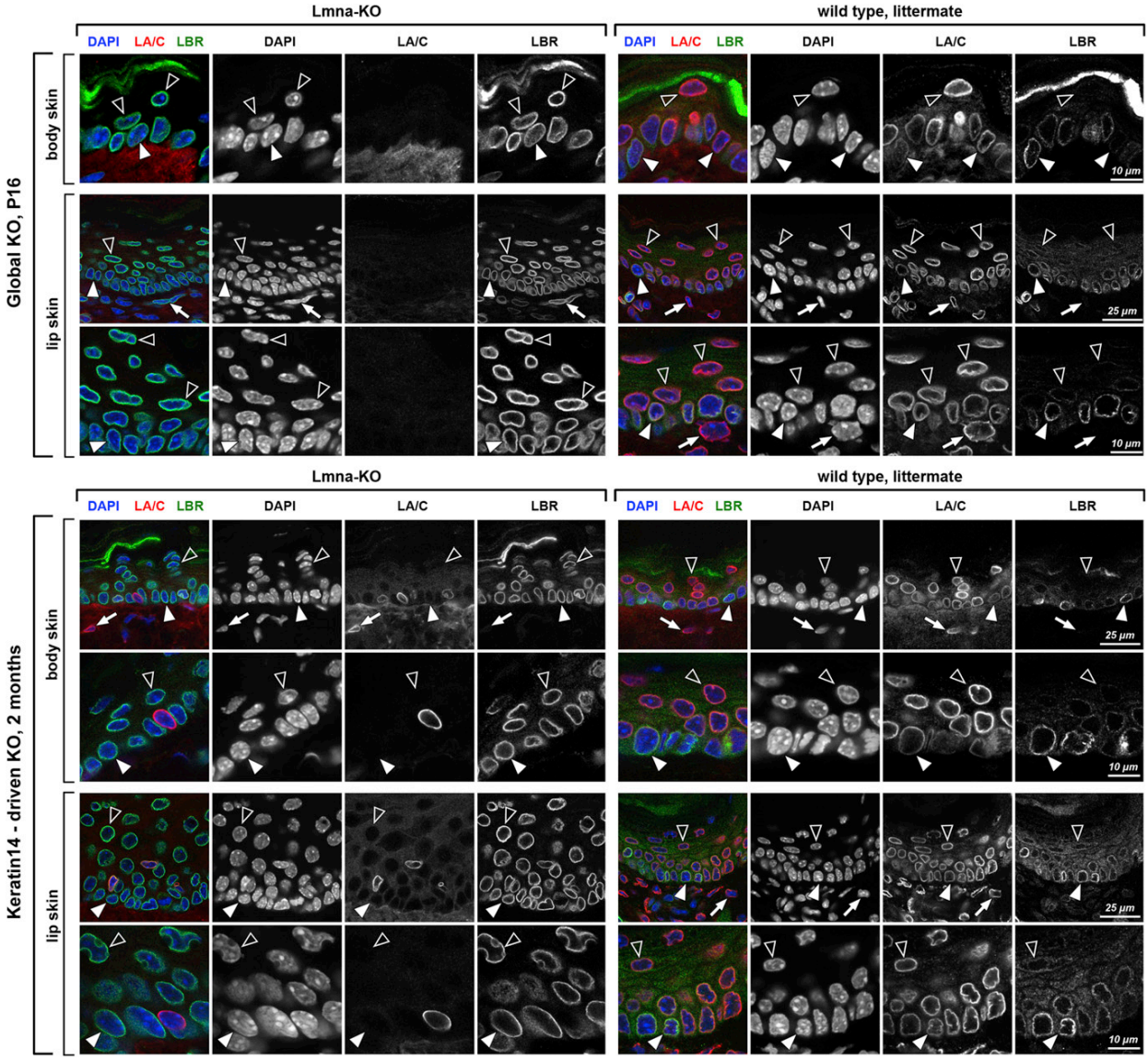

Figure S4. Compensation of LamA/C Deletion by Prolonged Expression of LBR in Keratinocytes, Related to Figures 5A and 5B

(A) Basal keratinocytes (solid arrowheads), suprabasal keratinocytes (empty arrowheads), and dermal fibroblasts (arrows). In both body skin and lip skin, deletion of LamA/C results in prolonged and enhanced expression of LBR in all keratinocytes. Fibroblasts do not express K14, therefore persistent LBR expression is observed only in keratinocytes from K14*Cre*-driven knockout mice, whereas fibroblasts express LamA/C. Single cells situated between basal keratinocytes but expressing LamA/C in K14*Cre*-driven *Lmna*-KO are melanocytes. Basal cells not expressing LBR probably are cells that already exited cell cycle but still have not moved apically.

(B) Summary of differences between the WT and Lmna-KO keratinocytes; compensatory changes in LBR expression are highlighted by green shading.

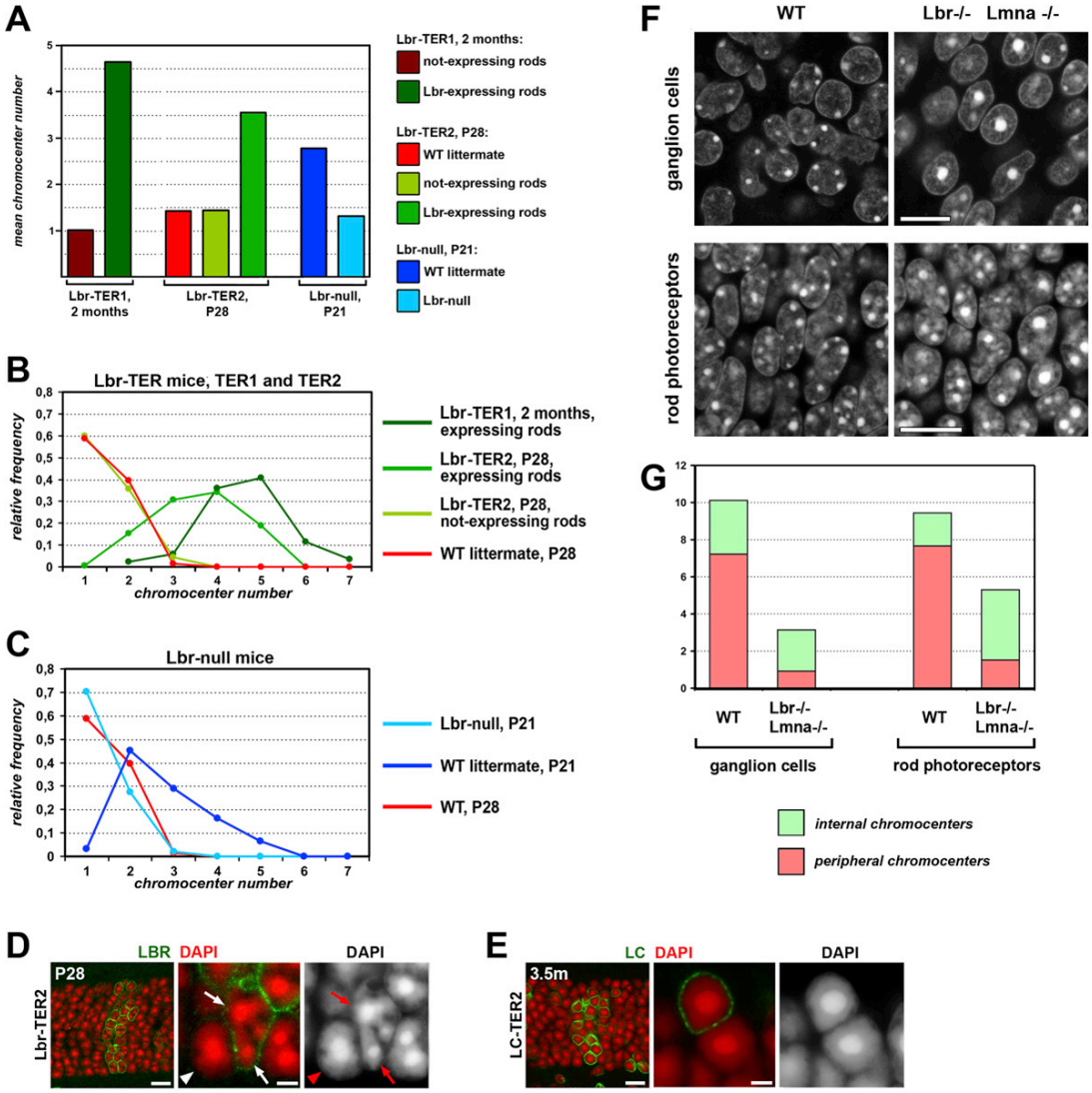

Figure S5. The Effect of Transgenic LBR and LamA/C Expression on Rod Nuclei, Related to Figures 5C–5E and 6A–6C

(A–C) The degree of inversion estimated by chromocenter number. Differences between the phenotypes of interest and controls were tested using chi-square method and are in all cases significant at the level of $p < 0.01$ or better. (A) Mean chromocenter number. Note that not-expressing rod nuclei in Lbr-TER1 have the same chromocenter number (a single chromocenter) as WT rods (not shown). (B) Relative frequency distribution of nuclei depending on chromocenter number for Lbr-TER rods. Note than WT and not-expressing rods of Lbr-TER2 show the same distribution. (C) Relative frequency distribution of LBR null rods depending on chromocenter number. For comparison, the distribution for WT rods in P28 mice (red line) is shown in both last diagrams (B and C). Note that inP21 LBR null rods inversion is even slightly more advanced, than in P28 WT mice.

(D) Lbr-TER2 mice show no signs of LBR overexpression, eventually LBR expression is almost completely silenced in Lbr-TER2 and rod nuclei invert, but at P28 they display clear, statistically significant retardation of inversion. Lbr-TER2, one month old retina. A positive clone (left panel) and nuclei at its border (middle and right panels). Note an LBR-negative, completely inverted nucleus (arrowhead) and a nucleus with retarded inversion; it has several chromocenters and they are abut the NE (arrows).

(E) Expression of lamin C (LC) does not affect rod nuclear architecture. A positive clone (left panel) and nuclei expressing and not expressing lamin C (middle and right panels).

(F and G) Ganglion cells and rod photoreceptor cells from WT (left) and double knockout (LBR−/− Lmna−/−, right) P0 mice. DAPI staining (F) shows a doubtless change in the size, number and position of chromocenters in ganglion cells and rod photoreceptor cells of double KO mice compared to the WT. The histogram (G) shows the mean numbers of peripheral and internal chromocenters scored in 50 nuclei of each cell type and genotype: note a reduction in total chromocenter number and that of the peripheral chromocenters.

Bars: D,E, 25 μm left panel, 2 μm middle and right panels; F, 10 μm.

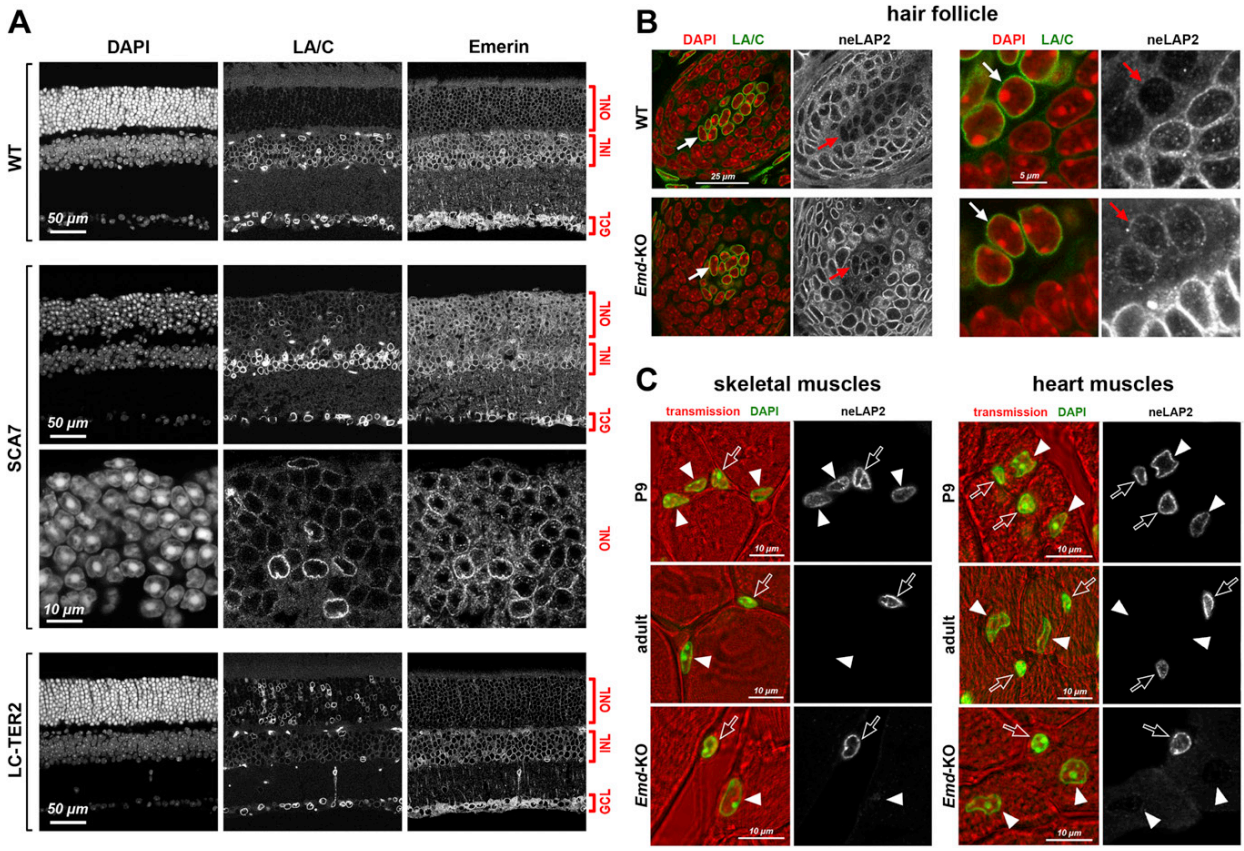

Figure S6. Expression of LamA/C and Emerin in the Retina of WT, SCA7, and LC-TER2 Mice; Expression of neLap2 in the Dermal Papilla Cells and Striated Muscles in WT and *Emd*-KO Mice, Related to Figure 6D

(A) Emerin is absent in the ONL of WT mice, whereas its level is equally high in INL and ONL of mice with advanced SCA7 (93 weeks); a higher magnification image shows a correlation in signal intensity of emerin and LamA/C in individual nuclei. Neither emerin, nor LamA/C are expressed in SCA7 mice at 4-6 weeks, by which time nuclei show complete inversion. The expression is initiated later, parallel to partial restoration of the conventional nuclear architecture. The inability of transgenic LamA/C to counteract nuclear inversion coincides with lack of emerin in rods expressing lamin C.

(B) Dermal papilla cell nuclei (arrows) are LamA/C-positive; they are surrounded by LamA/C negative hair matrix cells. Dermal papilla nuclei do not express neLap2 in WT mice (top row), whereas in *Emd*-KO mice (bottom row) they show a clear signal, though still weaker, than in the nuclei of the hair matrix cells.

(C) Myotube (left) and cardiomyocyte (right) nuclei from WT (P9 and adult) and Emd-KO (adult) mice. Myotube and cardiomyocyte nuclei (arrowheads) express neLap2b in young mice but not in adult WT or Emd-KO mice. Note that endothelial cells (arrows) in both tissues express neLap2 throughout life.

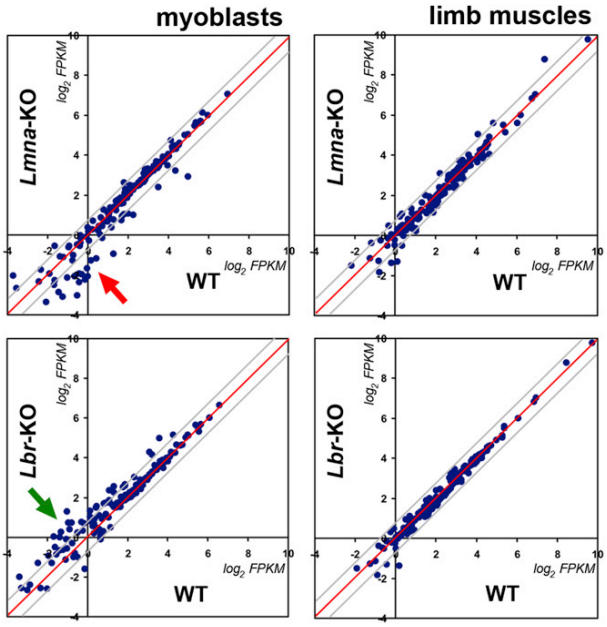

Figure S7. Genes from the GOC Striated Muscle Cell Differentiation: Myoblasts and Limb Muscles, Related to Figure 7B

Each point represents a gene, with its expression levels (log_2 FPKM) in WT and a KO as coordinates. Gray lines mark 2-fold downregulation (below the red line) and upregulation (above the red line). Arrows emphasize deregulation trends for Lmna (red) and Lbr (green).

The results are very similar to those for the GOC Structural constituent of muscle. The proportion of genes strongly deregulated in myoblasts is smaller, which may be explained by the fact that this GOC covers numerous genes (157 with non-zero expression in our data), many of which are not muscle-specific (e.g., Dicer1, Ezh2, Notch1, Rb1).

2.5 Autonomous and non-autonomous properties of small chromosome segments: spatial interactions, lamina-association and transcriptional regulation

Harmen van de Werken, Katharina Thanisch, Wouter Meulemann, Josien Haan, Dominika Bijos, An Weut, Yana Feodorova, Sjoerd Holwerda, Heinrich Leonhardt, Bas van Steensel*, Wouter de Laat*, Thierry Voet*, Irina Solovei*, and Boris Joffe

Summary

Spatial chromatin arrangement is pivotal for both normal and pathogenic nuclear processes. Although key features of the nuclear architecture have been unraveled, their interdependencies as well as relations to the underlying genomic sequence remain poorly understood. Here, we present the first comprehensive analysis of the features, which determine spatial genome positioning by comparing two variants of a Human Artificial Chromosome (HAC) within a xenospecific mouse background with their native mouse and human orthologs. Both HACs comprise genomic sequences corresponding to the main chromatin classes, including centromeric, gene-rich, gene-poor and desert subregions marked by a distinct GC-content, gene-richness and repeat repertoire. Importantly, the borders of the subregions match with the borders of topologically associated domains (TADs).

We performed 4Cseq, DamID and RT-qPCR on mouse rod photoreceptor cells, where the main chromatin classes are arranged in concentric shells. Our results reveal that small chromosome segments (500 kb) exhibit an inherent tendency to cluster autonomously with sequences of the same chromatin class in a context independent manner. Moreover, lamina-association of short chromosome segments (100 kb) within a gene-rich subregion strongly correlates with transcriptional activity. In contrast, establishment of lamina-association patterns between gene-rich and gene-poor subregions is chromosomal context dependend.

Our data suggest that the main chromatin classes play a crucial role in linking the genome not only to chromosomal functions but also to its spatial distribution in mammalian nuclei, serving as a blueprint of the overall nuclear architecture which is further specified by other factors.

Results

We sought to directly test whether small chromosomal regions build by different chromatin classes correctly segregate in the nuclei, establish proper lamina-association patterns and maintain transcriptional regulation. For this purpose, we studied a Human Artificial

Chromosome (HAC) in a xenospecific mouse background in relation to its orthologous regions of the native mouse and human chromosomes.

Genomic features of HACs and corresponding human and mouse orthologous regions

Two variants of a human artificial chromosome (HAC), a circular (C-HAC) and a linear (L-HAC), were generated as described earlier (Voet et al., 2001; 2003; Weuts et al., 2012) (Figure 1a). In brief, the HAC contains a 4.25 Mb region from human chromosome 1 (HSA1, 1p21.3-22.1, human HAC Orthology Region, hHOR) spanning from *MTF2* to the middle of the *DPYD* (Fig. 1b). In the HACs, the ends of the hHOR are joined by the centromere region containing at least 2 Mb of human alphoid repeats (Figure 1a).

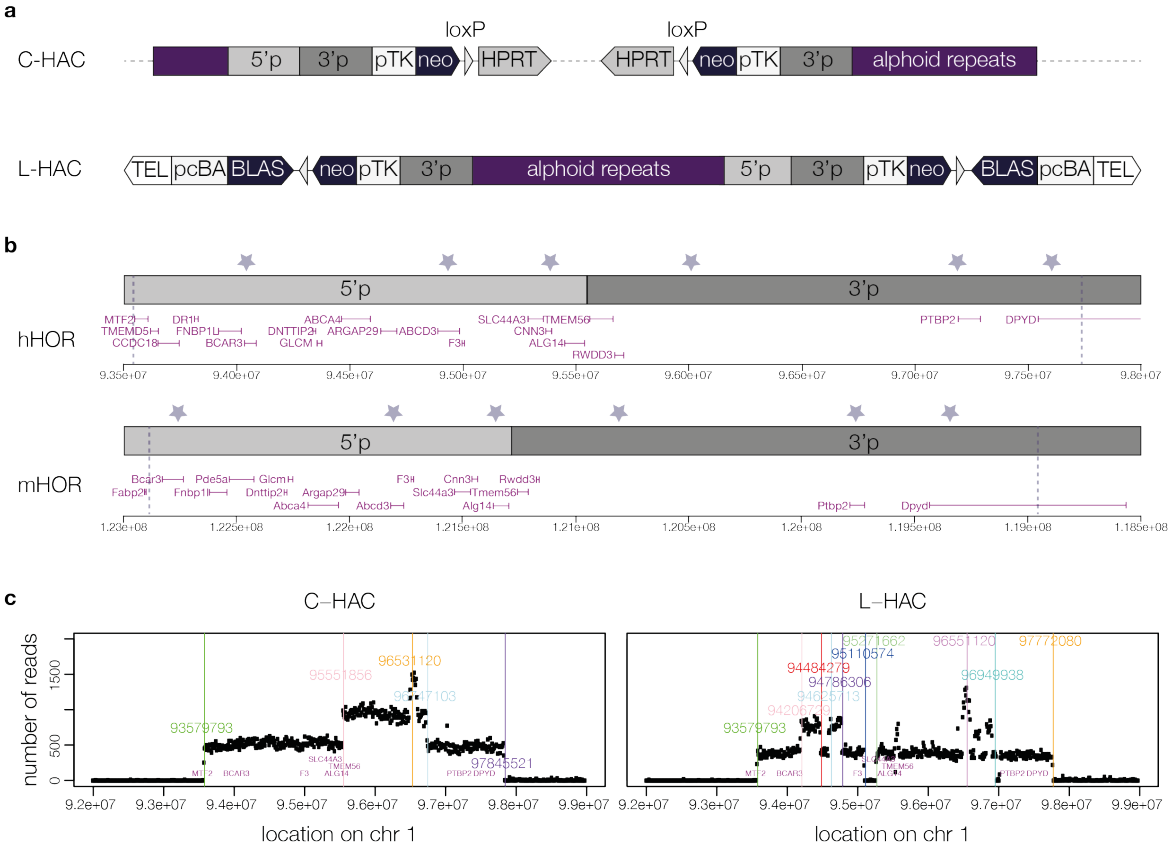

Figure 1: Genomic features of HACs and corresponding human and mouse orthology regions.
(a) Structure of circular and linear HAC (C-HAC and L-HAC, respectively). The upstream arm (5'p) contains the genomic region from MFT2 to ALG14, while the downstream arm (3'p) comprises the genomic region from TMEM56 to DPYD on human chromosome 1. In C-HAC, the two arms are separated on the one side by two inverted selection cassettes consisting of a neomycin (neo) selective marker driven by the thymidine kinase promoter (pTK), followed by a loxP site and the 3' end of a human HPRT minigene. On the other side, the arms are flanked by the centromere (alphoid repeats). The L-HAC comprises additional telomere ends (TEL) but lacks the HPRT minigene. Up- and downstream arms are separated by the centromere (alphoid repeats). (b) Genomic structure of the human and mouse orthology regions (hHOR and mHOR, respectively) on HSA1 and MMU3. Up- and downstream arms of the HAC are depicted above. (c) Genomic structure of C-HAC and L-HAC.

The central part of the C-HAC between *ALG14* and *TMEM56*, contains two inverted selection cassettes and a loxP site. The L-HAC was generated by Cre-loxP-mediated

addition of telomere ends to the existing C-HAC. Thus, both HAC variants have two arms joined by the centromere. The downstream arm comprises the chromosome region from *DPYD* to *TMEM56* (3'p). The upstream arm spans the region from *MTF2* down to *ALG14* (5'p). The portion of the L-HAC between *ALG14* and *BCAR3* is reorganised. In addition to a number of short deletions present in C-HAC, L-HAC carries a deletion of ca. 156 Kb between *F3* and *SLC44A3* in the upstream arm and a short deletion upstream of *PTBP2* in the downstream arm; it also lost a small piece at the downstream end (Fig. 1c). Both HACs contain four structurally different subregions: (i) a centromeric, (ii) a gene-rich, (iii) a gene desert, and (iv) a gene-poor subregion covered by the long gene *DPYD* and the intron-poor gene *PTBP2*. The mouse HAC Orthology Region (mHOR) on mouse chromosome 3 (MMU3) has the inverted orientation compared to hHOR and is syntenic with hHOR in the region from *Dpyd* to *Fnbp1* (Fig. 1b).

HAC and mHOR regions faithfully localise to the rod nuclei shells occupied by the same chromatin class

We based our topological study on rod photoreceptor nuclei where the main chromatin classes form distinct concentric shells: (i) C-band chromatin, represented by the major satellite repeats, is packed into a single chromocenter in the nuclear center, (ii) G-band heterochromatin enriched in LINEs encircles the chromocenter, forming the so-called L1-shell, (iii) and R-band euchromatin enriched in SINEs forms the outmost peripheral layer, the so-called B1-shell (Fig.2, Supplementary Fig.1). The arrangement of the chromatin classes in rods is inverted in comparison to that of all other known cell types possessing a conventional nuclear organisation with heterochromatin abutting nuclear periphery and euchromatin residing in the nuclear interior (Solovei et al., 2009; Eberhart et al., 2013).

In mice stably carrying the HAC, only a proportion of retinal clones exhibited the HACs suggesting that the HAC was lost in some of the progenitor cells (Fig.2 a1). FISH analysis using whole human genomic DNA or human Cot1 as probes revealed that both L-HAC and C-HAC adopt a rod- or V-shape and are stretched through the L1-shell situated between the central chromocenter and the nuclear periphery (Fig.2 a2). To study the localisation of the HAC subregions and mHOR we designed three respective BAC cocktail probes for FISH on cryosections encompassing the three non-centromeric subregions. For mouse, we additionally designed a probe against the gene-rich region outside of mHOR, upstream to *Dpyd* (Fig.2 b). Since the three concentric shells of rod nuclei are well distinguishable in retina cryosections by differential DAPI staining (Supplementary Fig.1), we used confocal image stacks to directly score the positions of HACs and mHOR subregions

in rod nuclei. Notably, HAC and HOR subregions faithfully localise to the rod nuclei shells built by chromatin of the same class. About 90% of the HAC and more than 80% of mHOR gene-rich subregions localise to B1-shell, while 90% of the deserts and 60-80% of gene poor regions localize to the L1-shell (Fig.2 c,d).

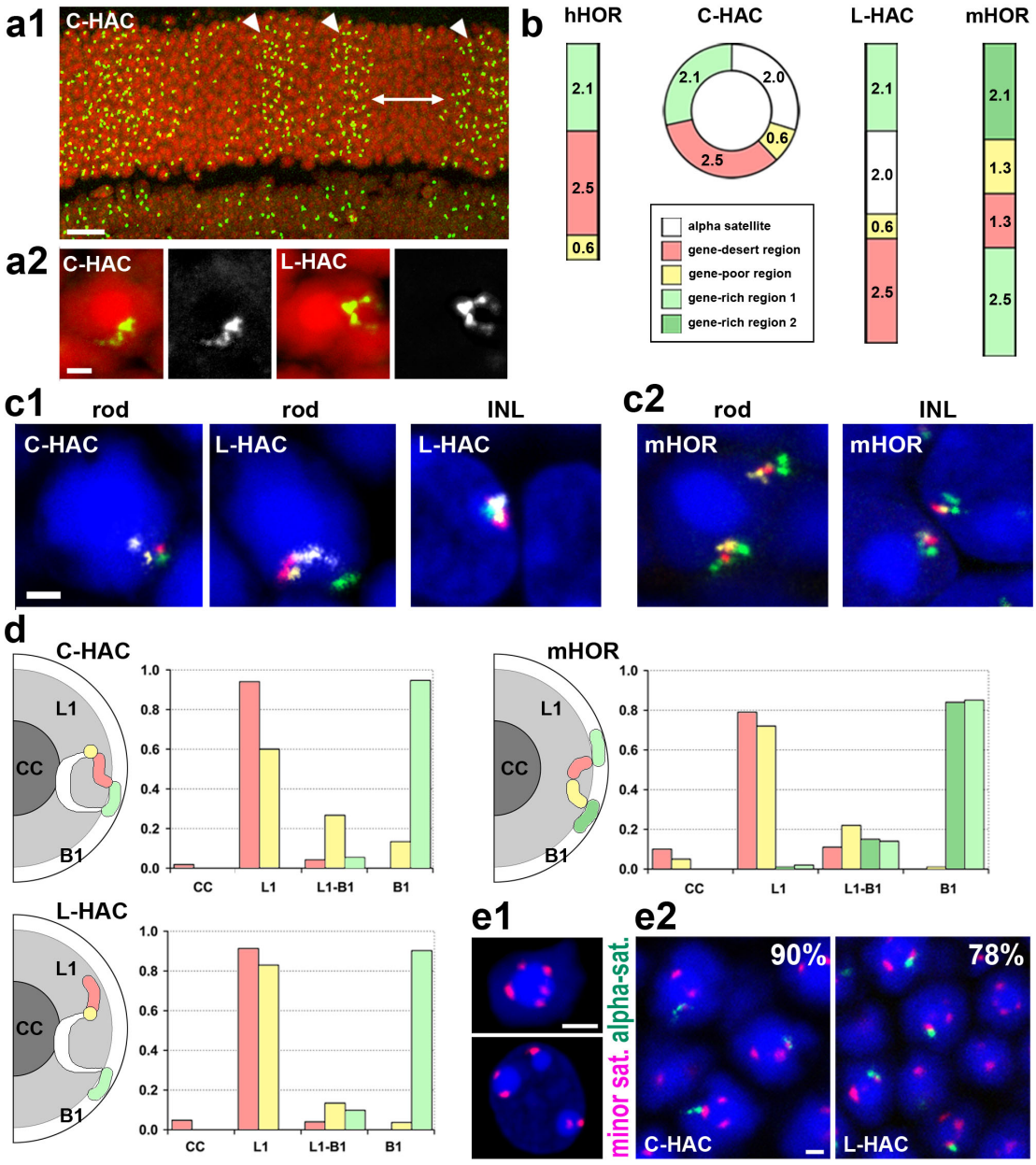

Figure 2: HAC and mHOR regions faithfully locate in the rod nuclei shells occupied by the same chromatin class. (a1) HAC visualised by FISH in mouse retinal cells. Note that some retinal clones are lacking HAC (as the one marked by arrow), in others (arrowheads) one HAC per cell is present. **(a2)** HAC is stretched from the central chromocenter to the nuclear periphery as a rod- (left) or v-like structure (right). **(b)** Scheme of the linear arrangement of gene-rich, gene-poor, and gene-deserts regions in HACs and HORs. c, examples of FISH with cocktail probes differentially staining regions of HAC or HOR in nuclei of rods or inner nuclear layer (INL) cells. **(d)** Scoring results and schemes of typical distribution of differential HAC and mHOR regions in rod nuclei. **(e1)** Distribution of centromeres in rod (upper) and bipolar (low) cells visualised by FISH with minor satellite repeat. e2, centromere region of HACs (α-satellite, green) is colocalised with mouse centromeres (minor satellite, red). All FISH images are projections of few optical sections encompassing ca. 2 µm. Scale bars: a1, 20 µm; a2, c, e, 2 µm.

Association of HAC genic segments with the B1-zone prompted us to investigate whether HAC genes are transcriptionally active and transcribed along with the mouse genes. Therefore, we tested expression of the two genes *Abca4/ABCA4* and *Cnn3/CNN3* in retinal cells carrying L- or C-HACs. *Abca4/ABCA4* is a member of the superfamily of ATP-binding cassette transporters and is expressed exclusively in photoreceptor cells, whereas *Cnn3/CNN3* is a ubiquitously expressed cytoskeleton protein. Indeed, both genes were expressed in rod cells irrespective of their mouse or human origin (Supplementary Fig. 2).

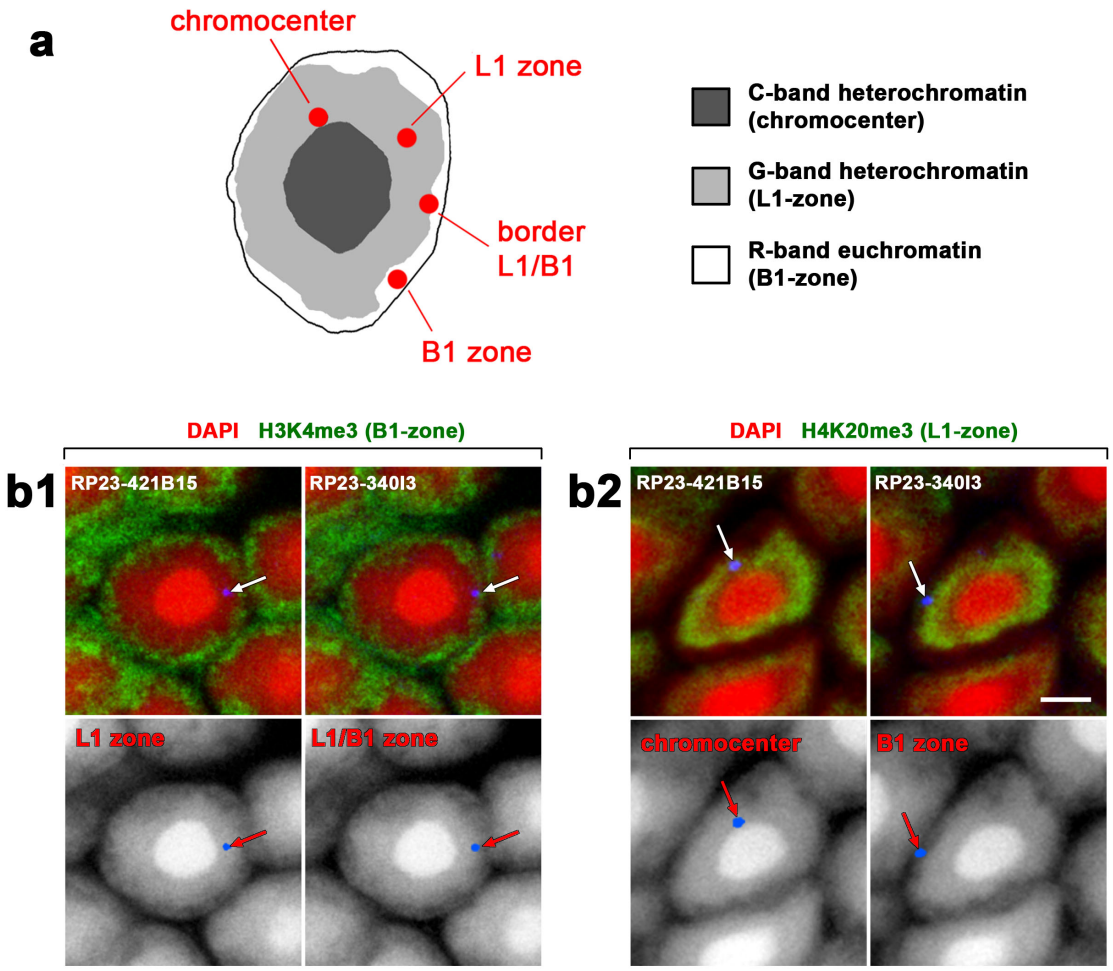

Supplementary Figure 1. Concentric arrangement of main chromatin classes in rod nuclei and BAC signal classification. (a) Classification of signal positions for qualitative analysis in nuclei of rod cells. BAC signal were classified according to their colocalisation with three concentric shells formed by main chromatin classes (chromocenter, L1-zone, B1-zone, border between L1 and B1). Chromocenter, *dark grey*; L1-rich heterochromatin, *light grey*; B1-rich euchromatin, *white*; BAC signals, *red*. **(b)** Spatial distribution of BAC signals after FISH combined with euchromatin (b1, H3K4me3) and heterochromatin (b2, H4K20me3) immunostaining of B1- and L1 zones, respectively. BAC probe encompassing relatively gene-rich chromosomal region (RP23-340I3) localise to B1-zone or L1/B1-zones border; BAC for gene-desert region (RP23-421B15) is found either in L1-zone or adjacent to the chromocenter. Top raw: DAPI (red) and immunostaining (green); bottom raw: grey scale images of DAPI with superimposed BAC signals (blue). Note that classification based on DAPI-staining conforms well to that based on immunostaining of histone modifications. Arrows point at the BAC signals. Single optical sections. Scale bar: 2 µm

In mouse nuclei, centromeres consisting of minor satellite repeats form small clusters on the surface of the chromocenters (Fig.2 e1). Notably, HAC centromeres formed by human alphoid repeats colocalised with the minor satellite repeats in about 80% or 90% of rods harboring L-HAC or C-HAC, respectively (Fig.2 e2). Obviously, association of HAC centromeres with its mouse counterparts on the surface of large chromocenters affects the distribution of other HAC subregions.

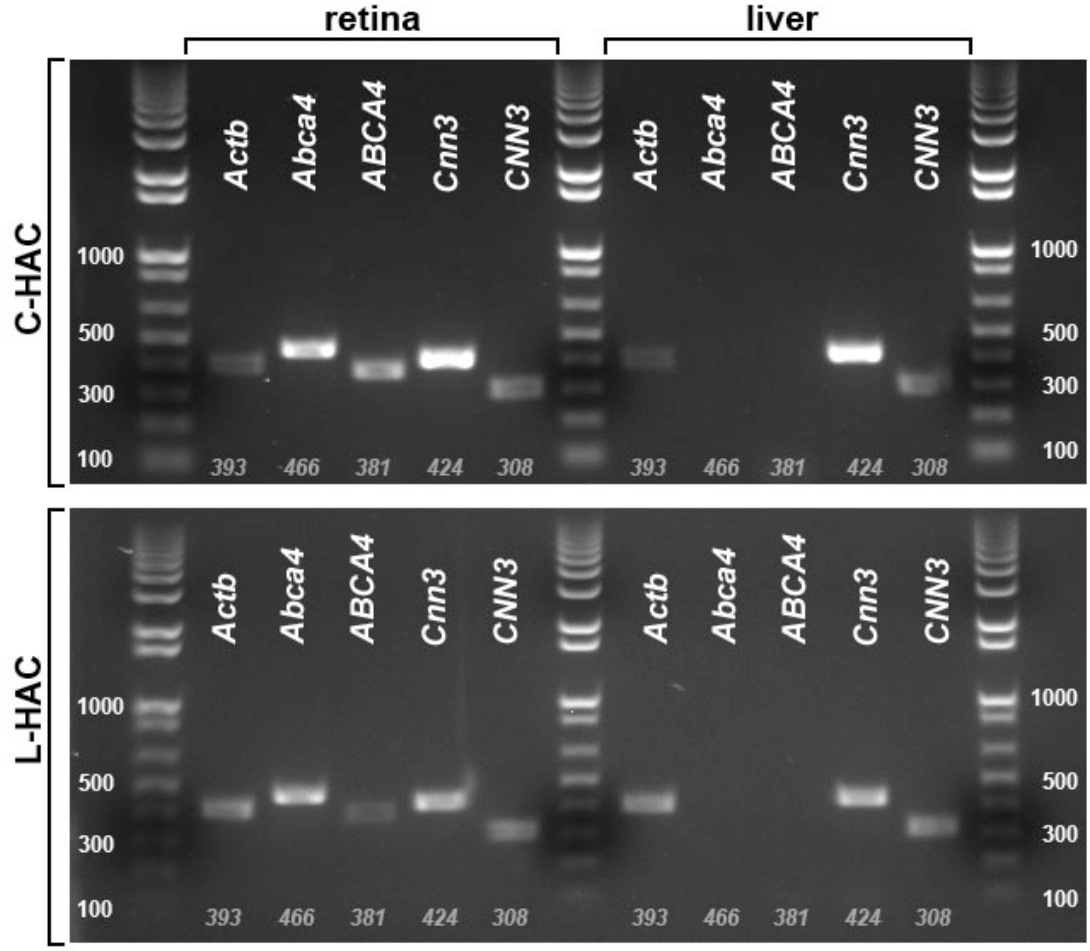

Supplementary Figure 2. Expression of mouse and human genes in rod cells carrying C- and L-HACs. *Abca4/ABCA4* is expressed exclusively in retina photoreceptor cells in both human and mouse; the *Cnn3/CNN3* is ubiquitously expressed. Note that *ABCA4* is expressed from both C- and L-HACs in rods but not in liver cells; *CNN3* is expressed in both cell types. As a control, expression of mouse *Actab* gene was tested in parallel. Numbers on left and right mark the length of the marker fragments (bp); italic numbers at the bottom show expected amplified fragment length (bp).

Accordingly, in mature rods, 91-94% of HAC and 72% of mHOR deserts localise in the LINE-rich zone. In neuroretinal cells, ca. 70% of HAC deserts abutted the nuclear envelope or both the envelope and a chromocenter, and only 30% were associated exclusively with the chromocenters. mHOR deserts showed an even higher affinity to the nuclear envelope (ca. 90%). On the one hand, the difference depends in part on the presence of peripheral chromocenters in none-rod cells and a distant position of mHOR from the centromere of

MMU3 (Supplementary Fig. 3). On the other hand, these results demonstrate that in presence of peripheral heterochromatin tethers (Solovei et al., 2013), the desert and gene-poor subregions have a pronouncedly higher affinity to the nuclear envelope compared to the chromocenters. This well conforms to the fact that gene-poor chromatin and deserts are commonly found within LADs (Guelen et al., 2008; Meuleman et al., 2013).

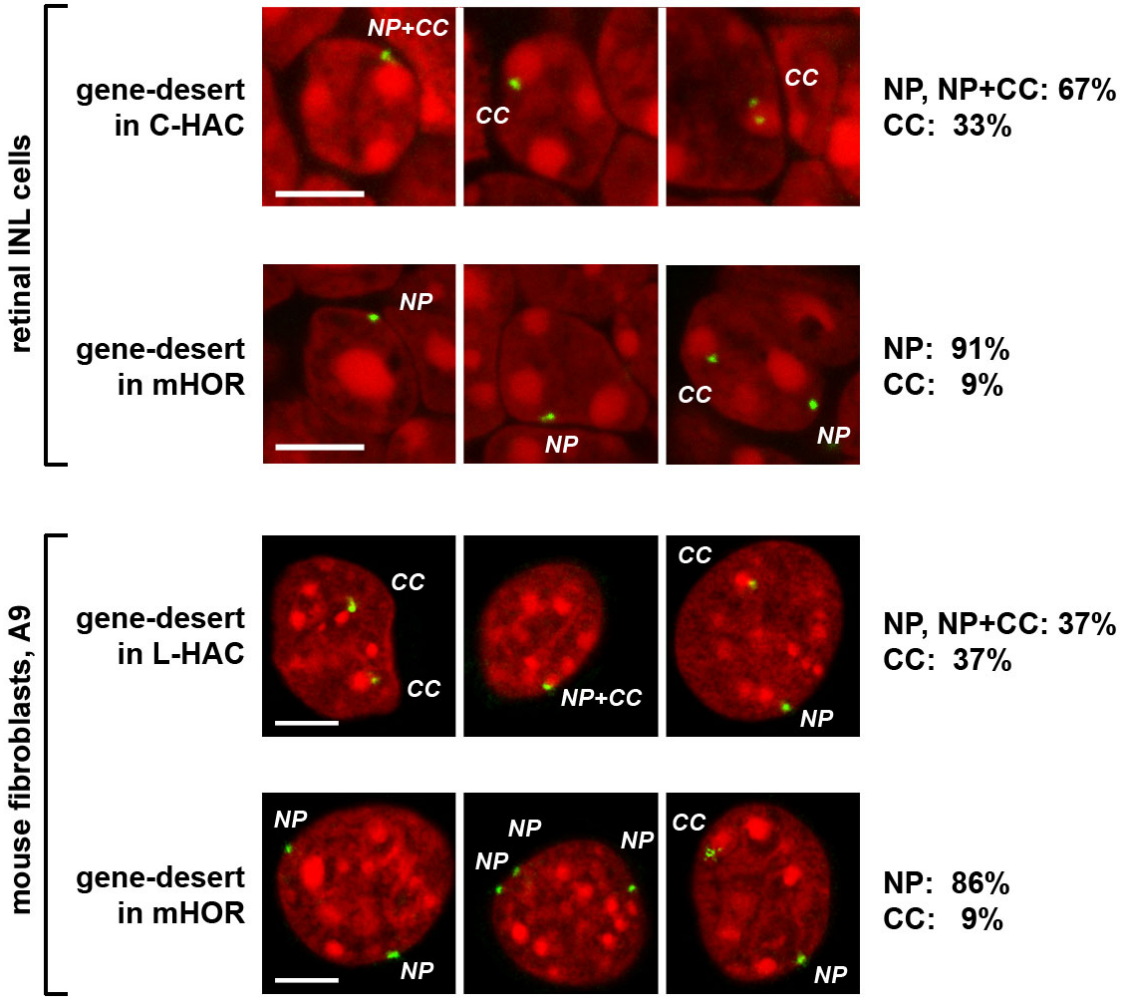

Supplementary Figure 3. Difference in distribution of gene-desert regions of HAC and mHOR in nuclei of neuroretina and cultured mouse fibroblasts bearing HACs. Gene-deserts (green) were visualised by FISH in retinal INL cells (top rows) and cultured fibroblasts A9 (bottom row). Gene-deserts of HACs are mostly adjacent to the chromocenter or both, chromocenters and nuclear periphery, whereas gene-desert of mouse chromosomes are found mostly at the nuclear border. Scoring of signal localisations is shown on the right. *NP*, nuclear periphery; *CC*, chromocenters. DNA was counterstained by DAPI (red). Images of INL cells are projections of confocal sections over 1 µm; images of cultured fibroblast nuclei are single optical sections. Scale bars: 5 µm

In cultured fibroblasts, HAC and mHOR subregions preferentially interact with chromatin of the same class

The very strong tendency of HAC and mHOR subregions to locate within chromatin of their own class in rods prompted us to explore whether positioning in the mouse nuclei with a conventional architecture takes place with the same fidelity. In a preliminary way, this is

already obvious from visual inspection of neurons in the inner nuclear layer (INL) after FISH with the same probes. However, as the main chromatin classes do not form regular shells in nuclei with a conventional nuclear architecture and HACs are considerably more condensed than in rods (Fig.2 c1), direct scoring is not reliable. Therefore, we applied 4Cseq (Circularised Chromosome Conformation Capture with sequencing) to cultured fibroblasts derived from mice carrying either C-HAC or L-HAC. We placed 6 viewpoints (sequences whose spatial interactions are analyzed) on three parts of HAC sequence: gene-rich (*BCAR3, ABCD3, ALG14*), gene-desert (ca. 30% of distance from *RWWD3* to *PTBP2*), and gene-poor (*PTBP2* and *DPYD*) (Fig. 1b). For mHOR, distinctly recognizable viewpoints were established for mouse DNA in the same positions, as for HACs (Fig. 1b). The interactions of human viewpoints were additionally studied for the hHOR in human fibroblasts.

First, we analyzed the spatial interactions of the viewpoints with sequences encompassed by HACs/HORs themselves. The spatial proximity of the viewpoints to the analyzed chromosome region predetermines a high level of spatial interactions. However, the correlation matrices for interactions between viewpoints showed that gene-rich and gene-poor subregions had clearly different spatial interactors within the HACs. Viewpoints within the gene-rich subregions interacted predominantly with gene-rich regions of HACs, while interactions of desert and gene-poor viewpoints were restricted to desert and gene-poor subregions (Fig.3A). Importantly, this trend was species-independent and observed in three different chromosomal contexts: (i) for L-HAC, where gene-rich and gene-poor subregions are separated from one side by a large centromeric region, (ii) for C-HAC where these subregions are separated by the chromocenter but are close to one other on the other side of the ring where they are separated by an insertion, and (iii) for the mHOR and hHOR where the subregions directly contact each other. Only a comparatively strong direct separation of *TMEM56* and *RWDD3* by an insertion switched interaction preferences of these genes (a ca. 150 Kb region) to the gene-poor HAC arm. Remarkably, the changed interactions preference did not affect the location of these genes in rod nuclei. All signals from the BAC encompassing the *ALG14* to *TMEM56* segment of the HACs preferably located to the B1 shell of rod nuclei suggesting that genes do not move from the normal chromatin environment but rather find a place at the border of the respective chromatin classes or form a border environment.

A similar trend was observed for genome-wide interactions (Fig 3C, D). For instance, *Ptbp2*, showed a more pronounced interaction with other mouse (Fig 3C) and human genes (Fig 3D), than *Dpyd* or the desert subregions. Importantly, spatial interactors across the whole genome showed that subregions of the HACs, just as well as the respective

subregions of mHOR and hHOR, preferably interacted with chromatin of their own class (Fig 3E).

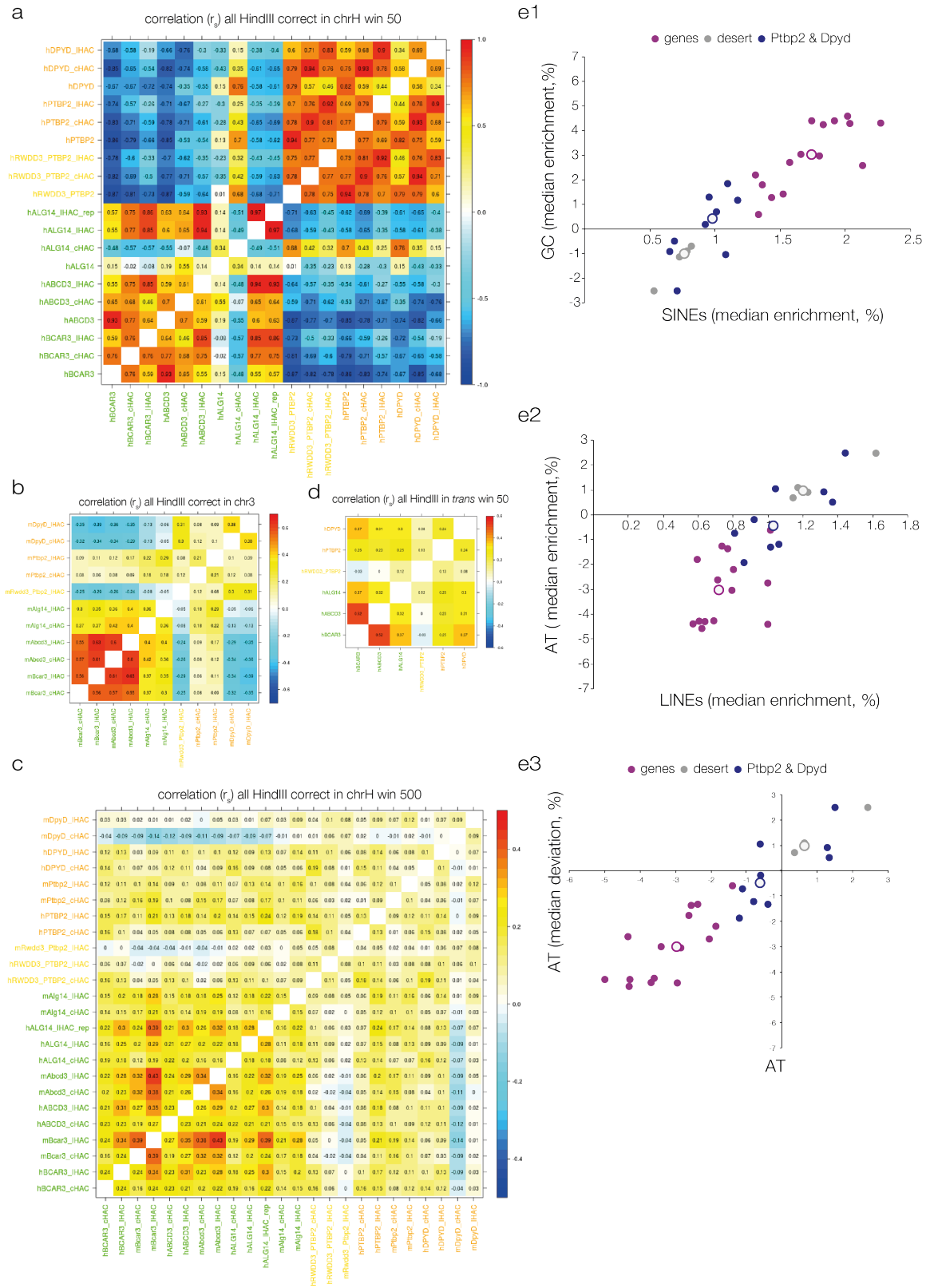

Figure 3. HAC and mHOR subregions preferentially interact with chromatin of the same class

Accordingly, interactors of genic viewpoints were mostly GC-rich, SINE-rich and LINE-poor, whereas interactors of the desert were mostly AT-rich, SINE-poor, and LINE-rich. The interactors of gene-poor viewpoints exhibited intermediate characteristics (Fig 3E1,2). Decreasing autocorrelations (diagonal squares) correspond to the high excess of DNA covered by deserts compared to long genes and, especially, to gene-rich areas. Hence, our results are in accordance with the concept of a preferential type rather a preferential set of neighbours (Simonis et al., 2006; Joffe et al., 2010).This notion is further corroborated by the strength of interactions over the HOR-carrying chromosomes (excluding HORs themselves to avoid the effect of positional proximity). The correlation observed for HOR viewpoints was notably stronger, than for HACs due to location on the same or different chromosomes, respectively. Correlation between the interactions of HOR and HAC viewpoints in mouse cells is the weakest of the three, which would not be the case if both HAC and HOR viewpoints had a limited number of strongly preferred individual interactors. One more confirmation of this conclusion comes from the fact that SINEs and LINEs together define the type of chromatin interacting with HAC subregions nearly as well as SINEs and AT-content, showing that the cardinal feature selecting likely interactors is correlated gene-, GC, SINE-richness (Fig. 3e3).

In cultured cells, small HAC segments correctly maintain strong or weak lamina-association, but HACs as a whole fail to maintain normal LAD/interLAD pattern

To analyze the pattern of lamina-association in conventional nuclei, we studied the distribution of LADs in the A9 cells containing linear HAC using DamID. Due to the high percentage of HACs associated with chromocenters rather than with the nuclear envelope (Supplementary Fig. 6) LADness has a narrower signal intensity range compared to HORs but still allows for a comparison of the HAC subregions. We calculated the normalised LADness for all genes and intergenic intervals within the L-HACs and mHOR. The mouse LADs were perfectly well detected in our experiment (Fig. 4) and strongly overlapped with previously detected LADs in mouse fibroblasts (Peric-Hupkes et al., 2010). Indeed, all LADness profiles obtained earlier for human and mouse native chromosomes (Peric-Hupkes et al., 2010; Meuleman et al., 2013) strongly correlated with each other ($R_{Spearman}$ of 0.6-0.9, $P<0.0001$) even in xenospecific comparisons. In contrast, the HAC showed an unexpectedly high LADness for the genic region (Fig. 5), and this inability to position the gene-rich region off from the nuclear lamina was the main difference observed between the L-HAC and HORs. Notably, we observed a striking decrease in LADness for *PTBP2* compared to the flanking regions in both human and, even more pronounced, in mouse sequences (Fig. 4).

This low LADness corresponds to a more central position, which conforms to “more gene-rich” interactions of the *Ptbp2* viewpoint within mHOR region detected by 4C technique.

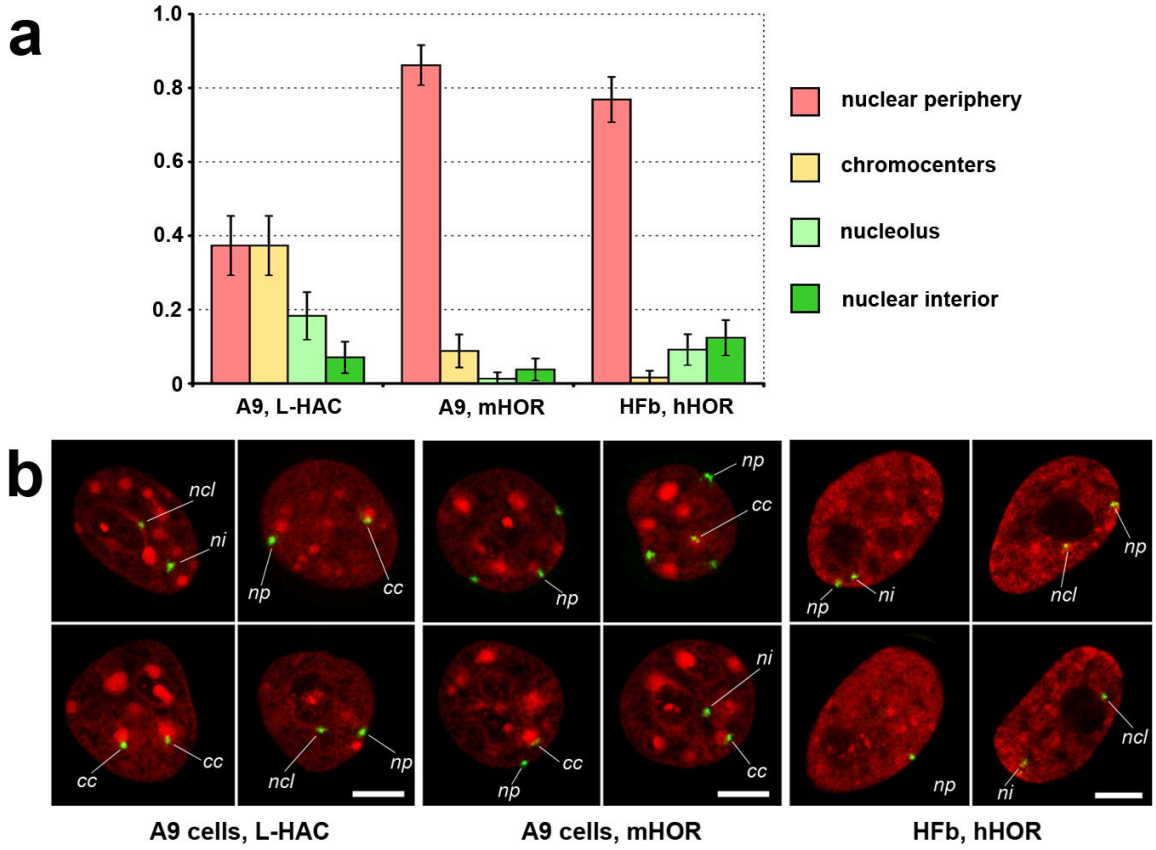

Supplementary Figure 6. Spatial distribution of the HACs and HORs desert region in L-HAC bearing mouse fibroblasts (A9 cells) and human fibroblasts (HFb). (a) Scoring of the desert FISH signal in four nuclear locations. **(b)** Typical examples of the desert signal location after 3D-FISH. *np*, nuclear periphery; *cc*, chromocenters; *ncl*, periphery of the nucleolus; *ni*, nuclear interior. Single optical sections. Scale bar: 5 μm

a

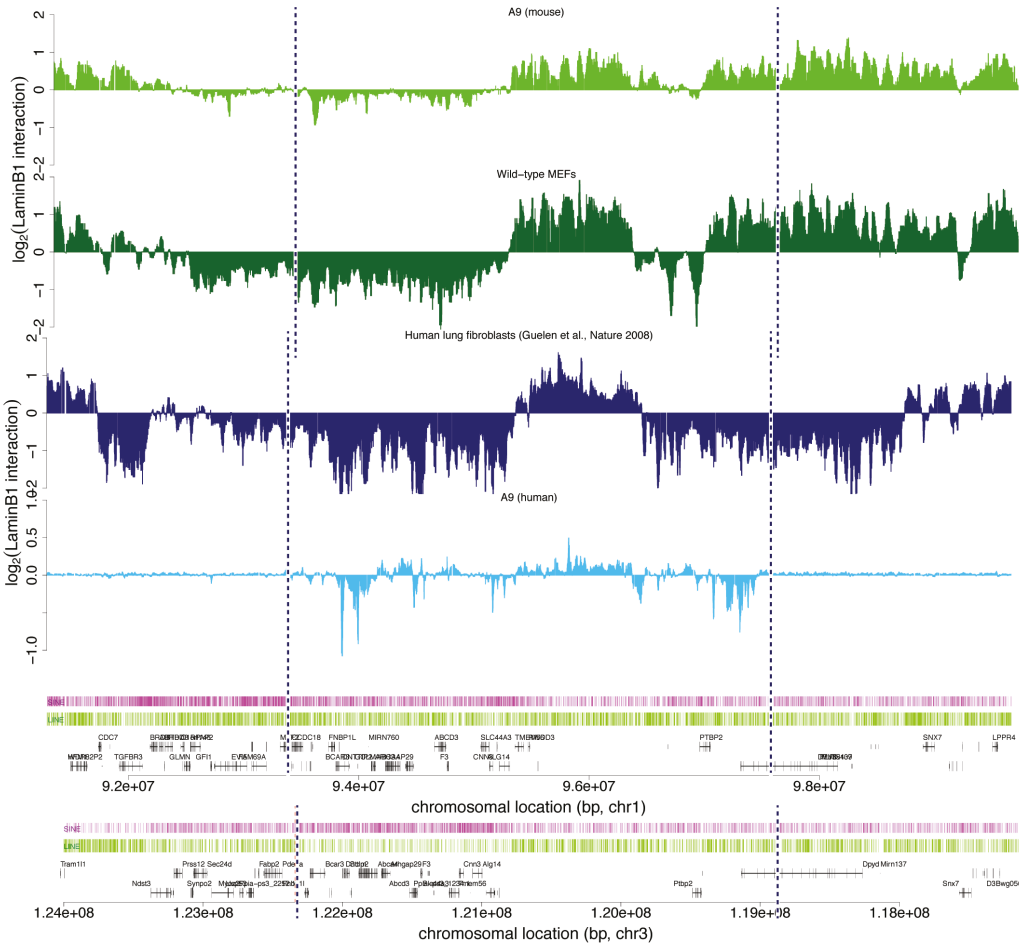

b

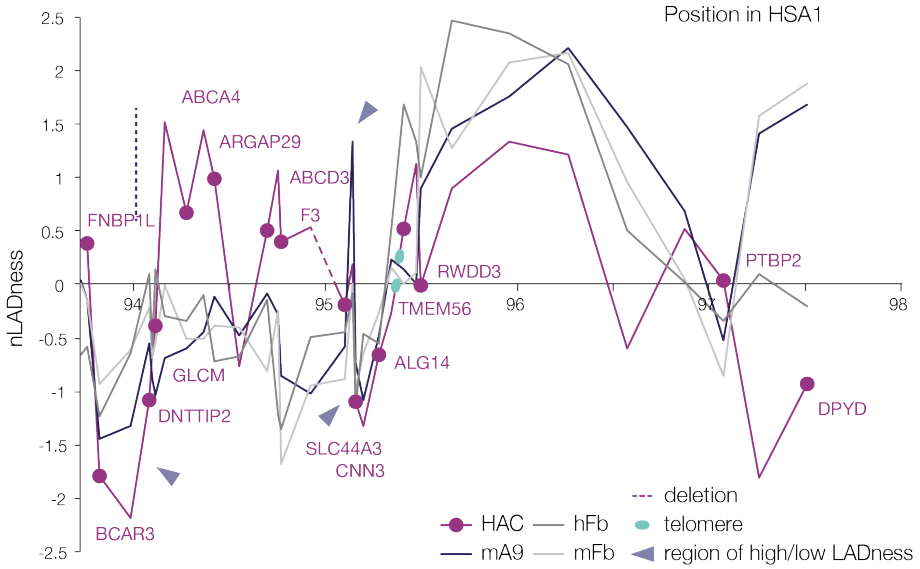

Figure 4. Maintenance of LAD / interLAD pattern in HACs

We next analysed the expression levels of genes present in both HACs and mHOR in 6 mouse and 2 human cell types by RT-qPCR. Indeed, transcription of human *PTBP2* is approximately 3-fold lower compared to mouse *Ptbp2* (Figure 5b).

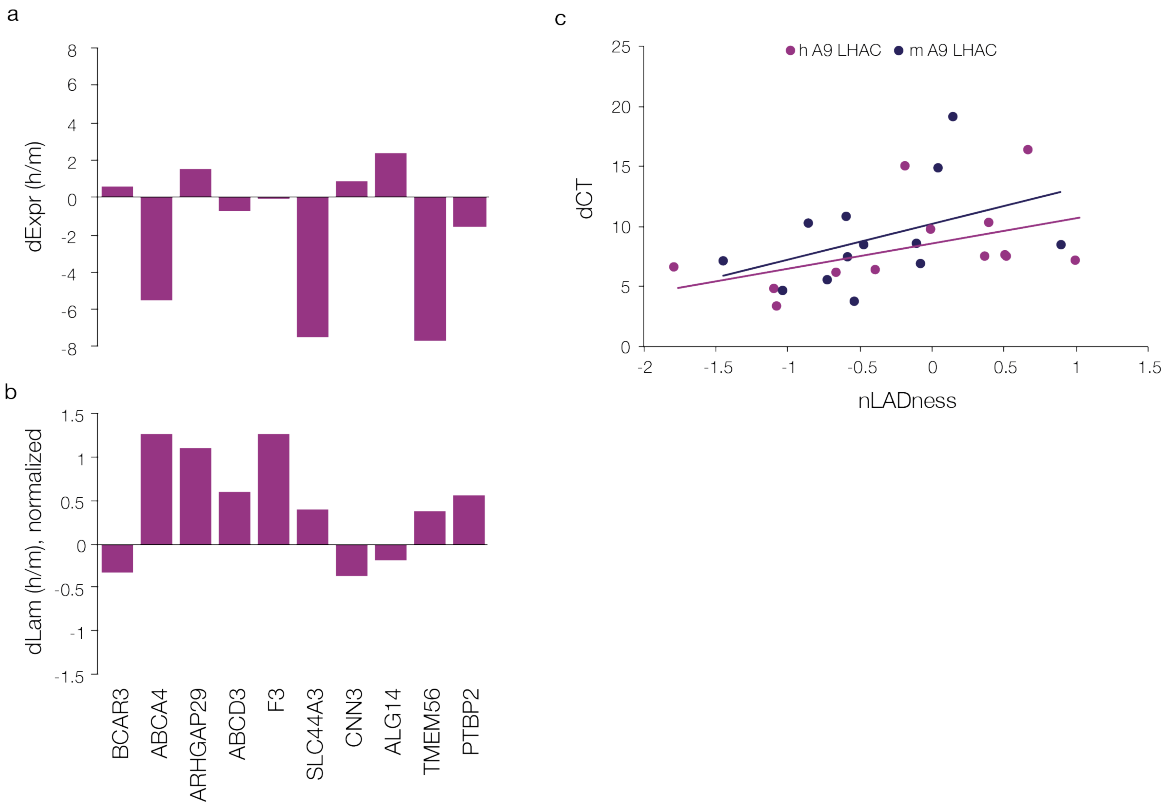

Figure 5. Correlation of gene expression and LADness.

The HAC *PTBP2* level varies in different mouse cell types and typically accounts for 2-22% of the mouse transcript. In A9 cells where LADs were studied, *Ptbp2* transcription levels are generally high and transcription from the HAC gene reaches up to 33% of the mouse transcript (Supplementary Figure 7). Considering other studied genes, we observed a significant correlation (P<0.035) between LADness and dCT for human genes, suggesting that LADness of individual genes is indeed related to their transcriptional level. For mouse genes, this correlation was also seen, though it was not statistically significant (Fig. 5c).

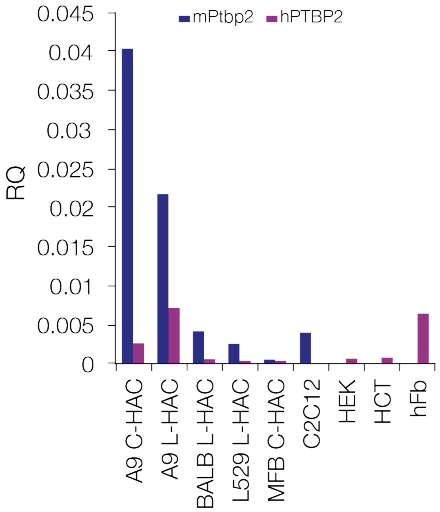

	hPTBP2 on total PTBP2 transcription
A9 C-HAC	6.32%
A9 L-HAC	32.79%
BALB L-HAC	13.45%
L529 L-HAC	1.73%
MFB C-HAC	21.88%
C2C12	n.d
HEK	100.00%
HCT	100.00%
hFb	100.00%

Supplementary Figure 7. Relative expression of human and mouse Ptbp2 in different cell lines.

Discussion

Segregation of the main chromatin classes is autonomous for small chromosome segments

Segregation of eu- and heterochromatin – more precisely, of pericentromeric, LINE-rich, and SINE-rich chromatin – has been established as a cardinal trait of nuclear organisation based on extensive microscopic observations (Bolzer et al., 2005; Solovei et al., 2009; Joffe et al., 2010) and 3C-based experiments (Lieberman-Aiden et al., 2009; Kalhor et al., 2011; Gibcus and Dekker, 2013; Phillips-Cremins et al., 2013). Although the chromatin classes are commonly characterised based on their differences in GC-content, gene-richness and repeat repertoire, our data provides a comprehensive analysis of these features in respect to spatial genome arrangements.

First, our results strongly emphasise that in mammals, the two A and B compartments revealed by Hi-C (Lieberman-Aiden et al., 2009) correspond to gene-rich (SINE-rich) and gene-poor to gene deserts (LINE-rich) chromosomal regions, that is, to eu- and heterochromatic chromosomal R- and G-bands (Korenberg and Rykowski, 1988; Chen and Manuelidis, 1989). Secondly, different range of neighbours for the desert and gene-poor region suggests that there can be an even more precise segregation of heterochromatin, with gene-poor regions and gene deserts being also at least partially segregated. Thirdly and most importantly, our data show that segregation of the main chromatin classes is autonomously established by small (at least down to 0.5 Mb) chromosome segments. This segregation is established independently on (i) chromosomal context (native chromosomes, linear or circular HAC), (ii) genomic neighbourhood (e.g., presence or absence of a significantly long separating region of chromatin of different nature), and (iii) cellular background (con- or xenospecific). Spatial interactions of the HAC gene-rich subregions imply that even when they are bound to the nuclear envelope, they form euchromatic environment, rather than changing their neighbours. Microscopically, this notion is supported by proven initiation of transcription and formation of typically euchromatic structures like speckles close to the nuclear envelope (Joffe et al., 2010).

Eu- and heterochromatin segregation likely depends on DNA/chromatin binding proteins

The notion that co-localisation of certain chromatin regions is due to sequestration by nuclear proteins specifically recognising DNA and chromatin regions of certain type has been discussed for quite a time, in particular, it was suggested as a mechanism for ordered chromosome arrangement in elongated sperm nuclei (Joffe et al., 1998; Solovei et al., 1998). Clustering of similar chromatin segments by proteins binding to them is now increasingly suggested as the probable mechanism for most of the static and dynamic features of the

nuclear architecture (Holwerda and de Laat, 2012), especially in connection to chromatin loop formation (Phillips-Cremins et al., 2013). Our data shed new light on this issue.

First of all, we show a very strong trend of colocalisation for human and mouse centromeres. Build of alphoid repeat and minor satellite repeat, respectively, their sequences actually have very little in common: only similar 17 bp long CENP-B boxes and centromeric histone CENP-A. However, these features, CENP-A in the first place, are sufficient to attract the whole set of proteins necessary to form a functional centromeres and correctly locate them (Black and Cleveland, 2011; Padeken and Heun, 2013; Mendiburo et al., 2011). This happens even in xenospecific genomic background and in a variety of different chromosomal contexts. For instance, human NORs are able to integrate in active mouse nucleoli in mouse-human hybrid cells although they remain silent, likely as a result of cross-recognition by the pivotal nucleolar factor UBF (Sullivan et al., 2001). Recent studies suggest that recognition sequences for nuclear proteins can cause differential association of chromatin with transcription factors, promoters and enhancers, splicing machinery and facilitate their clustering (Hu et al., 2010; Nagano et al., 2013; Fanucchi et al., 2013).

Genes in a gene-rich subregion show distinctly different lamina-association, whereas LAD/interLAD pattern for subregions is not reproduced by the HAC

Earlier observations on LADs demonstrated that the composition of LAD DNA has a similarity with that of LINE-rich heterochromatin (Guelen et al., 2008; Peric-Hupkes et al., 2010; Meuleman et al., 2013). Our study of HAC/HOR illustrates a clear correlation between the main chromatin classes and LAD/interLAD subregions (typically, above 100kb) including 1-2 genes, that is a strong or a low lamina-association depending on whether they are transcribed or not (Peric-Hupkes et al., 2010). In HAC/HOR region we have not observed clear relation between transcriptional upregulation of human genes and presence of LINE2 or some ancient LINE1 variants (Ward et al., 2013). While in our mice the differences account for more that 29% of transcription level, a higher transcription of human gene was actually observed where mouse transcription was low and not *vice versa*.

In addition to differentiation-dependent changes, our data show a clear correlation between LADness and transcription levels of individual genes within the gene-rich subregion. In particular, we observed that the high transcription level of *PTBP2* is accompanied by a sharply decreased LADness. Even more importantly, our data reveals a new role of lamina-association in the gene-rich region, as genes showed a consistent LADness pattern, which significantly correlated with the gene expression. Earlier microscopic studies (Joffe et al., 2010) showed that transcription can start at the nuclear periphery and that there is no direct

casual relation between more or less central position and higher or lower transcriptional level. Our data emphasise that there is a reliable relation, possibly depending on the fact that transcriptional activation can release a gene from its position and initiate its relocation (Bickmore).

Surprisingly, in HAC, gene-rich and gene-poor/desert subregions failed to reproduce the LAD/interLAD pattern observed for orthologous human and mouse sequences. This is actually surprising because the differences found between individual genes in gene-rich subregion are comparable to those between LADs and interLADs. Thus, our data show that maintenance of the proper LAD/interLAD pattern needs a proper chromosomal context – e.g., larger chromosome regions – and is non-autonomous in this sense.

Main chromatin classes are the bottom-level of the genomic blueprint of the nuclear architecture

It recently became clear that the linear genomic sequence is subdivided in the nucleus into a number of chromatin domains which could be classified according to their spatial distribution (e.g., LADs and NADs), interaction partners (e.g., TADs), replication timing, protein composition (e.g., Polycomb domains), DNA methylation status (e.g., PMD domains), etc. (Bickmore and van Steensel, 2013). Our results suggest a more transparent model explaining the relations between the genomic and nuclear genome organisation and uniting the various chromatin domains. We suggest that the basic structural units of genomic organisation are stretches of the main chromatin classes marked by GC content, gene richness, and repeat repertoire.

Thus main chromatin classes make a pivotal link not only between the genome and chromosomal functions but also as the bottom-level link between the genome and its spatial distribution in mammalian nuclei, blueprinting the overall nuclear architecture which is further specified by other factors.

3 Discussion

3.1 Designer TALEs (dTALEs) as a tool for genome activation

In eukaryotic cells, transcription initiation starts with recognition and binding of DNA response elements within a promoter by transcription activators, which serve as a platform to recruit and assemble additional TFs, chromatin remodelers and the basal transcription machinery (Hirai et al., 2010). Recent studies have started to explore the potential of dTALEs to selectively switch on and off transcription in mammals. Initial studies demonstrated the induction of reporter genes by dTALEs (Geissler et al., 2011; Zhang et al., 2011). Endogenous gene activation, however, was often modest and in some cases even failed (Geissler et al., 2011; Zhang et al., 2011; Tremblay et al., 2012; Cong et al., 2012; Garg et al., 2012), e.g. activation of endogenous *oct4* (Zhang et al., 2011).

Our study provided the first comparative assessment of *in vitro* binding properties, relative positioning within a promoter and transcriptional activation potential of dTALEs on active and silent episomal promoters. Demonstrating selective activation of endogenous *oct4* expression, we established dTALEs as a promising tool for both transcriptional activation and cellular reprogramming. All five tested dTALEs specifically recognised their cognate targeting sequence compared to a non-target template *in vitro* and exhibited a strong binding affinity with K_d values in the high picomolar to the low nanomolar range. Given the tight binding of all dTALEs to the target sequence *in vitro*, the varying potential for transcriptional activation is likely to depend on position and epigenetic status of the promoter. The local chromatin environment determines the accessibility for TF binding, which have to dynamically interact and remodel nucleosome positioning in order to bind. Proximity to TF binding sites, such as Sp1 sites thus increases the likelihood of targeting permissive sites in active promoters. Moreover, presence of additional factors might synergistically affect the activation capacity of TALEs through cooperative binding and stabilisation of the pre-initiation complex (Kim et al., 2000; Anthony et al., 2014). Accordingly, transcriptional activation is dependent on the particular target sequence and the rate of success highly increases when choosing DNase I hypersensitive sites (Perez-Pinera et al., 2013b; Maeder et al., 2013b). As the tandem-arrayed repeats of the TALE DNA binding domain have to wind almost twice around the DNA, regular and heterochromatinised nucleosomal arrays of repressed promoters instead appear to impede with binding of TALEs to its target sequences (Maeder et al., 2013b). Strikingly, natural TALEs have been suggested to preferentially target unmethylated promoters (de Lange et al., 2014). Consistently, dTALE T-83 readily elicited *oct4* activation in ESCs, but not in neural stem cells

(NSCs), where *oct4* is silenced. Combination with chemical inhibition of repressive DNA methylation or histone deacetylation by 5-aza-2'-deoxycytidine and valproic acid, respectively, facilitated the selective, dTALE-mediated reactivation of silent *oct4*. By increasing the chromatin accessibility, the epigenetic inhibitors likely promote binding of the dTALE to the chromatin.

The importance of target site choice for transcriptional activation, was demonstrated by a recent study, where dTALEs directed against the upstream distal enhancer in the *oct4* promoter could further increase *oct4* activation, reactivate endogenous *oct4* in MEFs, and in combination with other factors promote reprogramming (Gao et al., 2012). Transcriptional remodelling by TALEs relies on the AD. Importantly, dTALEs fused to the herpesviral VP16 AD, or its tetrameric repeat, VP64, are more potent than the wild-type AD (Zhang et al., 2011; Geissler et al., 2011; Miller et al., 2011; Bultmann et al., 2012). VP16 induces local chromatin decondensation by recruiting chromatin remodelers and interacts with proteins implicated in gene activation thereby facilitating the assembly of the transcriptional machinery (Tumbar et al., 1999; Carpenter et al., 2005; Hirai et al., 2010). Indeed, dTALEs without AD act as transcriptional repressors in yeast (Blount et al., 2012). Recently, combined administration of multiple TALEs was shown to greatly enhance transcriptional activation and cooperative binding of multiple TALEs even overcomes repressive chromatin states (Maeder et al., 2013b; Perez-Pinera et al., 2013b). Similarly, TALE-based reactivation of silenced promoters in presence of additional activators such as the TATA box binding protein coincidences with increased chromatin accessibility (Anthony et al., 2014).

Systematic analysis revealed how TALEs impact on transcription, which is an episodic process with pulsatile bursts of mRNA generation. While stronger activation domains yield higher transcription initiation rates, combinations of TALEs enhance the duration of transcription and the number of transcripts as the lifetime of the TALE on the promoter is increased (Senecal et al., 2014) (Figure 12).

Based on these initial studies, future work will be required to better understand the complex interplay between TF and the chromatin microenvironment to enable fine-tuning of transcriptional regulation of endogenous promoters and synthetic circuits by programmable DNA binders, such as TALEs.

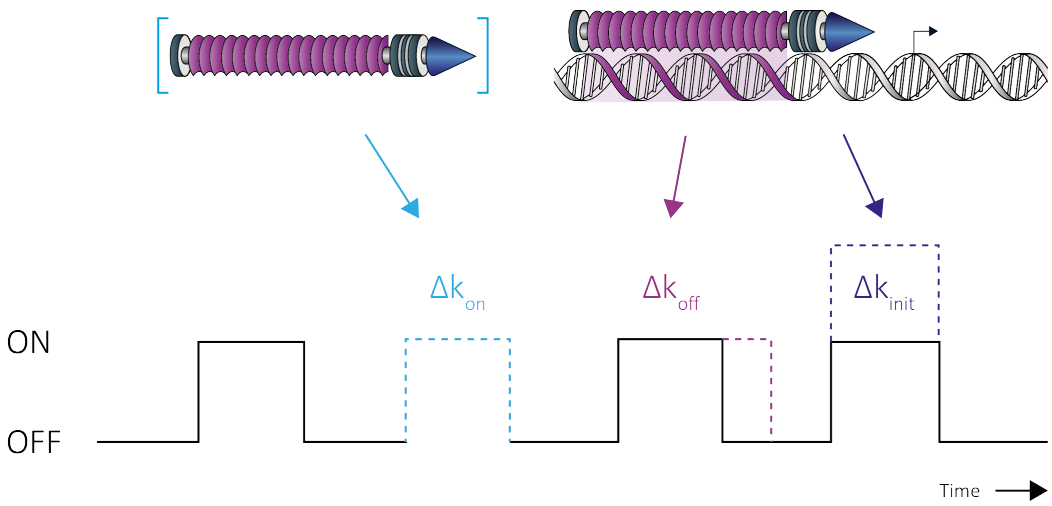

Figure 12: Kinetic model for modulation of transcriptional bursts by TALEs. Transcriptional burst frequency increases with TF concentration (k_{on}, light blue), duration is affected by the lifetime of the DNA binding domain on the promoter (k_{off}, magenta) and burst initiation is influenced by the strength of the activation domain (k_{init}, dark blue). Modified from (Senecal et al., 2014).

3.1.1 Further extension of the dTALE toolkit

By now, the number of different dTALE fusions and biotechnological application has been further expanded. Repression can be achieved by dTALEs either lacking the activation domain or fusions to repressive domains such as Serine-aspartate repeat X (SDRX) or Krüppel-associated box (KRAB) (Blount et al., 2012; Mahfouz et al., 2012; Cong et al., 2012; Gao et al., 2013; Garg et al., 2012).

Moreover, dTALEs fused to epigenetic factors, such as the histone demethylase LSD-1, Tet1, HMTs or HDACs (Mendenhall et al., 2013; Maeder et al., 2013a; Konermann et al., 2013) enabled targeted modification of chromatin states, thus paving the way to selective manipulation of the epigenetic landscape. Potentially, dTALEs could enable the selective epigenetic reactivation of aberrantly silenced genes, e.g. of tumour suppressor genes frequently subjected to promoter hypermethylation in various cancers. Another attractive target for targeted reactivation is the X-inactivated gene *mecp2*. Mutations in MeCP2, which is abundantly expressed in the brain, selectively binds 5mC, induces chromatin compaction and CC clustering (Shahbazian and Zoghbi, 2002; Nan et al., 1998; Jones et al., 1998; Brero et al., 2005), are associated with the neuronal disorder known as Rett syndrome (RTT) (Amir et al., 1999). Due to the X-linked, autosomal-dominant transmission mode, RTT almost exclusively affects females, which usually survive due to the remaining, unaffected copy expressed in a fraction of the randomly inactivated cells.

Selective reactivation of the transcriptionally silenced intact copy in affected cells could thus possibly rescue MeCP2 function.

Besides from holding a great promise for molecular biology and medical application, a number of recent publications revealed a great potential for dTALEs as regulators in synthetic biology and plant metabolic engineering (Blount et al., 2012; Lienert et al., 2014).

3.1.2 The CRISPR/Cas9 system as an alternative to dTALEs

Recently, the CRISPR/Cas9 system, a prokaryotic adaptive immune system which mediates the destruction of invading nucleic acids, emerged as a popular alternative to TALEs and ZPFs. The CRISPR/Cas9 platform is highly efficient for genome engineering, applicable for transcriptional regulation, and programming sequence-recognition is straightforward (as reviewed in Mali et al., 2013b; Sander and Joung, 2014).

In contrast to TALEs and ZPFs, which recognise their target by protein-DNA interaction, the Crisper-associated protein 9 (Cas9) nuclease contacts the DNA by a loaded RNA duplex (hence, they are also referred to as RNA-guided nucleases or RGNs). Naturally, two components expressed from the clustered regulatory interspaced short palindromic repeat locus (CRISPR) are involved, namely the CRISPR RNA (crRNA) and the trans-activating RNA (tracrRNA). Specificity is determined by the crRNA, which harbours the target sequence, while the tracrRNA facilitates crRNA processing and complex integration (Barrangou, 2014). Synthetic fusion of crRNA and tracrRNA to a chimeric small guide RNA (sgRNA) further simplified the system (Jinek et al., 2012) (Figure 13). Guidance of the Cas9 nuclease to the target sequence is achieved by complementarity of a 20-bp region within the sgRNA, termed spacer, to its target region (protospacer) flanked by a short proto-spacer adjacent motif (PAM) (Mojica et al., 2009). The CRISPR/Cas9 complex is then loaded onto the DNA by R-loop formation, where the sgRNA invades the complementary DNA to form a sgRNA-DNA heteroduplex, and cleaves the target sequence adjacent to the PAM (Barrangou, 2014) (Figure 13 C, D).

Crystallographic studies unravelled a bilobed structure of the Cas9 nuclease comprising recognition and nuclease lobes which accommodate the target DNA in a central channel (Nishimasu et al., 2014; Jinek et al., 2014) (Figure 13 D). Cleavage is mediated by the HNH and RuvC domains situated within the nuclease lobe (Figure 13 A, D). DNA target recognition and unwinding is suggested to depend on the PAM (Anders et al., 2014). Sequence-specific DNA targeting involves Cas9-RNA binding to the PAM GG dinucleotide, whereby the phosphor backbone of the dsDNA target gets in contact with the Cas9-RNA

complex. Subsequent local duplex melting allows the Cas9-RNA complex to interrogate the sequence identity immediately upstream to the PAM. Base pairing between the target DNA strand and the seed region (3' 10 -12 nts of the spacer most critical for DNA binding (Kabadi and Gersbach, 2014)) of the sgRNA then drives RNA-DNA heteroduplex formation towards the distal end of the target DNA.

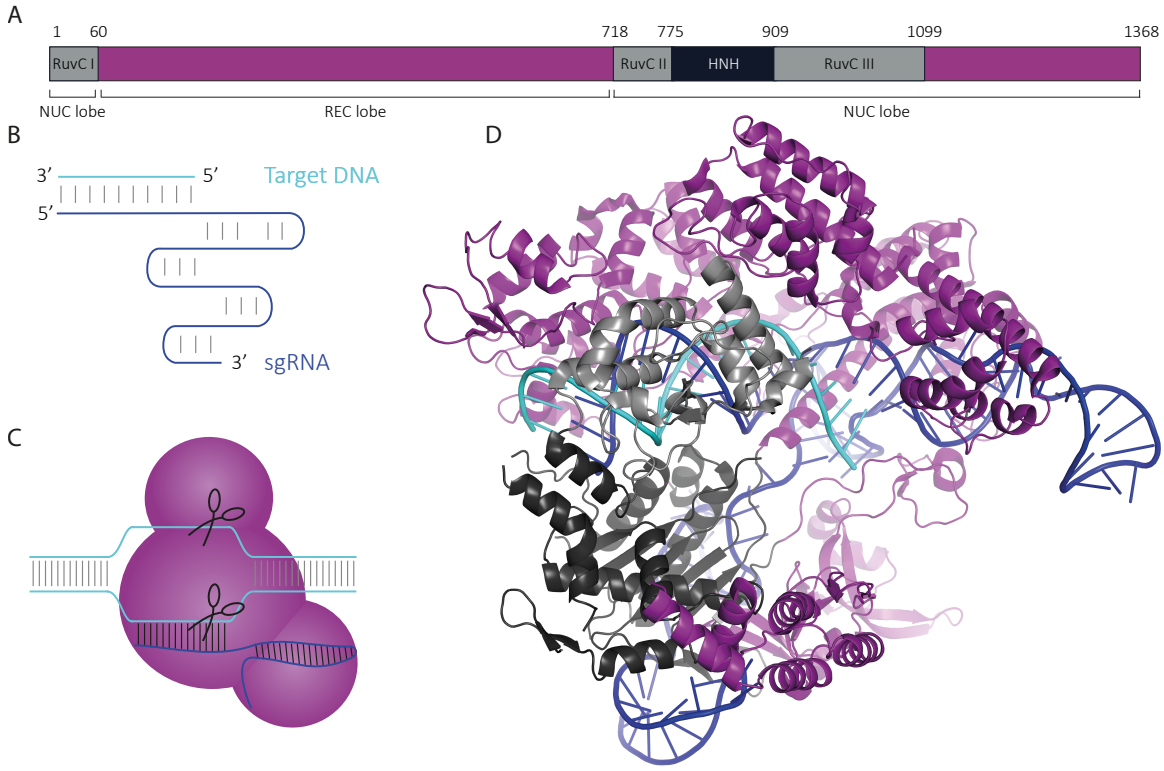

Figure 13: DNA target recognition by the CRISPR/Cas9 system. (A) Schematic representation of the *S.pyogenes* Cas9 comprising a nuclease (NUC) and recognition (REC) lobe. Within the NUC lobe, the nuclease domains HNH and RuvC I-III mediating target DNA cleavage are highlighted in black and grey, respectively. (B) Schematic depiction of the sgRNA:target DNA complex (sgRNA in blue, target DNA in cyan). The sgRNA is composed of crRNA and tracrRNA connected by an artificial tetraloop. (C) Schematic drawing of the Cas9 enzyme contacting the target DNA (cyan) by Watson-Crigg base pairing with the loaded sgRNA (blue). (D) Crystal structure of the Cas9 protein with a loaded sgRNA (blue) in complex with its target DNA (cyan). The sgRNA:target DNA complex adopts a T-shaped structure. The nuclease domains HNH and RuvC I-III mediating target DNA cleavage are highlighted in black and grey, respectively. (PDB 4008. Molecule A. Side view. Modified from (Nishimasu et al., 2014)).

User-defined DNA targeting can simply be addressed by adapting the sgRNA spacer sequence, which is easier and cheaper compared to the ZF and TALE technology, were a new protein has to be engineered for each target sequence. One of the main drawbacks of RGNs is the relatively high frequency of off-targets (Pattanayak et al., 2013; Ran et al., 2013; Fu et al., 2013; Hsu et al., 2013; Cradick et al., 2013). Attempts using mutant Cas9 nickases, where one of the two nuclease domains is inactivated, and pairs thereof, as well as truncated sgRNAs could at least partially reduce off-target cleavage (Ran et al., 2013; Fu et al., 2013). Recently, the impact of off-target binding of a catalytically inactive, dead Cas9

(dCas9) for applications beyond genome editing has been addressed. Compared to the active version, off-target binding was significantly increased for dCas9 with up to several thousand sites, often localised within genes, suggesting a model in which seed matching enables binding but cleavage requires more extensive RNA-DNA heteroduplex formation (Kuscu et al., 2014; Wu et al., 2014).

Based on dCas9, the CRISPR system has been repurposed amongst others to manipulate gene expression. Initially, gene expression has been blocked by presence of dCas9 itself, likely due to steric hindrance, and later by fusion of repressive domains, such as the KRAB domain (Qi et al., 2013; Gilbert et al., 2013). Similarly, fusion of transcriptional activator domains enabled transcriptional gene activation (Bikard et al., 2013; Cheng et al., 2013; Maeder et al., 2013c; Perez-Pinera et al., 2013a; Kearns et al., 2014). While the transcriptional activation potential is considerably reduced compared to TALEs (Mali et al., 2013a; Maeder et al., 2013b; Perez-Pinera et al., 2013a; Bultmann et al., 2012; Zhang et al., 2011), CRISPR/Cas9 appears to be more potent for transcriptional repression (Gao et al., 2014). In summary, both programmable DNA-binding platforms offer exciting possibilities to address, ideally in a combined approach, a wide spectrum of dynamic genome properties.

3.2 dTALEs as a tool to visualise chromatin dynamics

The three-dimensional organisation of the genome and its interactions with epigenetic factors and cellular components play a critical role in the epigenetic regulation of gene expression. Live cell approaches to spatiotemporally resolve the dynamics of endogenous genomic sequences have been limited until recently. Together with two independent studies, which were published almost in parallel, we first demonstrate the applicability of dTALEs for live imaging of repetitive endogenous loci (Miyanari et al., 2013; Ma et al., 2013; Thanisch et al., 2014). Using a GFP-dTALE directed against the ms-repeats (GFP-msTALE), we specifically highlighted the CCs in murine ESCs and followed their spatiotemporal positioning throughout the cell cycle (Figure 14 A, B). Moreover, we established double transgenic cell lines enabling simultaneous imaging of S-Phase progression and *in vivo* chromatin counterstaining.

dTALE-based genome visualisation provides a promising *in vivo* platform to study the genome organisation and its dynamics, which was so far mainly limited to static views. To date, most studies of genome organisation are based on either FISH or 3C-based methods which rely on fixation. While FISH microscopically visualises the spatial arrangements of genomic sequences, 3C-based methods provides indirect information about spatial arrangements by inferring the proximity of genomic loci based on their interaction

frequencies. Although it is generally assumed that FISH and 3C-based views on genome organisation are concordant, a recent study of the murine *HoxD* locus in different developmental and activity stages reveals in some cases incompatible results (Williamson et al., 2014). Given the contrasting views on genome organisation obtained by FISH and 3C-based methods, it will be necessary to compare the results obtained by either technique. Moreover, live imaging information will be required to validate the static snapshots provided so far. Although dTALE-mediated genome visualisation is, similarly to FISH, restricted to a limited set of chosen target sequences, whereas 5C and Hi-C provide genome-wide high-throughput information, it is especially attractive as it reflects the *in vivo* situation.

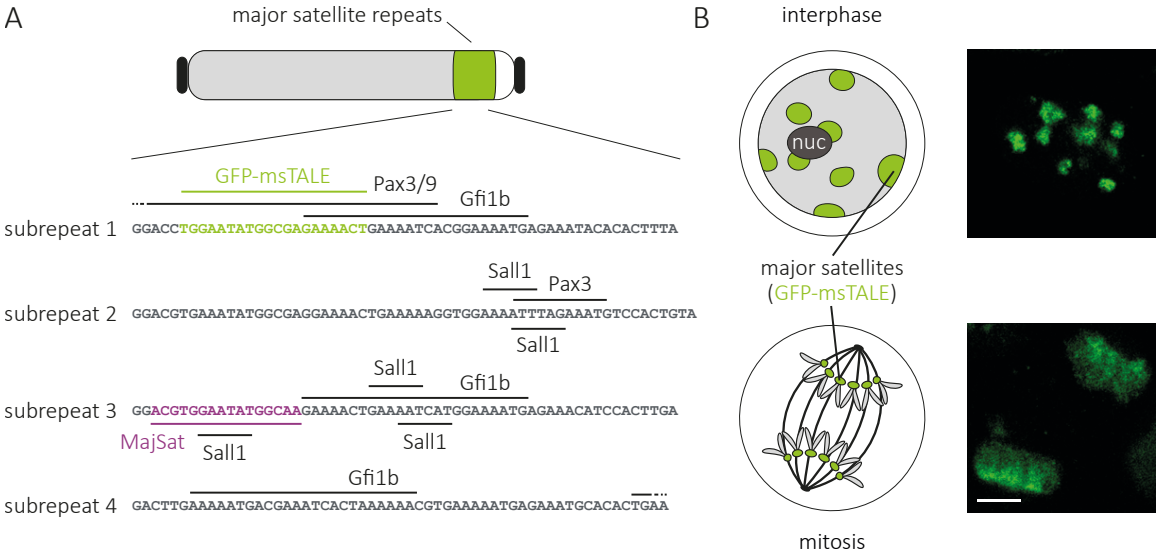

Figure 14: dTALE-based targeting and tracing of the murine major satellite repeats. (A) Schematic representation of a mouse acrocentric chromosome with the pericentromeric ms-repeats (green). Consensus sequence of the four subrepeats of one ms-repeat (green) (Vissel and Choo, 1989). Transcription factors binding to the sense (top) and antisense (below) strand (Bulut-Karslioglu et al., 2012). GFP-msTALE (green) (Thanisch et al., 2014) and MajSat (Miyanari et al., 2013) target sites are highlighted in green and magenta, respectively. (B) Schematic representation (left) and GFP-msTALE-based visualisation (right) of the interphase and mitotic organisation of the pericentromeric domain (green). During interphase, ms-repeats cluster in CCs abutting the nuclear periphery and the nucleoli (nuc, dark grey). Scale bar: 5 µm.

In this respect our double transgenic cell line stably coexpressing RFP-PCNA is particularly valuable as a tool to dissect the replication-dependent processes such as replication timing of the mid-to-late replicating ms-repeats *in vivo*. Using TALEs against different targets also other sequences could be assessed. In addition, by introducing activating epigenetic factors, such as Tets or HATs in fusion with the fluorescent TALE, changes in replication timing in dependence of chromatin state and condensation could be assessed.

Given that active and inactive compartments closely match early and late replicating chromatin, TADs have been proposed to coincide with replication domains. However, direct evidence is still missing. Simultaneous visualisation of constitutive late domains by TALEs

and the cellular DNA replication machinery in combination with 4C shed light on this issue. Alternatively to 4C, FISH probes directed against specific TADs could be applied. However, the most direct *in vivo* evidence would be programmable DNA binding proteins, such as TALEs, directed against repetitive sequences within the respective TADs.

3.2.1 Dynamics of dTALE binding during mitosis

While the GFP-msTALE stably bound to chromatin during interphase, CC association was significantly diminished during mitosis. Mitosis, however, is a period of drastic changes where many structures, including the nuclear envelope, temporarily dissolve and chromosomes are condensed. As revealed by both 5C and Hi-C, condensed mitotic chromosomes appear to be functionally distinct from interphase chromosomes regarding their 3D genome organisation. In contrast to the decondensed, in-homogenous folding state observed during interphase, metaphase chromosomes seem to be homogenously folded and exhibited a striking loss of genomic contacts, chromosome compartments and TADs (Naumova et al., 2013). Moreover, during mitosis most proteins, including RNA polymerases, are evicted from the highly condensed chromosomes. Key TFs, such as GATA-binding protein 1 (GATA1) (Kadauke et al., 2012) or cKrox (Zullo et al., 2012), as well as chromatin architectural proteins, such as Cohesins (Yan et al., 2013), remain however associated and thus might function as mitotic bookmarks transmitting the cellular transcriptional identity (Kadauke and Blobel, 2013).

Apparently, the GFP-msTALE shows similar characteristics to the vast majority of TFs. Binding of the GFP-msTALE is substantially diminished towards metaphase and is only fully re-acquired in late anaphase/early telophase (Figure 14, B). Similarly, for many TFs, the bound protein faction as well as the number of occupied sites is often significantly diminished during mitosis compared to interphase (Kadauke et al., 2012; Caravaca et al., 2013; Follmer et al., 2012). Consistently, we observed residual binding of the GFP-msTALE to its target region in cell clones with higher GFP-msTALE expression. Besides expression levels, mitotic binding might be also dependent on intrinsic TALE features such as number of repeats. Continuous labelling of repetitive sequences throughout mitosis in living cells so far was only achieved by one (Miyanari et al., 2013) of the four dTALE-based visualisation studies published to date (Miyanari et al., 2013; Ma et al., 2013; Thanisch et al., 2014; Yuan et al., 2014). Differently from the other studies, they employed relatively short dTALEs containing 15.5 repeats. Recently, dissociation of longer dTALEs has been confirmed in *Drosophila* using dTALEs with 20.5 repeats (Yuan et al., 2014). Thus, increased repeat domain length might interfere with stable binding in the compacted mitotic state.

Remarkably, repeat domains of naturally occurring TALEs vary drastic in lengths and comprise 1.5 to 33.5 repeats (Boch and Bonas, 2010). Short TALEs below 6.5 repeats, however, fail to induce gene expression and dTALEs below 15.5 repeats exhibit high nucleoplasmic background (Boch et al., 2009; Miyanari et al., 2013). As the TALE has to wind almost twice around the DNA, local chromatin environment and chromatin modifications are likely to affect dTALE binding. It is, thus, conceivable that specific histone modifications and proteins associated to the mitotic chromatin (Wang and Higgins, 2013) along with the high level of mitotic condensation pose a barrier for stable dTALE binding which likely involves remodelling of the nucleosome array. As presence of endogenous TF binding sites is considered indicative for accessible sites and co-loaded TFs might cooperate to open up the chromatin, our TALE was directed against the first subrepeat, which contains binding sites for Pax3, Pax9 and Gf1b TFs (Bulut-Karslioglu et al., 2012). The sequence target by Miyanari *et al.*, however, contains only one additional Sall TF site (Figure 14, A). Based on these results it is also possible, that instead of cooperative action, additional TFs targeting the same site might lead to competitive replacement during mitosis. It remains, however, unclear whether natural TALEs are binding throughout mitosis or not and or whether this is target locus dependent. For transcriptional activation, dedicated mechanisms to ensure TALE binding throughout mitosis might not be required, as most gene expression is ceased during mitosis. Retention of TALEs, however, could facilitate timely transcriptional reactivation of postmitotic host gene expression to the benefit of the pathogen.

3.2.2 *In vivo* kinetics of dTALE binding

Our study provides an important extension to the other published dTALE-based genome visualisation approaches, as we for the first time assess the *in vivo* kinetics of dTALE-DNA interaction. Consistent with our *in vitro* binding studies (Bultmann et al., 2012), fluorescence bleaching experiments revealed a tight association of the GFP-msTALE *in vivo*. We unravelled striking differences in the binding kinetics when comparing the GFP-msTALE to a previously published ZFP directed against the ms-repeats (PZF:GFP) (Lindhout et al., 2007). Complementary FRAP and FLIP experiments clearly demonstrated an increased strength of interaction of the GFP-msTALE over the PZF:GFP, as evidenced in particular by the large immobile fraction detected for the GFP-msTALE. In general, mean residence times of TFs can be short and rapid exchange is typical for many TFs (McNally et al., 2000; Bosisio et al., 2006; Sharp et al., 2006), however not for the GFP-msTALE. It is certainly plausible, that a

tight interaction with chromatin in interphase is inherent to TALEs and stems from superhelical tracking along the double helix during DNA recognition. In summary, mitotic depletion and tight interphase binding indicate that the TALE dynamically interacts with the chromatin environment during the cell cycle.

3.2.3 Alternative approaches and future directions

Recently, catalytically inactive Cas9 proteins were repurposed for genome imaging (Chen et al., 2013; Anton et al., 2014). Labelling of repetitive sequences was reported to be stable throughout mitosis, which might be due to differences in the recognition mode. While it is conceivable that recognition based on strand invasion is more stable, it likely perturbs the local chromatin structure to a greater extent, especially when applying multiple sgRNAs consecutively binding the DNA. For imaging, however, the multiplexing capacity of CRISPR-based approaches opens up exciting new perspectives for visualisation of non-repetitive single genomic loci, which still remains challenging with dTALEs (Chen et al., 2013). So far, CRISPR has not enabled multicolour detection. The commonly used *S.pyogenes* Cas9 protein universally attracts all present sgRNAs. In future, simultaneous use of various Cas9 orthologs and corresponding sgRNAs might help to overcome this limitation (Esvelt et al., 2013). Both platforms open exciting perspectives for genome visualisation with potential clinical applications. dTALEs were already employed to detect changes in the repeat copy number (Ma et al., 2013) and to distinguish sequences with single nucleotide polymorphisms (SNPs) (Miyanari et al., 2013). Similarly, programmable DNA-recognition technologies could be employed to distinguish different chromosomes *in vivo* by targeting repeats unique to a given chromosome. dTALEs could additionally be applied for the discrimination of methylated versus non-methylated sequences, as base-specifying residue for thymine but not the one for cytosine recognition additionally binds to methylated cytosine (Deng et al., 2012b). In future, differential labelling and *in vivo* discrimination could be achieved, possibly simultaneously in multicolour. Ultimately, programmable DNA-binding technologies might enable to follow the spatiotemporal dynamics of repetitive as well as non-repetitive loci to elucidate how genome organisation and epigenetic regulation of differentiation and development are linked.

3.3 dTALEs as a tool to manipulate spatial genome arrangements

The dynamics in the spatial genome organisation plays an important role in various nuclear processes such as replication, long-range gene regulation or translocations. However, in

most cell types the overall distribution of the main chromatin classes is conserved. Dramatic reorganisation of structures such as CCs is mainly restricted to early development and terminal differentiation (Probst et al., 2007; Solovei et al., 2004b; Brero et al., 2005; Solovei et al., 2009). During early development, the centromeric domain forms a ring-like structure around the nucleolar precursor bodies in the pronuclei. During the early cleavage stages, the pericentromeric regions then progressively cluster in CCs (Probst et al., 2007). CC formation coincidences with a burst in ms-repeat transcription, which is required for HC formation and developmental progression (Probst et al., 2010). Recently, the spatial localisation of the ms-repeats was revealed to be essential for embryonic development since peripheral reposition using the PZF:GFP-ZF fused to the NET Emerin impaired developmental progression (Jachowicz et al., 2013). Notably, tethering was time-sensitive as the construct could only elicit tethering in the early two-cell but not at later stages. Moreover, a significant portion of densely DAPI-stained HC was not repositioned and remained around the nucleolar precursor bodies (Jachowicz et al., 2013).

Based on the tight chromatin association of the GFP-msTALE, we independently undertook a similar approach. By coexpression of a high-affinity GFP-binding nanobody (GBP) fused to the nuclear lamina component LB1 (GBP-LB1) (Rothbauer et al., 2008) we could completely repositioned CCs to the nuclear periphery. Importantly, peripheral CC tethering was compatible with normal ESC proliferation even under conditions of a double transgenic cell line. Tethered CCs remained associated to the periphery over consecutive cell cycles and followed the dynamics of LB1 incorporation. During interphase LB1 constrains CCs to the periphery, whereas upon nuclear envelope breakdown and lamina dissociation chromosomes can freely align at the metaphase plate and segregate to the daughter cells (Figure 15, A).

LB1 recruitment during late anaphase newly establishes CC-NL interactions resulting in a patched distribution of the pericentromeric domains instead of a continuous lining beneath the NE. It is conceivable, that the patch-like pattern results from incorporation of GBP-LB1 into the polymerising LB1 meshwork starting from the spindle poles concomitantly serving as nucleation points for the progressive immobilisation of CCs at the NE. Probably, the force that tethers CCs to the periphery is not strong enough to disrupt pericentromeric HC associations completely; especially as histone modifications and hence the repressive status of the pericentromeric HC appear to be unaffected. It is thus conceivable that chromatin-binding proteins remain and mediate associations of the ms-repeats and therefore CCs are not completely dispersed but retained unevenly distributed as squashed patches.

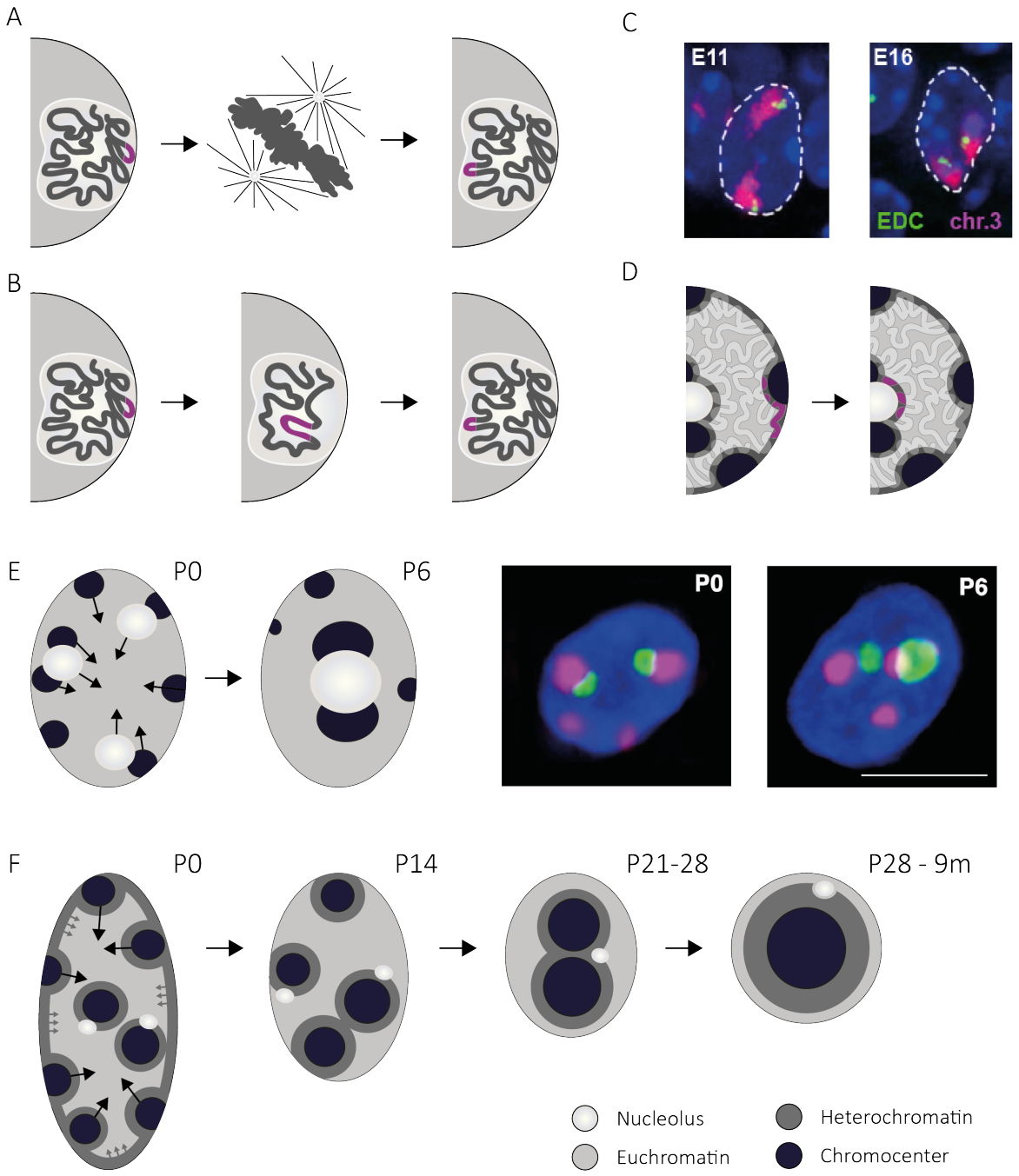

Figure 15: Dynamic spatial genome repositioning during proliferation and differentiation. (A) Following nuclear envelope breakdown and lamina dissociation, genomic positioning is reshuffled. Lamina-assocations can be re-established or more peripheral positions can be adopted. (B) During differentiation, genomic repositioning results from slow movements. Stable associations are favoured, as cells do not divide. (C) Dynamic repositioning of the EDC locus (green) upon activation (Embryonic development day 16 (E16), chromosome paint (magenta) for chromosome 3, DAPI counterstain (blue)) (immunostainings from Irina Solovei). (D) LAD-reshuffling following mitosis. LADs are re-established both perinuclearly and perinucleolarly. (E) Genome repositioning in differentiating Purkinje neurons. During differentiation, centromeres, nucleoli and CCs cluster and adopt a more central position (adapted from (Solovei et al., 2004b). Scheme of the positional changes occurring in the early postembryonic days 0 and 6 (P0, P6). Arrows indicate the central movements and clustering of nucleoli and HC. 3D-FISH with a mouse ms-repeat specific probe (magenta), immunostaining of the nucleolar marker B23 (green), TO-PRO-3 counterstain (blue). Scale bar: 10µm (Solovei et al., 2004b). (F) Changes in the nuclear architecture during postmitotic rod development. While CCs gradually fuse, LINE-rich HC separates from the NE, gets decompacted and accumulates around the large central CC. Arrows indicate the inward movements. By P28, inversion is completed. Chromatin spatially segregates into two concentric shells around the CC with a central layer of LINE-rich HC and an outmost layer of SINE-rich EC (adapted from (Solovei et al., 2009)).

Consistent with earlier studies revealing that peripheral targeting of lacO-tagged sequences depends passage through mitosis (Reddy et al., 2008; Kumaran and Spector, 2008; Finlan et al., 2008), we observe that initial tethering of CCs to the periphery is established following mitosis. The positioning of tethered CCs, however, is probably not maintained. Following mitosis, genes that become activated can lose lamina-association and adopt a more internal position (Figure 15, C). Similarly, LADs are reshuffled after division and contacts are newly established (Kind et al., 2013) (Figure 15, D). Perinuclear LAD positioning is correlated with transcriptional silent states, yet it remains unclear whether artificial recruitment to a repressive compartment suffices to repress gene expression. It is rather likely, that repressive modifications enhance the probability of a locus to be directed peripherally. Consistently, artificial targeting of lacO-tagged reporters, flanking genes and chromosomes to the nuclear periphery had varying impact on gene expression status (Reddy et al., 2008; Finlan et al., 2008; Kumaran and Spector, 2008) ranging from strong repression over moderate effects to normal expression status whereas a repressive chromatin status has been clearly linked to reposition (Zullo et al., 2012; Harr et al., 2015).

Besides transcriptional competence and cellular background, the observed differences presumably depend on a combination of epigenetic status, folding of adjacent chromosomal regions, DNA sequence, presence of NETs and their chromatin-binding or modifying partners. Due to interaction with HDAC3, peripheral targeting of active regions by the INM proteins EMD and Lap2ß (Holaska and Wilson, 2007; Somech et al., 2005; Demmerle et al., 2012; Zullo et al., 2012) coincides with chromatin remodelling by histone hyperacetylation while treatment with the HDAC-inhibitor trichostatin A (TSA) dislodged the tethered sequences (Reddy et al., 2008; Finlan et al., 2008; Zullo et al., 2012).

Recent evidence suggests, besides dependency on heterochromatic modifications/chromosomal context, at least some dependency of LAD specification on certain motifs. Repositioning assays revealed that ectopically integrated LAD-derived sequences were sufficient for the establishment of NL contacts of otherwise nucleoplasmic chromatin along with their transcriptional repression (Zullo et al., 2012). In the case of LAP2B, $(GA)_n$ repeats have been revealed to be sufficient for peripheral HC anchorage (Zullo et al., 2012). Similarly, the polycomb-binding tandem repeat D4Z4, which also contains $(GA)_n$ repeats, is involved in LmA and CTCF dependent peripheral HC association (Ottaviani et al., 2009). Genome-wide integration of reporter genes revealed that insertion in LADs caused their peripheral positioning and transcriptional silencing (Akhtar et al., 2014). Interestingly, similar sequence composition is found in NL-associated LADs and surrounding the nucleoli

and CCs. Indeed, during cell division LADs can be reshuffled, e.g. former NL-associated LADs can be found at the periphery of the nucleoli (Kind et al., 2013) (Figure 15, D).

Moreover, genome-wide analysis revealed at least a partial overlap to nucleolar-associated domains (NADs), which contain besides rDNA sequences mainly centromeric and pericentromeric satellite DNA and LINE-rich HC (Nemeth et al., 2010; van Koningsbruggen et al., 2010). A similar repositioning between the two compartments in dependence on the cell cycle is also found for the inactivated X (Zhang et al., 2007) or centromere clusters (Solovei et al., 2004a). Most but not all genes within LADs and NADs are transcriptionally silent indicating that chromatin compaction and positioning alone are not decisive for transcriptional regulation (Nemeth et al., 2010; van Koningsbruggen et al., 2010; Akhtar et al., 2013; Kind and van Steensel, 2014). Nevertheless, both nuclear and perinucleolar periphery can be regarded as a silencing zone, which can lock repressive ground states. Release from the HC domains instead poises genes for activation (Peric-Hupkes et al., 2010). It remains, however, a chicken and egg type question, which roles chromatin remodelling and transcriptional regulation play in this context. Strikingly, dynamic repositioning of loci towards or away from CCs during development coincidences with transcriptional suppression and activation, respectively, suggesting a role of CCs in transcriptional regulation (Brown et al., 1997; 1999; Skok et al., 2001; Roldan et al., 2005; Merkenschlager et al., 2004; Clowney et al., 2012). Clustering and dynamic repositioning of centromeric and pericentromeric regions, which is particularly pronounced in differentiating and postmitotic cells (Manuelidis, 1984; Solovei et al., 2004a; b; Brero et al., 2005; Solovei et al., 2009), likely drives the consolidation of the repressive intranuclear HC domain and thus global separation of the silencing from the EC compartment (Gibcus and Dekker, 2013). Such interchromosomal HC associations might be favoured by an intrinsic propensity of similar sequences to cluster and presence of chromatin-binding proteins. In non-dividing cells, interchromosomal HC associations might be facilitated, as chromosomes are no more redistributed following mitosis (Figure 15, B).

Peripheral tethering of CCs leads to their enrichment at the periphery, which is accompanied by a striking loss of perinucleolar HC. Importantly, we did not observe changes in histone modifications. Although forced reposition presumably counteracts the intrinsic tendency of the satellite repeats to self-associate and CCs disintegrate, the resulting patched pattern suggests a persistent interaction. A similar but complete disintegration of CCs along with peripheral repositioning and destabilisation of the NL was recently reported upon knockout of the H3K9me1-specific HMTs Prdm3 and Prdm6 (Pinheiro et al., 2012). While dTALE-LB1 mediated peripheral repositioning preserves the repressive chromatin

status and does not affect general HC integrity, abolishment of H3K9m1 and subsequent H3K9me2/3 leads to extensive chromatin remodelling and HC disruption (Pinheiro et al., 2012; Towbin et al., 2012). It will be interesting to study, whether and how peripheral repositioning impacts on transcriptional regulation. A crucial impairment due to peripheral tethering of ms-repeats is not expected since the positioning of EC and HC in the nucleus, despite of their conserved overall spatial arrangement in most cell types, appears not to be critical for nuclear function. In the extreme case of rod photoreceptor nuclei, where pericentromeric regions fuse and relocalise to build one large internal CC, neither peripheral relocalisation of EC nor continuous chromatin movements during reorganisation impede with transcription (Solovei et al., 2009). Consistently, in our experiments, forced repositioning of CCs to the periphery does not hamper differentiation into myotubes.

Interestingly, both rods and nuclei with peripheral tethered CCs deviate from conventional nuclei regarding the subnuclear sites of HC anchorage. In rods, NL-associated LADs are dislodged and accumulate intranuclearly, whereas forced CC-NL association probably disrupts nucleolar associations. Unlike in rods, however, peripheral repositioning does not involve chromatin remodelling and is therefore unlikely to affect chromosome folding. Besides manipulating the overall nuclear architecture, it will be extremely interesting to exploit programmable DNA binding platforms, either TALEs or CRISPR, for the repositioning of endogenous genes. Considering the exciting possibilities to probe and manipulate the nuclear architecture, we might start to understand the structure-function relationship between transcription and spatiotemporal genome organisation.

3.4 Mechanisms of peripheral heterochromatin tethering

Inversion of the nuclear architecture during terminal differentiation in rod photoreceptors is a slow process, which takes about two months and involves changes in chromatin folding (Solovei et al., 2009). Gradual CC fusion is accompanied by continuous chromatin movements and remodelling, as LINE-rich HC separates from the NE, is decompacted and accumulates around the converging CCs (Figure 15, F). Anchored by the large internal CC, chromatin spatially segregates in two concentric compartments of LINE-rich HC followed by SINE-rich EC beneath the NE. Only some small HC remnants present at the periphery bridge into the HC layer (Kizilyaprak et al., 2010; Solovei et al., 2009; Eberhart et al., 2013). Notably, basic chromosome folding in the inverted nuclear architecture is similar to the conventional nuclear architecture with linear chromosome threads weaving between the two compartments. Yet, due to a different subnuclear anchorage site and changes in CT

positioning, chromosome folds align in a parallel, petal-like fashion (Solovei et al., 2009) (Figure 16, A).

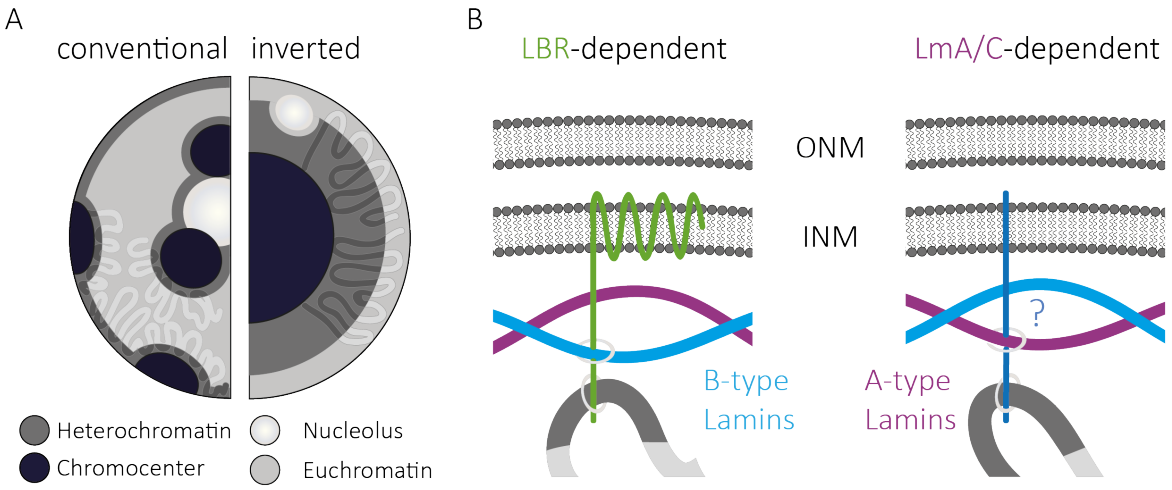

Figure 16: Chromosome folding and peripheral HC anchorage. (A) Chromosome folding in conventional and inverted nuclei. Chromosome threads weave back and forth between the active EC and inactive HC compartment in the interphase chromosome territory. In conventional nuclei, anchorage is provided by the HC domains at the periphery, surrounding the nucleoli and the CCs. In inverted nuclei, HC anchorage at the periphery is lost. Chromosome threads align parallel in a petal-like fashion. (B) Model of peripheral HC anchorage by the two tethers LBR (left) and Lamin A/C (LmA/C, right). While LBR can rescue peripheral HC anchorage, LmA/C likely requires at least one additional chromatin binding partner, which is absent in rod cells (adapted from (Solovei et al., 2013)).

Importantly, our study provides the first basis towards a mechanistic understanding of inversion linking peripheral HC maintenance to the NE-associated tethers LBR and LmA/C (Figure 16, B). Both tethers are differentially used, developmentally regulated, and oppositely affect both transcription and cellular differentiation. LBR is expressed first but in later differentiation stages either replaced or joined by LmA/C. Interestingly, depletion of LmA/C is often compensated by sustained LBR expression but not *vice versa* and depletion of both proteins coincides with inversion in all postmitotic cells. Consistently, inversion in rod nuclei of nocturnal mammals correlates with the absence of both LBR and LmA/C.

3.4.1 LBR rescues HC tethering in rods

Strikingly, LBR is important for the maintenance of LAD-NL associations as ectopic LBR expression in rods (LBR-TER) rescues peripheral HC tethering (Figure 16, B, left). LBR might exert this function by both tethering and compacting HC (Hirano et al., 2012). In the proposed two-step model, LBR initially binds HC by recognition of H4K20me2 by its N-terminal Tudor domain (Makatsori et al., 2004; Olins et al., 2010; Hirano et al., 2012). Multimerisation via the RS domain further promotes high affinity clustering and the nucleoplasmic part of the TM-domain recruits additional factors, such as Lamin B, HP1 or MeCP2 (Lin et al., 1996; Ye et al., 1997; Guarda et al., 2009) fostering transcriptional

repression and further heterochromatinisation of the tethered chromatin (Hirano et al., 2012). It remains, however, unclear whether LBR suffices to tether HC to the periphery or whether it relies on additional partners, which are present in rod cells.

Impaired HC organisation, clumping and internal repositioning, a phenotype similar to the CC aggregation observed in rods, is manifested in granulocytes of Pelger-Huët Anomaly and ichthyotic mice lacking functional LBR (Shultz et al., 2003; Hoffmann et al., 2002; Zwerger et al., 2008; Hoffmann et al., 2007; Cohen et al., 2008). A similar aggregation of CCs is also observed in mouse olfactory sensory neurons (OSNs) where LBR is absent (Clowney et al., 2012). OSNs are implicated in odorant detection and sensing is performed by a set of olfactory receptors (ORs), which are monogenically and monoallelically expressed (Chess et al., 1994). OSN identity is determined by the OR expressed. Interestingly, active and repressed OR alleles position differently within the nucleus, with the inactive allele localising in close proximity to the central CC aggregate and the active allele residing in the EC domain (Clowney et al., 2012). Upon ectopic expression of LBR, the central CC aggregate along with the OR gene disassociates. In contrast, LBR ablation causes CCs and OR gene clustering in non-OSN cell types. Irrespective of the similarities in CC fusion and internal reposition in the absence of LBR, the nuclear architecture in OSNs likely differs from the inverted nuclear architecture of rods as revealed by DAPI staining (Clowney et al., 2012; Solovei et al., 2009) and FISH experiments (I. Solovei, unpublished). In particular, LINE-rich HC seems neither to dissociate from the periphery nor to accumulate internally. Moreover, there is no evidence that LINE-rich HC and SINE-rich EC segregate in regular concentric shells. Thus, it is tempting to speculate that in OSNs, due to peripheral CC release in absence of LBR, heterochromatic self-association forces together with chromatin-binding proteins drive the clustering of nuclear organiser regions (NORs), CCs and centromeres, thereby globally separating active and inactive compartments. The inverted nuclear architecture of rods instead is characterised by concentric arrangements of LINE-rich HC and SINE-rich EC. Thus, it is likely that there are additional mechanisms in rod nuclei governing the dramatic movements and spatial reorganisation of the main chromatin.

3.4.2 Mouse models for the study of night vision

Notably, central HC aggregation in rod nuclei appears to act as a microlense focussing light traversing the retina and thereby improving vision at low light conditions (Solovei et al., 2009). The LBR-TER mouse model, in which clonal cells expressing LBR revert to the conventional architecture, provides the first model for the study of night vision in

dependence of photoreceptor nuclei inversion. Generation of an LBR-TER knock-in mouse would improve the existing model by providing a model where LBR is expressed all rods.

Close inspection of our LBR-TER mouse model revealed that rod nuclei rescued by LBR exhibit an increased nuclear envelope growth. Stimulated membrane growth is consistent with the known function of LBR in membrane growth regulation and the observation that high levels of LBR can cause extensive membrane production accompanied by NE invagination and formation of cytoplasmic vesicular aggregates *in vitro* (Olins et al., 1998; Olins and Olins, 2009; Ma et al., 2007). Notably, NE invaginations were attributed to the overexpression of the N-terminal domain (Ellenberg et al., 1997; Ma et al., 2007). In contrast, membrane overgrowth along with perinuclear aggregates appears to be induced by the TM-domain of LBR (Ma et al., 2007), which, besides mediating anchorage in the INM, exhibits sterol reductase activity (Ye and Worman, 1994; Silve et al., 1998; Waterham et al., 2003). Consistently, 3-hyroxy-3-methyl-glutaryl (HMG) coenzyme A (CoA) sterol reductase overexpression results in formation of stacked, perinuclear membrane pairs surrounding the nuclei in yeast (Wright et al., 1988). Since correct insertion of LBR relies only on the first transmembrane domain (TMD) (Smith and Blobel, 1993), rod-specific expression of a truncated LBR with a considerably shorter TMD and presumably impaired sterol reductase activity could possibly abolish membrane overproduction in transgenic or knock-in mice. It remains, however, to be tested whether truncated versions correctly fold, localise and bind HC.

3.4.3 Model of assisted HC-tethering for LmA/C

Interestingly, ectopic LBR but not LmC expression alone can revert the inverted nuclear architecture to the conventional one. Notably, different splicing forms of Lamins exist and the composition of the NL appears to be cell type specific. For example, LmC prevails in the central nervous system due to selective downregulation of the LmA splicing form by the brain-specific miRNA miR-9 (Jung et al., 2012). It is, however, unlikely that ectopic expression of the LmA splicing form would rescue inversion in rods. Although both LmC and prelamin A are differently processed, both splicing forms are considered functionally equivalent after removal of farnesylation and carboxymethylated residues and release from the INM during LmA maturation (Dechat et al., 2010).

Although LmA/C has been reported to bind at least to some degree directly to chromatin (Brachner and Foisner, 2011; Kubben et al., 2012), LmA/C-dependent maintenance of HC tethering appears to depend on the presence of at least one chromatin-

binding partner (Figure 16, B, right). Possible candidates are among the well-characterised LEM-domain proteins, such as MAN1, LAP2, LEM2 or EMD, which were assessed in our study. While MAN1 and LAP2 are present in rods at all stages, LEM2 is not expressed and EMD is strongly downregulated during rod differentiation. Notably, MAN1 or LAP2 expression cannot rescue the inverted nuclear architecture upon ectopic expression of LmC in rods. Likewise, EMD appears to be dispensable for HC tethering, as cells from EMD-KO mice, which lack LBR, show neither inversion nor compensation by prolonged or increased LBR expression. Moreover, except for one cell type, EMD is not functionally replaced with another LEM-domain protein.

Considering the highly divers protein composition of the NE between different cell types and developmental stages revealed by recent proteomic studies (Schirmer et al., 2003; Korfali et al., 2010; Wilkie et al., 2011; Korfali et al., 2012), it might be difficult to find the missing partner(s) of LmA/C. It is thus not only conceivable that the mediating partner of LmA/C is cell-type specific but moreover that even other proteins can replace LmA/C. Notably, many of the identified NETs have not been functionally characterised yet. The mechanisms of peripheral HC scaffolding remain largely elusive and have only been addressed for some of the best-characterised NETs, such as Lap2ß or EMD. Lap2ß-dependent tethering was revealed to depend on presence of the TF cKrox and HDAC3 (Zullo et al., 2012). Similarly, EMD is likely to tether chromatin in complex with HDAC3 (Demmerle et al., 2012) or BAF (Brachner and Foisner, 2011). Both, however, do clearly not account for all tethering. Regarding the various NETs found within a given cell type, it is certainly plausible that different NET proteins might facilitate anchorage at the same time in independent complexes either directly or indirectly with nucleoplasmic chromatin binding or modifying factors.

To identify the missing partner in rods, it might be beneficial to compare the protein composition in photoreceptor precursors and mature rods not only by immunostainings but also by mass spectrometry. Ultimately, however, specific knock-out and knock-in experiments will be required to assess the involvement of NET proteins in LmA/C dependent tethering. In summary, the picture that emerges is that the versatility of nuclear envelope composition in different tissues and developmental contexts significantly contributes to the dynamic spatial genome organisation thereby shaping cellular identity and functions.

3.5 The main chromatin classes blueprint the spatiotemporal genome organisation

The vast majority of the genome is made up by intergenic and intronic sequences as well as repetitive elements with no direct function long considered to be junk DNA. Recent evidence, however, suggests that many of these 'junk'-like sequences crucially contribute to genomic functions (Shen et al., 2012). Clustering of similar chromosomal segments in conjunction with chromatin-binding proteins shape the dynamic genome organisation, in particular by controlling transcription via chromatin looping (Holwerda and de Laat, 2012; Phillips-Cremins et al., 2013). Such genomic interactions are spatially confined within a small genomic neighbourhood in TADs. Strikingly, our study of a human artificial chromosome (HAC) in a xenospecific mouse background reveals that small chromosomal subregions corresponding to the main chromatin classes autonomously segregate depending on GC-content, gene-richness and repeat composition. Sharp borders corresponding to TADs demarcate the subregions. Genomic interactions are observed between preferred types of neighbours, similar in sequence but independent from their chromosomal context.

3.5.1 Repetitive sequences as basic units of nuclear architecture

As proposed by the birds-of-a-feather-flock-together model similarly typed sequences show a strong tendency for association (Gibcus and Dekker, 2013). Consistently, we observe a species-independent clustering of centromeric regions. As impressively demonstrated in rod nuclei, LINE-rich and SINE-rich HAC regions position to the respective active and inactive compartments while keeping away from the opposing one (Lieberman-Aiden et al., 2009). Genic regions within the active compartment are robustly expressed. According to the model, gene-poor/gene-desert segments associate equally well with both inactive compartments (nuclear periphery and margins of CCs and nucleoli) in conventional nuclei. In the presence of peripheral HC tethers, however, mouse or human orthologous regions exhibit an increased affinity towards the NE, whereas the HAC associates equally well with both CCs and NE. The influence of different sequences on genome positioning can be explained by the dogs-on-a-lead-model, in which highly repetitive sequences, such as rDNA and centromeres, represent strong dogs, which autonomously pull their owner (chromosome) to a particular place whereas submissive dogs (genes and regulatory sequences) follow their owners (Krijger and de Laat, 2013). Positioning is newly established in G1 and repetitive sequences, due to their linear succession over long stretches, have a higher probability to form stable contacts thereby serving as nucleation points.

Concomitantly, they constrain the mobility of the remainder of the chromosome and render autonomous positioning of single genes unlikely.

Apparently, peripheral tethers can outcompete against highly repetitive sequences, as evidenced by the preferential lamina-association of gene-poor chromatin and deserts of endogenous mouse and human orthologous sequences. This is consistent with the overwhelming number of such sequences being positioned in peripheral cLADs and their continuous re-establishment immediately after mitosis (Kind et al., 2013; Guelen et al., 2008; Meuleman et al., 2013). In rods, positioning is less constrained since peripheral HC is released and HC-associated repetitive sequences are situated in the nuclear interior. Furthermore, positioning and genomic contacts do not have to be re-establish but are stably maintained, as cells do not divide.

In comparison to an entire chromosome, the HAC is relatively small (ca. 4 – 5 Mb) and the centromere accounts for a large fraction. Thus, the competitive advantage of the repetitive sequences to establish stable contacts preferentially positions the HAC towards the CCs. On the chromosomal level, dispersed repetitive LINEs and SINEs exert a similar, inherent cooperativity facilitating polarised, gene-density related arrangements of chromosomal segments (Kupper et al., 2007; Goetze et al., 2007) and driving the global segregation into active and inactive A and B compartment (Lieberman-Aiden et al., 2009). LINEs, SINEs as well as centromeric sequences might thus represent basic modules of genome positioning.

3.5.2 Lamina-association and transcriptional regulation

LADs are characterised by LINE-rich, gene-poor HC with an overall low transcriptional activity (Guelen et al., 2008; Peric-Hupkes et al., 2010; Meuleman et al., 2013). Consistently, lamina-association of HAC and orthologous human subregions correlates with a decreased transcriptional activity. However, genic HAC regions exhibit an overall increased LADness compared to their orthologous human and mouse counterparts as well as gene-rich and gene-poor subregions failed to establish a proper LAD/interLAD pattern. Although surprising, this could be attributed to the relatively small size of the HAC, which does not allow proper positioning of genic regions away from the NE. Moreover, it is conceivable that LAD/interLAD positioning depends on the proper chromosomal context of native chromosomes. Possibly, long-range promoter-enhancer interactions are dependent on the cellular background/conspecific sequences and thus affected. In multigene complexes, rupture of chromosomal loops by TALENs directly affected the transcription of associated genes

(Fanucchi et al., 2013). Similarly, chromosomal translocations that cause local perturbations in the chromosome structure impact on the regulation of both proximal and distant genes (Harewood et al., 2010), as the spatial relocalisation of the sequences to another TAD is likely to disturb the genomic contacts. Consistently, the overall gene activity of the HAC is decreased and it is thus plausible that the gene-rich subregions, which might correspond to a fLAD, exhibit an increased affinity to the NE. Although overall increased, LADness of genic HAC regions strongly correlates and decreases with increasing gene activity. As most of the genes are less expressed, the more active genes in close proximity might relatively follow in their positioning since lamina-association exerts a strong relocating force. Yet, they maintain their transcriptional competence, probably by forming or relocating to an active TAD microenvironment either by an active or passive mechanism. Within this microenvironment, which can also be established close to the periphery and nuclear pores, active genes may share factors of the transcriptional and splicing machinery (Akhtar and Gasser, 2007; Joffe et al., 2010).

In summary, our study not only reveals that stretches of the main chromatin classes blueprint the nuclear architecture, but will also further enhance our understanding how the epigenetic landscape of the genome is dynamically regulated in differentiation, development as well as in disease.

4 Annex

4.1 References

Akhtar, A., and S.M. Gasser. 2007. The nuclear envelope and transcriptional control. *Nature Reviews Genetics*. 8:507–517. doi:10.1038/nrg2122.

Akhtar, W., A.V. Pindyurin, J. de Jong, L. Pagie, J. Ten Hoeve, A. Berns, L.F.A. Wessels, B. van Steensel, and M. van Lohuizen. 2014. Using TRIP for genome-wide position effect analysis in cultured cells. *Nat Protoc*. 9:1255–1281. doi:10.1038/nprot.2014.072.

Akhtar, W., J. de Jong, A.V. Pindyurin, L. Pagie, W. Meuleman, J. de Ridder, A. Berns, L.F.A. Wessels, M. van Lohuizen, and B. van Steensel. 2013. Chromatin Position Effects Assayed by Thousands of Reporters Integrated in Parallel. *Cell*. 154:914–927. doi:10.1016/j.cell.2013.07.018.

Almouzni, G., and A.V. Probst. 2011. Heterochromatin maintenance and establishment: lessons from the mouse pericentromere. *Nucleus*. 2:332–338. doi:10.4161/nucl.2.5.17707.

Amir, R.E., I.B. Van den Veyver, M. Wan, C.Q. Tran, U. Francke, and H.Y. Zoghbi. 1999. Rett syndrome is caused by mutations in X-linked MECP2, encoding methyl-CpG-binding protein 2. *Nat. Genet.* 23:185–188. doi:10.1038/13810.

Anders, C., O. Niewoehner, A. Duerst, and M. Jinek. 2014. Structural basis of PAM-dependent target DNA recognition by the Cas9 endonuclease. *Nature*. doi:10.1038/nature13579.

Anthony, K., A. More, and X. Zhang. 2014. Activation of Silenced Cytokine Gene Promoters by the Synergistic Effect of TBP-TALE and VP64-TALE Activators. *PLoS ONE*. 9:e95790. doi:10.1371/journal.pone.0095790.

Anton, T., S. Bultmann, H. Leonhardt, and Y. Markaki. 2014. Visualisation of specific DNA sequences in living mouse embryonic stem cells with a programmable fluorescent CRISPR/Cas system. *Nucleus*. 5. doi:10.4161/nucl.28488.

Azuara, V., P. Perry, S. Sauer, M. Spivakov, H.F. Jorgensen, R.M. John, M. Gouti, M. Casanova, G. Warnes, M. Merkenschlager, and A.G. Fisher. 2006. Chromatin signatures of pluripotent cell lines. *Nat. Cell Biol.* 8:532–538. doi:10.1038/ncb1403.

Bannister, A.J., and T. Kouzarides. 2011. Regulation of chromatin by histone modifications. *Cell Res.* 21:381–395. doi:10.1038/cr.2011.22.

Barrangou, R. 2014. RNA events. Cas9 targeting and the CRISPR revolution. *Science*. 344:707–708. doi:10.1126/science.1252964.

Beerli, R.R., and C.F.3. Barbas. 2002. Engineering polydactyl zinc-finger transcription factors. *Nat. Biotechnol.* 20:135–141.

Benavente, R., G. Krohne, and W.W. Franke. 1985. Cell type-specific expression of nuclear lamina proteins during development of Xenopus laevis. *Cell*. 41:177–190.

Berezney, R., D.D. Dubey, and J.A. Huberman. 2000. Heterogeneity of eukaryotic replicons, replicon clusters, and replication foci. *Chromosoma*. 108:471–484.

Berg, J.M. 1988. Proposed structure for the zinc-binding domains from transcription factor IIIA and related proteins. *Proceedings of the National Academy of Sciences of the United States of America*. 85:99–102.

Bernardi, G. 1989. The isochore organization of the human genome. *Annu Rev Genet*. 23:637–661. doi:10.1146/annurev.ge.23.120189.003225.

Bernstein, B.E., T.S. Mikkelsen, X. Xie, M. Kamal, D.J. Huebert, J. Cuff, B. Fry, A. Meissner, M. Wernig, K. Plath, R. Jaenisch, A. Wagschal, R. Feil, S.L. Schreiber, and E.S. Lander. 2006. A bivalent chromatin structure marks key developmental genes in embryonic stem cells. *Cell*. 125:315–326. doi:10.1016/j.cell.2006.02.041.

Beurdeley, M., F. Bietz, J. Li, S. Thomas, T. Stoddard, A. Juillerat, F. Zhang, D.F. Voytas, P. Duchateau, and G.H. Silva. 2013. Compact designer TALENs for efficient genome engineering. *Nat Commun*. 4:1762. doi:10.1038/ncomms2782.

Bickmore, W.A. 2014. The Spatial Organization of the Human Genome. *Annu. Rev. Genomics Hum. Genet.* 67–84.

Bickmore, W.A., and B. van Steensel. 2013. Genome architecture: domain organization of interphase chromosomes. *Cell*. 152:1270–1284. doi:10.1016/j.cell.2013.02.001.

Bikard, D., W. Jiang, P. Samai, A. Hochschild, F. Zhang, and L.A. Marraffini. 2013. Programmable repression and activation of bacterial gene expression using an engineered CRISPR-Cas system. *Nucleic acids research*. 41:7429–7437. doi:10.1093/nar/gkt520.

Bione, S., K. Small, V.M. Aksmanovic, M. D'Urso, A. Ciccodicola, L. Merlini, L. Morandi, W. Kress, J.R. Yates, and S.T. Warren. 1995. Identification of new mutations in the Emery-Dreifuss muscular dystrophy gene and evidence for genetic heterogeneity of the disease. *Human Molecular Genetics*. 4:1859–1863.

Black, B.E., and D.W. Cleveland. 2011. Epigenetic centromere propagation and the nature of CENP-a nucleosomes. *Cell*. 144:471–479. doi:10.1016/j.cell.2011.02.002.

Blount, B.A., T. Weenink, S. Vasylechko, and T. Ellis. 2012. Rational diversification of a promoter providing fine-tuned expression and orthogonal regulation for synthetic biology. *PLoS ONE*. 7:e33279.

Boch, J., and U. Bonas. 2010. Xanthomonas AvrBs3 family-type III effectors: discovery and function. *Annu Rev Phytopathol*. 48:419–436. doi:10.1146/annurev-phyto-080508-081936.

Boch, J., H. Scholze, S. Schornack, A. Landgraf, S. Hahn, S. Kay, T. Lahaye, A. Nickstadt, and U. Bonas. 2009. Breaking the code of DNA binding specificity of TAL-type III effectors. *Science*. 326:1509–1512. doi:10.1126/science.1178811.

Bogdanove, A.J., and D.F. Voytas. 2011. TAL Effectors: Customizable Proteins for DNA Targeting. *Science*. 333:1843–1846. doi:10.1126/science.1204094.

Bolzer, A., G. Kreth, I. Solovei, D. Koehler, K. Saracoglu, C. Fauth, S. Muller, R. Eils, C. Cremer, M.R. Speicher, and T. Cremer. 2005. Three-dimensional maps of all chromosomes in human male fibroblast nuclei and prometaphase rosettes. *PLoS Biol*. 3:e157. doi:10.1371/journal.pbio.0030157.

Bonne, G., K. Schwartz, M.R.D. Barletta, S. Varnous, H.-M. Bécane, E.-H. Hammouda, L. Merlini, F. Muntoni, C.R. Greenberg, F. Gary, J.-A. Urtizberea, D. Duboc, M. Fardeau, and D. Toniolo. 1999. Mutations in the gene encoding lamin A/C cause autosomal dominant Emery-Dreifuss muscular dystrophy. *Nat. Genet.* 21:285–288. doi:10.1038/6799.

Bornfleth, H., P. Edelmann, D. Zink, T. Cremer, and C. Cremer. 1999. Quantitative motion analysis of subchromosomal foci in living cells using four-dimensional microscopy. *Biophys J*. 77:2871–2886.

Bosisio, D., I. Marazzi, A. Agresti, N. Shimizu, M.E. Bianchi, and G. Natoli. 2006. A hyper-dynamic equilibrium between promoter-bound and nucleoplasmic dimers controls NF-kappaB-dependent gene activity. *EMBO J.* 25:798–810. doi:10.1038/sj.emboj.7600977.

Boyle, S., M.J. Rodesch, H.A. Halvensleben, J.A. Jeddeloh, and W.A. Bickmore. 2011. Fluorescence in situ hybridization with high-complexity repeat-free oligonucleotide probes generated by massively parallel synthesis. *Chromosome Res.* 19:901–909. doi:10.1007/s10577-011-9245-0.

Boyle, S., S. Gilchrist, J.M. Bridger, N.L. Mahy, J.A. Ellis, and W.A. Bickmore. 2001. The spatial organization of human chromosomes within the nuclei of normal and emerin-mutant cells. *Human Molecular Genetics*. 10:211–219.

Brachner, A., and R. Foisner. 2011. Evolvement of LEM proteins as chromatin tethers at the nuclear periphery. *Biochem. Soc. Trans.* 39:1735–1741. doi:10.1083/jcb.200210026.

Branco, M.R., and A. Pombo. 2006. Intermingling of chromosome territories in interphase suggests role in translocations and transcription-dependent associations. *PLoS Biol*. 4:e138. doi:10.1371/journal.pbio.0040138.

Brandeis, M., D. Frank, I. Keshet, Z. Siegfried, M. Mendelsohn, A. Nemes, V. Temper, A. Razin, and H. Cedar. 1994. Sp1 elements protect a CpG island from de novo methylation. *Nature*. 371:435–438. doi:10.1038/371435a0.

Brero, A., H.P. Easwaran, D. Nowak, I. Grunewald, T. Cremer, H. Leonhardt, and M.C. Cardoso. 2005. Methyl CpG-binding proteins induce large-scale chromatin reorganization during terminal differentiation. *J. Cell Biol.* 169:733–743. doi:10.1083/jcb.200502062.

Briggs, A.W., X. Rios, R. Chari, L. Yang, F. Zhang, P. Mali, and G.M. Church. 2012. Iterative capped assembly: rapid and scalable synthesis of repeat-module DNA such as TAL effectors from individual monomers. *Nucleic acids research*. 40:e117–e117. doi:10.1093/nar/gks624.

Brown, K.E., J. Baxter, D. Graf, M. Merkenschlager, and A.G. Fisher. 1999. Dynamic repositioning of genes in the nucleus of lymphocytes preparing for cell division. *Mol. Cell*. 3:207–217.

Brown, K.E., S.S. Guest, S.T. Smale, K. Hahm, M. Merkenschlager, and A.G. Fisher. 1997. Association of transcriptionally silent genes with Ikaros complexes at centromeric heterochromatin. *Cell*. 91:845–854.

Bultmann, S., R. Morbitzer, C.S. Schmidt, K. Thanisch, F. Spada, J. Elsaesser, T. Lahaye, and H. Leonhardt. 2012. Targeted transcriptional activation of silent oct4 pluripotency gene by combining designer TALEs and inhibition of epigenetic modifiers. *Nucleic acids research*. 40:5368–5377. doi:10.1093/nar/gks199.

Bulut-Karslioglu, A., V. Perrera, M. Scaranaro, I.A. de la Rosa-Velazquez, S. van de Nobelen, N. Shukeir, J. Popow, B. Gerle, S. Opravil, M. Pagani, S. Meidhof, T. Brabletz, T. Manke, M. Lachner, and T. Jenuwein. 2012. A transcription factor-based mechanism for mouse heterochromatin formation. *Nat. Struct. Mol. Biol.* 19:1023–1030. doi:10.1038/nsmb.2382.

Buttner, D., D. Gurlebeck, L.D. Noel, and U. Bonas. 2004. HpaB from Xanthomonas campestris pv. vesicatoria acts as an exit control protein in type III-dependent protein secretion. *Molecular Microbiology*. 54:755–768. doi:10.1111/j.1365-2958.2004.04302.x.

Capell, B.C., and F.S. Collins. 2006. Human laminopathies: nuclei gone genetically awry. *Nature Reviews Genetics*. 7:940–952. doi:10.1038/nrg1906.

Caravaca, J.M., G. Donahue, J.S. Becker, X. He, C. Vinson, and K.S. Zaret. 2013. Bookmarking by specific and nonspecific binding of FoxA1 pioneer factor to mitotic chromosomes. *Genes Dev.* 27:251–260. doi:10.1101/gad.206458.112.

Carpenter, A.E., S. Memedula, M.J. Plutz, and A.S. Belmont. 2005. Common effects of acidic activators on large-scale chromatin structure and transcription. *Mol Cell Biol*. 25:958–968. doi:10.1128/MCB.25.3.958-968.2005.

Carter-Dawson, L.D., and M.M. LaVail. 1979. Rods and cones in the mouse retina. I. Structural analysis using light and electron microscopy. *J Comp Neurol*. 188:245–262. doi:10.1002/cne.901880204.

Cavalli, G., and T. Misteli. 2013. Functional implications of genome topology. *Nat. Struct. Mol. Biol.* 20:290–299. doi:10.1038/nsmb.2474.

Cermak, T., E.L. Doyle, M. Christian, L. Wang, Y. Zhang, C. Schmidt, J.A. Baller, N.V. Somia, A.J. Bogdanove, and D.F. Voytas. 2011. Efficient design and assembly of custom TALEN and other TAL effector-based constructs for DNA targeting. *Nucleic acids research*. 39:7879–7879. doi:10.1093/nar/gkr739.

Chan, S.R.W.L., and E.H. Blackburn. 2004. Telomeres and telomerase. *Philos Trans R Soc Lond B Biol Sci*. 359:109–121. doi:10.1098/rstb.2003.1370.

Chen, B., L.A. Gilbert, B.A. Cimini, J. Schnitzbauer, W. Zhang, G.-W. Li, J. Park, E.H. Blackburn, J.S. Weissman, L.S. Qi, and B. Huang. 2013. Dynamic Imaging of Genomic Loci in Living Human Cells by an Optimized CRISPR/Cas System. *Cell*. 155:1479–1491. doi:10.1016/j.cell.2013.12.001.

Chen, T.L., and L. Manuelidis. 1989. SINEs and LINEs cluster in distinct DNA fragments of Giemsa band size. *Chromosoma*. 98:309–316.

Cheng, A.W., H. Wang, H. Yang, L. Shi, Y. Katz, T.W. Theunissen, S. Rangarajan, C.S. Shivalila, D.B. Dadon, and R. Jaenisch. 2013. Multiplexed activation of endogenous genes by CRISPR-on, an RNA-guided transcriptional activator system. *Cell Res.* 23:1163–1171. doi:doi:10.1038/cr.2013.122.

Chess, A., I. Simon, H. Cedar, and R. Axel. 1994. Allelic inactivation regulates olfactory receptor gene expression. *Cell*. 78:823–834.

Chuang, C.-H., A.E. Carpenter, B. Fuchsova, T. Johnson, P. de Lanerolle, and A.S. Belmont. 2006. Long-Range Directional Movement of an Interphase Chromosome Site. *Current Biology*. 16:825–831. doi:10.1016/j.cub.2006.03.059.

Chubb, J.R., S. Boyle, P. Perry, and W.A. Bickmore. 2002. Chromatin Motion Is Constrained by Association with Nuclear Compartments in Human Cells. *Current Biology*. 12:439–445. doi:10.1016/S0960-9822(02)00695-4.

Clowney, E.J., M.A. LeGros, C.P. Mosley, F.G. Clowney, E.C. Markenskoff-Papadimitriou, M. Myllys, G. Barnea, C.A. Larabell, and S. Lomvardas. 2012. Nuclear Aggregation of Olfactory Receptor Genes Governs Their Monogenic Expression. *Cell*. 151:724–737. doi:10.1016/j.cell.2012.09.043.

Cohen, T.V., K.D. Klarmann, K. Sakchaisri, J.P. Cooper, D. Kuhns, M. Anver, P.F. Johnson, S.C. Williams, J.R. Keller, and C.L. Stewart. 2008. The lamin B receptor under transcriptional control of C/EBP is required for morphological but not functional maturation of neutrophils. *Human Molecular Genetics*. 17:2921–2933. doi:10.1093/hmg/ddn191.

Cong, L., R. Zhou, Y.-C. Kuo, M. Cunniff, and F. Zhang. 2012. Comprehensive interrogation of natural TALE DNA-binding modules and transcriptional repressor domains. *Nat Commun*. 3:968–. doi:10.1038/ncomms1962.

Cradick, T.J., E.J. Fine, C.J. Antico, and G. Bao. 2013. CRISPR/Cas9 systems targeting beta-globin and CCR5 genes have substantial off-target activity. *Nucleic acids research*. 41:9584–9592. doi:10.1093/nar/gkt714.

Cremer, M., J. von Hase, T. Volm, A. Brero, G. Kreth, J. Walter, C. Fischer, I. Solovei, C. Cremer, and T. Cremer. 2001. Non-random radial higher-order chromatin arrangements in nuclei of diploid human cells. *Chromosome Res.* 9:541–567.

Cremer, M., K. Kupper, B. Wagler, L. Wizelman, J. von Hase, Y. Weiland, L. Kreja, J. Diebold, M.R. Speicher, and T. Cremer. 2003. Inheritance of gene density-related higher order chromatin arrangements in normal and tumor cell nuclei. *J. Cell Biol.* 162:809–820.

Cremer, T., and C. Cremer. 2001. Chromosome territories, nuclear architecture and gene regulation in mammalian cells. *Nature Reviews Genetics*. 2:292–301.

Cremer, T., and M. Cremer. 2010. Chromosome Territories. *Cold Spring Harb Perspect Biol*. 2:a003889–a003889. doi:10.1101/cshperspect.a003889.

Cremer, T., C. Cremer, H. Baumann, E.K. Luedtke, K. Sperling, V. Teuber, and C. Zorn. 1982. Rabl's model of the interphase chromosome arrangement tested in Chinese hamster cells by premature chromosome condensation and laser-UV-microbeam

experiments. *Hum Genet*. 60:46–56.

Croft, J.A. 1999. Differences in the Localization and Morphology of Chromosomes in the Human Nucleus. *J. Cell Biol.* 145:1119–1131. doi:10.1083/jcb.145.6.1119.

de Lange, O., A. Binder, and T. Lahaye. 2014. From dead leaf, to new life: TAL effectors as tools for synthetic biology. *Plant J*. 78:n/a–n/a. doi:10.1111/tpj.12431.

Deaton, A.M., and A. Bird. 2011. CpG islands and the regulation of transcription. *Genes Dev.* 25:1010–1022. doi:10.1101/gad.2037511.

Dechat, T., K. Gesson, and R. Foisner. 2010. Lamina-independent lamins in the nuclear interior serve important functions. *Cold Spring Harbor symposia on quantitative biology*. 75:533–543. doi:10.1101/sqb.2010.75.018.

Dekker, J., K. Rippe, M. Dekker, and N. Kleckner. 2002. Capturing chromosome conformation. *Science*. 295:1306–1311. doi:10.1126/science.1067799.

Dekker, J., M.A. Marti-Renom, and L.A. Mirny. 2013. Exploring the three-dimensional organization of genomes: interpreting chromatin interaction data. *Nature Reviews Genetics*. 14:390–403. doi:10.1038/nrg3454.

Demmerle, J., A.J. Koch, and J.M. Holaska. 2012. The nuclear envelope protein emerin binds directly to histone deacetylase 3 (HDAC3) and activates HDAC3 activity. *J. Biol. Chem.* 287:22080–22088. doi:10.1074/jbc.M111.325308.

Deng, D., C. Yan, X. Pan, M. Mahfouz, J. Wang, J.-K. Zhu, Y. Shi, and N. Yan. 2012a. Structural basis for sequence-specific recognition of DNA by TAL effectors. *Science*. 335:720–723. doi:10.1126/science.1215670.

Deng, D., P. Yin, C. Yan, X. Pan, X. Gong, S. Qi, T. Xie, M. Mahfouz, J.-K. Zhu, N. Yan, and Y. Shi. 2012b. Recognition of methylated DNA by TAL effectors. *Cell Res.* 22:1502–1504. doi:10.1038/cr.2012.127.

Dialynas, G., S. Speese, V. Budnik, P.K. Geyer, and L.L. Wallrath. 2010. The role of Drosophila Lamin C in muscle function and gene expression. *Development*. 137:3067–3077. doi:10.1242/dev.048231.

Dillon, N., and R. Festenstein. 2002. Unravelling heterochromatin: competition between positive and negative factors regulates accessibility. *Trends Genet.* 18:252–258.

Dimitrova, D.S., and R. Berezney. 2002. The spatio-temporal organization of DNA replication sites is identical in primary, immortalized and transformed mammalian cells. *Journal of cell science*. 115:4037–4051.

Dion, V., and S.M. Gasser. 2014. Chromatin movement in the maintenance of genome stability. *Cell*. 152:1355–1364. doi:10.1016/j.cell.2013.02.010.

Dixon, J.R., S. Selvaraj, F. Yue, A. Kim, Y. Li, Y. Shen, M. Hu, J.S. Liu, and B. Ren. 2012. Topological domains in mammalian genomes identified by analysis of chromatin interactions. *Nature*. 485:376–380. doi:10.1038/nature11082.

Dundr, M., J.K. Ospina, M.-H. Sung, S. John, M. Upender, T. Ried, G.L. Hager, and A.G.

Matera. 2007. Actin-dependent intranuclear repositioning of an active gene locus in vivo. *J. Cell Biol.* 179:1095–1103. doi:10.1083/jcb.200710058.

Eberhart, A., Y. Feodorova, C. Song, G. Wanner, E. Kiseleva, T. Furukawa, H. Kimura, G. Schotta, H. Leonhardt, B. Joffe, and I. Solovei. 2013. Epigenetics of eu- and heterochromatin in inverted and conventional nuclei from mouse retina. *Chromosome Res.* 21:535–554. doi:10.1007/s10577-013-9375-7.

Ellenberg, J., E.D. Siggia, J.E. Moreira, C.L. Smith, J.F. Presley, H.J. Worman, and J. Lippincott-Schwartz. 1997. Nuclear membrane dynamics and reassembly in living cells: targeting of an inner nuclear membrane protein in interphase and mitosis. *J. Cell Biol.* 138:1193–1206.

Ernst, J., and M. Kellis. 2010. Discovery and characterization of chromatin states for systematic annotation of the human genome. *Nat. Biotechnol.* 28:817–825. doi:10.1038/nbt.1662.

Esvelt, K.M., P. Mali, J.L. Braff, M. Moosburner, S.J. Yaung, and G.M. Church. 2013. Orthogonal Cas9 proteins for RNA-guided gene regulation and editing. *Nat. Methods*. 10:1116–1121. doi:doi:10.1038/nmeth.2681.

Fadloun, A., A. Eid, and M.-E. Torres-Padilla. 2013. Mechanisms and dynamics of heterochromatin formation during mammalian development: closed paths and open questions. *Curr. Top. Dev. Biol.* 104:1–45. doi:10.1016/B978-0-12-416027-9.00001-2.

Fanucchi, S., Y. Shibayama, S. Burd, M.S. Weinberg, and M.M. Mhlanga. 2013. Chromosomal Contact Permits Transcription between Coregulated Genes. *Cell*. 155:606–620. doi:10.1016/j.cell.2013.09.051.

Finlan, L.E., D. Sproul, I. Thomson, S. Boyle, E. Kerr, P. Perry, B. Ylstra, J.R. Chubb, and W.A. Bickmore. 2008. Recruitment to the Nuclear Periphery Can Alter Expression of Genes in Human Cells. *PLoS Genet.* 4:e1000039. doi:10.1371/journal.pgen.1000039.

Fisher, D.Z., N. Chaudhary, and G. Blobel. 1986. cDNA sequencing of nuclear lamins A and C reveals primary and secondary structural homology to intermediate filament proteins. *Proceedings of the National Academy of Sciences of the United States of America*. 83:6450–6454.

Flemming, W. 1882. Zellsubstanz, Kern und Zelltheilung.

Follmer, N.E., A.H. Wani, and N.J. Francis. 2012. A polycomb group protein is retained at specific sites on chromatin in mitosis. *PLoS Genet.* 8:e1003135.

Fu, Y., J.A. Foden, C. Khayter, M.L. Maeder, D. Reyon, J.K. Joung, and J.D. Sander. 2013. High-frequency off-target mutagenesis induced by CRISPR-Cas nucleases in human cells. *Nat. Biotechnol.* 31:822–826. doi:doi:10.1038/nbt.2623.

Fuks, F., W.A. Burgers, A. Brehm, L. Hughes-Davies, and T. Kouzarides. 2000. DNA methyltransferase Dnmt1 associates with histone deacetylase activity. *Nat. Genet.* 24:88–91. doi:10.1038/71750.

Gabsalilow, L., B. Schierling, P. Friedhoff, A. Pingoud, and W. Wende. 2013. Site- and strand-specific nicking of DNA by fusion proteins derived from MutH and I-SceI or TALE

repeats. *Nucleic acids research*. 41:e83. doi:10.1093/nar/gkt080.

Gaines, P., C.W. Tien, A.L. Olins, D.E. Olins, L.D. Shultz, L. Carney, and N. Berliner. 2008. Mouse neutrophils lacking lamin B-receptor expression exhibit aberrant development and lack critical functional responses. *Exp Hematol*. 36:965–976. doi:10.1016/j.exphem.2008.04.006.

Gao, H., D.A. Wright, T. Li, Y. Wang, K. Horken, D.P. Weeks, B. Yang, and M.H. Spalding. 2014. TALE activation of endogenous genes in Chlamydomonas reinhardtii. *Algal Research*. 5:52–60. doi:10.1016/j.algal.2014.05.003.

Gao, H., X. Wu, J. Chai, and Z. Han. 2012. Crystal structure of a TALE protein reveals an extended N-terminal DNA binding region. *Cell Res.* 22:1716–1720. doi:10.1038/cr.2012.156.

Gao, X., J. Yang, J.C.H. Tsang, J. Ooi, D. Wu, and P. Liu. 2013. Reprogramming to Pluripotency Using Designer TALE Transcription Factors Targeting Enhancers. *Stem Cell Reports*. 1:183–197. doi:10.1016/j.stemcr.2013.06.002.

Garg, A., J.J. Lohmueller, P.A. Silver, and T.Z. Armel. 2012. Engineering synthetic TAL effectors with orthogonal target sites. *Nucleic acids research*. 40:7584–7595. doi:10.1093/nar/gks404.

Gartenberg, M.R., F.R. Neumann, T. Laroche, M. Blaszczyk, and S.M. Gasser. 2004. Sir-mediated repression can occur independently of chromosomal and subnuclear contexts. *Cell*. 119:955–967. doi:10.1016/j.cell.2004.11.008.

Geissler, R., H. Scholze, S. Hahn, J. Streubel, U. Bonas, S.-E. Behrens, and J. Boch. 2011. Transcriptional activators of human genes with programmable DNA-specificity. *PLoS ONE*. 6:e19509.

Gersbach, C.A., and P. Perez-Pinera. 2014. Activating human genes with zinc finger proteins, transcription activator-like effectors and CRISPR/Cas9 for gene therapy and regenerative medicine. *Expert Opin Ther Targets*. 1–5. doi:10.1517/14728222.2014.913572.

Gesson, K., S. Vidak, and R. Foisner. 2014. Lamina-associated polypeptide (LAP)2alpha and nucleoplasmic lamins in adult stem cell regulation and disease. *Semin Cell Dev Biol*. 29:116–124. doi:10.1016/j.semcdb.2013.12.009.

Gibcus, J.H., and J. Dekker. 2013. The hierarchy of the 3D genome. *Mol. Cell*. 49:773–782. doi:10.1016/j.molcel.2013.02.011.

Gilbert, L.A., M.H. Larson, L. Morsut, Z. Liu, G.A. Brar, S.E. Torres, N. Stern-Ginossar, O. Brandman, E.H. Whitehead, J.A. Doudna, W.A. Lim, J.S. Weissman, and L.S. Qi. 2013. CRISPR-Mediated Modular RNA-Guided Regulation of Transcription in Eukaryotes. *Cell*. 154:442–451. doi:10.1016/j.cell.2013.06.044.

Goelz, S.E., B. Vogelstein, S.R. Hamilton, and A.P. Feinberg. 1985. Hypomethylation of DNA from benign and malignant human colon neoplasms. *Science*. 228:187–190.

Goetze, S., J. Mateos-Langerak, H.J. Gierman, W. de Leeuw, O. Giromus, M.H.G. Indemans, J. Koster, V. Ondrej, R. Versteeg, and R. van Driel. 2007. The three-

dimensional structure of human interphase chromosomes is related to the transcriptome map. *Mol Cell Biol*. 27:4475–4487. doi:10.1128/MCB.00208-07.

Grewal, S.I.S., and S. Jia. 2007. Heterochromatin revisited. *Nature Reviews Genetics*. 8:35–46. doi:10.1038/nrg2008.

Guarda, A., F. Bolognese, I.M. Bonapace, and G. Badaracco. 2009. Interaction between the inner nuclear membrane lamin B receptor and the heterochromatic methyl binding protein, MeCP2. *Exp Cell Res*. 315:1895–1903. doi:10.1016/j.yexcr.2009.01.019.

Guelen, L., L. Pagie, E. Brasset, W. Meuleman, M.B. Faza, W. Talhout, B.H. Eussen, A. de Klein, L. Wessels, W. de Laat, and B. van Steensel. 2008. Domain organization of human chromosomes revealed by mapping of nuclear lamina interactions. *Nature*. 453:948–951. doi:10.1038/nature06947.

Guenatri, M., D. Bailly, C. Maison, and G. Almouzni. 2004. Mouse centric and pericentric satellite repeats form distinct functional heterochromatin. *J. Cell Biol.* 166:493–505. doi:10.1083/jcb.200403109.

Hahn, M., S. Dambacher, S. Dulev, A.Y. Kuznetsova, S. Eck, S. Worz, D. Sadic, M. Schulte, J.-P. Mallm, A. Maiser, P. Debs, H. von Melchner, H. Leonhardt, L. Schermelleh, K. Rohr, K. Rippe, Z. Storchova, and G. Schotta. 2013. Suv4-20h2 mediates chromatin compaction and is important for cohesin recruitment to heterochromatin. *Genes Dev.* 27:859–872. doi:10.1101/gad.210377.112.

Hakim, O., and T. Misteli. 2012. SnapShot: Chromosome Conformation Capture. *Cell*. 148:1068–1068.e2.

Harewood, L., F. Schutz, S. Boyle, P. Perry, M. Delorenzi, W.A. Bickmore, and A. Reymond. 2010. The effect of translocation-induced nuclear reorganization on gene expression. *Genome Research*. 20:554–564. doi:10.1101/gr.103622.109.

Harr, J.C., T.R. Luperchio, X. Wong, E. Cohen, S.J. Wheelan, and K.L. Reddy. 2015. Directed targeting of chromatin to the nuclear lamina is mediated by chromatin state and A-type lamins. *J. Cell Biol.* 208:33–52. doi:10.1083/jcb.201405110.

Hatton, K.S., V. Dhar, E.H. Brown, M.A. Iqbal, S. Stuart, V.T. Didamo, and C.L. Schildkraut. 1988. Replication program of active and inactive multigene families in mammalian cells. *Mol Cell Biol*. 8:2149–2158.

He, Y.-F., B.-Z. Li, Z. Li, P. Liu, Y. Wang, Q. Tang, J. Ding, Y. Jia, Z. Chen, L. Li, Y. Sun, X. Li, Q. Dai, C.-X. Song, K. Zhang, C. He, and G.-L. Xu. 2011. Tet-mediated formation of 5-carboxylcytosine and its excision by TDG in mammalian DNA. *Science*. 333:1303–1307. doi:10.1126/science.1210944.

Heitz, E. 1928. Das Heterochromatin der Moose. 69:762–818–.

Helmlinger, D., S. Hardy, G. Abou-Sleymane, A. Eberlin, A.B. Bowman, A. Gansmuller, S. Picaud, H.Y. Zoghbi, Y. Trottier, L. Tora, and D. Devys. 2006. Glutamine-expanded ataxin-7 alters TFTC/STAGA recruitment and chromatin structure leading to photoreceptor dysfunction. *PLoS Biol*. 4:e67. doi:10.1371/journal.pbio.0040067.

Hemmerich, P., L. Schmiedeberg, and S. Diekmann. 2011. Dynamic as well as stable

protein interactions contribute to genome function and maintenance. *Chromosome Res.* 19:131–151. doi:10.1007/s10577-010-9161-8.

Herce, H.D., W. Deng, J. Helma, H. Leonhardt, and M.C. Cardoso. 2013. Visualization and targeted disruption of protein interactions in living cells. *Nat Commun*. 4:2660. doi:10.1038/ncomms3660.

Hewitt, S.L., F.A. High, S.L. Reiner, A.G. Fisher, and M. Merkenschlager. 2004. Nuclear repositioning marks the selective exclusion of lineage-inappropriate transcription factor loci during T helper cell differentiation. *Eur J Immunol*. 34:3604–3613. doi:10.1002/eji.200425469.

Hirai, H., T. Tani, and N. Kikyo. 2010. Structure and functions of powerful transactivators: VP16, MyoD and FoxA. *Int J Dev Biol*. 54:1589–1596. doi:10.1387/ijdb.103194hh.

Hirano, Y., K. Hizume, H. Kimura, K. Takeyasu, T. Haraguchi, and Y. Hiraoka. 2012. Lamin B receptor recognizes specific modifications of histone H4 in heterochromatin formation. *J. Biol. Chem.* 287:42654–42663. doi:10.1074/jbc.M112.397950.

Hiratani, I., T. Ryba, M. Itoh, T. Yokochi, M. Schwaiger, C.-W. Chang, Y. Lyou, T.M. Townes, D. Schübeler, and D.M. Gilbert. 2008. Global Reorganization of Replication Domains During Embryonic Stem Cell Differentiation. *PLoS Biol*. 6:e245. doi:10.1371/journal.pbio.0060245.

Hoffmann, K., C.K. Dreger, A.L. Olins, D.E. Olins, L.D. Shultz, B. Lucke, H. Karl, R. Kaps, D. Müller, A. Vayá, J. Aznar, R.E. Ware, N.S. Cruz, T.H. Lindner, H. Herrmann, A. Reis, and K. Sperling. 2002. Mutations in the gene encoding the lamin B receptor produce an altered nuclear morphology in granulocytes (Pelger-Huet anomaly). *Nat. Genet.* 31:410–414. doi:10.1038/ng925.

Hoffmann, K., K. Sperling, A.L. Olins, and D.E. Olins. 2007. The granulocyte nucleus and lamin B receptor: avoiding the ovoid. *Chromosoma*. 116:227–235. doi:10.1007/s00412-007-0094-8.

Holaska, J.M., and K.L. Wilson. 2007. An Emerin "Proteome": Purification of Distinct Emerin-Containing Complexes from HeLa Cells Suggests Molecular Basis for Diverse Roles Including Gene Regulation, mRNA Splicing, Signaling, Mechanosensing, and Nuclear Architecture †. *Biochemistry*. 46:8897–8908. doi:10.1021/bi602636m.

Holwerda, S., and W. de Laat. 2012. Chromatin loops, gene positioning, and gene expression. *Frontiers in Genetics*. 3:217. doi:10.3389/fgene.2012.00217.

Hou, C., L. Li, Z.S. Qin, and V.G. Corces. 2012. Gene density, transcription, and insulators contribute to the partition of the Drosophila genome into physical domains. *Mol. Cell*. 48:471–484. doi:10.1016/j.molcel.2012.08.031.

Hsu, P.D., D.A. Scott, J.A. Weinstein, F.A. Ran, S. Konermann, V. Agarwala, Y. Li, E.J. Fine, X. Wu, O. Shalem, T.J. Cradick, L.A. Marraffini, G. Bao, and F. Zhang. 2013. DNA targeting specificity of RNA-guided Cas9 nucleases. *Nat. Biotechnol.* 31:827–832. doi:10.1038/nbt.2647.

Hu, Y., M. Plutz, and A.S. Belmont. 2010. Hsp70 gene association with nuclear speckles is Hsp70 promoter specific. *J. Cell Biol.* 191:711–719. doi:10.1083/jcb.201004041.

Hübner, M.R., M.A. Eckersley-Maslin, and D.L. Spector. 2013. Chromatin organization and transcriptional regulation. *Curr. Opin. Genet. Dev.* 23:89–95. doi:10.1016/j.gde.2012.11.006.

Imakaev, M., G. Fudenberg, R.P. McCord, N. Naumova, A. Goloborodko, B.R. Lajoie, J. Dekker, and L.A. Mirny. 2012. Iterative correction of Hi-C data reveals hallmarks of chromosome organization. *Nat. Methods*. 9:999–1003. doi:10.1038/nmeth.2148.

Ito, S., L. Shen, Q. Dai, S.C. Wu, L.B. Collins, J.A. Swenberg, C. He, and Y. Zhang. 2011. Tet proteins can convert 5-methylcytosine to 5-formylcytosine and 5-carboxylcytosine. *Science*. 333:1300–1303. doi:10.1126/science.1210597.

Jachowicz, J.W., A. Santenard, A. Bender, J. Muller, and M.-E. Torres-Padilla. 2013. Heterochromatin establishment at pericentromeres depends on nuclear position. *Genes Dev.* 27:2427–2432. doi:10.1101/gad.224550.113.

Jegou, T., I. Chung, G. Heuvelman, M. Wachsmuth, S.M. Gorisch, K.M. Greulich-Bode, P. Boukamp, P. Lichter, and K. Rippe. 2009. Dynamics of telomeres and promyelocytic leukemia nuclear bodies in a telomerase-negative human cell line. *Mol Biol Cell*. 20:2070–2082. doi:10.1091/mbc.E08-02-0108.

Jinek, M., F. Jiang, D.W. Taylor, S.H. Sternberg, E. Kaya, E. Ma, C. Anders, M. Hauer, K. Zhou, S. Lin, M. Kaplan, A.T. Iavarone, E. Charpentier, E. Nogales, and J.A. Doudna. 2014. Structures of Cas9 endonucleases reveal RNA-mediated conformational activation. *Science*. 343:1247997–1247997. doi:10.1126/science.1247997.

Jinek, M., K. Chylinski, I. Fonfara, M. Hauer, J.A. Doudna, and E. Charpentier. 2012. A Programmable Dual-RNA-Guided DNA Endonuclease in Adaptive Bacterial Immunity. *Science*. 337:816–821. doi:10.1126/science.1225829.

Joffe, B., H. Leonhardt, and I. Solovei. 2010. Differentiation and large scale spatial organization of the genome. *Curr. Opin. Genet. Dev.* 20:562–569. doi:10.1016/j.gde.2010.05.009.

Joffe, B.I., I.V. Solovei, and H.C. Macgregor. 1998. Ordered arrangement and rearrangement of chromosomes during spermatogenesis in two species of planarians (Plathelminthes). *Chromosoma*. 107:173–183.

Jones, P.A., and S.B. Baylin. 2002. The fundamental role of epigenetic events in cancer. *Nature Reviews Genetics*. 3:415–428.

Jones, P.L., G.J. Veenstra, P.A. Wade, D. Vermaak, S.U. Kass, N. Landsberger, J. Strouboulis, and A.P. Wolffe. 1998. Methylated DNA and MeCP2 recruit histone deacetylase to repress transcription. *Nat. Genet.* 19:187–191. doi:10.1038/561.

Joseph, A., A.R. Mitchell, and O.J. Miller. 1989. The organization of the mouse satellite DNA at centromeres. *Exp Cell Res*. 183:494–500.

Jost, K.L., S. Haase, D. Smeets, N. Schrode, J.M. Schmiedel, B. Bertulat, H. Herzel, M. Cremer, and M.C. Cardoso. 2011. 3D-Image analysis platform monitoring relocation of pluripotency genes during reprogramming. *Nucleic acids research*. 39:e113. doi:10.1093/nar/gkr486.

Joung, J.K., and J.D. Sander. 2013. TALENs: a widely applicable technology for targeted genome editing. *Nat Rev Mol Cell Biol*. 14:49–55. doi:10.1038/nrm3486.

Jung, H.-J., C. Coffinier, Y. Choe, A.P. Beigneux, B.S.J. Davies, S.H. Yang, R.H.2. Barnes, J. Hong, T. Sun, S.J. Pleasure, S.G. Young, and L.G. Fong. 2012. Regulation of prelamin A but not lamin C by miR-9, a brain-specific microRNA. *Proceedings of the National Academy of Sciences of the United States of America*. 109:E423–31. doi:10.1073/pnas.1111780109.

Kabadi, A.M., and C.A. Gersbach. 2014. Engineering Synthetic TALE and CRISPR/Cas9 Transcription Factors for Regulating Gene Expression. *Methods*. doi:10.1016/j.ymeth.2014.06.014.

Kadauke, S., and G.A. Blobel. 2013. Mitotic bookmarking by transcription factors. *Epigenetics Chromatin*. 6:6. doi:10.1186/1756-8935-6-6.

Kadauke, S., M.I. Udugama, J.M. Pawlicki, J.C. Achtman, D.P. Jain, Y. Cheng, R.C. Hardison, and G.A. Blobel. 2012. Tissue-specific mitotic bookmarking by hematopoietic transcription factor GATA1. *Cell*. 150:725–737. doi:10.1016/j.cell.2012.06.038.

Kalhor, R., H. Tjong, N. Jayathilaka, F. Alber, and L. Chen. 2011. Genome architectures revealed by tethered chromosome conformation capture and population-based modeling. *Nat. Biotechnol.* 30:90–98. doi:10.1038/nbt.2057.

Kanda, T., K.F. Sullivan, and G.M. Wahl. 1998. Histone-GFP fusion protein enables sensitive analysis of chromosome dynamics in living mammalian cells. *Curr. Biol.* 8:377–385.

Kaufmann, U., J. Kirsch, A. Irintchev, A. Wernig, and A. Starzinski-Powitz. 1999. The M-cadherin catenin complex interacts with microtubules in skeletal muscle cells: implications for the fusion of myoblasts. *Journal of cell science*. 112 (Pt 1):55–68.

Kay, S., S. Hahn, E. Marois, G. Hause, and U. Bonas. 2007. A bacterial effector acts as a plant transcription factor and induces a cell size regulator. *Science*. 318:648–651. doi:10.1126/science.1144956.

Kearns, N.A., R.M.J. Genga, M.S. Enuameh, M. Garber, S.A. Wolfe, and R. Maehr. 2014. Cas9 effector-mediated regulation of transcription and differentiation in human pluripotent stem cells. *Development*. 141:219–223. doi:10.1242/dev.103341.

Kim, J.M., Y. Hong, and S. Kim. 2000. Artificial recruitment of Sp1 or TBP can replace the role of IE1 in the synergistic transactivation by IE1 and IE2. *Biochemical and Biophysical Research Communications*. 269:302–308.

Kim, S.H., P.G. McQueen, M.K. Lichtman, E.M. Shevach, L.A. Parada, and T. Misteli. 2004. Spatial genome organization during T-cell differentiation. *Cytogenet Genome Res*. 105:292–301.

Kim, T.H., L.O. Barrera, M. Zheng, C. Qu, M.A. Singer, T.A. Richmond, Y. Wu, R.D. Green, and B. Ren. 2005. A high-resolution map of active promoters in the human genome. *Nature*. 436:876–880. doi:10.1038/nature03877.

Kind, J., and B. van Steensel. 2014. Stochastic genome-nuclear lamina interactions: Modulating roles of Lamin A and BAF. *Nucleus*. 5:124–130. doi:10.4161/nucl.28825.

Kind, J., L. Pagie, H. Ortabozkoyun, S. Boyle, S.S. de Vries, H. Janssen, M. Amendola, L.D. Nolen, W.A. Bickmore, and B. van Steensel. 2013. Single-cell dynamics of genome-nuclear lamina interactions. *Cell*. 153:178–192. doi:10.1016/j.cell.2013.02.028.

Kipling, D., H.E. Ackford, B.A. Taylor, and H.J. Cooke. 1991. Mouse minor satellite DNA genetically maps to the centromere and is physically linked to the proximal telomere. *Genomics*. 11:235–241.

Kizilyaprak, C., D. Spehner, D. Devys, and P. Schultz. 2010. In vivo chromatin organization of mouse rod photoreceptors correlates with histone modifications. *PLoS ONE*. 5:e11039. doi:10.1371/journal.pone.0011039.

Konermann, S., M.D. Brigham, A. Trevino, P.D. Hsu, M. Heidenreich, Le Cong, R.J. Platt, D.A. Scott, G.M. Church, and F. Zhang. 2013. Optical control of mammalian endogenous transcription and epigenetic states. *Nature*. doi:10.1038/nature12466.

Korenberg, J.R., and M.C. Rykowski. 1988. Human genome organization: Alu, lines, and the molecular structure of metaphase chromosome bands. *Cell*. 53:391–400.

Korfali, N., G.S. Wilkie, S.K. Swanson, V. Srsen, D.G. Batrakou, E.A.L. Fairley, P. Malik, N. Zuleger, A. Goncharevich, J. de Las Heras, D.A. Kelly, A.R.W. Kerr, L. Florens, and E.C. Schirmer. 2010. The leukocyte nuclear envelope proteome varies with cell activation and contains novel transmembrane proteins that affect genome architecture. *Mol Cell Proteomics*. 9:2571–2585. doi:10.1074/mcp.M110.002915.

Korfali, N., G.S. Wilkie, S.K. Swanson, V. Srsen, J. de Las Heras, D.G. Batrakou, P. Malik, N. Zuleger, A.R.W. Kerr, L. Florens, and E.C. Schirmer. 2012. The nuclear envelope proteome differs notably between tissues. *Nucleus*. 3:552–564. doi:10.4161/nucl.22257.

Kosak, S.T., J.A. Skok, K.L. Medina, R. Riblet, M.M. Le Beau, A.G. Fisher, and H. Singh. 2002. Subnuclear compartmentalization of immunoglobulin loci during lymphocyte development. *Science*. 296:158–162.

Kouzarides, T. 2007. Chromatin modifications and their function. *Cell*. 128:693–705. doi:10.1016/j.cell.2007.02.005.

Kriaucionis, S., and N. Heintz. 2009. The nuclear DNA base 5-hydroxymethylcytosine is present in Purkinje neurons and the brain. *Science*. 324:929–930. doi:10.1126/science.1169786.

Krijger, P.H.L., and W. de Laat. 2013. Identical cells with different 3D genomes; cause and consequences? *Curr. Opin. Genet. Dev.* 23:191–196. doi:10.1016/j.gde.2012.12.010.

Kubben, N., M. Adriaens, W. Meuleman, J.W. Voncken, B. van Steensel, and T. Misteli. 2012. Mapping of lamin A- and progerin-interacting genome regions. *Chromosoma*. 121:447–464. doi:10.1007/s00412-012-0376-7.

Kumaran, R.I., and D.L. Spector. 2008. A genetic locus targeted to the nuclear periphery in living cells maintains its transcriptional competence. *J. Cell Biol.* 180:51–65. doi:10.1083/jcb.200404107.

Kupper, K., A. Kolbl, D. Biener, S. Dittrich, J. von Hase, T. Thormeyer, H. Fiegler, N.P.

Carter, M.R. Speicher, T. Cremer, and M. Cremer. 2007. Radial chromatin positioning is shaped by local gene density, not by gene expression. *Chromosoma*. 116:285–306. doi:10.1007/s00412-007-0098-4.

Kuscu, C., S. Arslan, R. Singh, J. Thorpe, and M. Adli. 2014. Genome-wide analysis reveals characteristics of off-target sites bound by the Cas9 endonuclease. *Nat. Biotechnol.* 32:677–683. doi:10.1038/nbt.2916.

Lachner, M., D. O'Carroll, S. Rea, K. Mechtler, and T. Jenuwein. 2001. Methylation of histone H3 lysine 9 creates a binding site for HP1 proteins. *Nature*. 410:116–120.

Lange, O. de, C. Wolf, J. Dietze, J. Elsaesser, R. Morbitzer, and T. Lahaye. 2014. Programmable DNA-binding proteins from Burkholderia provide a fresh perspective on the TALE-like repeat domain. *Nucleic acids research*. 42:7436–7449. doi:10.1093/nar/gku329.

Lehner, C.F., R. Stick, H.M. Eppenberger, and E.A. Nigg. 1987. Differential expression of nuclear lamin proteins during chicken development. *J. Cell Biol.* 105:577–587.

Lehnertz, B., Y. Ueda, A.A.H.A. Derijck, U. Braunschweig, L. Perez-Burgos, S. Kubicek, T. Chen, E. Li, T. Jenuwein, and A.H.F.M. Peters. 2003. Suv39h-mediated histone H3 lysine 9 methylation directs DNA methylation to major satellite repeats at pericentric heterochromatin. *Curr. Biol.* 13:1192–1200.

Leonhardt, H., H.P. Rahn, P. Weinzierl, A. Sporbert, T. Cremer, D. Zink, and M.C. Cardoso. 2000. Dynamics of DNA replication factories in living cells. *J. Cell Biol.* 149:271–280.

Li, E., T.H. Bestor, and R. Jaenisch. 1992. Targeted mutation of the DNA methyltransferase gene results in embryonic lethality. *Cell*. 69:915–926.

Lichter, P., T. Cremer, J. Borden, L. Manuelidis, and D.C. Ward. 1988. Delineation of individual human chromosomes in metaphase and interphase cells by in situ suppression hybridization using recombinant DNA libraries. *Hum Genet*. 80:224–234.

Lieberman-Aiden, E., N.L. van Berkum, L. Williams, M. Imakaev, T. Ragoczy, A. Telling, I. Amit, B.R. Lajoie, P.J. Sabo, M.O. Dorschner, R. Sandstrom, B. Bernstein, M.A. Bender, M. Groudine, A. Gnirke, J. Stamatoyannopoulos, L.A. Mirny, E.S. Lander, and J. Dekker. 2009. Comprehensive mapping of long-range interactions reveals folding principles of the human genome. *Science*. 326:289–293. doi:10.1126/science.1181369.

Lienert, F., J.J. Lohmueller, A. Garg, and P.A. Silver. 2014. Synthetic biology in mammalian cells: next generation research tools and therapeutics. *Nat Rev Mol Cell Biol*. 15:95–107. doi:10.1038/nrm3738.

Lin, F., and H.J. Worman. 1993. Structural organization of the human gene encoding nuclear lamin A and nuclear lamin C. *J. Biol. Chem.* 268:16321–16326.

Lin, F., C.M. Noyer, Q. Ye, J.C. Courvalin, and H.J. Worman. 1996. Autoantibodies from patients with primary biliary cirrhosis recognize a region within the nucleoplasmic domain of inner nuclear membrane protein LBR. *Hepatology*. 23:57–61. doi:10.1002/hep.510230109.

Lin, F., D.L. Blake, I. Callebaut, I.S. Skerjanc, L. Holmer, M.W. McBurney, M. Paulin-

Levasseur, and H.J. Worman. 2000. MAN1, an inner nuclear membrane protein that shares the LEM domain with lamina-associated polypeptide 2 and emerin. *J. Biol. Chem.* 275:4840–4847.

Lindhout, B.I., P. Fransz, F. Tessadori, T. Meckel, P.J.J. Hooykaas, and B.J. van der Zaal. 2007. Live cell imaging of repetitive DNA sequences via GFP-tagged polydactyl zinc finger proteins. *Nucleic acids research*. 35:e107–e107. doi:10.1093/nar/gkm618.

Luger, K., A.W. Mader, R.K. Richmond, D.F. Sargent, and T.J. Richmond. 1997. Crystal structure of the nucleosome core particle at 2.8 A resolution. *Nature*. 389:251–260. doi:10.1038/38444.

Ma, H., P. Reyes-Gutierrez, and T. Pederson. 2013. Visualization of repetitive DNA sequences in human chromosomes with transcription activator-like effectors. *Proceedings of the National Academy of Sciences of the United States of America*. 110:21048–21053. doi:10.1073/pnas.1319097110.

Ma, Y., S. Cai, Q. Lv, Q. Jiang, Q. Zhang, Sodmergen, Z. Zhai, and C. Zhang. 2007. Lamin B receptor plays a role in stimulating nuclear envelope production and targeting membrane vesicles to chromatin during nuclear envelope assembly through direct interaction with importin beta. *Journal of cell science*. 120:520–530. doi:10.1242/jcs.03355.

Macleod, D., J. Charlton, J. Mullins, and A.P. Bird. 1994. Sp1 sites in the mouse aprt gene promoter are required to prevent methylation of the CpG island. *Genes Dev.* 8:2282–2292.

Maeder, M.L., J.F. Angstman, M.E. Richardson, S.J. Linder, V.M. Cascio, S.Q. Tsai, Q.H. Ho, J.D. Sander, D. Reyon, B.E. Bernstein, J.F. Costello, M.F. Wilkinson, and J.K. Joung. 2013a. Targeted DNA demethylation and activation of endogenous genes using programmable TALE-TET1 fusion proteins. *Nat. Biotechnol.* 31:1137–1142. doi:10.1038/nbt.2726.

Maeder, M.L., S.J. Linder, D. Reyon, J.F. Angstman, Y. Fu, J.D. Sander, and J.K. Joung. 2013b. Robust, synergistic regulation of human gene expression using TALE activators. *Nat. Methods*. 10:243–245. doi:10.1038/nmeth.2366.

Maeder, M.L., S.J. Linder, V.M. Cascio, Y. Fu, Q.H. Ho, and J.K. Joung. 2013c. CRISPR RNA-guided activation of endogenous human genes. *Nat. Methods*. 10:977–979. doi:doi:10.1038/nmeth.2598.

Mahfouz, M.M., L. Li, M. Piatek, X. Fang, H. Mansour, D.K. Bangarusamy, and J.-K. Zhu. 2012. Targeted transcriptional repression using a chimeric TALE-SRDX repressor protein. *Plant Mol Biol*. 78:311–321. doi:10.1007/s11103-011-9866-x.

Maison, C., and G. Almouzni. 2004. HP1 and the dynamics of heterochromatin maintenance. *Nat Rev Mol Cell Biol*. 5:296–304.

Mak, A.N.-S., P. Bradley, A.J. Bogdanove, and B.L. Stoddard. 2013. TAL effectors: function, structure, engineering and applications. *Curr Opin Struct Biol*. 23:93–99. doi:10.1016/j.sbi.2012.11.001.

Mak, A.N.-S., P. Bradley, R.A. Cernadas, A.J. Bogdanove, and B.L. Stoddard. 2012. The

crystal structure of TAL effector PthXo1 bound to its DNA target. *Science*. 335:716–719. doi:10.1126/science.1216211.

Makatsori, D., N. Kourmouli, H. Polioudaki, L.D. Shultz, K. McLean, P.A. Theodoropoulos, P.B. Singh, and S.D. Georgatos. 2004. The inner nuclear membrane protein lamin B receptor forms distinct microdomains and links epigenetically marked chromatin to the nuclear envelope. *J. Biol. Chem.* 279:25567–25573.

Mali, P., J. Aach, P.B. Stranges, K.M. Esvelt, M. Moosburner, S. Kosuri, L. Yang, and G.M. Church. 2013a. CAS9 transcriptional activators for target specificity screening and paired nickases for cooperative genome engineering. *Nat. Biotechnol.* 31:833–838. doi:10.1038/nbt.2675.

Mali, P., K.M. Esvelt, and G.M. Church. 2013b. Cas9 as a versatile tool for engineering biology. *Nat. Methods*. 10:957–963. doi:doi:10.1038/nmeth.2649.

Malik, P., N. Korfali, V. Srsen, V. Lazou, D.G. Batrakou, N. Zuleger, D.M. Kavanagh, G.S. Wilkie, M.W. Goldberg, and E.C. Schirmer. 2010. Cell-specific and lamin-dependent targeting of novel transmembrane proteins in the nuclear envelope. *Cell Mol Life Sci*. 67:1353–1369. doi:10.1007/s00018-010-0257-2.

Manders, E.M., H. Kimura, and P.R. Cook. 1999. Direct imaging of DNA in living cells reveals the dynamics of chromosome formation. *J. Cell Biol.* 144:813–821.

Mansfield, J., S. Genin, S. Magori, V. Citovsky, M. Sriariyanum, P. Ronald, M. Dow, V. Verdier, S.V. Beer, M.A. Machado, I. Toth, G. Salmond, and G.D. Foster. 2012. Top 10 plant pathogenic bacteria in molecular plant pathology. *Mol Plant Pathol*. 13:614–629. doi:10.1111/j.1364-3703.2012.00804.x.

Manuelidis, L. 1978. Chromosomal localization of complex and simple repeated human DNAs. *Chromosoma*. 66:23–32.

Manuelidis, L. 1984. Different central nervous system cell types display distinct and nonrandom arrangements of satellite DNA sequences. *Proceedings of the National Academy of Sciences of the United States of America*. 81:3123–3127.

Manuelidis, L. 1985. Individual interphase chromosome domains revealed by in situ hybridization. *Hum Genet*. 71:288–293.

Marois, E., G. Van den Ackerveken, and U. Bonas. 2002. The xanthomonas type III effector protein AvrBs3 modulates plant gene expression and induces cell hypertrophy in the susceptible host. *Mol Plant Microbe Interact*. 15:637–646. doi:10.1094/MPMI.2002.15.7.637.

Marshall, W.F., A. Straight, J.F. Marko, J. Swedlow, A. Dernburg, A. Belmont, A.W. Murray, D.A. Agard, and J.W. Sedat. 1997. Interphase chromosomes undergo constrained diffusional motion in living cells. *Curr. Biol.* 7:930–939.

Martin, R.M., and M.C. Cardoso. 2010. Chromatin condensation modulates access and binding of nuclear proteins. *FASEB J*. 24:1066–1072. doi:10.1096/fj.08-128959.

Mattout, A., and E. Meshorer. 2010. Chromatin plasticity and genome organization in pluripotent embryonic stem cells. *Curr. Opin. Cell Biol.* 22:334–341.

doi:10.1016/j.ceb.2010.02.001.

Mayer, R., A. Brero, J. von Hase, T. Schroeder, T. Cremer, and S. Dietzel. 2005. Common themes and cell type specific variations of higher order chromatin arrangements in the mouse. *BMC Cell Biol*. 6:44. doi:10.1186/1471-2121-6-44.

McCord, R.P., A. Nazario-Toole, H. Zhang, P.S. Chines, Y. Zhan, M.R. Erdos, F.S. Collins, J. Dekker, and K. Cao. 2013. Correlated alterations in genome organization, histone methylation, and DNA-lamin A/C interactions in Hutchinson-Gilford progeria syndrome. *Genome Research*. 23:260–269. doi:10.1101/gr.138032.112.

McKeon, F.D., M.W. Kirschner, and D. Caput. 1986. Homologies in both primary and secondary structure between nuclear envelope and intermediate filament proteins. *Nature*. 319:463–468. doi:10.1038/319463a0.

McNally, J.G., W.G. Muller, D. Walker, R. Wolford, and G.L. Hager. 2000. The glucocorticoid receptor: rapid exchange with regulatory sites in living cells. *Science*. 287:1262–1265.

Meaburn, K.J., E. Cabuy, G. Bonne, N. Levy, G.E. Morris, G. Novelli, I.R. Kill, and J.M. Bridger. 2007. Primary laminopathy fibroblasts display altered genome organization and apoptosis. *Aging Cell*. 6:139–153. doi:10.1111/j.1474-9726.2007.00270.x.

Mendenhall, E.M., K.E. Williamson, D. Reyon, J.Y. Zou, O. Ram, J.K. Joung, and B.E. Bernstein. 2013. Locus-specific editing of histone modifications at endogenous enhancers. *Nat. Biotechnol.* 31:1133–1136. doi:doi:10.1038/nbt.2701.

Mendiburo, M.J., J. Padeken, S. Fulop, A. Schepers, and P. Heun. 2011. Drosophila CENH3 is sufficient for centromere formation. *Science*. 334:686–690. doi:10.1126/science.1206880.

Mercer, A.C., T. Gaj, R.P. Fuller, and C.F.3. Barbas. 2012. Chimeric TALE recombinases with programmable DNA sequence specificity. *Nucleic acids research*. 40:11163–11172. doi:10.1093/nar/gks875.

Merkenschlager, M., S. Amoils, E. Roldan, A. Rahemtulla, E. O'connor, A.G. Fisher, and K.E. Brown. 2004. Centromeric repositioning of coreceptor loci predicts their stable silencing and the CD4/CD8 lineage choice. *J Exp Med*. 200:1437–1444. doi:10.1084/jem.20041127.

Meshorer, E., and T. Misteli. 2006. Chromatin in pluripotent embryonic stem cells and differentiation. *Nat Rev Mol Cell Biol*. 7:540–546. doi:10.1038/nrm1938.

Meuleman, W., D. Peric-Hupkes, J. Kind, J.-B. Beaudry, L. Pagie, M. Kellis, M. Reinders, L. Wessels, and B. van Steensel. 2013. Constitutive nuclear lamina-genome interactions are highly conserved and associated with A/T-rich sequence. *Genome Research*. 23:270–280. doi:10.1101/gr.141028.112.

Mewborn, S.K., M.J. Puckelwartz, F. Abuisneineh, J.P. Fahrenbach, Y. Zhang, H. MacLeod, L. Dellefave, P. Pytel, S. Selig, C.M. Labno, K. Reddy, H. Singh, and E. McNally. 2010. Altered chromosomal positioning, compaction, and gene expression with a lamin A/C gene mutation. *PLoS ONE*. 5:e14342. doi:10.1371/journal.pone.0014342.

Miller, J.C., S. Tan, G. Qiao, K.A. Barlow, J. Wang, D.F. Xia, X. Meng, D.E. Paschon, E.

Leung, S.J. Hinkley, G.P. Dulay, K.L. Hua, I. Ankoudinova, G.J. Cost, F.D. Urnov, H.S. Zhang, M.C. Holmes, L. Zhang, P.D. Gregory, and E.J. Rebar. 2011. A TALE nuclease architecture for efficient genome editing. *Nat. Biotechnol.* 29:143–148. doi:10.1038/nbt.1755.

Misteli, T. 2007. Beyond the sequence: cellular organization of genome function. *Cell*. 128:787–800. doi:10.1016/j.cell.2007.01.028.

Miyanari, Y., C. Ziegler-Birling, and M.-E. Torres-Padilla. 2013. Live visualization of chromatin dynamics with fluorescent TALEs. *Nat. Struct. Mol. Biol.* 20:1321–1324. doi:10.1038/nsmb.2680.

Moindrot, B., B. Audit, P. Klous, A. Baker, C. Thermes, W. de Laat, P. Bouvet, F. Mongelard, and A. Arneodo. 2012. 3D chromatin conformation correlates with replication timing and is conserved in resting cells. *Nucleic acids research*. 40:9470–9481. doi:10.1093/nar/gks736.

Mojica, F.J.M., C. Diez-Villasenor, J. Garcia-Martinez, and C. Almendros. 2009. Short motif sequences determine the targets of the prokaryotic CRISPR defence system. *Microbiology*. 155:733–740. doi:10.1099/mic.0.023960-0.

Molenaar, C., K. Wiesmeijer, N.P. Verwoerd, S. Khazen, R. Eils, H.J. Tanke, and R.W. Dirks. 2003. Visualizing telomere dynamics in living mammalian cells using PNA probes. *EMBO J.* 22:6631–6641. doi:10.1093/emboj/cdg633.

Morbitzer, R., J. Elsaesser, J. Hausner, and T. Lahaye. 2011. Assembly of custom TALE-type DNA binding domains by modular cloning. *Nucleic acids research*. 39:5790–5799. doi:10.1093/nar/gkr151.

Moscou, M.J., and A.J. Bogdanove. 2009. A simple cipher governs DNA recognition by TAL effectors. *Science*. 326:1501. doi:10.1126/science.1178817.

Nagano, T., Y. Lubling, T.J. Stevens, S. Schoenfelder, E. Yaffe, W. Dean, E.D. Laue, A. Tanay, and P. Fraser. 2013. Single-cell Hi-C reveals cell-to-cell variability in chromosome structure. *Nature*. 502:59–64. doi:10.1038/nature12593.

Nakamura, H., T. Morita, and C. Sato. 1986. Structural organizations of replicon domains during DNA synthetic phase in the mammalian nucleus. *Exp Cell Res*. 165:291–297.

Nakayasu, H., and R. Berezney. 1989. Mapping replicational sites in the eucaryotic cell nucleus. *J. Cell Biol.* 108:1–11.

Nan, X., H.H. Ng, C.A. Johnson, C.D. Laherty, B.M. Turner, R.N. Eisenman, and A. Bird. 1998. Transcriptional repression by the methyl-CpG-binding protein MeCP2 involves a histone deacetylase complex. *Nature*. 393:386–389. doi:10.1038/30764.

Naumova, N., M. Imakaev, G. Fudenberg, Y. Zhan, B.R. Lajoie, L.A. Mirny, and J. Dekker. 2013. Organization of the mitotic chromosome. *Science*. 342:948–953. doi:10.1126/science.1236083.

Nemeth, A., A. Conesa, J. Santoyo-Lopez, I. Medina, D. Montaner, B. Peterfia, I. Solovei, T. Cremer, J. Dopazo, and G. Langst. 2010. Initial genomics of the human nucleolus. *PLoS Genet.* 6:e1000889. doi:10.1371/journal.pgen.1000889.

Nishimasu, H., F.A. Ran, P.D. Hsu, S. Konermann, S.I. Shehata, N. Dohmae, R. Ishitani, F. Zhang, and O. Nureki. 2014. Crystal structure of Cas9 in complex with guide RNA and target DNA. *Cell*. 156:935–949. doi:10.1016/j.cell.2014.02.001.

Noordermeer, D., M. Leleu, P. Schorderet, E. Joye, F. Chabaud, and D. Duboule. 2014. Temporal dynamics and developmental memory of 3D chromatin architecture at Hox gene loci. *eLife Sciences*. 3:e02557.

Nora, E.P., B.R. Lajoie, E.G. Schulz, L. Giorgetti, I. Okamoto, N. Servant, T. Piolot, N.L. van Berkum, J. Meisig, J. Sedat, J. Gribnau, E. Barillot, N. Blüthgen, J. Dekker, and E. Heard. 2012. Spatial partitioning of the regulatory landscape of the X-inactivation centre. *Nature*. 485:381–385. doi:10.1038/nature11049.

O'Keefe, R.T., S.C. Henderson, and D.L. Spector. 1992. Dynamic organization of DNA replication in mammalian cell nuclei: spatially and temporally defined replication of chromosome-specific alpha-satellite DNA sequences. *J. Cell Biol.* 116:1095–1110.

Okano, M., D.W. Bell, D.A. Haber, and E. Li. 1999. DNA methyltransferases Dnmt3a and Dnmt3b are essential for de novo methylation and mammalian development. *Cell*. 99:247–257.

Olins, A.L., A. Ernst, M. Zwerger, H. Herrmann, and D.E. Olins. 2010. An in vitro model for Pelger-Huet anomaly: stable knockdown of lamin B receptor in HL-60 cells. *Nucleus*. 1:506–512. doi:10.4161/nucl.1.6.13271.

Olins, A.L., and D.E. Olins. 1974. Spheroid chromatin units (v bodies). *Science*. 183:330–332.

Olins, A.L., and D.E. Olins. 2004. Cytoskeletal influences on nuclear shape in granulocytic HL-60 cells. *BMC Cell Biol*. 5:30.

Olins, A.L., B. Buendia, H. Herrmann, P. Lichter, and D.E. Olins. 1998. Retinoic acid induction of nuclear envelope-limited chromatin sheets in HL-60. *Exp Cell Res*. 245:91–104. doi:10.1006/excr.1998.4210.

Olins, A.L., H. Herrmann, P. Lichter, and D.E. Olins. 2000. Retinoic acid differentiation of HL-60 cells promotes cytoskeletal polarization. *Exp Cell Res*. 254:130–142.

Olins, D.E., and A.L. Olins. 2003. Chromatin history: our view from the bridge. *Nat Rev Mol Cell Biol*. 4:809–814. doi:10.1038/nrm1225.

Olins, D.E., and A.L. Olins. 2009. Nuclear envelope-limited chromatin sheets (ELCS) and heterochromatin higher order structure. *Chromosoma*. 118:537–548. doi:10.1007/s00412-009-0219-3.

Ottaviani, A., C. Schluth-Bolard, S. Rival-Gervier, A. Boussouar, D. Rondier, A.M. Foerster, J. Morere, S. Bauwens, S. Gazzo, E. Callet-Bauchu, E. Gilson, and F. Magdinier. 2009. Identification of a perinuclear positioning element in human subtelomeres that requires A-type lamins and CTCF. *EMBO J.* 28:2428–2436. doi:10.1038/emboj.2009.201.

Owens, J.B., D. Mauro, I. Stoytchev, M.S. Bhakta, M.-S. Kim, D.J. Segal, and S. Moisyadi. 2013. Transcription activator like effector (TALE)-directed piggyBac transposition in human cells. *Nucleic acids research*. 41:9197–9207. doi:10.1093/nar/gkt677.

Padeken, J., and P. Heun. 2013. Centromeres in nuclear architecture. *Cell Cycle*. 12:3455–3456. doi:10.4161/cc.26697.

Pardue, M.L., and J.G. Gall. 1970. Chromosomal localization of mouse satellite DNA. *Science*. 168:1356–1358.

Parelho, V., S. Hadjur, M. Spivakov, M. Leleu, S. Sauer, H.C. Gregson, A. Jarmuz, C. Canzonetta, Z. Webster, T. Nesterova, B.S. Cobb, K. Yokomori, N. Dillon, L. Aragon, A.G. Fisher, and M. Merkenschlager. 2008. Cohesins functionally associate with CTCF on mammalian chromosome arms. *Cell*. 132:422–433. doi:10.1016/j.cell.2008.01.011.

Pattanayak, V., S. Lin, J.P. Guilinger, E. Ma, J.A. Doudna, and D.R. Liu. 2013. High-throughput profiling of off-target DNA cleavage reveals RNA-programmed Cas9 nuclease specificity. *Nat. Biotechnol.* 31:839–843. doi:10.1038/nbt.2673.

Pavletich, N.P., and C.O. Pabo. 1991. Zinc finger-DNA recognition: crystal structure of a Zif268-DNA complex at 2.1 A. *Science*. 252:809–817.

Peng, J.C., and G.H. Karpen. 2008. Epigenetic regulation of heterochromatic DNA stability. *Curr. Opin. Genet. Dev.* 18:204–211. doi:10.1016/j.gde.2008.01.021.

Pepperkok, R., and W. Ansorge. 1995. Direct visualization of DNA replication sites in living cells by microinjection of fluorescein-conjugated dUTPs. *Methods in Molecular and Cellular Biology*. 5:112–117.

Perez-Pinera, P., D.D. Kocak, C.M. Vockley, A.F. Adler, A.M. Kabadi, L.R. Polstein, P.I. Thakore, K.A. Glass, D.G. Ousterout, K.W. Leong, F. Guilak, G.E. Crawford, T.E. Reddy, and C.A. Gersbach. 2013a. RNA-guided gene activation by CRISPR-Cas9-based transcription factors. *Nat. Methods*. 10:973–976. doi:doi:10.1038/nmeth.2600.

Perez-Pinera, P., D.G. Ousterout, J.M. Brunger, A.M. Farin, K.A. Glass, F. Guilak, G.E. Crawford, A.J. Hartemink, and C.A. Gersbach. 2013b. Synergistic and tunable human gene activation by combinations of synthetic transcription factors. *Nat. Methods*. 10:239–242. doi:10.1038/nmeth.2361.

Peric-Hupkes, D., W. Meuleman, L. Pagie, S.W.M. Bruggeman, I. Solovei, W. Brugman, S. Gräf, P. Flicek, R.M. Kerkhoven, M. van Lohuizen, M. Reinders, L. Wessels, and B. van Steensel. 2010. Molecular Maps of the Reorganization of Genome-Nuclear Lamina Interactions during Differentiation. *Mol. Cell*. 38:603–613. doi:10.1016/j.molcel.2010.03.016.

Persikov, A.V., E.F. Rowland, B.L. Oakes, M. Singh, and M.B. Noyes. 2014. Deep sequencing of large library selections allows computational discovery of diverse sets of zinc fingers that bind common targets. *Nucleic acids research*. 42:1497–1508. doi:10.1093/nar/gkt1034.

Peters, A.H., D. O'Carroll, H. Scherthan, K. Mechtler, S. Sauer, C. Schofer, K. Weipoltshammer, M. Pagani, M. Lachner, A. Kohlmaier, S. Opravil, M. Doyle, M. Sibilia, and T. Jenuwein. 2001. Loss of the Suv39h histone methyltransferases impairs mammalian heterochromatin and genome stability. *Cell*. 107:323–337.

Pfaffeneder, T., B. Hackner, M. Truss, M. Munzel, M. Muller, C.A. Deiml, C. Hagemeier, and T. Carell. 2011. The discovery of 5-formylcytosine in embryonic stem cell DNA. *Angew*

Chem Int Ed Engl. 50:7008–7012. doi:10.1002/anie.201103899.

Phair, R.D., and T. Misteli. 2001. Kinetic modelling approaches to in vivo imaging. *Nat Rev Mol Cell Biol*. 2:898–907.

Phillips-Cremins, J.E., M.E.G. Sauria, A. Sanyal, T.I. Gerasimova, B.R. Lajoie, J.S.K. Bell, C.-T. Ong, T.A. Hookway, C. Guo, Y. Sun, M.J. Bland, W. Wagstaff, S. Dalton, T.C. McDevitt, R. Sen, J. Dekker, J. Taylor, and V.G. Corces. 2013. Architectural protein subclasses shape 3D organization of genomes during lineage commitment. *Cell*. 153:1281–1295. doi:10.1016/j.cell.2013.04.053.

Pickersgill, H., B. Kalverda, E. de Wit, W. Talhout, M. Fornerod, and B. van Steensel. 2006. Characterization of the Drosophila melanogaster genome at the nuclear lamina. *Nat. Genet.* 38:1005–1014. doi:10.1038/ng1852.

Pinheiro, I., R. Margueron, N. Shukeir, M. Eisold, C. Fritzsch, F.M. Richter, G. Mittler, C. Genoud, S. Goyama, M. Kurokawa, J. Son, D. Reinberg, M. Lachner, and T. Jenuwein. 2012. Prdm3 and Prdm16 are H3K9me1 methyltransferases required for mammalian heterochromatin integrity. *Cell*. 150:948–960. doi:10.1016/j.cell.2012.06.048.

Pinkel, D., J. Landegent, C. Collins, J. Fuscoe, R. Segraves, J. Lucas, and J. Gray. 1988. Fluorescence in situ hybridization with human chromosome-specific libraries: detection of trisomy 21 and translocations of chromosome 4. *Proceedings of the National Academy of Sciences of the United States of America*. 85:9138–9142.

Plohl, M., N. Mestrovic, and B. Mravinac. 2012. Satellite DNA evolution. *Genome Dyn*. 7:126–152. doi:10.1159/000337122.

Probst, A.V., and G. Almouzni. 2008. Pericentric heterochromatin: dynamic organization during early development in mammals. *Differentiation*. 76:15–23. doi:10.1111/j.1432-0436.2007.00220.x.

Probst, A.V., F. Santos, W. Reik, G. Almouzni, and W. Dean. 2007. Structural differences in centromeric heterochromatin are spatially reconciled on fertilisation in the mouse zygote. *Chromosoma*. 116:403–415. doi:10.1007/s00412-007-0106-8.

Probst, A.V., I. Okamoto, M. Casanova, F. El Marjou, P. Le Baccon, and G. Almouzni. 2010. A strand-specific burst in transcription of pericentric satellites is required for chromocenter formation and early mouse development. *Developmental Cell*. 19:625–638. doi:10.1016/j.devcel.2010.09.002.

Prokocimer, M., M. Davidovich, M. Nissim-Rafinia, N. Wiesel-Motiuk, D.Z. Bar, R. Barkan, E. Meshorer, and Y. Gruenbaum. 2009. Nuclear lamins: key regulators of nuclear structure and activities. *J Cell Mol Med*. 13:1059–1085. doi:10.1111/j.1582-4934.2008.00676.x.

Pyrpasopoulou, A., J. Meier, C. Maison, G. Simos, and S.D. Georgatos. 1996. The lamin B receptor (LBR) provides essential chromatin docking sites at the nuclear envelope. *EMBO J.* 15:7108–7119.

Qi, L.S., M.H. Larson, L.A. Gilbert, J.A. Doudna, J.S. Weissman, A.P. Arkin, and W.A. Lim. 2013. Repurposing CRISPR as an RNA-Guided Platform for Sequence-Specific Control of Gene Expression. *Cell*. 152:1173–1183. doi:10.1016/j.cell.2013.02.022.

Ragoczy, T., M.A. Bender, A. Telling, R. Byron, and M. Groudine. 2006. The locus control region is required for association of the murine beta-globin locus with engaged transcription factories during erythroid maturation. *Genes Dev.* 20:1447–1457. doi:10.1101/gad.1419506.

Rajapakse, I., M.D. Perlman, D. Scalzo, C. Kooperberg, M. Groudine, and S.T. Kosak. 2009. The emergence of lineage-specific chromosomal topologies from coordinate gene regulation. *Proceedings of the National Academy of Sciences of the United States of America*. 106:6679–6684. doi:10.1073/pnas.0900986106.

Ran, F.A., P.D. Hsu, C.-Y. Lin, J.S. Gootenberg, S. Konermann, A.E. Trevino, D.A. Scott, A. Inoue, S. Matoba, Y. Zhang, and F. Zhang. 2013. Double nicking by RNA-guided CRISPR Cas9 for enhanced genome editing specificity. *Cell*. 154:1380–1389. doi:10.1016/j.cell.2013.08.021.

Rao, S.S.P., M.H. Huntley, N.C. Durand, E.K. Stamenova, I.D. Bochkov, J.T. Robinson, A.L. Sanborn, I. Machol, A.D. Omer, E.S. Lander, and E.L. Aiden. 2014. A 3D Map of the Human Genome at Kilobase Resolution Reveals Principles of Chromatin Looping. *Cell*. doi:10.1016/j.cell.2014.11.021.

Reddy, K.L., J.M. Zullo, E. Bertolino, and H. Singh. 2008. Transcriptional repression mediated by repositioning of genes to the nuclear lamina. *Nature*. 452:243–247. doi:10.1038/nature06727.

Reyon, D., S.Q. Tsai, C. Khayter, J.A. Foden, J.D. Sander, and J.K. Joung. 2012. FLASH assembly of TALENs for high-throughput genome editing. *Nat. Biotechnol.* 30:460–465. doi:10.1038/nbt.2170.

Rhind, N., and D.M. Gilbert. 2013. DNA Replication Timing. *Cold Spring Harb Perspect Med*. 3:1–26.

Robinett, C.C., A. Straight, G. Li, C. Willhelm, G. Sudlow, A. Murray, and A.S. Belmont. 1996. In vivo localization of DNA sequences and visualization of large-scale chromatin organization using lac operator/repressor recognition. *J. Cell Biol.* 135:1685–1700. doi:10.1083/jcb.135.6.1685.

Roldan, E., M. Fuxa, W. Chong, D. Martinez, M. Novatchkova, M. Busslinger, and J.A. Skok. 2005. Locus “decontraction” and centromeric recruitment contribute to allelic exclusion of the immunoglobulin heavy-chain gene. *Nat Immunol*. 6:31–41. doi:10.1038/ni1150.

Romer, T., H. Leonhardt, and U. Rothbauer. 2011. Engineering antibodies and proteins for molecular in vivo imaging. *Curr Opin Biotechnol*. 22:882–887. doi:10.1016/j.copbio.2011.06.007.

Ronneberger, O., D. Baddeley, F. Scheipl, P.J. Verveer, H. Burkhardt, C. Cremer, L. Fahrmeir, T. Cremer, and B. Joffe. 2008. Spatial quantitative analysis of fluorescently labeled nuclear structures: problems, methods, pitfalls. *Chromosome Res.* 16:523–562. doi:10.1007/s10577-008-1236-4.

Rothbauer, U., K. Zolghadr, S. Muyldermans, A. Schepers, M.C. Cardoso, and H. Leonhardt. 2008. A versatile nanotrap for biochemical and functional studies with fluorescent fusion proteins. *Mol Cell Proteomics*. 7:282–289. doi:10.1074/mcp.M700342-MCP200.

Rothbauer, U., K. Zolghadr, S. Tillib, D. Nowak, L. Schermelleh, A. Gahl, N. Backmann, K. Conrath, S. Muyldermans, M.C. Cardoso, and H. Leonhardt. 2006. Targeting and tracing antigens in live cells with fluorescent nanobodies. *Nat. Methods*. 3:887–889. doi:10.1038/nmeth953.

Rubio, E.D., D.J. Reiss, P.L. Welcsh, C.M. Disteche, G.N. Filippova, N.S. Baliga, R. Aebersold, J.A. Ranish, and A. Krumm. 2008. CTCF physically links cohesin to chromatin. *Proceedings of the National Academy of Sciences of the United States of America*. 105:8309–8314. doi:10.1073/pnas.0801273105.

Ryba, T., I. Hiratani, J. Lu, M. Itoh, M. Kulik, J. Zhang, T.C. Schulz, A.J. Robins, S. Dalton, and D.M. Gilbert. 2010. Evolutionarily conserved replication timing profiles predict long-range chromatin interactions and distinguish closely related cell types. *Genome Research*. 20:761–770. doi:10.1101/gr.099655.109.

Sadoni, N., M.C. Cardoso, E.H.K. Stelzer, H. Leonhardt, and D. Zink. 2004. Stable chromosomal units determine the spatial and temporal organization of DNA replication. *Journal of cell science*. 117:5353–5365. doi:10.1242/jcs.01412.

Sander, J.D., and J.K. Joung. 2014. CRISPR-Cas systems for editing, regulating and targeting genomes. *Nat. Biotechnol.* 32:347–355. doi:doi:10.1038/nbt.2842.

Santos-Rosa, H., R. Schneider, A.J. Bannister, J. Sherriff, B.E. Bernstein, N.C.T. Emre, S.L. Schreiber, J. Mellor, and T. Kouzarides. 2002. Active genes are tri-methylated at K4 of histone H3. *Nature*. 419:407–411.

Sanyal, A., B.R. Lajoie, G. Jain, and J. Dekker. 2012. The long-range interaction landscape of gene promoters. *Nature*. 489:109–113. doi:10.1038/nature11279.

Scaffidi, P., and T. Misteli. 2006. Good news in the nuclear envelope: loss of lamin A might be a gain. *J. Clin. Invest.* 116:632–634. doi:10.1172/JCI27820.

Schatten, G., G.G. Maul, H. Schatten, N. Chaly, C. Simerly, R. Balczon, and D.L. Brown. 1985. Nuclear lamins and peripheral nuclear antigens during fertilization and embryogenesis in mice and sea urchins. *Proceedings of the National Academy of Sciences of the United States of America*. 82:4727–4731.

Schermelleh, L., I. Solovei, D. Zink, and T. Cremer. 2001. Two-color fluorescence labeling of early and mid-to-late replicating chromatin in living cells. *Chromosome Res.* 9:77–80.

Schermelleh, L., P.M. Carlton, S. Haase, L. Shao, L. Winoto, P. Kner, B. Burke, M.C. Cardoso, D.A. Agard, M.G.L. Gustafsson, H. Leonhardt, and J.W. Sedat. 2008. Subdiffraction multicolor imaging of the nuclear periphery with 3D structured illumination microscopy. *Science*. 320:1332–1336. doi:10.1126/science.1156947.

Schirmer, E.C., L. Florens, T. Guan, J.R.3. Yates, and L. Gerace. 2003. Nuclear membrane proteins with potential disease links found by subtractive proteomics. *Science*. 301:1380–1382.

Schmid, M., G. Arib, C. Laemmli, J. Nishikawa, T. Durussel, and U.K. Laemmli. 2006. Nup-PI: the nucleopore-promoter interaction of genes in yeast. *Mol. Cell*. 21:379–391. doi:10.1016/j.molcel.2005.12.012.

Schmid-Burgk, J.L., T. Schmidt, V. Kaiser, K. Honing, and V. Hornung. 2013. A ligation-independent cloning technique for high-throughput assembly of transcription activator-like effector genes. *Nat. Biotechnol.* 31:76–81. doi:10.1038/nbt.2460.

Schneider, K., C. Fuchs, A. Dobay, A. Rottach, W. Qin, P. Wolf, J.M. Alvarez-Castro, M.M. Nalaskowski, E. Kremmer, V. Schmid, H. Leonhardt, and L. Schermelleh. 2013. Dissection of cell cycle-dependent dynamics of Dnmt1 by FRAP and diffusion-coupled modeling. *Nucleic acids research*. 41:4860–4876. doi:10.1093/nar/gkt191.

Schotta, G., M. Lachner, K. Sarma, A. Ebert, R. Sengupta, G. Reuter, D. Reinberg, and T. Jenuwein. 2004. A silencing pathway to induce H3-K9 and H4-K20 trimethylation at constitutive heterochromatin. *Genes Dev.* 18:1251–1262.

Senecal, A., B. Munsky, F. Proux, N. Ly, F.E. Braye, C. Zimmer, F. Mueller, and X. Darzacq. 2014. Transcription Factors Modulate c-Fos Transcriptional Bursts. *Cell Rep*. 8:75–83.

Sexton, T., E. Yaffe, E. Kenigsberg, F. Bantignies, B. Leblanc, M. Hoichman, H. Parrinello, A. Tanay, and G. Cavalli. 2012. Three-dimensional folding and functional organization principles of the Drosophila genome. *Cell*. 148:458–472. doi:10.1016/j.cell.2012.01.010.

Shahbazian, M.D., and H.Y. Zoghbi. 2002. Rett syndrome and MeCP2: linking epigenetics and neuronal function. *Am J Hum Genet*. 71:1259–1272. doi:10.1086/345360.

Sharp, Z.D., M.G. Mancini, C.A. Hinojos, F. Dai, V. Berno, A.T. Szafran, K.P. Smith, T.P. Lele, D.E. Ingber, and M.A. Mancini. 2006. Estrogen-receptor-alpha exchange and chromatin dynamics are ligand- and domain-dependent. *Journal of cell science*. 119:4101–4116. doi:10.1242/jcs.03161.

Shelby, R.D., K.M. Hahn, and K.F. Sullivan. 1996. Dynamic elastic behavior of alpha-satellite DNA domains visualized in situ in living human cells. *J. Cell Biol.* 135:545–557.

Shen, Y., F. Yue, D.F. McCleary, Z. Ye, L. Edsall, S. Kuan, U. Wagner, J. Dixon, L. Lee, V.V. Lobanenkov, and B. Ren. 2012. A map of the cis-regulatory sequences in the mouse genome. *Nature*. 488:116–120. doi:10.1038/nature11243.

Shultz, L.D., B.L. Lyons, L.M. Burzenski, B. Gott, R. Samuels, P.A. Schweitzer, C. Dreger, H. Herrmann, V. Kalscheuer, A.L. Olins, D.E. Olins, K. Sperling, and K. Hoffmann. 2003. Mutations at the mouse ichthyosis locus are within the lamin B receptor gene: a single gene model for human Pelger-Huet anomaly. *Human Molecular Genetics*. 12:61–69.

Shumaker, D.K., T. Dechat, A. Kohlmaier, S.A. Adam, M.R. Bozovsky, M.R. Erdos, M. Eriksson, A.E. Goldman, S. Khuon, F.S. Collins, T. Jenuwein, and R.D. Goldman. 2006. Mutant nuclear lamin A leads to progressive alterations of epigenetic control in premature aging. *Proceedings of the National Academy of Sciences of the United States of America*. 103:8703–8708. doi:10.1073/pnas.0602569103.

Silve, S., P.H. Dupuy, P. Ferrara, and G. Loison. 1998. Human lamin B receptor exhibits sterol C14-reductase activity in Saccharomyces cerevisiae. *Biochim Biophys Acta*. 1392:233–244.

Simonis, M., P. Klous, E. Splinter, Y. Moshkin, R. Willemsen, E. de Wit, B. van Steensel, and W. de Laat. 2006. Nuclear organization of active and inactive chromatin domains

uncovered by chromosome conformation capture-on-chip (4C). *Nat. Genet.* 38:1348–1354. doi:10.1038/ng1896.

Skok, J.A., K.E. Brown, V. Azuara, M.L. Caparros, J. Baxter, K. Takacs, N. Dillon, D. Gray, R.P. Perry, M. Merkenschlager, and A.G. Fisher. 2001. Nonequivalent nuclear location of immunoglobulin alleles in B lymphocytes. *Nat Immunol*. 2:848–854.

Smith, S., and G. Blobel. 1993. The first membrane spanning region of the lamin B receptor is sufficient for sorting to the inner nuclear membrane. *J. Cell Biol.* 120:631–637.

Smith, Z.D., and A. Meissner. 2013. DNA methylation: roles in mammalian development. *Nature Reviews Genetics*. 14:204–220. doi:10.1038/nrg3354.

Solovei, I., A.S. Wang, K. Thanisch, C.S. Schmidt, S. Krebs, M. Zwerger, T.V. Cohen, D. Devys, R. Foisner, L. Peichl, H. Herrmann, H. Blum, D. Engelkamp, C.L. Stewart, H. Leonhardt, and B. Joffe. 2013. LBR and lamin A/C sequentially tether peripheral heterochromatin and inversely regulate differentiation. *Cell*. 152:584–598. doi:10.1016/j.cell.2013.01.009.

Solovei, I., and M. Cremer. 2010. 3D-FISH on cultured cells combined with immunostaining. *Methods Mol. Biol.* 659:117–126. doi:10.1007/978-1-60761-789-1_8.

Solovei, I., L. Schermelleh, K. During, A. Engelhardt, S. Stein, C. Cremer, and T. Cremer. 2004a. Differences in centromere positioning of cycling and postmitotic human cell types. *Chromosoma*. 112:410–423. doi:10.1007/s00412-004-0287-3.

Solovei, I., M. Kreysing, C. Lanctôt, S. Kösem, L. Peichl, T. Cremer, J. Guck, and B. Joffe. 2009. Nuclear architecture of rod photoreceptor cells adapts to vision in mammalian evolution. *Cell*. 137:356–368. doi:10.1016/j.cell.2009.01.052.

Solovei, I., N. Grandi, R. Knoth, B. Volk, and T. Cremer. 2004b. Positional changes of pericentromeric heterochromatin and nucleoli in postmitotic Purkinje cells during murine cerebellum development

. *Cytogenet Genome Res*. 105:302–310. doi:10.1159/000078202.

Solovei, I.V., B.I. Joffe, T. Hori, P. Thomson, S. Mizuno, and H.C. Macgregor. 1998. Unordered arrangement of chromosomes in the nuclei of chicken spermatozoa. *Chromosoma*. 107:184–188.

Somech, R., S. Shaklai, O. Geller, N. Amariglio, A.J. Simon, G. Rechavi, and E.N. Gal-Yam. 2005. The nuclear-envelope protein and transcriptional repressor LAP2beta interacts with HDAC3 at the nuclear periphery, and induces histone H4 deacetylation. *Journal of cell science*. 118:4017–4025. doi:10.1242/jcs.02521.

Soutoglou, E., and T. Misteli. 2007. Mobility and immobility of chromatin in transcription and genome stability. *Curr. Opin. Genet. Dev.* 17:435–442. doi:10.1016/j.gde.2007.08.004.

Sporbert, A., A. Gahl, R. Ankerhold, H. Leonhardt, and M.C. Cardoso. 2002. DNA polymerase clamp shows little turnover at established replication sites but sequential de novo assembly at adjacent origin clusters. *Mol. Cell*. 10:1355–1365.

Steglich, B., G.J. Filion, B. van Steensel, and K. Ekwall. 2012. The inner nuclear membrane

proteins Man1 and Ima1 link to two different types of chromatin at the nuclear periphery in S. pombe. *Nucleus*. 3:77–87.

Streubel, J., C. Blücher, A. Landgraf, and J. Boch. 2012. TAL effector RVD specificities and efficiencies. *Nat. Biotechnol.* 30:593–595. doi:10.1038/nbt.2304.

Subramanian, G., P. Chaudhury, K. Malu, S. Fowler, R. Manmode, D. Gotur, M. Zwerger, D. Ryan, R. Roberti, and P. Gaines. 2012. Lamin B receptor regulates the growth and maturation of myeloid progenitors via its sterol reductase domain: implications for cholesterol biosynthesis in regulating myelopoiesis. *J. Immunol.* 188:85–102. doi:10.4049/jimmunol.1003804.

Sullivan, G.J., J.M. Bridger, A.P. Cuthbert, R.F. Newbold, W.A. Bickmore, and B. McStay. 2001. Human acrocentric chromosomes with transcriptionally silent nucleolar organizer regions associate with nucleoli. *EMBO J.* 20:2867–2874. doi:10.1093/emboj/20.11.2867.

Sullivan, T., D. Escalante-Alcalde, H. Bhatt, M. Anver, N. Bhat, K. Nagashima, C.L. Stewart, and B. Burke. 1999. Loss of A-type lamin expression compromises nuclear envelope integrity leading to muscular dystrophy. *J. Cell Biol.* 147:913–920.

Szurek, B., E. Marois, U. Bonas, and G. Van den Ackerveken. 2001. Eukaryotic features of the Xanthomonas type III effector AvrBs3: protein domains involved in transcriptional activation and the interaction with nuclear import receptors from pepper. *Plant J*. 26:523–534.

Taddei, A., G. Van Houwe, F. Hediger, V. Kalck, F. Cubizolles, H. Schober, and S.M. Gasser. 2006. Nuclear pore association confers optimal expression levels for an inducible yeast gene. *Nature*. 441:774–778. doi:10.1038/nature04845.

Tahiliani, M., K.P. Koh, Y. Shen, W.A. Pastor, H. Bandukwala, Y. Brudno, S. Agarwal, L.M. Iyer, D.R. Liu, L. Aravind, and A. Rao. 2009. Conversion of 5-methylcytosine to 5-hydroxymethylcytosine in mammalian DNA by MLL partner TET1. *Science*. 324:930–935. doi:10.1126/science.1170116.

Takizawa, T., P.R. Gudla, L. Guo, S. Lockett, and T. Misteli. 2008. Allele-specific nuclear positioning of the monoallelically expressed astrocyte marker GFAP. *Genes Dev.* 22:489–498. doi:10.1101/gad.1634608.

Thanisch, K., K. Schneider, R. Morbitzer, I. Solovei, T. Lahaye, S. Bultmann, and H. Leonhardt. 2014. Targeting and tracing of specific DNA sequences with dTALEs in living cells. *Nucleic acids research*. 42:e38. doi:10.1093/nar/gkt1348.

Towbin, B.D., C. Gonzalez-Aguilera, R. Sack, D. Gaidatzis, V. Kalck, P. Meister, P. Askjaer, and S.M. Gasser. 2012. Step-wise methylation of histone H3K9 positions heterochromatin at the nuclear periphery. *Cell*. 150:934–947. doi:10.1016/j.cell.2012.06.051.

Tremblay, J.P., P. Chapdelaine, Z. Coulombe, and J. Rousseau. 2012. Transcription activator-like effector proteins induce the expression of the frataxin gene. *Hum Gene Ther*. 23:883–890. doi:10.1089/hum.2012.034.

Tumbar, T., and A.S. Belmont. 2001. Interphase movements of a DNA chromosome region

modulated by VP16 transcriptional activator. *Nat. Cell Biol.* 3:134–139. doi:10.1038/35055033.

Tumbar, T., G. Sudlow, and A.S. Belmont. 1999. Large-scale chromatin unfolding and remodeling induced by VP16 acidic activation domain. *J. Cell Biol.* 145:1341–1354.

Tupler, R., G. Perini, and M.R. Green. 2001. Expressing the human genome. *Nature*. 409:832–833. doi:10.1038/35057011.

van Bemmel, J.G., G.J. Filion, A. Rosado, W. Talhout, M. de Haas, T. van Welsem, F. van Leeuwen, and B. van Steensel. 2013. A network model of the molecular organization of chromatin in Drosophila. *Mol. Cell*. 49:759–771. doi:10.1016/j.molcel.2013.01.040.

Van den Ackerveken, G., E. Marois, and U. Bonas. 1996. Recognition of the bacterial avirulence protein AvrBs3 occurs inside the host plant cell. *Cell*. 87:1307–1316.

van Koningsbruggen, S., M. Gierlinski, P. Schofield, D. Martin, G.J. Barton, Y. Ariyurek, J.T. den Dunnen, and A.I. Lamond. 2010. High-resolution whole-genome sequencing reveals that specific chromatin domains from most human chromosomes associate with nucleoli. *Mol Biol Cell*. 21:3735–3748. doi:10.1091/mbc.E10-06-0508.

Vergnes, L., M. Peterfy, M.O. Bergo, S.G. Young, and K. Reue. 2004. Lamin B1 is required for mouse development and nuclear integrity. *Proceedings of the National Academy of Sciences of the United States of America*. 101:10428–10433.

Vissel, B., and K.H. Choo. 1989. Mouse major (gamma) satellite DNA is highly conserved and organized into extremely long tandem arrays: implications for recombination between nonhomologous chromosomes. *Genomics*. 5:407–414.

Voet, T., E. Schoenmakers, S. Carpentier, C. Labaere, and P. Marynen. 2003. Controlled transgene dosage and PAC-mediated transgenesis in mice using a chromosomal vector. *Genomics*. 82:596–605.

Voet, T., J. Vermeesch, A. Carens, J. Durr, C. Labaere, H. Duhamel, G. David, and P. Marynen. 2001. Efficient male and female germline transmission of a human chromosomal vector in mice. *Genome Research*. 11:124–136.

Voss, T.C., and G.L. Hager. 2014. Dynamic regulation of transcriptional states by chromatin and transcription factors. *Nature Reviews Genetics*. 15:69–81. doi:10.1038/nrg3623.

Walter, J., B. Joffe, A. Bolzer, H. Albiez, P.A. Benedetti, S. Muller, M.R. Speicher, T. Cremer, M. Cremer, and I. Solovei. 2006. Towards many colors in FISH on 3D-preserved interphase nuclei. *Cytogenet Genome Res*. 114:367–378. doi:10.1159/000094227.

Walter, J., L. Schermelleh, M. Cremer, S. Tashiro, and T. Cremer. 2003. Chromosome order in HeLa cells changes during mitosis and early G1, but is stably maintained during subsequent interphase stages. *J. Cell Biol.* 160:685–697.

Wang, F., and J.M.G. Higgins. 2013. Histone modifications and mitosis: countermarks, landmarks, and bookmarks. *Trends Cell Biol*. 23:175–184. doi:10.1016/j.tcb.2012.11.005.

Ward, M.C., M.D. Wilson, N.L. Barbosa-Morais, D. Schmidt, R. Stark, Q. Pan, P.C.

Schwalie, S. Menon, M. Lukk, S. Watt, D. Thybert, C. Kutter, K. Kirschner, P. Flicek, B.J. Blencowe, and D.T. Odom. 2013. Latent regulatory potential of human-specific repetitive elements. *Mol. Cell*. 49:262–272. doi:10.1016/j.molcel.2012.11.013.

Waterham, H.R., J. Koster, P. Mooyer, G.V. Noort Gv, R.I. Kelley, W.R. Wilcox, R.J.A. Wanders, R.C.M. Hennekam, and J.C. Oosterwijk. 2003. Autosomal recessive HEM/Greenberg skeletal dysplasia is caused by 3 beta-hydroxysterol delta 14-reductase deficiency due to mutations in the lamin B receptor gene. *Am J Hum Genet*. 72:1013–1017.

Wendt, K.S., K. Yoshida, T. Itoh, M. Bando, B. Koch, E. Schirghuber, S. Tsutsumi, G. Nagae, K. Ishihara, T. Mishiro, K. Yahata, F. Imamoto, H. Aburatani, M. Nakao, N. Imamoto, K. Maeshima, K. Shirahige, and J.-M. Peters. 2008. Cohesin mediates transcriptional insulation by CCCTC-binding factor. *Nature*. 451:796–801. doi:10.1038/nature06634.

Weuts, A., T. Voet, J. Verbeeck, N. Lambrechts, E. Wirix, L. Schoonjans, S. Danloy, P. Marynen, and G. Froyen. 2012. Telomere length homeostasis and telomere position effect on a linear human artificial chromosome are dictated by the genetic background. *Nucleic acids research*. 40:11477–11489. doi:10.1093/nar/gks926.

Wilkie, G.S., N. Korfali, S.K. Swanson, P. Malik, V. Srsen, D.G. Batrakou, J. de Las Heras, N. Zuleger, A.R.W. Kerr, L. Florens, and E.C. Schirmer. 2011. Several novel nuclear envelope transmembrane proteins identified in skeletal muscle have cytoskeletal associations. *Mol Cell Proteomics*. 10:M110.003129. doi:10.1074/mcp.M110.003129.

Williams, R.R.E., V. Azuara, P. Perry, S. Sauer, M. Dvorkina, H. Jorgensen, J. Roix, P. McQueen, T. Misteli, M. Merkenschlager, and A.G. Fisher. 2006. Neural induction promotes large-scale chromatin reorganisation of the Mash1 locus. *Journal of cell science*. 119:132–140. doi:10.1242/jcs.02727.

Williamson, I., S. Berlivet, R. Eskeland, S. Boyle, R.S. Illingworth, D. Paquette, J. Dostie, and W.A. Bickmore. 2014. Spatial genome organization: contrasting views from chromosome conformation capture and fluorescence in situ hybridization. *Genes Dev.* 28:2778–2791. doi:10.1101/gad.251694.114.

Wilson, E.B. 1925. The Cell in Development and Heredity. The Macmillan Company, New York.

Wilson, K.L., and R. Foisner. 2010. Lamin-binding Proteins. *Cold Spring Harb Perspect Biol*. 2:a000554–a000554. doi:10.1101/cshperspect.a000554.

Wong, A.K., and J.B. Rattner. 1988. Sequence organization and cytological localization of the minor satellite of mouse. *Nucleic acids research*. 16:11645–11661.

Wong, X., T.R. Luperchio, and K.L. Reddy. 2014. NET gains and losses: the role of changing nuclear envelope proteomes in genome regulation. *Curr. Opin. Cell Biol.* 28C:105–120. doi:10.1016/j.ceb.2014.04.005.

Worman, H.J. 2012. Nuclear lamins and laminopathies. *J Pathol*. 226:316–325. doi:10.1002/path.2999.

Worman, H.J., C.D. Evans, and G. Blobel. 1990. The lamin B receptor of the nuclear

envelope inner membrane: a polytopic protein with eight potential transmembrane domains. *J. Cell Biol.* 111:1535–1542.

Worman, H.J., J. Yuan, G. Blobel, and S.D. Georgatos. 1988. A lamin B receptor in the nuclear envelope. *Proceedings of the National Academy of Sciences of the United States of America*. 85:8531–8534.

Wright, R., M. Basson, L. D'Ari, and J. Rine. 1988. Increased amounts of HMG-CoA reductase induce “karmellae”: a proliferation of stacked membrane pairs surrounding the yeast nucleus. *J. Cell Biol.* 107:101–114.

Wu, J.C., and L. Manuelidis. 1980. Sequence definition and organization of a human repeated DNA. *Journal of Molecular Biology*. 142:363–386.

Wu, X., D.A. Scott, A.J. Kriz, A.C. Chiu, P.D. Hsu, D.B. Dadon, A.W. Cheng, A.E. Trevino, S. Konermann, S. Chen, R. Jaenisch, F. Zhang, and P.A. Sharp. 2014. Genome-wide binding of the CRISPR endonuclease Cas9 in mammalian cells. *Nat. Biotechnol.* 32:670–676. doi:10.1038/nbt.2889.

Xu, G.L., T.H. Bestor, D. Bourc'his, C.L. Hsieh, N. Tommerup, M. Bugge, M. Hulten, X. Qu, J.J. Russo, and E. Viegas-Pequignot. 1999. Chromosome instability and immunodeficiency syndrome caused by mutations in a DNA methyltransferase gene. *Nature*. 402:187–191. doi:10.1038/46052.

Yan, J., M. Enge, T. Whitington, K. Dave, J. Liu, I. Sur, B. Schmierer, A. Jolma, T. Kivioja, M. Taipale, and J. Taipale. 2013. Transcription factor binding in human cells occurs in dense clusters formed around cohesin anchor sites. *Cell*. 154:801–813. doi:10.1016/j.cell.2013.07.034.

Yang, J., Y. Zhang, P. Yuan, Y. Zhou, C. Cai, Q. Ren, D. Wen, C. Chu, H. Qi, and W. Wei. 2014. Complete decoding of TAL effectors for DNA recognition. *Cell Res.* 24:628–631. doi:doi:10.1038/cr.2014.19.

Ye, Q., and H.J. Worman. 1994. Primary structure analysis and lamin B and DNA binding of human LBR, an integral protein of the nuclear envelope inner membrane. *J. Biol. Chem.* 269:11306–11311.

Ye, Q., I. Callebaut, A. Pezhman, J.C. Courvalin, and H.J. Worman. 1997. Domain-specific interactions of human HP1-type chromodomain proteins and inner nuclear membrane protein LBR. *J. Biol. Chem.* 272:14983–14989.

Yin, P., D. Deng, C. Yan, X. Pan, J.J. Xi, N. Yan, and Y. Shi. 2012. Specific DNA-RNA hybrid recognition by TAL effectors. *Cell Rep*. 2:707–713. doi:10.1016/j.celrep.2012.09.001.

Yuan, K., A.W. Shermoen, and P.H. O'Farrell. 2014. Illuminating DNA replication during Drosophila development using TALE-lights. *Curr. Biol.* 24:R144–5. doi:10.1016/j.cub.2014.01.023.

Zhang, F., Le Cong, S. Lodato, S. Kosuri, G.M. Church, and P. Arlotta. 2011. Efficient construction of sequence-specific TAL effectors for modulating mammalian transcription. *Nat. Biotechnol.* 29:149–153. doi:doi:10.1038/nbt.1775.

Zhang, L.-F., K.D. Huynh, and J.T. Lee. 2007. Perinucleolar targeting of the inactive X during

S phase: evidence for a role in the maintenance of silencing. *Cell*. 129:693–706. doi:10.1016/j.cell.2007.03.036.

Zhang, Y., R.P. McCord, Y.-J. Ho, B.R. Lajoie, D.G. Hildebrand, A.C. Simon, M.S. Becker, F.W. Alt, and J. Dekker. 2012. Spatial organization of the mouse genome and its role in recurrent chromosomal translocations. *Cell*. 148:908–921. doi:10.1016/j.cell.2012.02.002.

Zhu, C., A. Gupta, V.L. Hall, A.L. Rayla, R.G. Christensen, B. Dake, A. Lakshmanan, C. Kuperwasser, G.D. Stormo, and S.A. Wolfe. 2013. Using defined finger-finger interfaces as units of assembly for constructing zinc-finger nucleases. *Nucleic acids research*. 41:2455–2465. doi:10.1093/nar/gks1357.

Zink, D., T. Cremer, R. Saffrich, R. Fischer, M.F. Trendelenburg, W. Ansorge, and E.H. Stelzer. 1998. Structure and dynamics of human interphase chromosome territories in vivo. *Hum Genet*. 102:241–251.

Zullo, J.M., I.A. Demarco, R. Pique-Regi, D.J. Gaffney, C.B. Epstein, C.J. Spooner, T.R. Luperchio, B.E. Bernstein, J.K. Pritchard, K.L. Reddy, and H. Singh. 2012. DNA sequence-dependent compartmentalization and silencing of chromatin at the nuclear lamina. *Cell*. 149:1474–1487. doi:10.1016/j.cell.2012.04.035.

Zwerger, M., H. Herrmann, P. Gaines, A.L. Olins, and D.E. Olins. 2008. Granulocytic nuclear differentiation of lamin B receptor-deficient mouse EPRO cells. *Exp Hematol*. 36:977–987. doi:10.1016/j.exphem.2008.03.003.

4.2 Abbreviations

1D	one-dimensional
3C	Chromatin conformation capture
3D	three-dimensional
3D-SIM	superresolution three-dimensional structured illumination
4C	circular chromosome conformation capture or 3C-on-chip
5C	chromosome conformation capture carbon copy
5mC	cytosine methylated at position C5
A	adenine
aa	amino acid
AD	activation domain
AD-EDMD	Emery-Dreifuss muscular dystrophy
AOTF	acousto-optic tunable filter
ATP	adenosine triphosphate
B1	short interspersed nuclear element, class B1
B23	nucleophosmin
BAC	bacterial artificial chromosome
BAF	Barrier-to-autointegration factor
bp	base pairs
C	cytosine
C-HAC	circular human artificial chromosome
C-terminal	carboxy-terminal
Cas	Crisper-associated protein
CC	chromocenter
CD	chromatin domain
CENP	centromere protein
cHC	constitutive heterochromatin
ChIP	chromatin immunoprecipitation
ChIP-seq	chromatin immunoprecipitation combined with DNA-sequencing
cLADs	constitutive LADs
CoA	coenzyme A
CRISPR	clustered regulatory interspaced short palindromic repeats
crRNA	CRISPR RNA
CT	chromosome territory
CTCF	CCCTC-binding factor
CTD	C-terminal domain
D4Z4	polycomb-binding tandem repeat protein
Dam	adenine DNA methyltransferase
DamID	DNA adenine methyltransferase identification
DAPI	4',6-diamindino-2-phenylindole
dCas9	catalytically inactive, dead Cas9
DNA	Deoxyribonucleic acid
Dnmt	DNA methyltranferase
Dnmt1	DNA methyltransferase 1
Dnmt3a	DNA methyltransferase 3a

Dnmt3b	DNA methyltransferase 3b
DSB	double strand break
dTALE	designer transcription activator-like effector
dUTP	dexoyuridine triphophate
E	day of embryonic development
EC	euchromatin
EMD	Emerin
ER	endoplasmatic reticulum
ESC	embryonic stem cells
FACS	fluorescence-activated cell sorting
fHC	facultative heterochromatin
FISH	fluorescence in situ hybridisation
fLADs	facultative LADs
FLIP	fluorescence loss in photobleaching
FRAP	fluorescence recovery after photobleaching
G	guanine
G1	Gap 1 phase of the cell cycle
G2	Gap 2 phase of the cell cycle
G9a	histone methyltransferase for H3K9me2
GATA1	GATA-binding protein 1
GBP	GFP-binding protein
GFP	green fluorescent protein
GFP-msTALE	designer transcription activator-like effector directed against the major satellites, N-terminally fused to GFP
GFP-nanotrap	GFP-binding protein in fusion with Lamin B1
h	hours
H2A	histone 2 variant A
H2B	histone 2 variant B
H3	histone 3
H3K27me3	lysine 27 trimethylated histone 3, repressive mark
H3K36me3	lysine 36 trimethylated histone 3, euchromatic mark
H3K4me3	lysine 4 trimethylated histone 3, euchromatic mark
H3K9me2	lysine 9 dimethylated histone 3, repressive mark
H3K9me3	lysine 9 trimethylated histone 3, repressive mark
H3S10P	histone 3 serine 10 phosphorylation
H4	histone 4
H4K20m3	lysine 24 trimethylated histone 4, repressive mark
HAC	human artificial chromosome
HAT	histone acetyltransferase
HC	heterochromatin
HDAC	histone deacetylase
HGPS	Hutchinson-Gilford progeria syndrome
hHOR	human HAC Orthology Region
HMG	3-hyroxy-3-methyl-glutaryl
HMT	histone methyltransferase
HNH	HNH endonuclease domain

Hox	homeodomain, family of transcription factors
HP1	heterochromatin protein 1
HR	homologous recombination
HSA	Homo sapiens
ICF	immunodeficiency, centromeric instability and facial anomaly
Ig	Immunoglobulin
INL	inner nuclear layer
INM	inner nuclear membrane
kb	kilo base
Kd	Dissociation constant
kDa	kilo Dalton
KO	knock-out
KRAB	Krüppel-associated box
L-HAC	linear human artificial chromosome
L1	long interspersed nuclear element, class L1
L2	long interspersed nuclear element, class L2
lacO	lac operator
LAD	Lamina-associating domain
LADness	degree of lamina-association
LAP	Lamina-associated polypeptide
LB1	Lamin B1
LBR	Lamin B receptor
LEM	LEM domain containing
LINE	long interspersed nuclear element
LmA	Lamin A
LmA/C	Lamin A/C
LmC	Lamin C
LSH	lymphoid specific helicase
m6A	adenine methylated at position C6
Mb	mega base
MBD	methylcytosine binding domain
MeCP2	methylcytosine binding protein 2
mHOR	mouse HAC Orthology Region
min	minutes
MLL	myeloid/lymphoid leukaemia
MMU	mouse chromosome
mRFP	monomeric red fluorescent protein
ms-repeats	major satellite repeats
N	amino-terminal
NAD	nuclear associated domain
NAD	Nucleolus-associated domain
NE	nuclear envelope
NET	nuclear envelope transmembrane protein
NHEJ	non-homologous end joining
NL	nuclear lamina
NLS	nuclear localization signal

nm	nano meter
NOR	nuclear organizer regions
NTD	N-terminal domain
NUC	nuclease lobe
Oct4	Octamer binding factor 4
ONM	outer nuclear membrane
OR	olfactory receptor
OSN	olfactory senory neuron
P	day of postembryonic development
PAM	protospacer adjacent motif
PCNA	proliferating nuclear antigen
PCR	polymerase chain reaction
PMT	post translational modification
Prdm3	PRDI-BF1 and RIZ homology domain containing protein 3, histone methyltransferase specific for H3K9me1
Prdm6	PRDI-BF1 and RIZ homology domain containing protein 6, histone methyltransferase specific for H3K9me1
PZF:GFP	Zinc finger directed to the major satellite repeats fused to GFP
rDNA	ribosomal DNA
REC	recognition lobe
RFP	red fluorescent protein
RGN	RNA-guided nucleases
RNA	ribonucleic acid
RPOII	RNA polymerase II
RT-PCR	real time PCR
RuvC	RuvC endonuclease domain
RVD	repeat variable diresidue
S-Phase	synthesis phase of the cell cycle
SDRX	Serine-aspartate repeat X
SetD	Set domain containing
sgRNA	short guide RNA
SINE	short interspersed nuclear element
SNP	single nucleotide polymorphism
Sox2	Sex-determining region (SRY)-Box2
Suv	suppressor of variegation
Suv39h1	histone methyltransferase for H3K9me3
Suv39h2	histone methyltransferase for H3K9me3
Suv40h1	histone methyltransferase for H4K20me3
Suv40h2	histone methyltransferase for H4K20me3
T	thymidine
T3S	Type III secretion system
TAD	Topology associated domain
TALE	transcription activator-like effector
TALEN	transcription activator-like effector nuclease fusion
Tet	ten eleven translocation
TF	transcritpion factor

TM	transmembrane
TMD	transmembrane domain
tracrRNA	transactivating RNA
TSA	trichostatin A
TSS	transcriptional start site
VP16	viral protein 16
ZF	zinc finger
ZFP	zinc finger proteins
µm	micro meter